

Magnetic carbon-coated cobalt nanoparticles as a versatile platform for polymer-design, scavenging and catalysis

Dissertation

Zur Erlangung des Doktorgrades der Naturwissenschaften

Dr. rer. nat.

der Fakultät für Chemie und Pharmazie

der Universität Regensburg



vorgelegt von

Lisa Stadler

aus Starnberg

Regensburg 2020

Die Arbeit wurde angeleitet von: Prof. Dr. Oliver Reiser

Promotionsgesuch eingereicht am: 30.06.2020

Promotionskolloquium am: 11.09.2020

| | | |
|--------------------|---------------|---------------------------------|
| Prüfungsausschuss: | Vorsitz: | Apl. Prof. Dr. Rainer Müller |
| | 1. Gutachter: | Prof. Dr. Oliver Reiser |
| | 2. Gutachter: | Prof. Dr. Alexander Breder |
| | 3. Prüfer: | Prof. Dr. Frank-Michael Matysik |

Der experimentelle Teil der vorliegenden Arbeit wurde im Zeitraum von November 2016 bis Januar 2020 unter der Anleitung von Prof. Dr. Oliver Reiser am Institut für Organische Chemie der Universität Regensburg angefertigt.

Besonders bedanken möchte ich mich bei Herrn Prof. Dr. Oliver Reiser für die Aufnahme in seinen Arbeitskreis, die Überlassung des interessanten Themas, die anregenden Diskussionen und die stete Unterstützung.

Für meine Familie

*“If you thought that science was certain
– well, that is just an error on your part.”*

Richard P. Feynman (1918-1988)

Table of contents

| | | |
|------|---------------------------------------------------------------------------------------------------------------------------------------------|----|
| A. | Introduction..... | 1 |
| 1. | Magnetic metal nanoparticles..... | 3 |
| 1.1. | Superparamagnetism – unique property of metal nanoparticles..... | 3 |
| 1.2. | Nanoparticle synthesis – overview..... | 4 |
| 1.3. | Coatings and surface functionalization of magnetic nanoparticles..... | 6 |
| 1.4. | Applications of carbon-coated magnetic nanoparticles..... | 13 |
| B. | Main part..... | 19 |
| 1. | Magnetic microporous organic polymers encapsulated with palladium nanoparticles as recyclable catalysts for hydrogenation reactions..... | 19 |
| 1.1. | Introduction..... | 20 |
| 1.2. | Results and Discussion..... | 21 |
| 2. | Palladium-catalyzed Suzuki-Miyaura coupling under mild reaction conditions..... | 35 |
| 2.1. | Suzuki-Miyaura coupling – the dynamic nature of palladium catalysis..... | 36 |
| 2.2. | Synthesis of magnetic palladium nanocatalysts..... | 38 |
| 2.3. | Application of the magnetic Co/C nanocatalysts in the Suzuki-Miyaura coupling..... | 42 |
| 3. | Recyclable aza-bis(oxazoline) ligands for the asymmetric cyclopropanation..... | 49 |
| 3.1. | Immobilization of aza-bis(oxazoline) ligands for the Cu(I)-catalyzed cyclopropanation .. | 50 |
| 3.2. | Immobilization of aza-bis(oxazolines) onto magnetic Co/C nanoparticles..... | 53 |
| 3.3. | Application of magnetic aza-bis(oxazolines) in the asymmetric cyclopropanation..... | 59 |
| 4. | Reversible extraction of toxic heavy metals from water..... | 67 |
| 4.1. | Introduction..... | 68 |
| 4.2. | Results and Discussion..... | 70 |
| C. | Summary..... | 79 |
| D. | Zusammenfassung..... | 82 |
| E. | Experimental Part..... | 85 |
| 1. | General Information..... | 85 |
| 2. | Hydrogenation reactions using microporous organic polymers..... | 90 |

| | | |
|------|----------------------------------------------------------------------------|-----|
| 2.1. | Synthesis of catalyst and starting materials | 90 |
| 2.2. | Catalysis | 92 |
| 2.3. | Sample preparation and miscellaneous | 96 |
| 3. | Suzuki-Miyaura coupling under mild reaction conditions..... | 101 |
| 3.2. | Catalysis..... | 104 |
| 3.3. | Sample preparation and miscellaneous | 107 |
| 4. | Cyclopropanation using chiral azaBOX-based copper catalysts..... | 108 |
| 4.1. | Synthesis of catalysts and starting materials | 108 |
| 4.2. | Catalysis | 122 |
| 4.3. | Sample preparation and miscellaneous | 125 |
| 5. | Heavy metal extraction from water using microporous organic polymers | 126 |
| 5.1. | Synthesis of magnetic materials..... | 126 |
| 5.2. | Heavy metal adsorption | 132 |
| 5.3. | Additional figures and miscellaneous..... | 138 |
| F. | References..... | 140 |
| G. | Appendix..... | 150 |
| 1. | NMR spectra | 150 |
| 2. | GC chromatograms..... | 159 |
| 3. | HPLC chromatograms | 172 |
| 4. | Curriculum Vitae..... | 174 |
| H. | Acknowledgment - Danksagung..... | 177 |
| I. | Declaration | 179 |

Abbreviations

| | | | |
|-----------|---------------------------------------------|-------------|----------------------------------------------------------|
|))) | ultrasound | EDTA | ethylenediaminetetraacetic acid |
| AD | <i>anno domini</i> | <i>ee</i> | enantiomeric excess |
| AIBN | 2,2'-azobis(2-methylpropionitrile) | emu | electromagnetic unit |
| aq. | aqueous | equiv. | equivalent(s) |
| atm | atmosphere | Et | Ethyl |
| ATR | attenuated total reflection | FDA | formaldehyde dimethyl acetal |
| azaBOX | aza-bis(oxazoline) | Fe/C | carbon-coated iron nanoparticle |
| BCE | before the common era | FID | flame ionization detector |
| BET | Brunauer-Emmett-Teller | FT | fourier transformation |
| BJH | Barrett-Joyner-Halenda | GC | gas chromatography |
| Boc | <i>tert</i> -butyloxycarbonyl | h | hour(s) |
| BOX | bis(oxazoline) | HPLC | high performance liquid chromatography |
| BuLi | butyl lithium | <i>i</i> - | <i>iso</i> - |
| Co/C | carbon-coated cobalt nanoparticle | ICP-MS | inductively coupled plasma-mass spectrometry |
| conc. | concentrated | ICP-OES | inductively coupled plasma-optical emission spectrometry |
| CuAAC | copper-catalyzed azide-alkyne cycloaddition | IL | ionic liquid |
| d | day(s) | <i>i</i> Pr | <i>iso</i> -propyl |
| dba | dibenzylideneacetone | IR | infrared |
| DCE | 1,2-dichloroethane | IR | infrared |
| DCM | dichloromethane | L (X) | loading of the element (X) in mmol/g |
| DIPEA | <i>N,N</i> -diisopropylethylamine | Me | methyl |
| dist. | distilled | Mes | mesityl (2,4,6-trimethylphenyl) |
| DMF | <i>N,N</i> -dimethylformamide | min | minute(s) |
| <i>dr</i> | diastereomeric ratio | MoM | monomer-on-monomer |
| EA | elemental microanalysis | MOP | microporous organic polymer |
| EDS | energy-dispersive X-ray spectroscopy | MS | mass spectrometry |

| | | | |
|----------------------|----------------------------------------|-----------------------------|------------------------------------------------------|
| MW | microwave | S | surface area |
| <i>n.d.</i> | not determined | s | second(s) |
| Nb | norbornyl | sat. | saturated |
| NHC | <i>N</i> -heterocyclic carbene | T | temperature |
| NMP | <i>N</i> -methyl-2-pyrrolidinone | TBAB | tetra- <i>n</i> -butylammonium bromide |
| NMR | nuclear magnetic resonance | ^t Bu | <i>tert</i> -butyl |
| NP | nanoparticle | TEM | transmission electron microscopy |
| PEG | poly(ethylene glycol) | Tf | trifluoromethanesulfonate |
| PEI | poly(ethyleneimine) | TGA | thermo-gravimetric analysis |
| Ph | phenyl | THF | tetrahydrofuran |
| ppb | parts per billion | TLC | thin-layer chromatography |
| ppm | parts per million | TOF | turn over frequency |
| PS | polystyrene | TON | turn over number |
| PTFE | polytetrafluoroethylene | <i>t_r</i> | retention time |
| quant. | quantitative | UV-vis | Ultraviolet-visible (spectroscopy) |
| R | arbitrary residue | v/v | volume to volume ratio |
| r.t. | room temperature | <i>V</i> _{0.1/tot} | ratio of micropore volume over the total pore volume |
| ref. | reference | w/w | weight to weight ratio |
| <i>R_f</i> | retardation factor | wt% | weight percent |
| ROMP | ring-opening metathesis polymerization | XPS | X-ray photoelectron spectroscopy |
| rpm | revolutions per minute | | |

A. Introduction

With the speech “There’s Plenty of Room at the Bottom” of Richard Feynman in 1959, the physicist and Nobel Prize laureate is perceived as the founder of nanoscience and nanotechnology.^[1] Nanochemistry emerged as one of the subcategories, laying the focus on synthetic chemistry to construct nanostructures or nanoscale building blocks for their potential technological applications.^{[2],[3]} These nanomaterials are defined as materials with at least one spatial dimension in the size range of 1-100 nm (Figure 1). Classifying these nanomaterials based on their dimensions of nanoscale (<100 nm), four different classes are possible: (i) zero-dimensional nanomaterials, *e.g.* nanoparticles, (ii) one-dimensional nanomaterials, *e.g.* nanorods, nanotubes, nanowires, (iii) two-dimensional nanomaterials, *e.g.* nanofilms, nanolayers, and (iv) three dimensional or bulk nanomaterials where all dimensions are above 100 nm, *e.g.* multi nanolayers, bundles of nanowires or nanotubes.

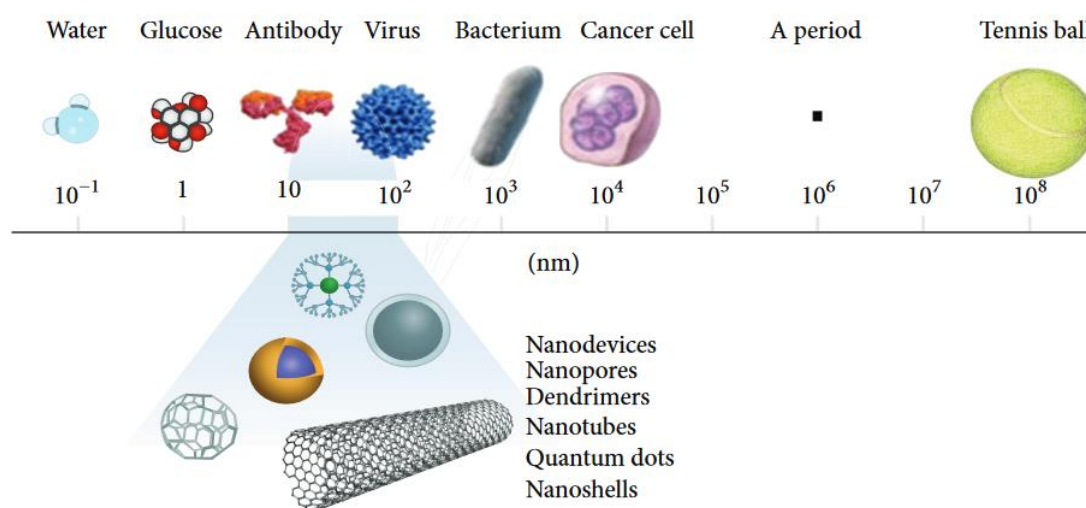


Figure 1. Size comparison of nanomaterials with larger-sized materials. The scale bar is given in nm. Reprinted with permission from [4]. Copyright © 2014, M. T. Amin *et al.*

Nanoparticles (NPs) are considered as zero-dimensional nanomaterials since all three dimensions are in the nanoscale region.^{[5],[6]} By downsizing to the nanometer scale, metals reveal unique physicochemical properties that differ decisively from their bulk counterparts, depending on the size and shape. Of these, especially the optical properties gained fundamental interest since ancient times and are probably the most prominent and earliest example for the characteristics of nanoparticles. Dating back to the time period of BCE, metallic nanoparticles were utilized due to their extraordinary features in numerous sculptures, paintings, and glasses.^[7] The Lycurgus Cup, dating back to the fourth century AD, has become particularly famous for the outstanding achievements of the ancient glass industry. Its dichroic glass changes color from jade green to blood-red when it is illuminated internally,

caused by the change of reflected to transmitted light. Modern science revealed the colloidal dispersion of silver-gold alloys (typically 50-100 nm) with a ratio of silver to gold about 7:3 (about 300 ppm to 40 ppm, with additionally 10% copper) as a reason for the light scattering and absorption.^{[7],[8]} During the medieval period, colorful stained glass windows like the rose windows of Notre-Dame were created due to the presence of dispersed gold, silver, and copper nanoparticles.^{[7],[9]} Certainly, the ancient stained-glass makers were unaware of the nanotechnology.^[7] Nowadays, the relation between nanoparticles and their associated colors is widely known (depicted in Figure 2), showing a red reflected color is assigned to either Ag nanoprisms with 100 nm or spherical Au NPs with 25 nm, whereas a green color can be achieved by 50 nm Au NPs. The historically widespread yellow stained glass is caused by 100 nm sized spherical Ag NPs and can be changed to blue by decreasing the size to 40 nm.^{[10],[11]} This knowledge is based on the proceeding development of enhanced synthesis, fabrication, and characterization methods allowing a controlled impact on the sizes, shapes, and compositions of metal nanoparticles and further enables their explicit investigation. Consequently, further physicochemical properties become relevant, such as *e.g.* superparamagnetism, which will be addressed in the following chapter. Afterwards, an overview of the most common methods for the preparation of magnetic nanoparticles is presented, followed by an introduction to surface coatings and functionalizations which are especially suitable for further approaches. Special focus will be on air-stable, so-called core-shell carbon-coated metallic nanoparticles. A highlight of selected applications of these materials is given in the last chapter, emphasizing their potential use as versatile catalysts, scavengers, and reagents.

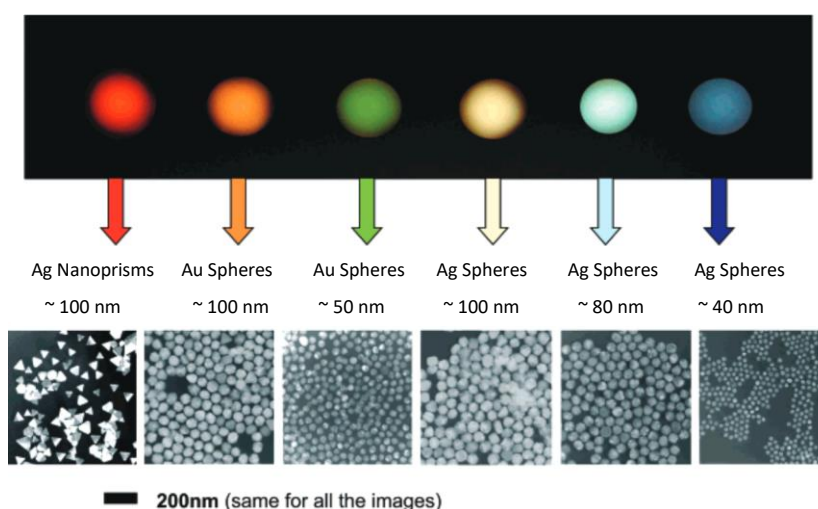


Figure 2. Sizes, shapes, and compositions of metal nanoparticles can be systematically varied to produce materials with distinct light-scattering properties. Adapted with permission from [11]. Copyright © 2005, American Chemical Society.

1. Magnetic metal nanoparticles

1.1. Superparamagnetism – unique property of metal nanoparticles

Although macromolecules and aggregates of organic molecules bear the possibility to form particles in the nanometer range,^[12] metals and semiconductor oxides are among the most well-known nanoparticles.^[3] Decreasing the size to the nanoscale region enlarges the surface-area-to-volume ratio significantly and consequently increases the number of surface atoms, which in turn influences the material properties. In the case of ferri- and ferromagnetic metals, downsizing below a critical size may entail the development of superparamagnetism. It is generally known that spinning particles containing both, mass and electric charge, cause magnetic effects by the formation of a magnetic dipole. These so-called magnetons are grouped in domains ('Weiss domains'). The size of magnetic domains is typically in the micrometer region. Decreasing the particle size below a critical nanometer-scale value (around 50 nm, depending on the material), means that the maintenance of domain walls costs more energy than to support the external magnetostatic energy (stray field) of the single-domain state. Consequently, single-domains become predominant, as depicted in Figure 3A.^[13] If an external magnetic field (H) is applied until the saturation magnetization (M_s) is reached, the multi-domain (green) and single-domain curves are well described as hysteresis loops (Figure 3B) with two main parameters: remanence (M_r) and coercivity (H_c). Remanence is described *via* the intersection ($H=0$) of the hysteresis loop by reducing the magnetic field to zero. Coercivity is apparent *via* the intersection at $M=0$.^[14] Reduction of the particle size to single-domains results in an enlargement of the coercivity to the maximum (blue curve), however, reducing the particle size even further, H_c becomes zero without any magnetic remanence (orange curve).^[13] This phenomenon is caused by thermal fluctuations which spontaneously demagnetize a previously saturated assembly and is known as superparamagnetism. Above a certain temperature (blocking temperature), superparamagnetic particles behave like independent atomic paramagnets with high magnetic susceptibility.^[14]

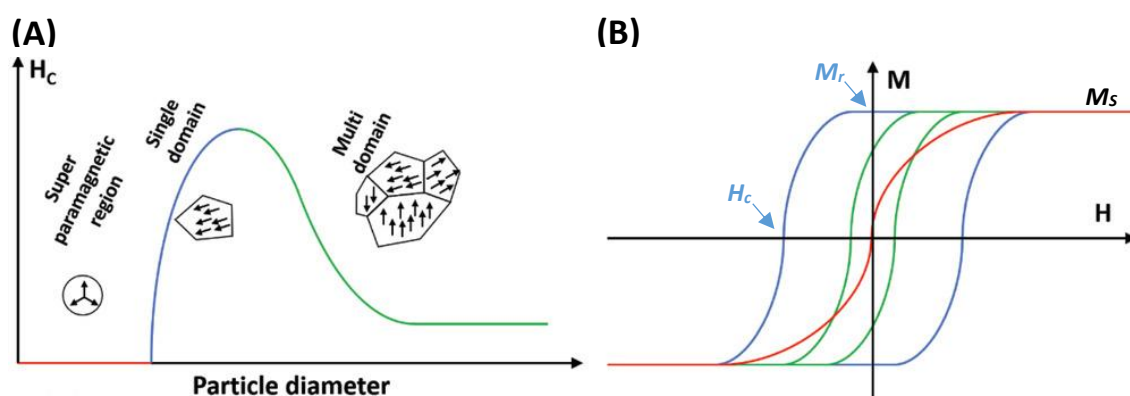


Figure 3. General dependence of ferromagnetic bulk materials on the reduction of physical size: multidomain (green), single domain (blue), and superparamagnetism (red). (A) Plot of magnetic coercivity versus particle size. (B) Magnetization hysteresis loops for the different domain size behaviors. H_c and M_r of the single domain (blue) are shown as an example. Adapted with permission from [13]. Copyright © 2018, WILEY-VCH Verlag GmbH & Co. KGaA, Weinheim.

1.2. Nanoparticle synthesis – overview

For the synthesis of nanoparticles, two common strategies can be employed. On the one hand, there is the top-down approach, where an external force is applied to downsize bulk materials to the nanoscale region. On the other hand, the so-called bottom-up approach utilizes precursor molecules or atoms to build up these structures. An overview of various preparation techniques for nanoparticles is depicted in Figure 4, with physical, chemical, and biological methods as superordinate categories. As synthesizing the desired particle sizes and shapes is more challenging for top-down methods and may diminish the magnetic properties of the material due to defects of lattice parameters,^{[5],[15]} the bottom-up approach is preferred for the synthesis of nanoparticles, offering a more defined control over the size and shape of the particles with a wide array of possible methods. Among these, co-precipitation and thermal decomposition are the most common methods to synthesize magnetic nanoparticles and offer high yields and a convenient scale-up as the main advantages.^[16]

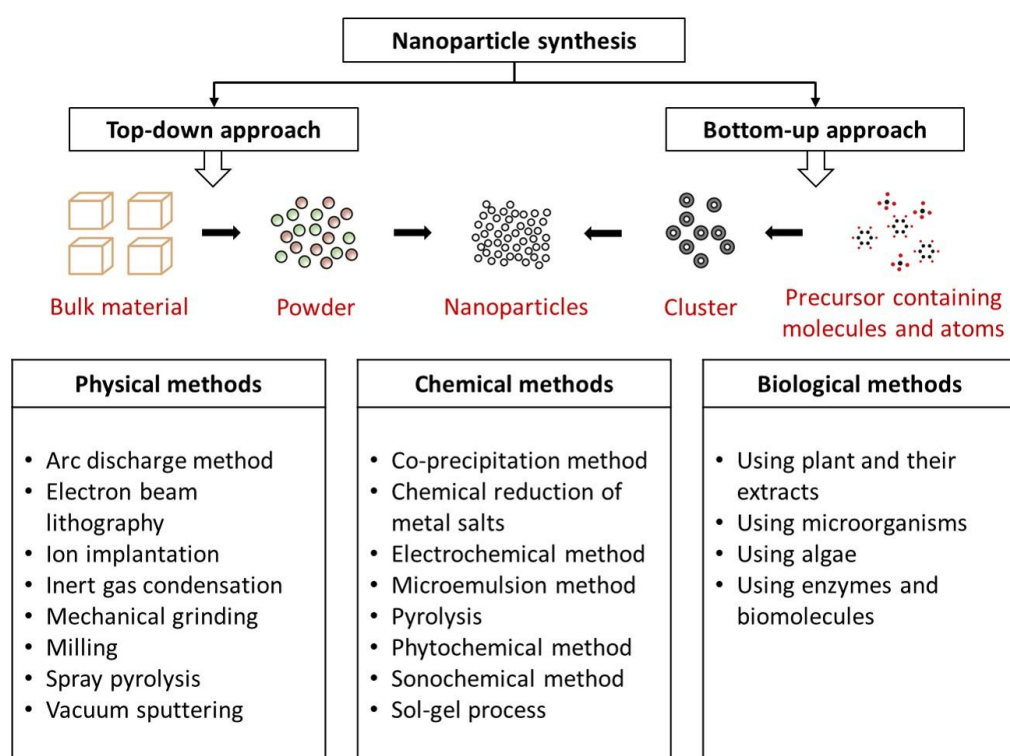


Figure 4. Top-down and bottom-up approaches for the synthesis of nanoparticles. Adapted with permission from [17]. Copyright © 2018, Elsevier.

Co-precipitation is a facile and efficient method for the synthesis of iron nanoparticles (e.g. Fe_3O_4 , Fe_2O_3 , Zn-Mn ferrite, Co-Zn ferrite) from dissolved metal salt solutions with the aid of alkaline solutions like ammonia or sodium hydroxide solutions. Thereby, the size, composition, and morphology are influenced by the type of salt used, the ratio of the different metal ions, and further reaction conditions like the pH value and reaction temperature.^{[18],[19]} In general, co-precipitation is performed in aqueous solutions at ambient conditions with temperatures between 20 to 90 °C and commonly requires short

reaction times.^[16] The high yields, low operation costs, short reaction periods, and comparably easy synthesis make co-precipitation convenient for large-scale reactions. However, this method suffers from agglomeration during the work-up (washing, filtering, or drying),^[18] difficult size and shape control, and wide size distribution.^[19] Thermal decomposition (or pyrolysis) offers the opportunity of smaller nanoparticle sizes than co-precipitation and further meets the requirements of a narrow size distribution and shape control. Organometallic precursors (*e.g.* $\text{Fe}(\text{acac})_3$, $\text{Fe}(\text{CO})_5$, $\text{Co}_2(\text{CO})_8$) are decomposed at high temperatures and pressures for the fabrication of monodisperse nanoparticles in high yields with tunable size.^{[18],[20]} Besides these two, microemulsion, hydrothermal methods, or microwave-assisted nanoparticle syntheses are widely employed methods (Figure 5).

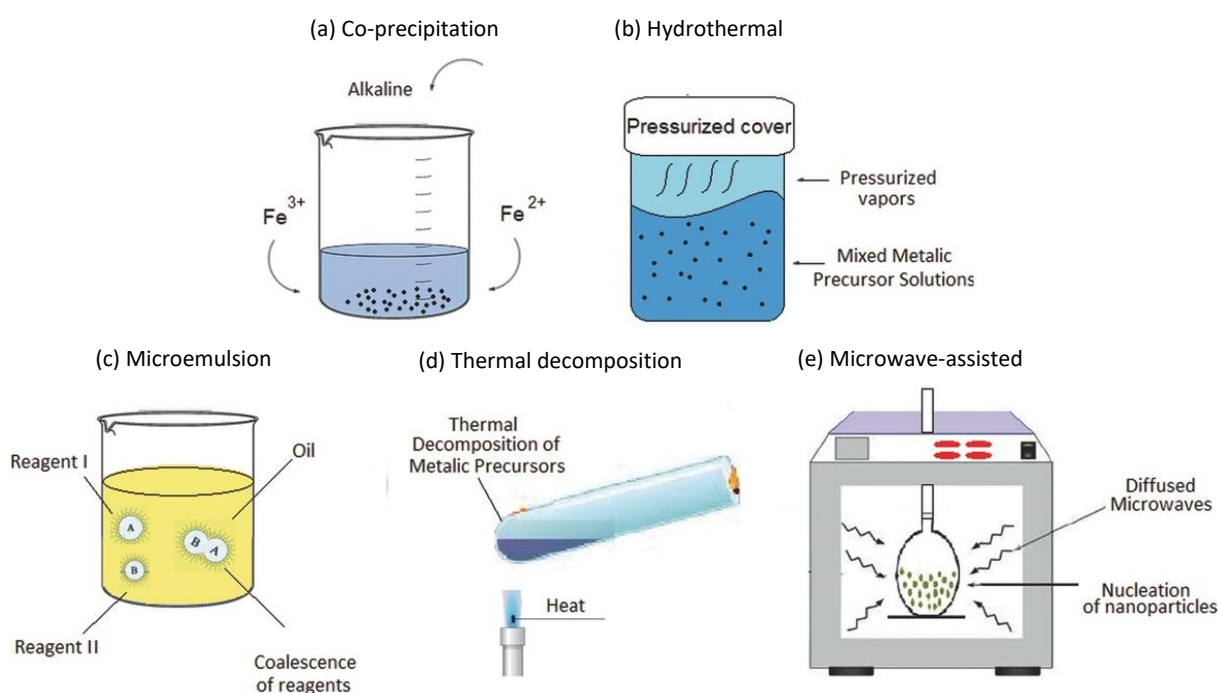


Figure 5. Schemes of selected types of bottom-up approaches. Adapted with permission from [21]. Copyright © 2017, WILEY-VCH Verlag GmbH & Co. KGaA, Weinheim.

Microemulsion, a thermodynamically stable isotropic dispersion of two immiscible liquids fixed by an amphiphilic surfactant, can be divided into two types: water-in-oil and the oil-in-water microemulsions.^[22] The surfactant can have a beneficial effect by limiting the size of the nanoparticles and influencing their shape during the synthesis.^{[21],[23]} However, low yields, the necessity for large amounts of solvent, and a time-consuming and elaborate separation from the surfactant diminish these benefits.^[19] The hydrothermal method involves high temperatures with high pressures, *e.g.* in an autoclave, where the metallic precursor and surfactants are dissolved in an aqueous solution to generate a critical supersaturated solution for nucleation, which subsequently produces size- and shape-controlled uniform nanoparticles. However, this method suffers from long reaction times and energy inefficiency.^{[21],[24]} In recent years, microwave-irradiation also gained attention for the synthesis

of nanoparticles due to uniform heating, which enables more homogeneous nucleation combined with shorter reaction times (compared to conventional heating), high yields, and narrow size distribution.^[25] Bioinspired methods emerged as eco-friendly alternatives for a clean and efficient nanoparticle synthesis utilizing fungi, viruses, bacteria, etc.^[5] Even though the detailed synthesis methods are not well-acknowledged and would require further investigations,^[19] *e.g.* Fe₃O₄ nanoparticles with defined sizes and shapes could be prepared *via* co-precipitation method with a biomineralization peptide (inspired from magnetotactic bacteria) as efficient nucleation promoter and growth modifier.^[26]

1.3. Coatings and surface functionalization of magnetic nanoparticles

Upon decreasing the size of metals to the nanometer scale, the surface-area-to-volume ratio and surface energy are increased, causing a thermodynamically and kinetically unstable or metastable state.^[27] The excess energy may enhance the process of diffusion and aggregation to larger clusters or clumps, resulting in partial or complete damaging^[28] of the nanoparticles and, thus, a loss of their unique properties, like the above-mentioned presence of single domains.^[29] To circumvent this issue and allow a controlled nanoparticle formation and their further application, diverse protocols for the utilization of stabilizing agents, surface-capping agents, and coatings were established.^[30] However, surface protectants and functionalizations diminish the magnetic properties of the nanomaterial and, hence, lower their recovery and application potential.^{[16],[31]} Therefore, the use of 'non-oxidic' metal nanoparticles turned out to be a promising alternative, exceeding the saturation magnetization of oxides (magnetite: $M_{S,bulk} \leq 92 \text{ emu}\cdot\text{g}^{-1}$) decisively (Co: $M_{S,bulk} \leq 163 \text{ emu}\cdot\text{g}^{-1}$, Fe: $M_{S,bulk} \leq 222 \text{ emu}\cdot\text{g}^{-1}$).^[32] To access air-stable magnetic nanoparticles, several coatings were investigated, such as *e.g.* gold,^[33] silica,^[34] polymers,^[16] transition-metal oxides,^[35] and carbon.^[36] While the gold coating is considered to be not cost-efficient,^[37] polymer coatings like *e.g.* polystyrene have a relatively low intrinsic stability of the coating at high temperatures and do not effectively avoid oxygen diffusion and are, thus, not suitable for reactive metal cores.^{[16],[32]} The deposition of silica shells is challenging due to the lack of OH groups on the metal surface. Further, silica shells are prone to restructuring or hydrolysis of the covalent bonds on silica under harsh environments.^{[16],[32],[37],[38]} Carbon-coatings have ascended as a research area due to their higher chemical and thermal stability as well as biocompatibility.^{[16],[29]} Encouraged by the investigations of fullerenes, the first carbon-encapsulated metal and metal carbide nanoparticles were synthesized shortly after in 1995.^{[16],[39]} Up to date, these ongoing studies revealed a variety of carbon-coated nanoparticle syntheses. These include gas-phase^{[36],[40]} methods like arc discharger or vapor deposition, solution-phase^[41] fabrications (*e.g.* hydrothermal methods) as well as flame syntheses, which evolved as a useful route for the production of high-quality materials in reasonable quantities.^{[42],[43]}

1.3.1. Synthesis of carbon-coated cobalt nanoparticles via flame-spray pyrolysis

The controlled synthesis of uniformly carbon-coated metal nanoparticles was significantly expanded by the publication of Stark *et al.*^[37] in 2007, reporting a large-scale synthesis for highly stable, non-agglomerated cobalt nanoparticles coated with 'graphene-like', sp^2 -hybridized carbon layers. In this method, the metal precursor (cobalt(II) 2-ethylhexanoate in mineral spirit) is dispersed by an oxygen jet forming a spray, which is ignited by a premixed pilot flame to form metal oxide clusters (Figure 6). Due to the operation in an oxygen-free environment (glove-box), these oxide clusters are subsequently reduced to zero-valent metals by the reducing flame conditions and aggregate to nanoparticles. By the injection of acetylene into the flame atmosphere, thin carbon layers (≈ 1 nm) are deposited onto the metal nanoparticles (≈ 50 nm) in a self-limiting process. This results in the formation of two to four homogeneously, onion-type arranged graphene layers around the metallic core (Figure 7A).

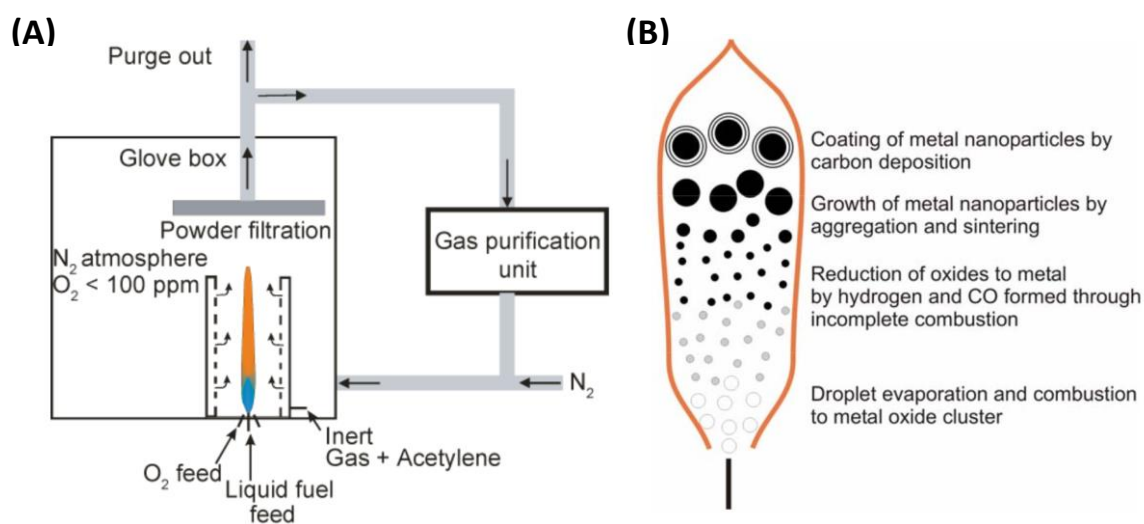


Figure 6. (A) Experimental set-up for fabrication of Co/C nanoparticles *via* reducing flame-spray pyrolysis. (B) Subsequent transformations from precursor to oxide, metal and carbon-coated metal nanoparticles during reducing flame-spray synthesis. Reprinted with permission from [37]. Copyright © 2007, WILEY-VCH Verlag GmbH & Co. KGaA, Weinheim.

With this one-step synthesis up to 30 g carbon-coated cobalt nanoparticles (Co/C) could be synthesized within one hour, proving its scalability.^{[32],[38],[44]} The resulting nanomaterial showed an excellent saturation magnetization of $158 \text{ emu}\cdot\text{g}^{-1}$, close to the value of bulk cobalt (Co: $M_{S,\text{bulk}} \leq 163 \text{ emu}\cdot\text{g}^{-1}$), which allows the rapid separation of the nanoparticles from a suspension with, *e.g.*, a commercial neodymium magnet (see Figure 7B).^{[37],[43]} Moreover, the carbon-coating gave rise to air-stable metallic nanoparticles with remarkable stability under acidic, basic, and thermal (no metal oxidation up to 190°C) conditions.^[37] In 2009, the synthesis was further expanded by the successful fabrication of carbon-coated iron nanoparticles (Fe/C), again performing the flame-spray pyrolysis under reducing atmosphere with adding acetylene. Thus, air-stable non-oxidic iron core-shell nanomagnets (≈ 30 nm) were synthesized with a high saturation magnetization up to $140 \text{ emu}\cdot\text{g}^{-1}$, good thermal stability (up to 200°C) and exceptional resistance against acidic dissolution (1 week in 24% HCl).^[32]

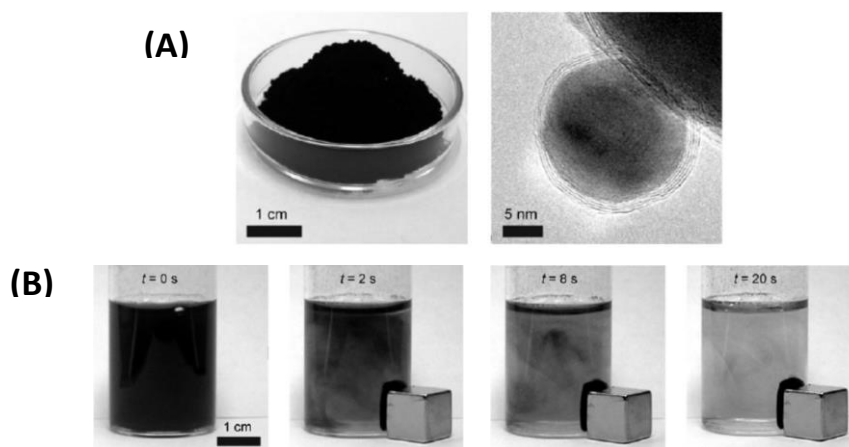
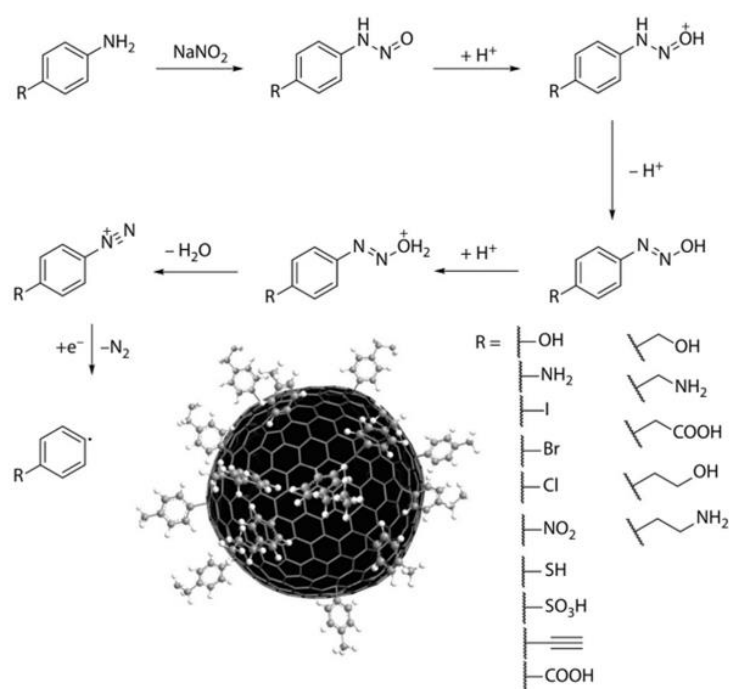


Figure 7. (A) Left: Image of about 5 g of the air-stable, carbon-coated Co NPs. Right: Transmission electron microscopic image of the powder shows two to four homogeneous graphene layers coating the metallic cobalt core. (B) Separation of cobalt nanoparticles from a suspension ($1 \text{ g}\cdot\text{L}^{-1}$) in water by a commercial neodymium magnet ($B = 1.4 \text{ T}$). Photographs were taken at indicated times ($t = 0\text{s}, 2\text{s}, 8\text{s}, 20\text{s}$) after placement of the magnet. Adapted with permission from [37]. Copyright © 2007, WILEY-VCH Verlag GmbH & Co. KGaA, Weinheim.

1.3.2. Surface functionalization of carbon-coated nanomagnets

The so prepared carbon-coated nanoparticles combine the benefits of the magnetic properties of the core with the functionalization potential of chemically related graphene layers or multiwalled carbon nanotubes. In order to implement functional groups to the carbon-coating of the nanomagnets, diazonium chemistry proved its efficiency.^{[32],[37],[43]} Scheme 1 shows an overview of possible surface functionalization derived by this procedure. The reaction quickly proceeds at ambient temperature with the aid of an ultrasonic bath.^[37] Thereupon, the key step is an electron transfer from the graphene layer to the *in situ* formed diazonium salt, causing an evolution of nitrogen to generate the phenyl radical. The radical readily reacts with the particle surface to form covalent C-C bonds.^{[43],[45]} The degree of functionalization revealed a relatively high surface density with circa 6 molecules per nm^2 , corresponding to a functionalization of circa every 12th surface atom (calculated by quantitative microanalysis).^[43] Moreover, the thermal stability even increased with the surface functionalization, making them attractive for further derivatizations and applications.^[37]

The introduction of halogen-, hydroxyl-, carboxyl-, nitro-, and amine groups *via* diazonium chemistry (Scheme 1) provides a versatile anchoring point for the covalent attachment of functional molecules like ligands, catalysts, or scavengers onto the carbon-coated metal nanoparticles. Besides the direct linking of catalysts or reagents onto the pre-functionalized nanobeads, *e.g. via* Cu(I)-catalyzed ‘click’ reactions, resulting in comparably low loadings per gram of material ($\approx 0.1\text{-}0.2 \text{ mmol}\cdot\text{g}^{-1}$), the introduction of a shell of dendrimers or polymers considerably increases the loading of the functional groups ($\approx 3 \text{ mmol}\cdot\text{g}^{-1}$). While dendrimers enable a higher degree of functional end groups compared to linear polymers, the synthesis is usually more challenging.^[38]

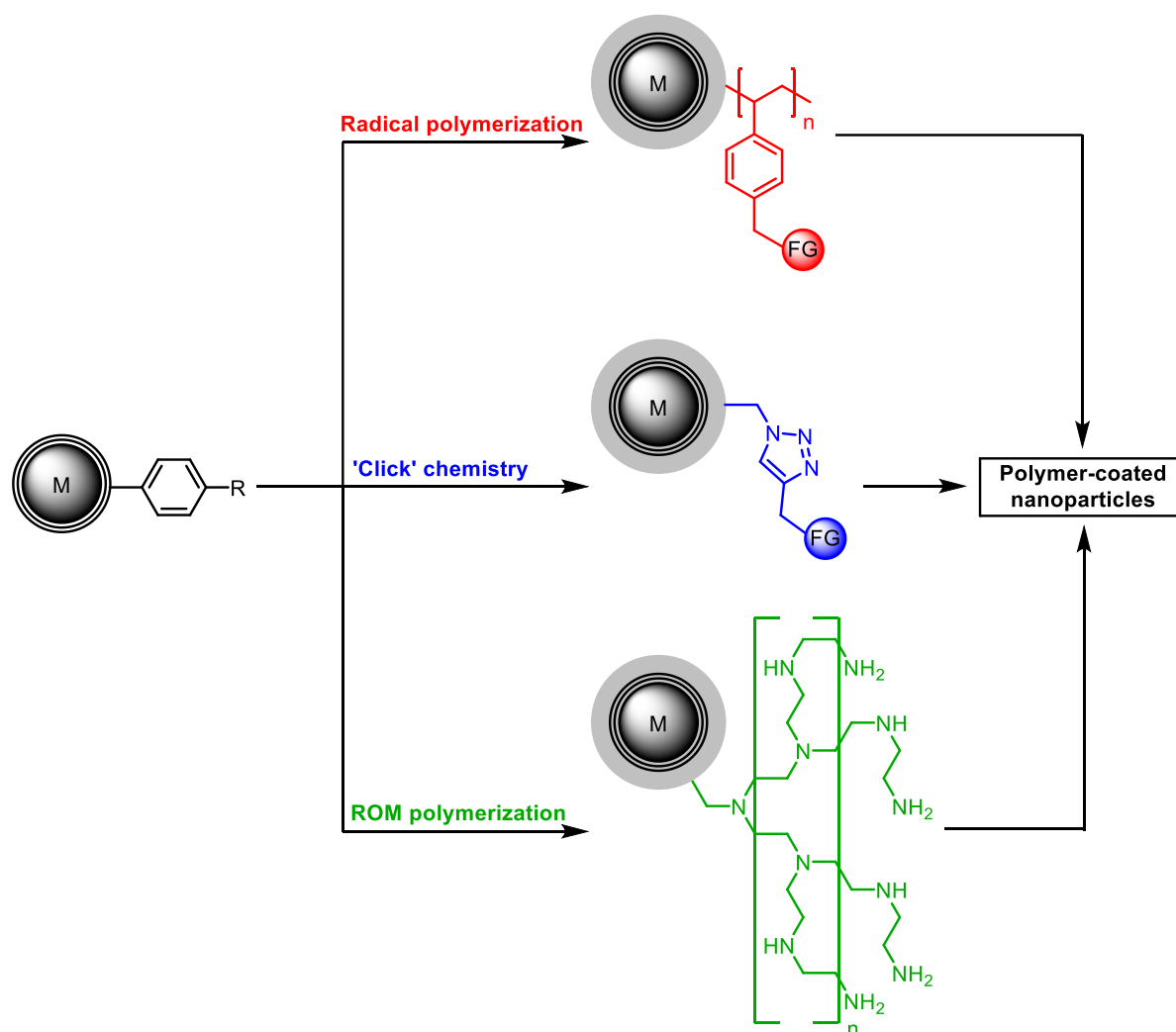


Scheme 1. Nanoparticle functionalization *via* diazonium chemistry. The diazo intermediate decomposes to an aryl radical and reacts with the carbon surface. The obtained surface density is relatively high, on average every 12th surface carbon atom functionalized). Reprinted with permission of The Licensor through PLSclear from [43]. Copyright © 2018, Taylor & Francis Group, LLC.

In Scheme 2, three common strategies for the preparation of polymer-coated metal nanoparticles are illustrated. One method to generate covalently bound polymers onto carbon-coated metal nanoparticles *via* radical polymerization was reported by Stark *et al.*^[46] in 2011. Poly(benzyl chloride)styrene-coated Co/C nanoparticles were synthesized with chloride loadings up to 3 mmol per gram by a surface-initiated grafting polymerization of 4-(chloromethyl)styrene onto vinyl-tagged Co/C nanobeads in presence of AIBN (2,2'-azobis(2-methylpropionitrile)) as radical starter. The stability of the scaffold was demonstrated by their functionalization with a trialkylsilane reagent. The resulting material served as recyclable 'magnetic protecting group' for primary and secondary alcohols. The high functionalization degree of the polymer enabled the application of reasonable amounts of the 'magnetic protecting group' and improved the long-term stability of the material, even at the harsh acidic conditions applied in the recycling process. Building on these results, a variety of polystyrene-coated metal- and organocatalysts, as well as scavengers, were prepared, *e.g.* immobilized variations of Pd-NHC complexes,^[47] Jørgenson-Hayashi organocatalysts,^[48] borohydride exchange and Wang aldehyde resins,^[49] zinc(II)-cyclen complexes,^[50] or Noyori-type ruthenium complexes.^[51]

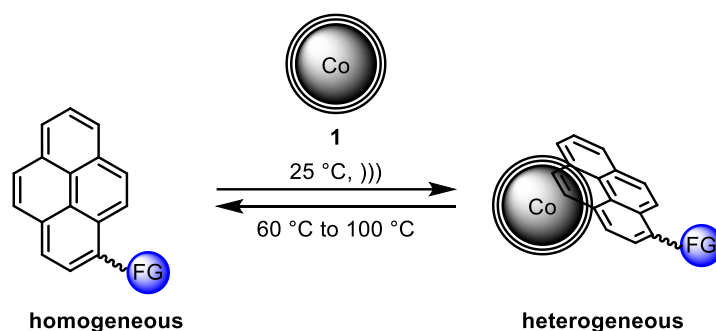
Another versatile strategy for the implementation of polymer shells onto the carbon-coated nanobeads is the copper(I)-catalyzed alkyne-azide cycloaddition (CuAAC, 'click' reaction). Besides the afore-mentioned direct attachment of catalytic moieties to the azide-nanoparticles, resulting in rather low loadings, pre-synthesized polymers, modified with an alkyne-moiety, can be linked to the azide-

nanoparticles. With this method, *e.g.* poly(ethylene glycol) (PEG)-coated Co/C nanoparticles with a loading of 0.9 mmol ether groups per gram have been successfully synthesized.^[52] The 'click' reaction further enables the possibility to synthesize norbornene-modified nanobeads *via* the linking of alkyne-functionalized norbornene derivatives. Upon activation of these with a Grubbs second-generation catalyst, surface-initiated ring-opening metathesis polymerization (ROMP) gives rise to high loadings (up to 2.6 mmol·g⁻¹) *e.g.* of a triphenylphosphine-functionalized ROMP-derived magnetic polymer for Suzuki-Miyaura reactions,^[53] and a magnetically recyclable acylation reagent derived from acylated *N*-hydroxysuccinimide ROMPgels.^[54] On the other hand, direct ROMP was carried out to obtain outstanding loadings up to 10 mmol per gram of nanomaterial.^[52] Therefore, benzylamine-functionalized Co/C nanobeads were polymerized with aziridine under acid catalysis. These covalently functionalized poly(ethyleneimine) Co/C nanobeads (PEI@Co/C) exhibited extraordinary dispersion stability in water up to several days without agglomeration or sedimentation.^{[52],[55]}



Scheme 2. General scheme for the preparation of polymer-coated magnetic nanoparticles (M = Co, Fe) *via* free radical polymerization, 'click chemistry', and ROMP starting with aryl-tagged nanobeads. The graphene-layers are illustrated by the black rings around the metal core, whereas the gray shell represents the functionalization of the first step. FG = functional group or functional molecule.

Complementary to the covalent surface modification, non-covalent functionalization methods were developed with impressive advances. In general, these can be divided into two main categories of organic and inorganic approaches. Whereas the former one utilizes π - π stacking interactions to attach the desired organic compounds *via* their aromatic building blocks to the graphene layers, the latter method directly deposits *e.g.* catalytically active metal nanoparticles onto the surface of the nanomagnets. In Scheme 3, the reversible immobilization of pyrene-tagged palladium complexes to the graphene layers of the magnetic Co/C nanobeads **1** is shown. This ‘boomerang’-type magnetic catalyst was first reported by Reiser *et al.*^[56] in 2010 for the non-covalent grafting of a palladium *N*-heterocyclic carbene (Pd-NHC), pyrene-tagged complex. The catch-release methodology was performed in water, where ultrasonication at ambient temperatures resulted in grafting to the nanobeads (heterogeneous) and high temperatures released the Pd-NHC to obtain the homogeneous complex. The feasibility of the catalyst was demonstrated in the efficient hydroxycarbonylation of aryl halides in water under atmospheric pressure of carbon monoxide for at least 16 cycles. The dissociation of the Pd-NHC complex at elevated temperatures resulted in high activities. Upon cooling to room temperature, the re-absorbed catalyst allowed facile and quantitative recycling from the reaction solution by magnetic decantation.

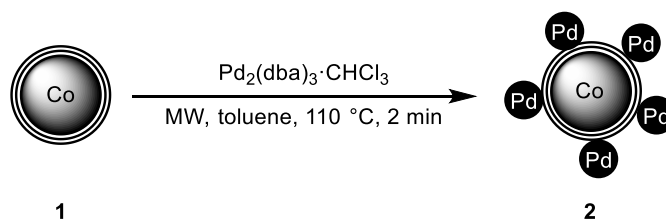


Scheme 3. ‘Boomerang’-type catalyst for the thermally triggered catch-release of pyrene-tagged palladium catalysts on Co/C nanobeads **1** *via* π - π stacking interactions. Elevated temperatures enable the release of the catalyst for a homogeneous catalysis, whereby the heterogeneous ‘captured’ catalyst facilitates the recycling from the reaction solution. FG = Pd-NHC, or dendritic Pd phosphine complexes;))) = ultrasound.

The same strategy was later utilized for the reversible immobilization of dendritic palladium phosphine catalysts. Due to the radial structure of the dendrimers, higher catalyst loadings per gram of nanomaterial have been achieved, making the applications more convenient from an economic and environmental perspective. In a joint publication, Caminade, Majoral, Ouali *et al.*^[57] reported a magnetic dendritic palladium phosphine catalyst with up to five times higher loadings ($0.5 \text{ mmol}\cdot\text{g}^{-1}$) than compared to the above-mentioned approach.^[56] This catalyst was applied for the iterative synthesis of Felbinac, a non-steroidal anti-inflammatory drug (NSAID) for the treatment of arthritis and muscle inflammation, *via* Suzuki-Miyaura cross-coupling. The reaction was performed in THF/H₂O at 60 °C to release the homogeneous palladium complex. Although the palladium contamination of the

crude product was relatively high for the first runs (1st run: 274 ppm Pd, 2nd run: 110 ppm, corresponding to 20% Pd loss within two cycles), the yield was not diminished for at least 12 cycles. After extraction with dichloromethane, the metal contamination of the product was found to be surprisingly low with less than 5 ppm Pd and even < 0.005 ppm Co, meeting the pharmaceutical specification limits without the need of a tedious chromatographic purification.^[57]

Stark *et al.*^[58] utilized the probably easiest way to synthesize polymer-coated nanoparticles by stirring the carbon-coated iron nanoparticles in a solution of PEI to adsorb the polymer irreversible on the surface. The stability of the non-covalently attached polymer-coating was demonstrated by several washing steps in an acidic solution, proving no polymer loss as determined by elemental analysis. Further functionalization of the amino groups resulted in magnetically EDTA-like chelators for the efficient removal of heavy metal ions (copper, cadmium, lead) from contaminated water. The same method was also applied for the reversible adsorption of organic contaminants from water by the linking of β -cyclodextrin to the PEI coated nanoparticles.^[59] However, this coating strategy achieved considerably lower polymer loadings compared to the covalent approach.



Scheme 4. Non-covalent deposition of Pd(0) nanoparticles on the graphene layers of Co/C **1** via microwave irradiation.

A straightforward way for the immobilization of inorganic catalysts, here palladium nanoparticles (Pd NPs), onto the magnetic graphene-layers was accomplished by microwave irradiation of a Pd(0) source in presence of the Co/C nanobeads **1** by Reiser *et al.*^[60] The resulting Pd@Co/C nanoparticles **2** revealed a distinct trend to higher activities in the hydrogenation of alkenes when lower Pd loadings on the nanobeads were used. The nanocatalyst **2** with 0.2 wt% Pd exhibited an excellent catalytic activity with turnover frequencies up to 11095 h⁻¹. Additionally, the recyclability of the catalyst **2** exceeded conventional palladium on charcoal (Pd/C). Its efficiency was demonstrated for up to six hydrogenation cycles with a low Pd leaching (≤ 6 ppm per cycle). Characterization of the recycled catalyst indicated an effective stabilization of the Pd NPs against aggregation (determined by particle size) as well as agglomeration (determined by Pd distribution), presumably due to the known π -interactions of carbon materials *via* sp² carbon atoms.^[60]

1.4. Applications of carbon-coated magnetic nanoparticles

1.4.1. Catalysis

Nanometer-sized catalysts hold the promise to combine the advantages of heterogeneous with homogeneous catalysis, being expressed with the terms quasi-homogeneous or semi-heterogeneous catalysts (Figure 8). In the last decades, a great effort has been made investigating various immobilized versions of homogeneous catalysts targeting benign and easy recycling.^[61] Thereby, a wide spectrum of diverse soluble and insoluble supports, reaching from polymers^[62] and dendrimers^[63] to nanoparticles,^{[38],[64]} were explored. In terms of green and sustainable chemistry, the design of new catalysts that meet these demands is, amongst others, one of the key research areas in the academic field. A “green catalyst”, by definition, provides high activity and selectivity, recovery and recycling, and is cost-efficient. Most of these requirements can be addressed by the usage of nanoparticles, offering a high activity due to the high surface-to-volume-ratio and an enhanced dispersion capacity in the reaction solution.^[65]

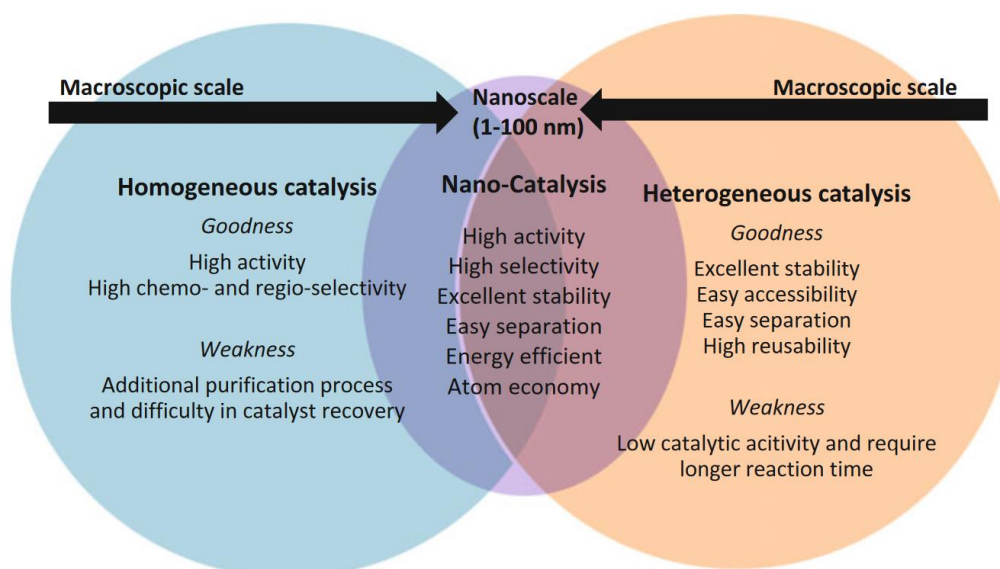


Figure 8. Characteristics of bulk (homogeneous and heterogeneous) catalysts with nano-catalysts as semi-heterogeneous/quasi-homogeneous catalysts. Reprinted with permission from [66]. Copyright © 2017, Springer International Publishing Switzerland.

Consequently, the development of novel nanocatalysts has received considerable attention during recent years. Over the years, a variety of magnetic carbon-coated metal nanocatalysts were investigated, reaching from immobilized organocatalysts^{[48],[67]} or metal complexes^{[47],[56],[57],[68]} to deposited^[60] and incorporated^{[69],[70]} metal nanoparticles onto the the magnetic support. These catalysts were, *e.g.*, employed in hydrogenation, oxidation, and cross-coupling reactions with a straightforward recycling strategy *via* magnetic decantation, made possible by the high saturation magnetization of the metal core.

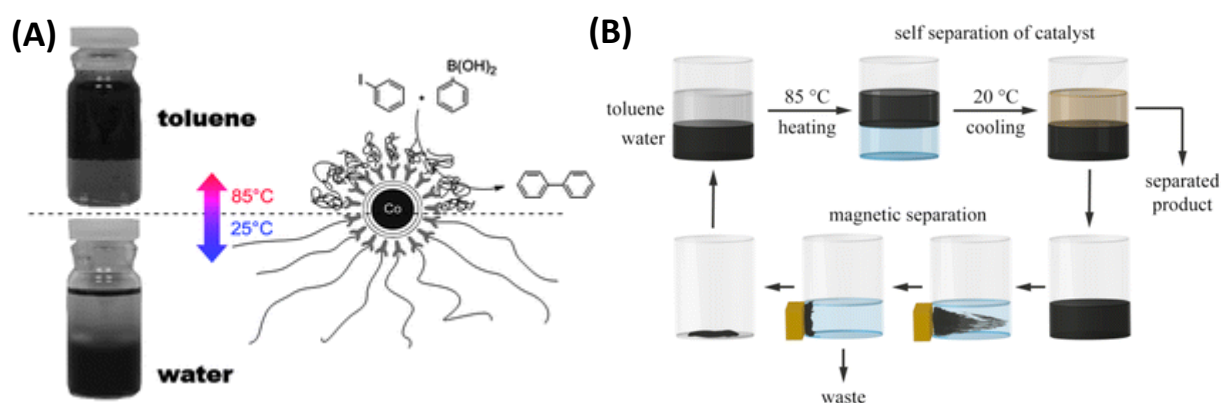


Figure 9. (A) Distribution of the magnethothermally responsive magnetic catalyst in a biphasic water/toluene-system. The magnetic NPs are reversibly shifted from the aqueous into the organic layer by heating, caused by collapsed polymer branches (upper part) and unfolded hydrophilic branches (lower part). Reprinted with permission from [71]. Copyright © 2011, The Royal Society of Chemistry. (B) Representation of the concept of the self-separating magnetic catalyst. Reprinted with permission from [38]. Copyright © 2014, American Chemical Society.

To further facilitate the reaction work-up, a thermally triggered ‘self-separating’ phase-switching palladium catalyst was developed for the Suzuki-Miyaura cross-coupling in a biphasic water/toluene system.^[71] Synthesizing carbon-coated cobalt nanoparticles with amphiphilic *N*-isopropylacrylamide polymer branches enabled the controlled shift from the organic to the aqueous phase and back. Upon heating the reaction mixture above the lower critical solution temperature (LCST > 36 °C), the thermoresponsive part of the polymer collapses, shifting the nanocatalyst to the organic phase where the cross-coupling reaction takes place. By cooling the reaction solution to room temperature, the hydrophilic polymer branches unfold again to form stable dispersions in water. Thus, the product can be separated from the organic phase without the need for further purification, whereas the magnetic catalyst can be recovered from the wastewater by magnetic decantation and recycled (Figure 9).^[71]

Further research resulted in immobilized versions of asymmetric organo- and metal catalysts with high enantioselectivities, *e.g.* a magnetically recyclable Noyori-type ruthenium catalyst for the asymmetric transfer hydrogenation of aromatic ketones in water.^[51] The high magnetization of the carbon-coated nanoparticles offers an alternative to commercial fixed-bed reactors *via* a novel designed continuous-flow setup. The feasibility of this approach was demonstrated with carbon-coated cobalt nanoparticles tagged with aza-bis(oxazoline)-copper(II) complexes for the kinetic resolution of 1,2-diphenylethane-1,2-diol through Cu(II)-catalyzed asymmetric monobenzylation (Figure 10). Three successive batches confirmed almost no leaching of the magnetic catalyst, resulting in excellent enantioselectivities of 98-99% *ee* and high yields (39-47% yield with a potential maximum of 50% yield) under the continuous flow conditions.^[72]

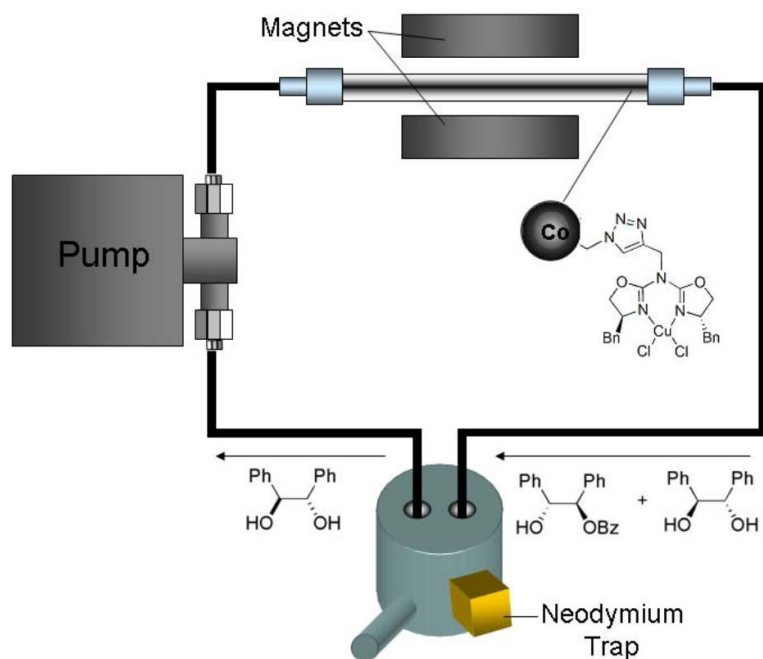


Figure 10. Cu(II)-aza-bis(oxazoline) complexes immobilized on magnetic Co/C nanoparticles for continuous-flow kinetic resolution of racemic 1,2-diphenylethane-1,2-diol *via* asymmetric monobenzylation. Reprinted with permission from [72]. Copyright © 2010, American Chemical Society.

1.4.2. Scavenging

Industrialization, as well as the growth of the world population, entailed environmental grand challenges of worldwide concern for industrialized and developing countries.^{[73],[74]} The spread of a variety of pollutants in surface and groundwater has a decisive influence on the water quality, thus purification methods to remove harmful contaminants (*e.g.* heavy metals, pesticides, organic pollutants) persisting in wastewater gained reasonable attention.^[73] With the rise of nanotechnology, magnetic nanoparticles emerged as potential pioneering scavengers, taking advantage of their high surface-area-to-volume-ratio and facile recycling properties.^{[74],[75]} Indeed, the use of magnetic nanoparticles for environmental treatments benefits from large removal capacities, fast kinetics, high reactivities, and magnetically recycling protocols, which lead the way to more convenient methods and might provide an economical, cost-effective solution.^{[75],[76]} However, when considering the applicability of nanoparticles in environmental technologies, care should be taken to a holistic approach, ensuring no adverse side effects to the human health with a minimal environmental footprint.^{[76],[77]}

As an example, mercury poisoning is a well-known effect caused by heavy metal contamination with extensive and drastic consequences, as shown by a notorious case in 1956 in Japan, leading to over 2200 victims of mercury poisoning throughout the twentieth century.^[74] As a facile and potent way to decontaminate mercury-contaminated water, Reiser *et al.*^[55] developed a magnetically recyclable scavenger for the selective and reversible extraction of mercury(II) ions with poly(ethyleneimine)

covalently functionalized on carbon-coated cobalt nanobeads (PEI@Co/C). Combining the high saturation magnetization of the core with a high amino-group loading (10 mmol per gram) gave rise to a highly dispersible nanoscavenger with excellent adsorption capacities (up to 550 mg Hg²⁺ per gram of PEI@Co/C). Simultaneously, they offered a facile recycling strategy for at least six cycles without loss in extraction capacity *via* magnetic separation. Further relevance was demonstrated in a large-scale experiment, decontaminating 20 L of mercury-spiked drinking water (30 µg·L⁻¹ Hg²⁺) with solely 60 mg of the nanomagnets.^[55] A different concept was published in 2011, where Stark *et al.*^[78] reported a moving bed reactor system for the concentration of diluted streams, applying modified polymer-coated Fe/C for the adsorption and desorption of As(V) as model ions. Poly(benzylchloride)styrene@Fe/C were functionalized with *N*-methyl-*D*-glucamine (NMDG) for the application in a cyclic, two-step process with a pH-dependent adsorption equilibrium. In the first, larger tank, the diluted arsenate ions are adsorbed by the nanoparticles, which in return are subsequently desorbed in the second, smaller tank by an appropriate desorption solution (pH above 12). This gives rise to a purified output stream, as well as a concentrated stream with an enrichment of the toxic metal ions up to 430 times (Figure 11). This approach demonstrated an energy-efficient method to concentrate diluted contaminated solutions with recyclability of the used nanoscavengers over five consecutive cycles on a small scale (up to 1 L).^[78]

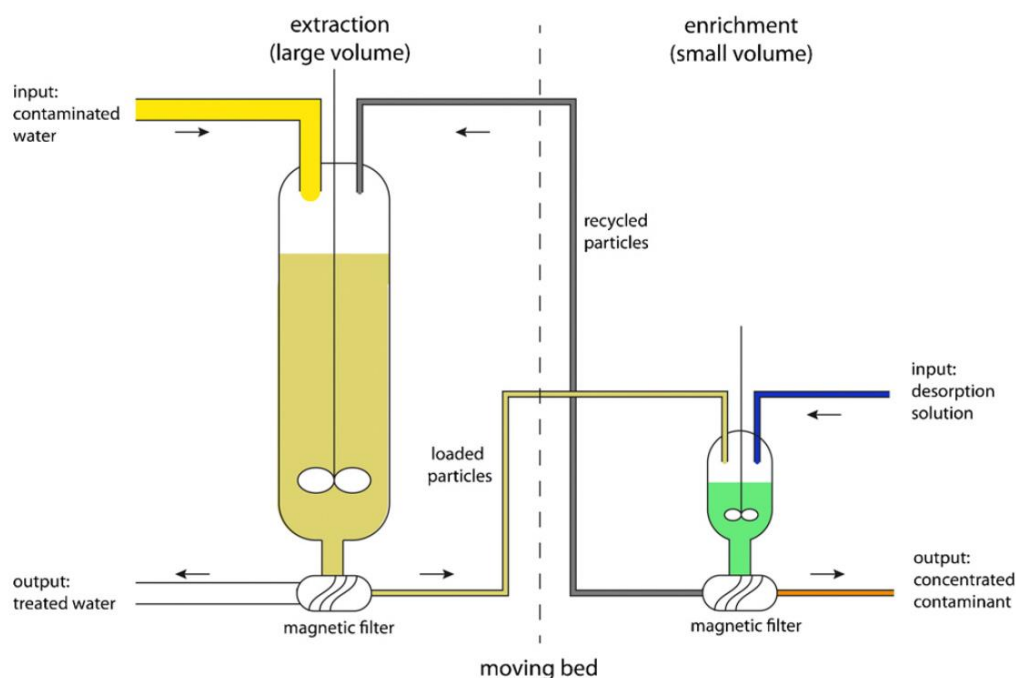
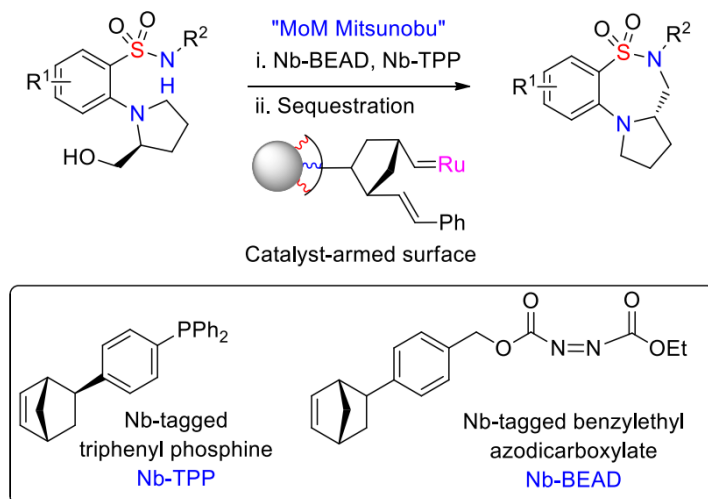


Figure 11. Schematic description of the moving bed reactor system: on the left side, the low concentrated contaminated solution is decontaminated from the toxic metal ions by the magnetic nanoparticles in the first reactor. In the second part (right), the loaded magnetic nanoparticles are washed (enrichment) and release the solute into a small volume (up to 430 times more concentrated). Reprinted with permission from [78]. Copyright © 2011, Elsevier.

Contrary to the extraction of heavy metal ions from aqueous solution, Stark *et al.*^[59] further published an immobilized version of β -cyclodextrin on surface-modified Co/C nanobeads. This material was used as pre-treatment for the reversible extraction of organic contaminants from water, considering low concentration as it may occur in process water in various industries (*e.g.* textile coloring, mining industry, fine chemistry, food industry, or pharmaceutical industry), before biological sludge treatment. The presence of organic contaminants can decisively influence microbiota or bacteria and thus decrease the water purification efficiency. In this approach, magnetically recyclable cyclodextrins were employed for the adsorption of eco-toxicologically problematic contaminants (*e.g.* dyes, phenolphthalein) with a subsequent substitution through microbiologically well-accepted benzyl alcohols, by making use of the host/guest interactions in the cavity. After the enrichment of the organic dye, the adsorbed benzyl alcohol was released by washing the nanoparticles in acetone. The cyclodextrin pocket offered a reversible, controllable adsorption/desorption process, whereas the magnetic support allowed an efficient recovery for the repetitive recycling of the nanobeads for over 16 cycles.^[59] Likewise, the covalent immobilization of zinc(II)-cyclen on polystyrene-coated Fe/C nanobeads proved a quantitative extraction and release of riboflavin (vitamin B₂) from a vitamin tablet within six cycles.^[50]

1.4.3. Further applications

Besides the utilization of magnetic nanoparticles for the purification of wastewaters from toxic heavy metals and organic pollutants, a different research-aspect focused on facilitating the separation of the desired product from organic reactions. In a joint publication of Reiser and Hanson *et al.*,^{[79],[80]} norbornenyl-tagged triphenylphosphine (Nb-TPP) and norbornenyl-tagged azodicarboxylate, here benzylethyl azodicarboxylate (Nb-BEAD), were employed for intermolecular^[79] as well as intramolecular^[80] monomer-on-monomer (MoM) Mitsunobu reaction. To allow facile isolation of the desired product from unwanted Mitsunobu by-products, excess and spent reagents were separated *via* a ring-opening metathesis polymerization (ROMP). Therefore, the crude reaction mixture was stirred with a pre-synthesized dispersion of norbornenyl-tagged Co/C nanobeads with a Grubbs catalyst to initiate the ROMP by the catalyst-armed surfaces (Scheme 5). After collecting the magnetic nanobeads, the crude products were obtained in reasonable purities (> 95%).^[80]



Scheme 5. Synthesis of benzofused thiadiazepine-dioxides *via* an intramolecular monomer-on-monomer (MoM) Mitsunobu cyclization. Reprinted with permission from [80]. Copyright © 2011, The Royal Society of Chemistry.

Another application was reported by Reiser *et al.*, combining three different magnetic reagents and scavengers to enable the multistep synthesis of trisubstituted (thio)ureas with magnetic decantation as the sole purification step. The reductive amination of aldehydes to secondary amines was carried out by a magnetic borohydride exchange resin to reduce the formed imines, followed by a Wang aldehyde resin to scavenge the residual primary amines. By the aid of benzylamine-tagged nanobeads, the excess iso(thio)cyanate reagent, used for the conversion of the secondary amines to trisubstituted (thio)ureas, was efficiently removed in the last step. Applying these work-up procedures, high product purities were obtained combined with a good regeneration and recyclability of the magnetic materials.^[49]

Attracted by the high magnetization of the air-stable carbon-coated nanobeads combined with their high thermal and chemical stability, these nanomaterials were also investigated regarding their potential in biomedical and clinical applications,^{[14],[43],[81]} including *e.g.* drug delivery,^{[81],[82]} blood purification,^[83] carrier for enzymes,^[84] or magnetic resonance imaging.^[85]

While these examples are only a small excerpt of the substantial advances that have been accomplished in the last years, their versatility as well as potential advantages for diverse applications is clearly demonstrated. In the following chapters, polymer-coated Co/C nanobeads will be highlighted for their capability as recyclable catalysts for organic transformations and their feasibility as reversible scavengers for heavy metal ions.

B. Main part

1. Magnetic microporous organic polymers encapsulated with palladium nanoparticles as recyclable catalysts for hydrogenation reactions*

Microporous organic polymers (MOPs) immobilized on magnetic Co/C nanobeads were employed for the incorporation of palladium nanoparticles (NPs), resulting in highly active catalysts for the hydrogenation of alkenes, alkynes, and nitro arenes with high turnover frequencies (TOFs) up to 3000 h^{-1} . The magnetic core of the nanobeads ensures an easy and fast recyclability for at least six consecutive runs by applying an external magnet to recapture the catalyst. The reported catalytic system uses cross-linked arenes, *e.g.* toluene, as polymeric network and is readily prepared *via* a cost-efficient and versatile synthesis route based on commercially available starting materials. These novel catalysts combine the advantages of heterogeneous magnetic support with MOPs that prevent NPs from agglomeration or deactivation. In addition, the advantages of palladium NPs as exceedingly active catalysts due to their high surface-area-to-volume ratio are exploited. Furthermore, the polymeric structure can easily be varied by the change of the aromatic monomer. Introducing hydroxyl groups *via* 2,2'-biphenol as monomer into the MOP, metal leaching from the catalyst can be reduced to a minimum.[†]

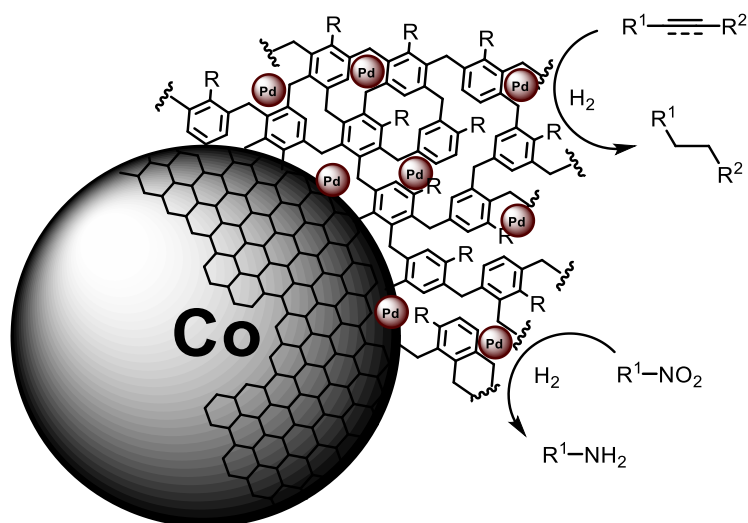


Figure 12. Microporous organic polymers immobilized on Co/C and encapsulated with Pd NPs for hydrogenation reactions.

* Reprinted (adapted) with permission from: L. Stadler, M. Homafar, A. Hartl, S. Najafshirtari, M. Colombo, R. Zboril, P. Martin, M. B. Gawande, J. Zhi, O. Reiser, *ACS Sustainable Chem. Eng.* **2019**, *7*, 2388-2399. Copyright © 2019, American Chemical Society.

[†] TEM was carried out by J. Zweck. TEM and BET were performed by S. Najafshirtari and M. Colombo. XPS spectra, HAADF images and EDS chemical mapping were performed, visualized and evaluated by R. Zboril, P. Martin and M. B. Gawande. TGA was measured by R. Müller. Polymers **4b-4e**, **5b-5e** and their catalytic application was carried out by M. Homafar. A. Hartl synthesized **5a-α** to **5a-γ** in Table 2 (entry 1-3). Evaluation and graphical presentation of BET measurements were carried out by L. Stadler in consultation with S. Najafshirtari. All other experiments synthesizing and utilizing **4a**, **5a** were performed by L. Stadler.

1.1. Introduction

Catalytic hydrogenation is one of the most important and widely distributed methods in the chemical industry. This transformation is a highly atom efficient process and one of the cleanest possible ways to reduce an organic compound if molecular hydrogen and an entirely recyclable catalyst are used.^[86] Over the past decade, catalyst recycling has generated intense interest, not only from an economical but also an ecological point of view due to the rise of green and sustainable chemistry.^[87] In this context, magnetic nanoparticles have emerged as excellent catalysts and supports due to their simple and fast separation from the reaction mixture by magnetic decantation.^{[38],[88]}

Porous materials gained wide interest due to their broad spectrum of possible applications, *e.g.* in separation,^{[89],[90]} heterogeneous catalysis,^[91] and gas storage.^{[92],[93]} During the last years, this led to a large variety of novel porous materials including metal-organic frameworks (MOFs),^[94] covalent organic frameworks (COFs),^[95] organic cages,^[96] and microporous organic polymers (MOPs)^{[97],[98]} besides the already well-known porous materials such as zeolites or activated carbon. MOPs possess attractive attributes, such as a high surface area, low skeletal density, and high chemical stability. One of the earliest types of MOPs are “Davankov resins”, representing styrene-type polymers that are hyper-cross-linked using a Friedel-Crafts reaction,^[99] with the drawback of hydrogen halide as by-product, which is difficult to remove.^{[100],[101]} In 2011, Tan and co-workers^[98] proposed a new strategy to synthesize microporous polymers, involving “knitting” rigid aromatic building blocks by an external cross-linker. The polymer was formed by a simple one-step Friedel-Crafts reaction, applying formaldehyde dimethyl acetal (FDA) as a low-cost and commercially available external cross-linker with various aromatic monomers, *e.g.* benzene, to synthesize cost-efficient microporous polymers with high surface areas (Figure 13). These investigations established a basis for MOPs encapsulated with metal nanoparticles as heterogeneous catalysts.^{[102],[103]}

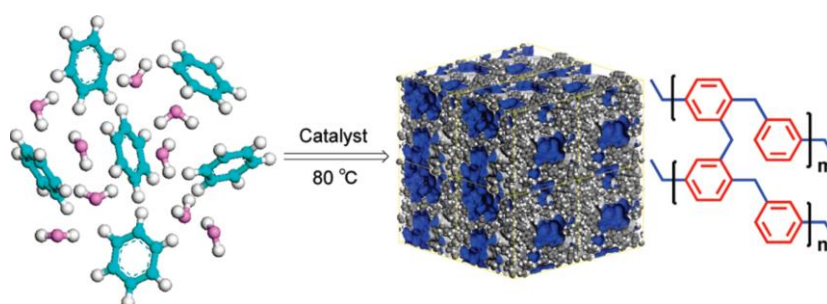


Figure 13. “Knitting” aromatic monomers with FDA as external cross-linker resulting in a microporous network. Reprinted with permission from [98]. Copyright © 2011, American Chemical Society.

In this work, microporous organic polymers encapsulated with palladium NPs were synthesized with commercially available Co/C nanobeads as magnetic support aiming at the development of a highly active and easily recyclable hydrogenation catalyst. The microporous material cages the palladium NPs

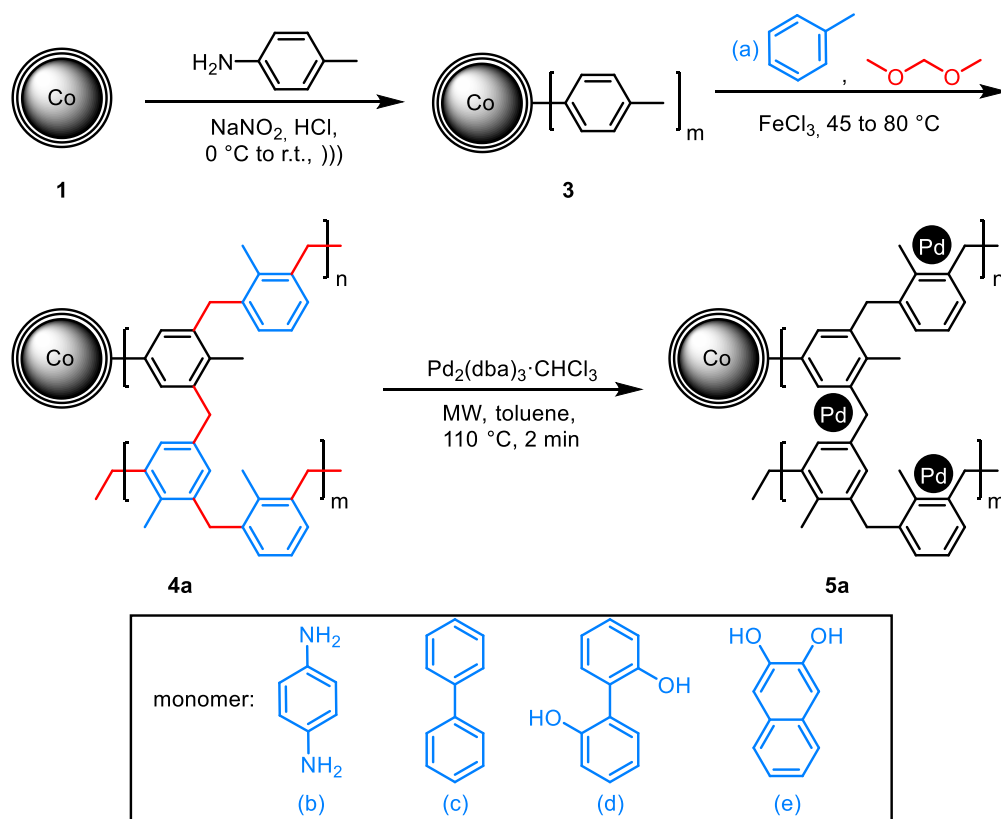
to control their size, prevent agglomeration, and allows access to the surface of the latter due to its native porosity.^[104] Combining these advantages of MOPs with the high magnetization value of the cobalt nanobeads (Co/C) enables a rapid and facile way to recycle the catalyst with the aid of an external magnet. Key features of this study include the variation of the external cross-linker content, leading to diverse surface areas and pore diameters of the supporting porous polymer, and the investigation on the influence of these supports regarding the catalytic activity of the entire hybrid system. This includes the effect of various palladium loadings on their dispersion and catalytic efficiency. Furthermore, the best catalytic system was further analyzed by focusing on the metal leaching, the recyclability, and the substrate scope in catalytic hydrogenation reactions.

1.2. Results and Discussion[‡]

Carbon-coated ferromagnetic cobalt nanobeads (Co/C) were used as magnetic support due to their high chemical and thermal stability. Their high magnetization value ($158 \text{ emu}\cdot\text{g}^{-1}$)^[37] is almost five times higher compared to common iron oxide particles,^[105] allowing a rapid recovery of the particles from a suspension by the aid of an external magnet within seconds. The one-step, large-scale reducing flame-spray pyrolysis ($> 30 \text{ g}\cdot\text{h}^{-1}$) of these nanomagnets was originally described by Stark *et al.*,^[37] which are by now commercially available. The graphene-like shell enables a number of further functionalizations, such as *e.g.* the covalent grafting of phenyl groups to the surface of carbon-coated cobalt nanobeads (Co/C) by *in situ* formed aryl radicals from their corresponding diazonium salts.^[37] Taking this as a starting point, a microporous polymer was grown on the surface of the nanoparticles by “knitting” rigid aromatic building blocks with formaldehyde dimethyl acetal (FDA) as external cross-linker.^[98] First, pristine Co/C nanobeads **1** were covalently functionalized *via* diazonium chemistry by dispersing **1** in water together with 4-toluidine and hydrochloric acid as catalyst. Subsequently, a pre-cooled solution of sodium nitrite was added dropwise at 0 °C (Scheme 6). In order to decompose the formed arene diazonium salt and ligate the aryl radical to the carbon shell, the mixture was stirred for a given time, followed by ultrasonication to yield toluene-functionalized nanobeads **3**. The polymeric network was then generated with the different monomer building blocks a-e and FDA, resulting in microporous polymers attached to the nanobeads **4a-4e**. Owing to the high initial magnetization of the

[‡] This chapter is based on the preliminary investigations of **5a** as magnetic catalyst for Heck couplings (fundamental experiments performed by J. Zhi (postdoctoral research) and continued by S. Ranjbar (PhD thesis) and L. Stadler (Master thesis)) and hydrogenation reactions (initial hydrogenation of *trans*-stilbene with **5a** performed by S. Ranjbar (PhD thesis), screening of reaction conditions and substrate scope carried out by L. Stadler (Master thesis) and the recycling of the catalyst applying *trans*-stilbene **6** (A. Hartl, Master thesis)) at the University of Regensburg under supervision of Prof. Dr. O. Reiser.

unfunctionalized nanoparticles **1**, the resulting hybrid materials MOPs@Co/C **4** are still highly magnetic, thus making them easy and fast to recover.



Scheme 6. Synthesis of Pd@toluene@Co/C **5a**. Analogous to **4a** and **5a**, MOPs **4b-4e** and Pd catalysts **5b-5e** were synthesized with the aromatic building blocks b-e.))) = ultrasound.

In order to determine the effect of the cross-linker on the pore sizes and catalyst activity, toluene was chosen first as the monomer. Thus, the microporous polymer toluene@Co/C **4a** was synthesized with 1.25 (**4a- α**), 2.00 (**4a- β**), and 2.50 (**4a- γ**) equivalents of FDA, the latter corresponding to the potential maximum of cross-linker for toluene as a monomer. The porous properties of these hybrid materials were investigated by N_2 sorption analysis at 77.3 K (Table 1 and graphical representation in Figure 14).

Table 1. Nitrogen adsorption isotherms at 77.3 K of **4a**.

| No. | FDA ^a | S_{BET}^b [m^2/g] | S_{BJH}^c [m^2/g] | $V_{0.1/\text{tot}}^d$ [cm^3/g] |
|-------------------------------|------------------|----------------------------------------------|----------------------------------------------|---------------------------------------------------|
| 4a-α | 1.25 | 43 | 15 | 0.14 |
| 4a-β | 2.00 | 85 | 22 | 0.23 |
| 4a-γ | 2.50 | 277 | 55 | 0.37 |

[a] Molar ratio with respect to toluene; [b] Surface area calculated using BET equation; [c] Surface area calculated using BJH equation; [d] Ratio of micropore volume (at $P/P_0=0.1$) over the total pore volume.

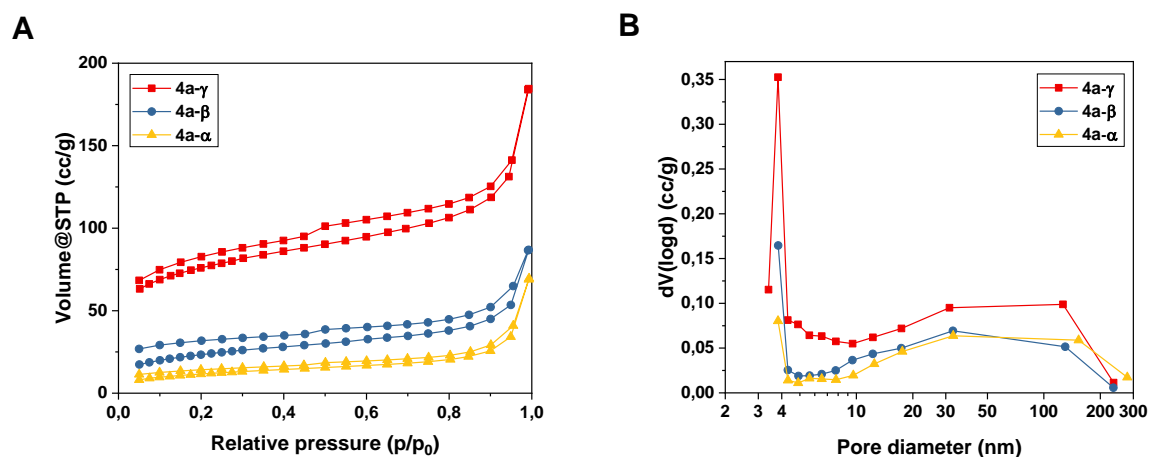


Figure 14. (A) N_2 adsorption-desorption isotherm of **4a-α** to **4a-γ**. (B) Logarithmic presentation of the pore size distribution calculated by Barrett-Joyner-Halenda (BJH) method for **4a-α** to **4a-γ**.

In Figure 14A, the rise of the adsorbed nitrogen in the low relative pressure area ($P/P_0 < 0.1$) implies the presence of micropores, while the steep nitrogen uptake in the middle and high relative pressure region ($0.8 < P/P_0 > 1.0$) is characteristic for macropores.^[106] The slight hysteresis loop indicates a spot of mesopores.^[101] However, such a loop can also be caused by the softness of the organic material, leading to the deformation and swelling of the polymer in the low-pressure region at 77.3 K by N_2 .^[107] The Barrett-Joyner-Halenda (BJH) pore size distribution of **4a** in Figure 14B assumes a heterogeneous pore structure, including micro-, meso-, and macropores, which is favorable for catalytic reactions. Micro- and mesopores with appropriate sizes can contribute to anchor metal catalysts and influence the nanoparticle formation. The macroporous structure accelerates the mass transfer of reactants to the embedded metal catalysts and of the corresponding products.^[102] The highest Brunauer-Emmett-Teller (BET) surface area was calculated to be $277 \text{ m}^2 \cdot \text{g}^{-1}$ in the case of **4a-γ**, Table 1, whereby it should be noted that the apparent low surface area in comparison to the literature^[98] is a result of the heavy Co/C nanobeads, having a comparably low surface area of $20.5 \text{ m}^2 \cdot \text{g}^{-1}$ in their pristine form.^[46] The micropore content was calculated by the ratio of micropore volume ($P/P_0 = 0.1$) over the total pore volume to be 0.37 for **4a-γ**. Thus, micropores are outnumbered and meso- and macropores are predominant.^[93]

There is a great effort to immobilize palladium nanoparticles (Pd NPs) on a variety of supports, including porous materials like silica,^[108] zeolites,^[109] MOFs,^[110] or MOPs^{[97],[102]} to generate heterogeneous catalytic systems. Since the catalytic activity of Pd NPs is size- and shape-dependent, these porous supports turned out to be excellent for such approaches, not only because of their ability to control the nanoparticle size by spatial restriction, but further because they are able to prevent aggregation and precipitation. In order to generate and embed the palladium NPs into the porous support **4a**, a decomposition method^[111] modified by Reiser *et al.*^[112] was applied (Scheme 6): Upon

microwave irradiation of $\text{Pd}_2(\text{dba})_3\text{-CHCl}_3$ in the presence of **4a** (1 mg $\text{Pd}_2(\text{dba})_3\text{-CHCl}_3$ per 50 mg of the MOPs **4a- α** to **4a- γ**), **5a- α** to **5a- γ** were obtained with palladium loadings from 0.2 to 0.4 wt% and incorporation rates between 36% and 87% (Table 2, entries 1-3). The palladium incorporation rate of only 36% for **5a- α** and 71% for **5a- β** indicate a lower capacity uptake for the metal nanoparticles and reflects the results of the nitrogen adsorption measurements (Figure 14). Based on this, **4a- γ** was concluded to be the most effective polymer, for which the capacity for the palladium incorporation was further explored. Thus, a series of materials **5a- γ** (Table 2, entries 4-9) was synthesized using different amounts of $\text{Pd}_2(\text{dba})_3\text{-CHCl}_3$ aiming at diverse Pd wt% loadings. The incorporation of palladium was high (81-97%), when up to 10 mg of palladium precursor per 50 mg of **4a- γ** were employed, resulting in materials with 0.2-3.9 wt% Pd (entries 3-8). However, an appreciable decline to 67% Pd incorporation was observed, if 50 mg of palladium precursor were used (entry 9), corresponding to 14 wt% Pd. This result suggested that the limit for the uptake of palladium into the porous material **4a- γ** was reached at this point.

Table 2. Palladium incorporation into **4a- α** to **4a- γ** , resulting in materials **5a- α** to **5a- γ** with various Pd wt% loadings.

| Entry | No. | FDA [equiv.] | 4a [mg] | $\text{Pd}_2(\text{dba})_3\text{-CHCl}_3$ [mg] | Pd incorporation ^a [%] | Pd ^a [wt%] |
|-------|-------------------------------|--------------|----------------|------------------------------------------------|-----------------------------------|-----------------------|
| 1 | 5a-α | 1.25 | 50 | 1.0 | 36 | 0.2 |
| 2 | 5a-β | 2.00 | 50 | 1.0 | 71 | 0.3 |
| 3 | 5a-γ | 2.50 | 50 | 1.0 | 87 | 0.4 |
| 4 | 5a-γ | 2.50 | 50 | 0.5 | 97 | 0.2 |
| 5 | 5a-γ | 2.50 | 50 | 1.0 | 87 | 0.4 |
| 6 | 5a-γ | 2.50 | 50 | 2.5 | 91 | 1.0 |
| 7 | 5a-γ | 2.50 | 50 | 5.0 | 81 | 1.7 |
| 8 | 5a-γ | 2.50 | 50 | 10 | 91 | 3.9 |
| 9 | 5a-γ | 2.50 | 50 | 50 | 67 | 14 |

[a] Determined by ICP-OES.

The palladium nanoparticle size distribution of the synthesized materials was evaluated by TEM measurements and was found to be quite narrow for **5a- γ** with 0.4 to 1.7 wt% Pd with main particle sizes of 3 and 4 nm (Figure 15A; Figure 48-Figure 50, Experimental Part). For higher loadings (3.9 and 14 wt%) a broader size distribution was observed, resulting on average in bigger and more agglomerated nanoparticles (Figure 15B; Figure 51, Figure 52, Experimental Part). However, especially for the catalysts with a high palladium loading, the determination of the palladium nanoparticles was rather challenging due to the partially broad size distribution of the carbon-coated cobalt nanoparticles themselves, thus an unambiguous assignment of the particle size distribution was not possible. In the case of the material containing 0.2 wt% Pd, the Pd nanoparticles were not observable with the

equipment available to us, thus the determination of their size distribution was not possible (Figure 47, Experimental Part).

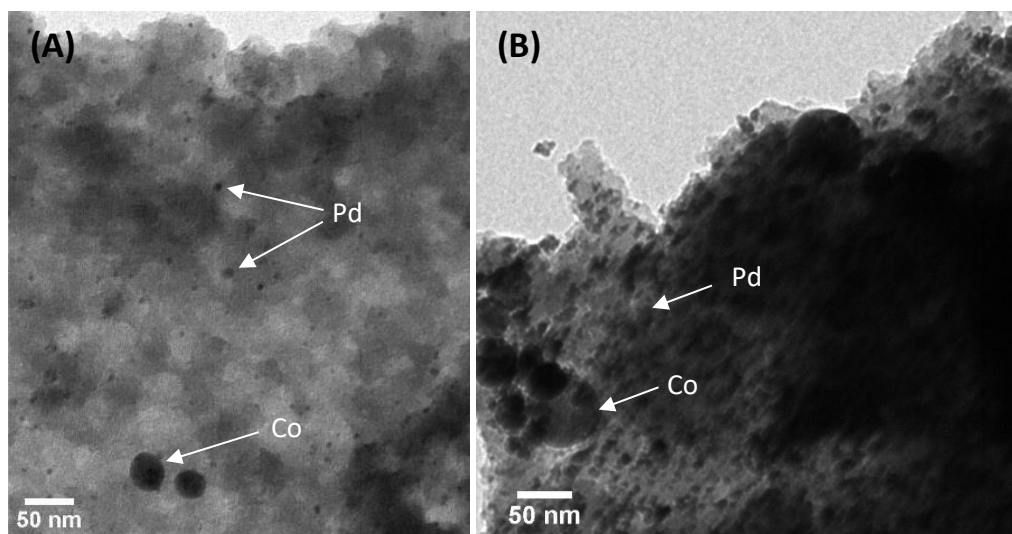


Figure 15. Exemplary TEM images of Pd materials **5a-γ** with (A) 1.7 wt% Pd and (B) 14 wt% Pd.

X-ray photoelectron spectroscopy (XPS) has been employed to further elucidate the composition of catalyst **5a-γ** (1.9 wt% Pd). The survey spectrum shows elemental compositions of C, O, Co, and Pd, which were found to be 86.8, 11.4, 1.1, and 0.8 atomic%, respectively (Figure 53, Experimental Part). The high-resolution XPS spectra in the C 1s region can be deconvoluted into three major peak components with binding energies of 284.6, 285.2, and 286.4 eV corresponding to C-C sp^3 , C=C sp^2 , and C-O types of carbon bonds (Figure 16A, B). The binding energy of Co 2p_{3/2} peak at 779.0 eV is attributed to the cobalt metal Co(0) (Figure 16C).^[113] The high-resolution XPS spectrum of Pd 3d at 335.59 and 340.85 eV is assigned to metallic Pd(0) and the second set of peaks at 337.45 and 342.71 eV is assigned to Pd(II) (Figure 16D). The peak at the higher binding energy may indicate the presence of palladium oxide, which may arise due to handling the material under air.^[114] The Pd(II)/Pd(0) ratio (64:36) further reflects that no special precaution was taken, *i.e.* the material was handled open to air, thus making its application in catalytic hydrogenations convenient. Upon performing reductions with molecular hydrogen, Pd(II) is largely reduced to Pd(0) *in situ*, resulting in high turnover numbers and rates for these reactions (*vide infra*). Thermogravimetric analysis (TGA) of **5a-γ** (1.9 wt%) detected no weight loss up to 200 °C and only a small weight loss of 2% at temperatures up to 300 °C, demonstrating excellent thermal stability of the material and making it suitable for most organic reactions (Figure 55, Experimental Part).

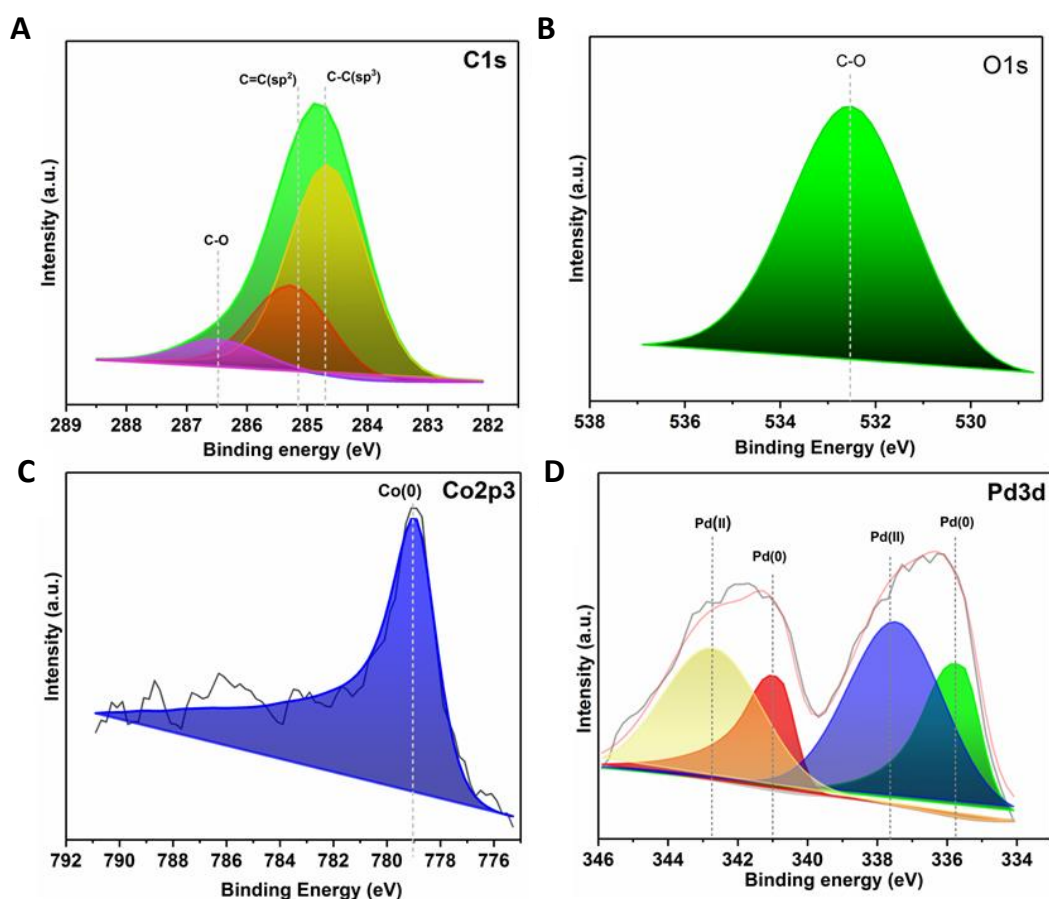


Figure 16. XPS spectra of **5a-γ** with 1.9 wt% Pd. Ratio of Pd(0)/Pd(II) = 36:64.

Energy-dispersive X-ray spectroscopy (EDS) detected the elements C, Co, and Pd, resulting from the cobalt core, their carbon shell, the organic polymer, and the palladium nanoparticles (survey spectrum Figure 56, Experimental Part). The high-angle annular dark-field scanning transmission electron microscopy (HAADF-STEM) and element mapping show a uniform distribution of the Pd nanoparticles within the carbon-based polymer (Figure 17). The presence of nitrogen, predominately near the cobalt core, results from the first functionalization step, the diazonium chemistry (Figure 17E). Furthermore, iron nanoparticles were detected, which were probably embedded during the iron-catalyzed polymer synthesis (1.4 wt% Fe, corresponding to 2% incorporation of the original FeCl₃; Figure 57, Experimental Part). Control experiments established that these particles were not active for hydrogenation reactions.[§] The distribution of oxygen, predominately present near the iron nanoparticles, suggests an oxidized form of iron.

[§] Control experiments: hydrogenation of trans-stilbene **6** (0.5 mmol) without any catalyst and with 5 mg of **4a-γ** for 70 min led to only negligible background conversion of < 4% without detectable amounts of product. A further experiment with 0.2 mol% **5a-γ** led to a yield of 71% after 50 min, and after removing the catalyst, the solution was hydrogenated for further 60 min without a change in yield.

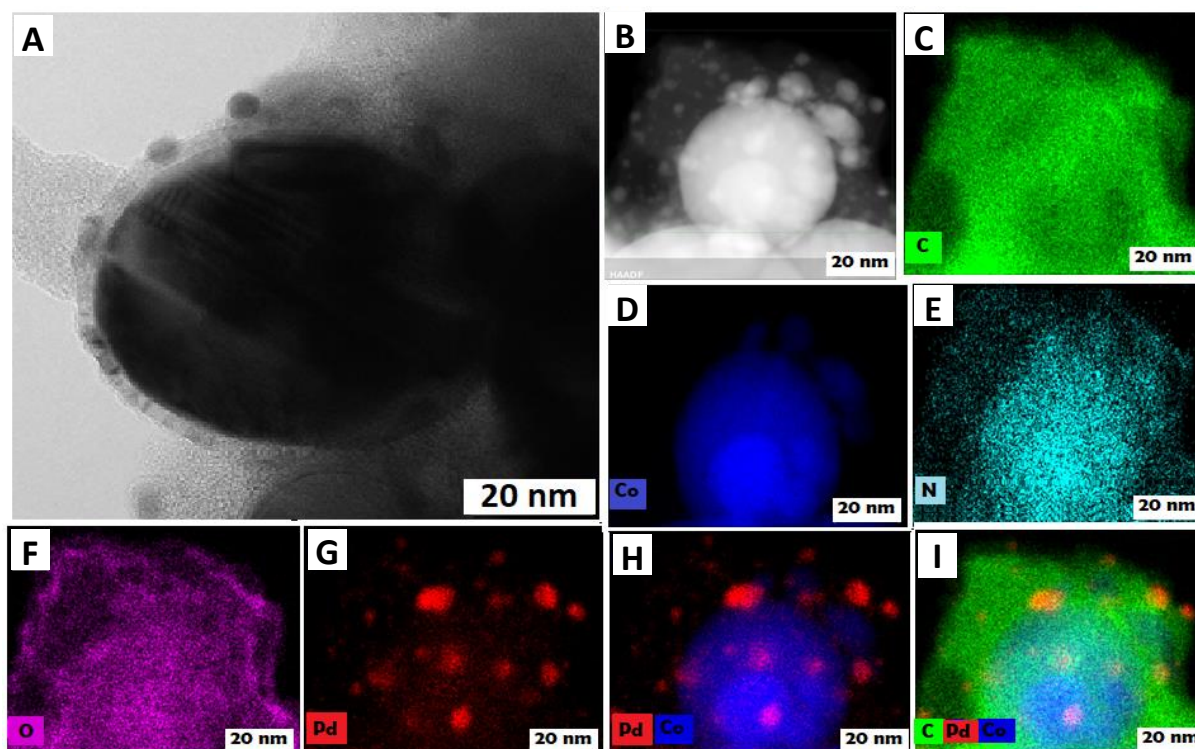
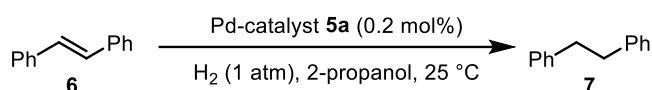


Figure 17. HAADF images and EDS chemical mapping of **5a-gamma** (1.9 wt%) (A) HRTEM image showing single cobalt nanoparticle covered with carbon and Pd NPs. (B-I) Elemental mapping of C, Co, N, O, Pd, Pd-Co, and C-Pd-Co together.

To investigate the catalytic activity of the new hybrid materials **5a-alpha** to **5a-gamma** (0.2 to 14 wt%), the hydrogenation of *trans*-stilbene **6** in 2-propanol at 25 °C was selected as a model reaction. For sake of comparison, all reactions were performed with the same low palladium content of 0.2 mol% and stopped after a given time (Table 3). **5a-gamma** showed the highest catalytic activity with full conversion after only 30 min (Table 3, entry 3) compared to the two systems with lower cross-linker content **5a-alpha** and **5a-beta** (Table 3, entries 1 and 2). To further explore the differences in activity for the catalytic materials **5a-gamma** with diverse Pd loadings of 0.2 to 14 wt%, the reaction time was shortened to 10 min. Entries 4-8 revealed that the activity is approximately the same for the materials containing up to 3.9 wt% Pd. Only the material with the highest palladium content (14 wt% Pd, entry 9) showed a reduced activity in the hydrogenation. These results give credit to the supporting effect of the microporous polymer regarding the prevention of metal NPs from agglomeration up to high Pd wt% loadings. For the related unsupported catalytic system, where the Pd NPs are directly deposited onto the graphene layer of the Co/C nanobeads (Pd@Co/C **2**),^[112] the catalytic activity drastically dropped with increasing Pd loadings, whereby 0.2 wt% Pd gave the most active catalyst. Taking into account these data as well as the more favorable narrow size distribution of the Pd nanoparticles (Figure 50, Experimental Part), catalyst **5a-gamma** with 1.7 wt% Pd was considered to be optimal with respect to its activity, the palladium loading per gram of material, and the high palladium incorporation in the course of its preparation.

Table 3. Hydrogenation of *trans*-stilbene **6** with 0.2 mol% of Pd-catalysts **5a-α** to **5a-γ**.

| Entry | No. | Pd ^a [wt%] | Time [min] | Conversion ^b [%] | TOF ^c [h ⁻¹] | Mean particle size ^d [nm] |
|-------|-------------|--------------------------|---------------|--------------------------------|----------------------------------------|-----------------------------------------|
| 1 | 5a-α | 0.2 | 30 | 75 | 750 | <i>n.d.</i> |
| 2 | 5a-β | 0.3 | 30 | 86 | 860 | <i>n.d.</i> |
| 3 | 5a-γ | 0.4 | 30 | 100 | 1000 | 3.6 |
| 4 | 5a-γ | 0.2 | 10 | 32 | 960 | <i>n.d.</i> |
| 5 | 5a-γ | 0.4 | 10 | 33 | 990 | 3.6 |
| 6 | 5a-γ | 1.0 | 10 | 36 | 1080 | 3.9 |
| 7 | 5a-γ | 1.7 | 10 | 37 | 1110 | 3.4 |
| 8 | 5a-γ | 3.9 | 10 | 37 | 1110 | 5.3 |
| 9 | 5a-γ | 14 | 10 | 28 | 840 | 5.2 |

[a] Determined by ICP-OES; [b] Conversion to yield 1,2-diphenylethane **7** (single product) was determined by GC analysis using dodecane as an internal standard; [c] TOF is calculated as mmol substrate per mmol palladium (obtained by ICP-OES measurements) per time; [d] Determined by TEM; *n.d.* = not determined.

Thus, the as-described material **5a-γ** (Table 2, entry 7) was resynthesized on a larger scale (500 mg), resulting in 1.9 wt% Pd (89% Pd incorporation) in good agreement with the analytical results obtained for the small scale reaction. TEM analysis of the nanocomposite further confirmed a well-developed polymer with evenly distributed palladium and cobalt nanoparticles. This material was tested for its recyclability and metal leaching in the hydrogenation of diphenylacetylene **8** to the fully hydrogenated 1,2-diphenylethane **7** using the reaction setup shown in Figure 18. Hydrogenations were carried out with 0.2 mol% palladium catalyst **5a-γ** (1.9 wt%) at room temperature and ambient hydrogen pressure in 2-propanol, not only advantageous from a sustainability point of view but also proving superior to MeOH, toluene, CH₂Cl₂, or CHCl₃** with respect to conversion and yield. Control experiments in the absence of hydrogen showed no conversion, proving that 2-propanol is not taking the role of a hydrogen donor within this catalytic system. Likewise, formic acid/triethylamine or sodium formate could not be used as a hydrogen donor for the herein reported catalyst reported. The polymers **4**, having no palladium incorporated, did not promote the hydrogenation and neither did the reaction solution if catalyst **5a-γ** was removed.

** This preliminary results were already reported in the master thesis of L. Stadler (University of Regensburg, 2016) and the PhD thesis of S. Ranjbar^[115] in a joint cooperation project with A. Hartl (Master thesis at University of Regensburg, 2016). The experimental work was performed as following: hydrogenation of *trans*-stilbene in MeOH, 2-PrOH with initial, non-optimized Pd@toluene@Co/C **5a** were tested by S. Ranjbar; hydrogenations in toluene, CH₂Cl₂, CHCl₃ as well as control experiments and substrate scope was carried out by L. Stadler.

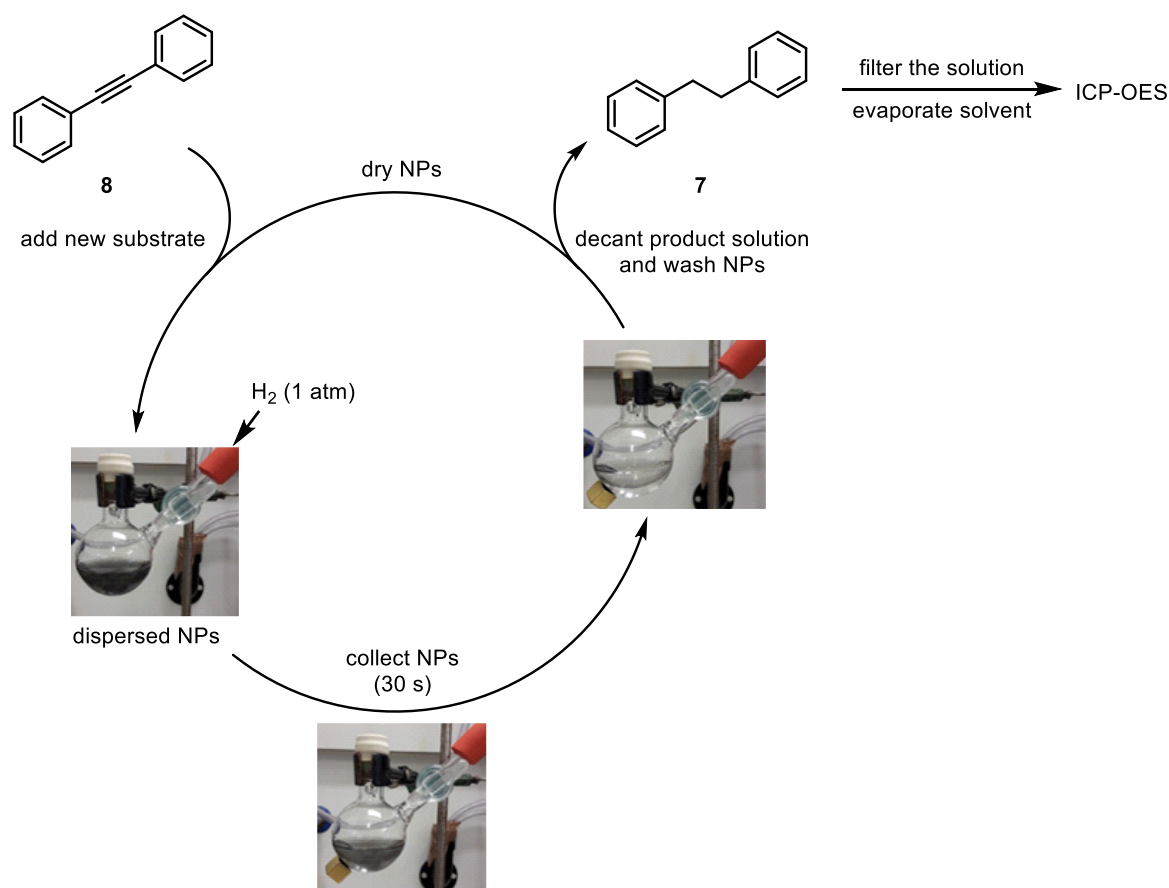


Figure 18. Consecutive hydrogenation of **8** using 0.2 mol% Pd-catalyst **5a-γ** (1.9 wt%) in 2-propanol.

Evaluating six consecutive cycles (Table 4), the catalyst showed an overall high activity of up to 1500 turnover numbers/h. Nevertheless, a doubling of the reaction time was necessary to reach full conversion, comparing the first and sixth cycle. On average, low palladium contamination of about 15 ppm in the product was detected (Table 4), while the leached cobalt (average of 26 ppm cobalt) is a result of small defects in the graphene layer of the cobalt support.

Table 4. Consecutive hydrogenation of **8** with **5a-γ** (1.9 wt%) and determination of metal contamination in the product.^a

| Cycle | TOF ^b [h ⁻¹] | Time ^c [min] | Yield [%] | Leaching Pd ^d [ppm] | Leaching Co ^d [ppm] |
|-------|-------------------------------------|-------------------------|-----------|--------------------------------|--------------------------------|
| 1 | 1500 | 20 | 94 | 9 | 25 |
| 2 | 1200 | 25 | 89 | <2 | 34 |
| 3 | 1000 | 30 | 76 | 4 | 13 |
| 4 | 857 | 35 | 93 | 38 | 42 |
| 5 | 667 | 45 | 96 | 28 | 27 |
| 6 | 667 | 45 | 93 | 10 | 15 |

[a] Diphenylacetylene **8** (1 mmol) in 2-propanol (20 mL) was hydrogenated by 0.2 mol% **5a-γ** (1.9 wt%). Each run was stopped after full conversion in order to determine the leaching; [b] TOF is calculated as mmol substrate per mmol of palladium per time; [c] Hydrogenation carried out until complete conversion was determined by GC analysis; [d] Leaching determined by ICP-OES, calculated in μg per g of product.

Overall, approximately 7% Pd have leached from the magnetic support within the six runs, while 10% of the total material **5a-γ** (mass balance) were lost due to handling during the decantation procedure. Thus, the decrease in activity (approximately by half comparing the first and the sixth cycle) cannot be explained solely by the leached palladium or the loss of catalyst material. TEM analysis of the recycled catalyst **5a-γ** (1.9 wt%) showed almost no agglomeration of the Pd nanoparticles, which again demonstrates that the microporous polymer acts as protective support (Figure 19A). Comparing the XPS spectra of the freshly prepared catalyst **5a-γ** (Figure 16) with the recycled catalyst **5a-γ** after six runs (Figure 19B) shows an increase of the Pd(0)/Pd(II) ratio from 36:64 to 82:18. This was also observed in a pretreatment experiment, in which the catalyst was exposed to a hydrogen atmosphere before measuring the XPS (Figure 54, Experimental Part). These results demonstrate an *in situ* reduction of the oxidized palladium species upon hydrogenation to the catalytically active Pd(0) nanoparticles.

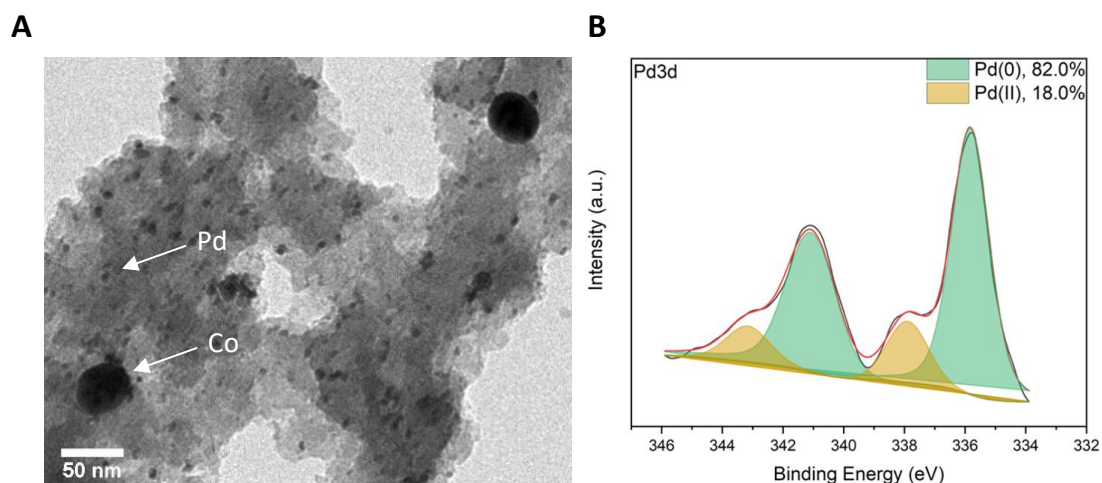


Figure 19. Pd catalyst **5a-γ** (1.9 wt%) after six consecutive recycling steps (A) TEM image and (B) XPS spectra.

Next, magnetically supported materials were built up with the monomers b-e (Scheme 6 and Table 5), analogous to the synthesis of catalyst **5a**, aiming to further improve the activity and recyclability. Since the results described above demonstrated the benefit of high cross-linker content, these new polymers were synthesized employing 2.5 to 3.0 equivalents of FDA. Notably, monomers 1,4-diaminobenzene (b) or 1,1'-biphenyl (c) resulted in unsatisfactory palladium incorporation even when low palladium amounts were used (entries 1 and 2), while materials **5d** and **5e** comprising of phenol monomers gave excellent results in this respect (entries 3-5). Benchmarking the materials **5b** to **5e** regarding their catalytic activity in the model hydrogenation of *trans*-stilbene **6** showed the best results for **5c** and **5d** (entries 2-4). In contrast, materials with strong donor groups (**5b**, entry 1) or chelators (**5e**, entry 5) did not perform well.

Table 5. Synthesis of various Pd@MOPs@Co/C following the procedure in Scheme 6 and their evaluation in the catalytic hydrogenation of *trans*-stilbene **6**.^{††}

| Entry | No. | Monomer | FDA ^a [equiv.] | Pd incor- poration ^b [%] | Pd ^b [wt%] | Conversion ^c [%] | TOF ^d [h ⁻¹] |
|-------|-----------|---------------------|------------------------------|----------------------------------------|--------------------------|--------------------------------|----------------------------------------|
| 1 | 5b | 1,4-diaminobenzene | 3 | 64 | 0.3 | traces | <i>n.d.</i> |
| 2 | 5c | 1,1'-biphenyl | 3 | 73 | 0.3 | 100 (94) | 940 |
| 3 | 5d | 2,2'-biphenol | 3 | 95 | 0.4 | 94 (93) | 930 |
| 4 | 5d | 2,2'-biphenol | 2.5 | 97 | 2.0 | 89 (70) | 700 |
| 5 | 5e | 2,3-naphthalenediol | 3 | 93 | 0.4 | 57 (47) | 470 |

[a] Molar ratio with respect to the monomer; [b] Determined by ICP-OES. 2.0 mg (1.9 μmol) of Pd₂dba₃·CHCl₃ (entries 1-3, 5) and 52 mg (50 μmol) of Pd₂dba₃·CHCl₃ (entry 4) were employed; [c] Hydrogenation of *trans*-stilbene **6** with 0.2 mol% Pd after 30 min. Conversion and yield (in brackets) were determined by GC analysis using dodecane as an internal standard. [d] TOF is calculated as mmol substrate per mmol of palladium per time; *n.d.* = not determined.

Recycling studies with catalyst **5c** showed quite high leaching, being in accordance with the results obtained during the recycling of catalyst **5a-y**, which also does not contain any functional groups in the monomer. Gratifyingly, the Pd and Co leaching could be reduced close to the detection limit of 2 ppm in every run when catalyst **5d** was used (Table 6), being below the limit of heavy metal traces allowed in pharmaceutical products (< 10 ppm).^[117] Presumably, the introduced hydroxyl groups are capable to stabilize the Pd nanoparticles efficiently but also might act as an internal scavenger for cobalt ions that might leach from the support. Furthermore, the different pore size (mainly micropores with $V_{0.1/\text{tot}} = 0.63$) and higher surface area ($S_{\text{BET}} = 389 \text{ m}^2\cdot\text{g}^{-1}$, Table 24, Experimental Part) of **4d** may play a decisive role for the nanoparticle formation, size distribution (mean particle size = 2.9 nm) as well as the mass transfer to the active sites.

Table 6. Consecutive hydrogenation of **8** with **5d** (2.0 wt%) and determination of metal contamination in the product.^a

| Cycle | TOF ^b [h ⁻¹] | Time ^c [min] | Yield [%] | Leaching Pd ^d [ppm] | Leaching Co ^d [ppm] |
|-------|-------------------------------------|-------------------------|-----------|--------------------------------|--------------------------------|
| 1 | 2000 | 15 | 94 | 2 | 6 |
| 2 | 1500 | 20 | 91 | 2 | 3 |
| 3 | 1200 | 25 | 84 | 2 | 3 |
| 4 | 1000 | 30 | 96 | 3 | 5 |
| 5 | 1000 | 30 | 87 | 2 | 5 |
| 6 | 857 | 35 | 85 | 2 | 2 |

[a] Diphenylacetylene **8** (1 mmol) in 2-propanol (20 mL) was hydrogenated by 0.2 mol% **5d** (2.0 wt%). Each run was stopped after full conversion in order to determine the leaching; [b] TOF is calculated as mmol substrate per mmol of palladium per time; [c] Hydrogenation carried out until complete conversion was determined by GC analysis; [d] Leaching determined by ICP-OES, calculated in μg per g of product.

^{††} These polymers, as well as all reactions utilizing **4b-4e** or **5b-5e**, were performed by M. Homafar. For experimental details and further characterization see online at the Supporting Information of the Publication.^[116]

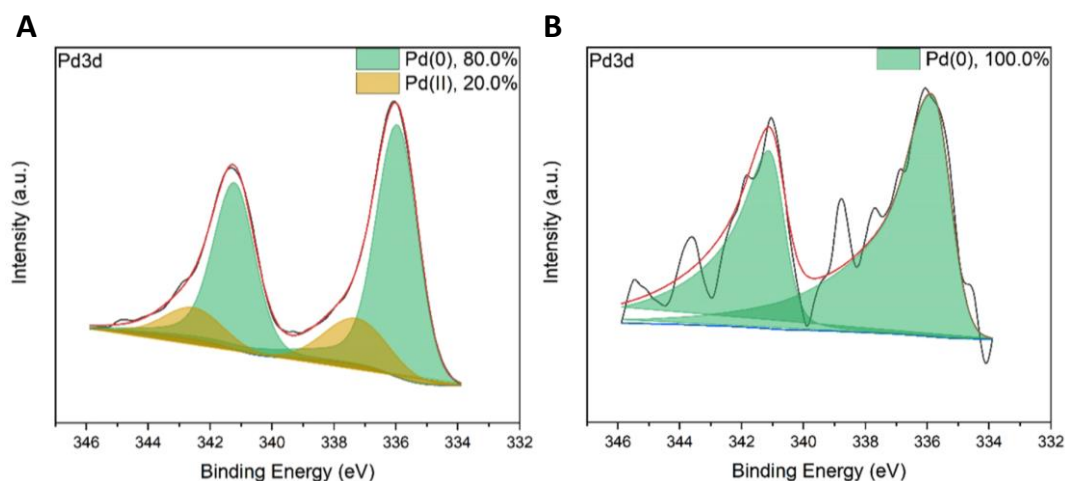


Figure 20. XPS spectra of Pd 3d of the catalyst **5d** with 2.0 wt% Pd. (A) freshly prepared and (B) after six recycling steps.

Notably, significantly less Pd(II) was observed during preparation and recycling for **5d** (Pd(0)/Pd(II) 80:20 upon preparation of **5d**, 100:0 after six cycles), indicating that the hydroxyl groups present in the microporous polymer protect Pd(0) from oxidation, presumably through coordination (Figure 20).

Further evaluation of the new hybrid materials **5a-y** (1.9 wt%) and **5d** (2.0 wt%) regarding their porous properties showed a significant change of the surface area (S_{BET} (**5d**) = 248 m²·g⁻¹) and pore size distribution, when the material **4d** was loaded with Pd nanoparticles. This effect was, *e.g.*, apparent by the loss of 36% of the surface area from **4d** to **5d** (Figure 21). Comparing **4a-y** with **5a-y** (S_{BET} (**5a-y**) = 224 m²·g⁻¹, Figure 22), resulted only in 19% loss of surface area. Determining the micropore volume ($V_{0.1}$) showed a loss of 35% for **5d** and 18% for **5a-y**. The meso-/macropore volume ($V_{\text{tot-0.1}}$) was not significantly affected for **5d** (0.04%), while 18% were lost in the case of **5a-y**. These results suggest that the Pd nanoparticles in **5d** are almost exclusively incorporated into the micropores of the material, which may lead to more efficient anchoring of the metal. The changes of $V_{0.1}$ and $V_{\text{tot-0.1}}$ of **5a-y** indicate that the metal is incorporated into micro- as well as meso-, and macropores, which may also be a reason for the higher metal leaching compared to **5d**.

The benchmarking of the catalytic activities of **5a-y** (1.9 wt%) and **5d** (2.0 wt%) was implemented by hydrogenating various alkynes, alkenes, α,β -unsaturated compounds, and nitro arenes with molecular hydrogen under atmospheric pressure (Table 7). Sterically less demanding alkynes as well as primary and strained alkenes were successfully hydrogenated to the corresponding alkanes within short reaction times, yielding high TOFs up to 3000 h⁻¹ (Table 7, entries 1-4). Di- and trisubstituted olefins required longer reaction times to reach full conversion (40-540 min, entries 5-9). For α,β -unsaturated carbonyl compounds, the C-C double bond was hydrogenated selectively. Furthermore, the hydrogenation of nitro arenes proceeded well (entries 10-12). In particular, the conversion of 4-nitrophenol to 4-aminophenol, being relevant for environmental reasons as well as for drug

syntheses, is possible with good efficiency and full recovery by magnetic capture of the catalyst (entry 12). This provides an alternative to other supported palladium catalysts^[118] and to the conventional iron-acid reduction, generating a large amount of Fe/Fe oxide sludge (1.2 kg/kg of product), which cannot be reused and complicates the workup and isolation of the product.^[119]

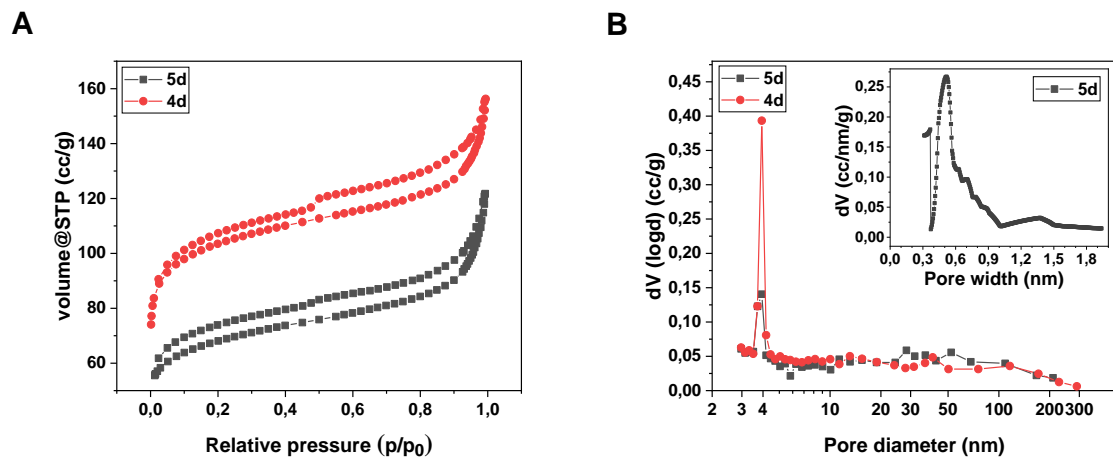


Figure 21. (A) N₂ adsorption-desorption isotherms of **4d** (red) and **5d** (gray). (B) Logarithmic presentation of the pore size distribution calculated by the Barrett-Joyner-Halenda (BJH) method for **4d** (red) and **5d** (gray). Inset: Size distribution of the micropores of **5d** obtained by the Horvath-Kawazoe (HK) method.

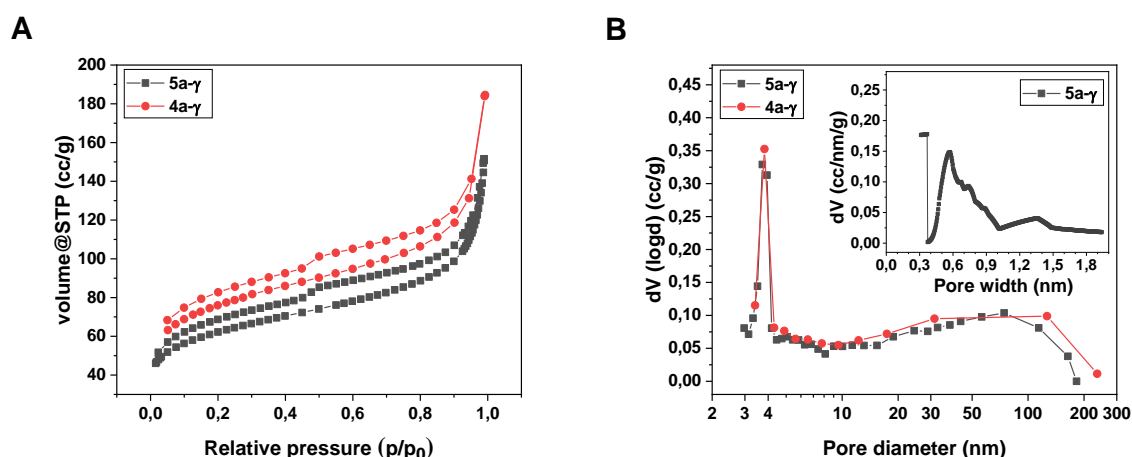
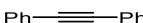

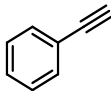
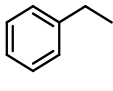
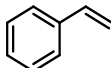
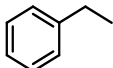


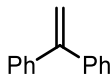
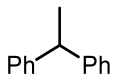
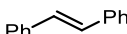
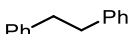
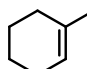
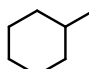
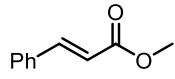
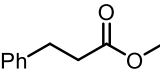
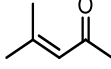
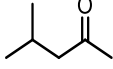
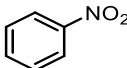
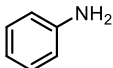
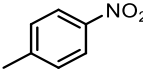
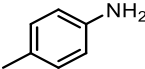
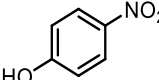
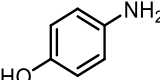


Figure 22. (A) N₂ adsorption-desorption isotherms of **4a-γ** (red) and **5a-γ** (gray). (B) Logarithmic presentation of the pore size distribution calculated by the Barrett-Joyner-Halenda (BJH) method for **4a-γ** (red) and **5a-γ** (gray). Inset: Size distribution of the micropores of **5a-γ** obtained by the Horvath-Kawazoe (HK) method.

In summary, new magnetically retrievable palladium nanocatalysts embedded into a microporous organic polymer support were developed, being efficiently synthesized in three steps from commercially available starting materials. The key step has been the polymerization of aromatic monomers with FDA as cross-linker onto carbon-coated cobalt nanoparticles, being pre-functionalized with 4-methylphenyl groups. 2,2'-Biphenol was found to be the most efficient monomer in the process, allowing a quantitative incorporation of palladium nanoparticles into the microporous network. Catalytic hydrogenation of alkynes, alkenes, and nitro arenes could be carried out successfully with up to 3000 turnover cycles/h, with a minimal leaching of palladium and cobalt from the supported system

into the products. Moreover, the catalysts were easily recovered by an external magnet and reused for six consecutive runs. The combination of magnetic nanoparticles as a primary platform with the microporous polymeric matrix for palladium nanocatalysts prevents the agglomeration and deactivation of the catalytically active sites, but, nevertheless, enables an efficient mass transfer to the latter and finally allows convenient recycling by making use of the magnetic properties of the materials.

Table 7. Hydrogenation of alkenes, alkynes, and nitro compounds with **5a-γ** (1.9 wt%) and **5d** (2.0 wt%).

| Entry ^a | Substrate | Product | Catalyst 5a-γ | | Catalyst 5d | |
|--------------------|-------------------------------------------------------------------------------------|-------------------------------------------------------------------------------------|----------------------|------------------------|--------------------|------------------------|
| | | | t [min] | TOF [h ⁻¹] | t [min] | TOF [h ⁻¹] |
| 1 |  |  | 20 | 1500 | 15 | 2000 |
| 2 |  |  | 30 | 1000 | 30 | 1000 |
| 3 |  |  | 10 | 3000 | 10 | 3000 |
| 4 |  |  | 10 | 3000 | 10 | 3000 |
| 5 |  |  | 40 | 750 | 70 | 429 |
| 6 |  |  | 70 | 429 | 65 | 462 |
| 7 |  |  | 540 | 56 | 480 | 63 |
| 8 |  |  | 30 | 1000 | 45 | 667 |
| 9 |  |  | 90 | 333 | 65 | 462 |
| 10 |  |  | 120 | 250 | 110 | 273 |
| 11 |  |  | 110 | 273 | 100 | 300 |
| 12 ^b |  |  | 60 | 100 | 65 | 92 |

[a] Substrate (0.5 mmol) in 2-propanol (10 mL) was hydrogenated by 0.2 mol% **5a-γ** (1.9 wt%) or **5d** (2.0 wt%) until full conversion was determined by GC analysis using dodecane (ethylbenzene in entry 10) as an internal standard; [b] 1 mol% catalyst **5a-γ** (1.9 wt%) or **5d** (2.0 wt%), 50 °C.

2. Palladium-catalyzed Suzuki-Miyaura coupling under mild reaction conditions

A palladium-based nanocatalyst was developed for the Suzuki-Miyaura coupling with focus on mild reaction conditions with low temperatures up to 50 °C. An immobilized *N*-heterocyclic carbene palladium(II) complex enabled the efficient coupling of aryl iodides as well as aryl bromides with boronic acids for up to six cycles. The linking of this complex to polystyrene-functionalized Co/C nanobeads facilitated the recycling protocol by simple magnetic decantation combined with an overall low metal leaching. The aim of this project was the design of an easy practicable magnetic catalyst for the Suzuki-Miyaura coupling, which was further investigated in a joint collaboration with the technical university of Dortmund regarding its efficiency in the coupling of small molecule scaffolds to DNA. Consequently, the preliminary studies in this chapter consider reaction conditions, which in principle are tolerated by DNA sequences.

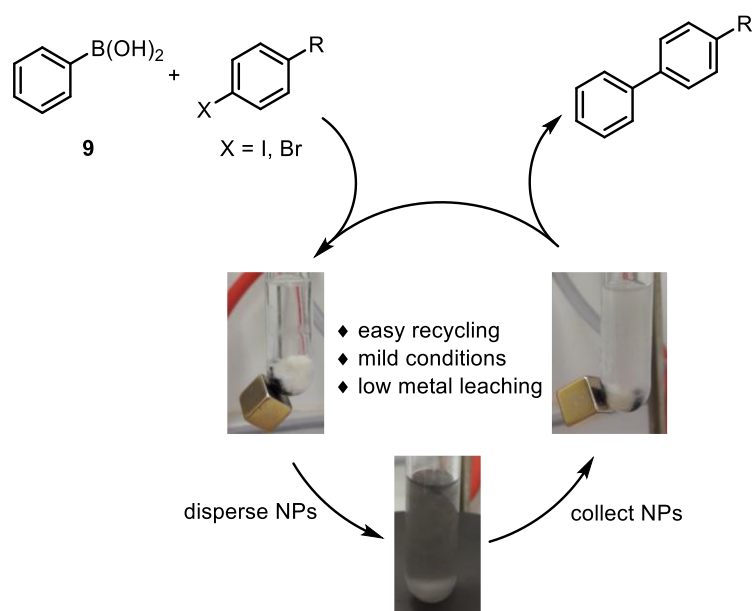
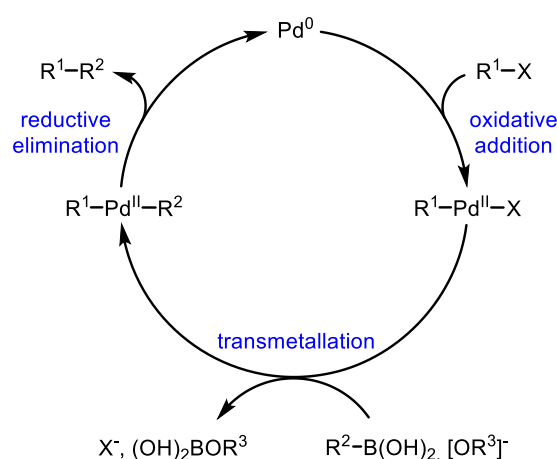


Figure 23. Pd-catalyzed Suzuki-Miyaura coupling applying magnetic Pd-nanocatalysts for a facile recovery.

2.1. Suzuki-Miyaura coupling – the dynamic nature of palladium catalysis

Palladium-catalyzed cross-couplings are still among the most powerful and widely explored reactions for the formation of carbon-carbon bonds, as proven by a variety of applications for academic as well as industrial purposes.^{[120]–[123]} The relevance of this research was also appreciated with the award of the Nobel Prize in 2010, jointly for the pioneering work of Richard F. Heck, Ei-ichi Negishi, and Akira Suzuki.^[123] In the following, some general remarks on the C-C bond-forming process of the latter one, namely the Suzuki-Miyaura coupling, should be described. This reaction type mainly benefits from (i) mild reaction conditions, (ii) a broad tolerance of functional groups, (iii) the ready availability, stability and sustainability of the organoboron compounds, (iv) the low toxicity of the organoboron compounds, and (v) the facile removal of the inorganic by-products.^{[121],[124]} These aspects contributed to the design of new transition-metal catalysts, with palladium-based catalysts being predominant.^[120]



Scheme 7. Typical catalytic cycle for the Suzuki-Miyaura cross-coupling. Reproduced with permission from [125]. Copyright © 2006, WILEY-VCH Verlag GmbH & Co. KGaA, Weinheim.

Besides great advances in homogeneous catalysis regarding the development of ligand and ligand-free processes, heterogeneous catalysts emerged as a sustainable alternative with a simplified separation protocol.^[120] With the proceeding achievements in the fast-growing field of palladium catalysis, the desire for mechanistic evidence and the question for the active species in the cross-coupling became more important.^{[125],[126]} A typical textbook catalytic cycle of the Suzuki-Miyaura reaction is shown in Scheme 7, including oxidative addition, transmetallation and reductive elimination as key steps. Eremin and Ananikov^[126] summarized a historical overview of the most influential mechanistic studies towards the ‘real nature’ of the catalyst, as well as the resultant novel approaches utilizing these catalysts according to their respective time period (Figure 24). While some palladium complexes are well defined as molecular catalysts, others entailed further developments in terms of mechanistic studies to identify the catalytically active species.^{[123],[125],[127]} The application of nanosized catalysts and the investigation of leaching-driven mechanisms achieved outstanding advances in the early 2000s.

Among these, the possibility to perform cross-coupling reactions with Pd amounts down to the ppb level,^[128] also termed ‘homeopathic’ catalysis.^{[120],[126]} Subsequently, more detailed mechanistic investigations disclosed the concept of a ‘cocktail’ of catalysts with a dynamic interconversion of molecular complexes, clusters, and nanoparticles. These Pd species can be generated from the precursors by *e.g.* aggregation as well as leaching, crushing or destruction during the overall catalytic process. The dynamic nature of catalytic systems and their active species are described in several reviews and publications and are still debated today. Its understanding has led to an improvement in catalyst design as well as their applications.^{[120],[126],[127],[129]}

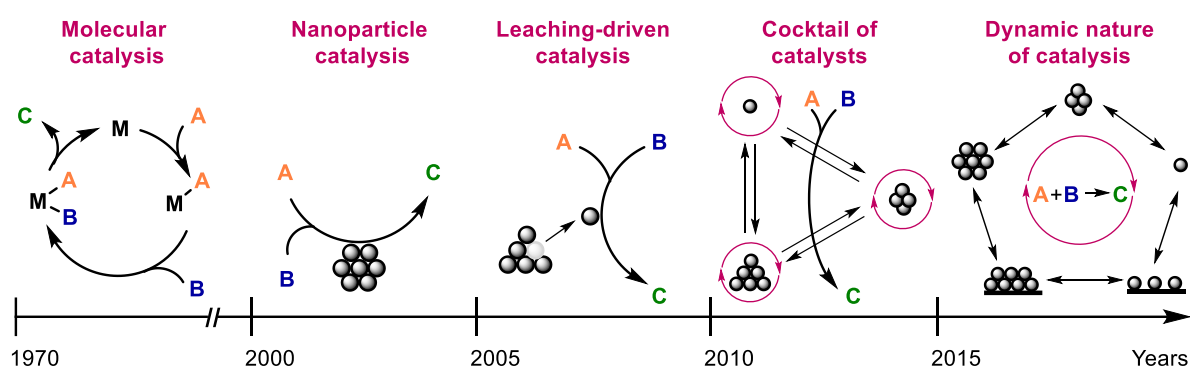
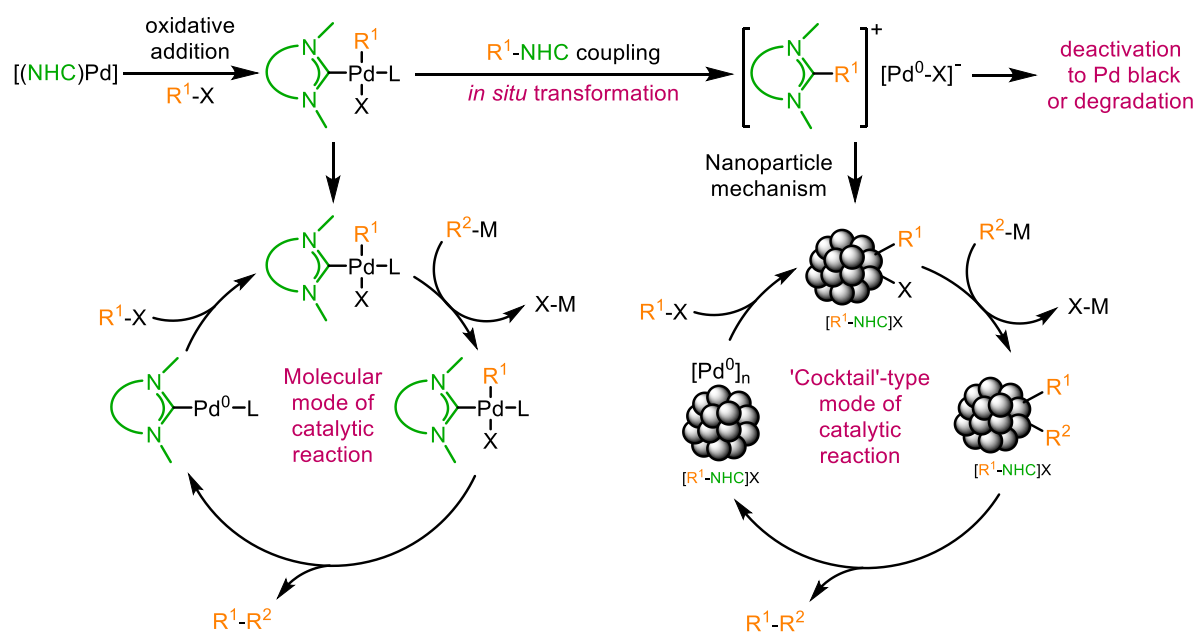


Figure 24. Proposed mechanistic studies of the nature of transition-metal catalysis, whereby the time axis shows the influential periods of mechanistic studies rather than the first publication. Adapted with permission from [126]. Copyright © 2017, Elsevier.

As mentioned above, for the design of new efficient catalysts, a clear understanding of their dynamic nature is of fundamental relevance.^{[126],[130]} Highlighting the investigations of Ananikov and co-workers in this research area, extensive studies resulted in continuous improvements. In 2017, they reported that the lability of palladium-*N*-heterocyclic carbene (Pd-NHC) systems was the reason for the catalytic efficiency in the performed Heck-type cross-couplings, rather than their defined stability.^[131] Typically, Pd-NHCs are assumed to act as well-defined homogeneous catalysts. However, the examined Pd-NHC complexes evidenced a cleavage of the Pd-C_{carbene} bond to form a ‘cocktail’ of catalytically active species, involving Pd nanoparticles and Pd clusters.^{**} The derived azolium salts were supposed to act as N⁺X⁻ stabilizing agents to prevent agglomeration of the palladium. Further studies by Ananikov and co-workers followed in 2019,^[127] combining theoretical calculations with appropriate experiments for a more detailed mechanistic insight. These investigations were in good agreement with the concept of the dynamic behavior of the Pd/NHC system during the catalysis, dependent on the NHC ligand, the reaction conditions, and the reactants (Scheme 8).

^{**} Especially benzimidazole, imidazole, and triazole NHC ligands underwent this ‘cocktail’-type mechanistic proposal based on the break of the Pd-NHC bond. Bulkier NHC ligands, with *e.g.* *N*-alkyl(aryl) groups, showed only a retarded decomposition.



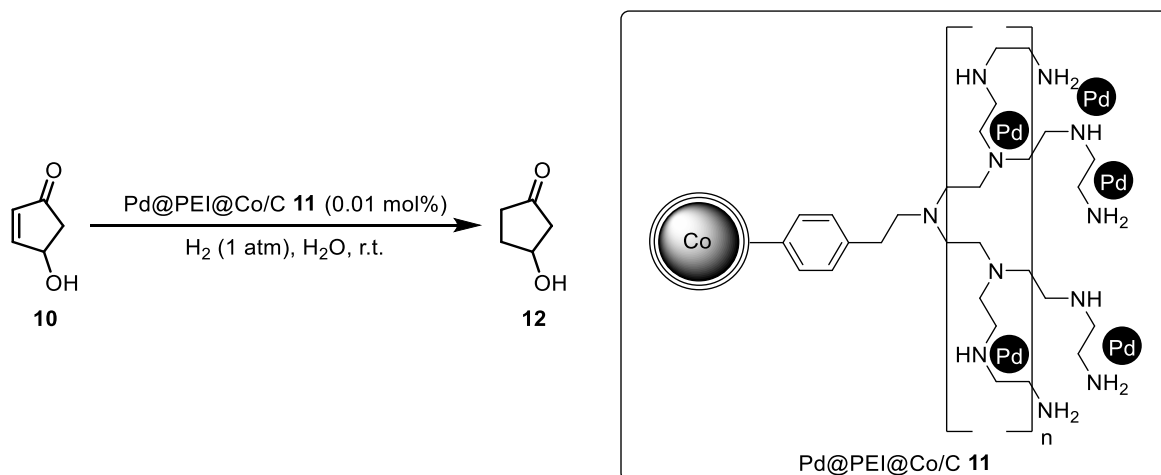
Scheme 8. Two possible mechanistic modes for Pd/NHC catalytic systems. Adapted with permission from [127]. Copyright © 2018, The Royal Society of Chemistry.

2.2. Synthesis of magnetic palladium nanocatalysts

2.2.1. Preliminary considerations

In this chapter, a suitable magnetic palladium catalyst had to be developed in cooperation with the TU Dortmund. As the catalyst was planned for the use with DNA sequences, given specifications regarding reaction conditions had to be upheld. Especially its performance under mild reaction conditions in the Suzuki-Miyaura coupling was of interest, ensuring low temperatures up to 50 °C as well as a restricted selection of bases and solvents. At the same time, an easy separation *via* magnetic decantation should still be achievable. After careful consideration, three different palladium-based magnetic systems were investigated.

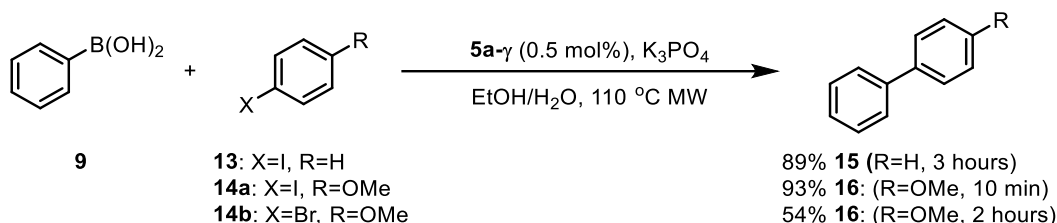
Two of these systems were examined due to their preceding successful application in palladium-catalyzed hydrogenation reactions. Pd@PEI@Co/C **11** is known for its high catalytic activity in water combined with good recyclability up to seven runs with only a minor loss in yield (98% to 92% in the hydrogenation of hydroxyl-2-cyclopentenone **10** in water, Scheme 9).^[132]



Scheme 9. Pd@PEI@Co/C **11** catalyzed hydrogenation of hydroxyl-2-cyclopentenone **10** in water, performed by B. Kastl.^[132]

In contrast to Pd@PEI@Co/C **11**, Pd@toluene@Co/C **5a-γ** were utilized bearing a highly hydrophobic nature of the polymer. This catalyst already proved its efficiency for the hydrogenation in 2-propanol (chapter 1). Even though the Pd leaching during the hydrogenation of diphenylacetylene **8** was higher for the recycling of catalyst **5a-γ** than for the corresponding Pd@2,2'-biphenol@Co/C **5d**, **5a-γ** was further investigated due to its successful application in the Suzuki-Miyaura coupling carried out by a former colleague, Sara Ranjbar, utilizing **5a-γ** with 0.43 wt% Pd.^[115] The Pd-catalyzed cross-couplings of boronic acids with aryl iodides as well as bromides were performed in a mixture of ethanol/water (1:1), however, solely harsh microwave conditions (110 °C) were tested.

S. Ranjbar, 2016:



Scheme 10. Preliminary results applying **5a-γ** (0.43 wt% Pd). Results are taken from PhD thesis of S. Ranjbar.^[115]

The third palladium-loaded magnetic material was synthesized combining the aforementioned advantages of utilizing *N*-heterocyclic carbenes as ligands with an additional trapping effect of polystyrene network. In 2012, Reiser *et al.*^[47] reported a palladium NHC-pincer complex **17** supported onto polystyrene-modified carbon-coated iron nanoparticles (Figure 25) for the microwave-assisted Suzuki-Miyaura coupling with fixed power of 200 W, corresponding to temperatures up to 140 °C. Furthermore, the recycling of the catalyst was carried out at lower temperatures of 70 °C, showing no loss in activity over six cycles for the coupling of phenylboronic acid **9** with 4-bromoanisole **14b** (> 95% conversion, 12 hours). During the recycling process, the formation of palladium nanoparticles, trapped within the polystyrene matrix, was observed *via* TEM analysis after the first cycle (left image, Figure

25). After four cycles (right image, Figure 25), an enrichment of the nanoparticles was determined without an increase in size, suggesting a good stabilizing effect of the polymer from metal leaching.

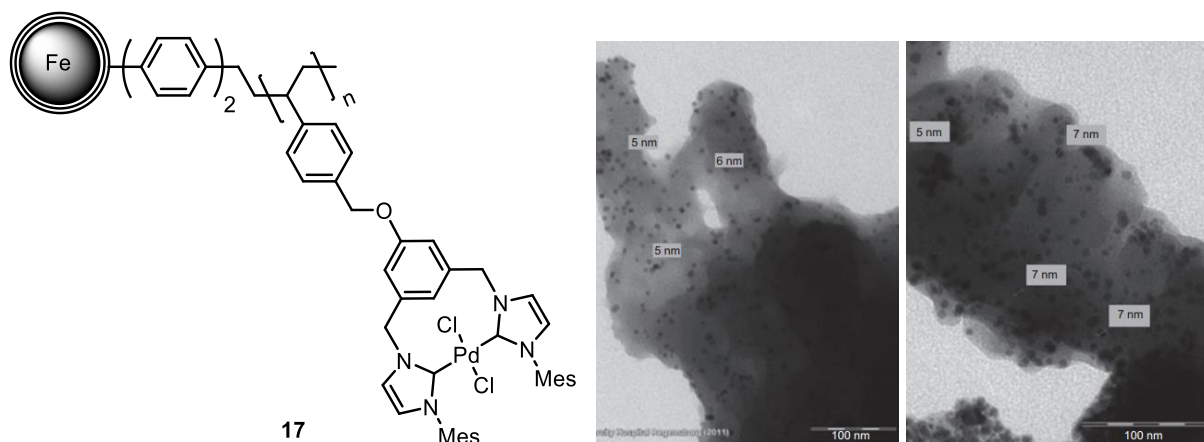


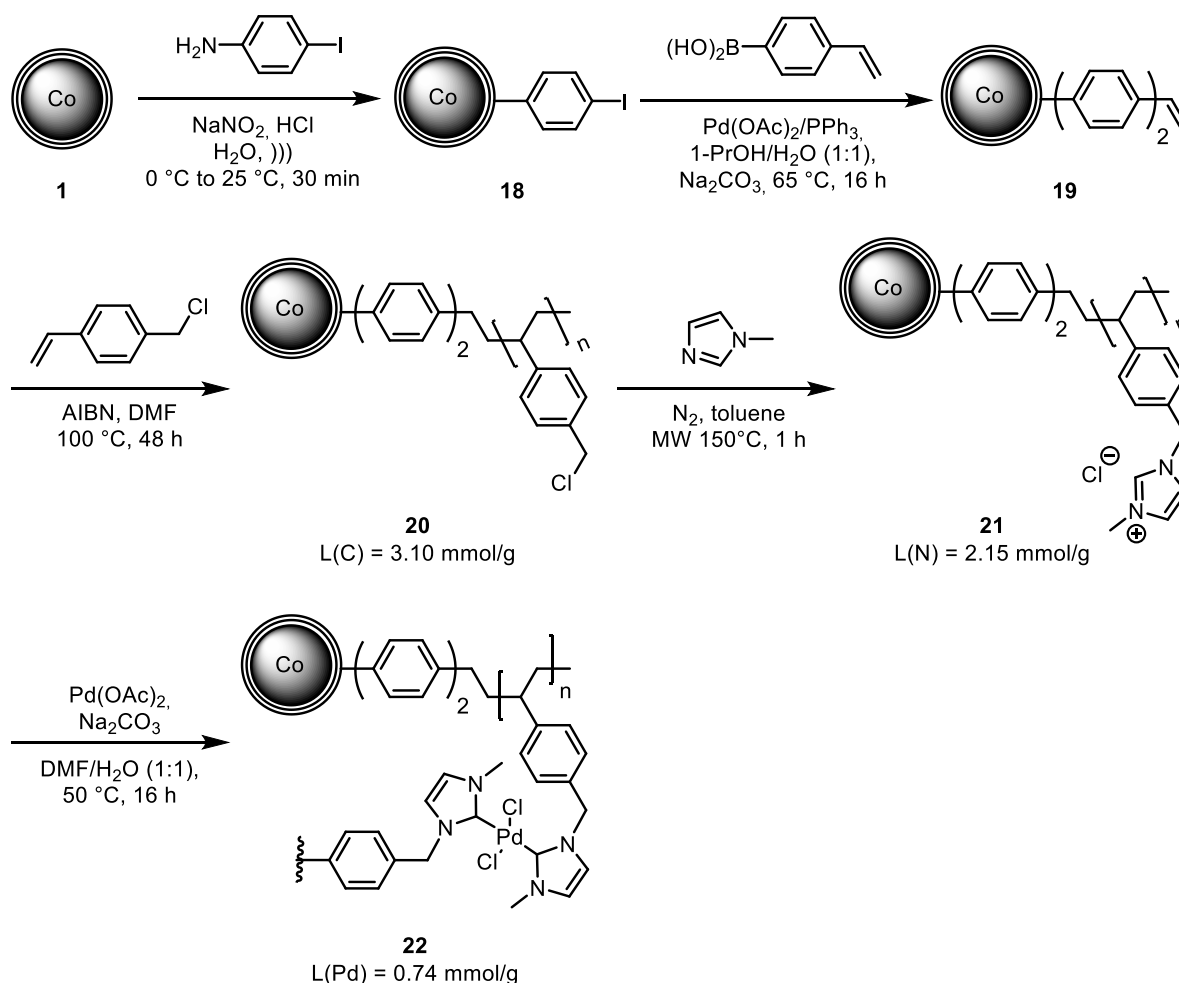
Figure 25. Palladium NHC-pincer complex **17** and TEM images of the recycled catalyst after one (left side) and after four (right side) reaction cycles of the Suzuki-Miyaura cross-coupling at 70 °C (conventional heating), showing Pd NPs of 5-7 nm in the polystyrene network. Reprinted from [47]. De Gruyter 2012, licensed under CC BY-NC-ND 3.0.

Another example for the successful application and recycling of Pd-NHC complexes is based on 1-methylimidazole as readily available NHC precursor.^[133] Therefore, Gao *et al.* examined superparamagnetic iron oxide (Fe₂O₃) nanocrystals with a thin layer of lightly cross-linked polystyrene as a platform for the immobilization of 1-methylimidazole, resulting in an efficient Pd-NHC-based complex. This catalyst showed good recyclability for the coupling of 4-iodotoluene and phenylboronic acid **9** at low temperatures (50 °C) for five runs (88% yield, 12 hours) in a mixture of water/DMF.

2.2.2. Synthesis of Pd-NHC complex immobilized onto carbon-coated cobalt nanoparticles

Combining the promising results of 1-methylimidazole, being sufficient to form active Pd-NHC complexes for the catalysis of the Suzuki-Miyaura coupling at low temperatures, with the high functionalization potential of polystyrene-based supports, polystyrene-coated Co/C nanoparticles **20** were synthesized. According to the literature protocol of Reiser *et al.*,^[46] pristine Co/C nanobeads **1** were tagged with iodobenzene moieties *via* diazonium chemistry to yield **18** (Scheme 11). Subsequent coupling with 4-vinylphenylboronic acid by a palladium-catalyzed Suzuki cross-coupling reaction obtained vinyl-functionalized Co/Cs **19**.^[134] Polymerization of 4-(chloromethyl)styrene on vinylbiphenyl@Co/C **19** in presence of AIBN gave rise to poly(benzyl chloride) styrene nanoparticles PS-Cl@Co/C **20** with a high polymer loading of 3.10 mmol·g⁻¹ based on the carbon content derived from elemental analysis.^[46] Next, methyl imidazole was immobilized onto the polystyrene network *via* microwave reaction at 150 °C to yield the ionic liquid (IL) supported polystyrene nanoparticles PS-IL@Co/C **21**.^[69] However, after 30 minutes reaction time, incomplete conversion was observed based

on the nitrogen loading, corresponding to roughly 55% substituted chloride. By prolonging the reaction time to 60 minutes, PS-IL@Co/C **21** could be achieved with an IL loading of $2.15 \text{ mmol}\cdot\text{g}^{-1}$. This loading was in good agreement with the literature value of $2.1 \text{ mmol}\cdot\text{g}^{-1}$ reported by Reiser *et al.*^[69] Finally, the imidazolium groups were deprotonated with the aid of Na_2CO_3 to generate the NHCs followed by complexation of Pd(II), according to the adapted protocol from Lee^[135] and Gao *et al.*^[133] ICP-OES analysis revealed a palladium content of $0.74 \text{ mmol}\cdot\text{g}^{-1}$ with a ligand loading of $1.42 \text{ mmol}\cdot\text{g}^{-1}$ for **22**, based on nitrogen elemental analysis, suggesting that the synthesized material is almost quantitatively available as Pd(II) complex as depicted in Scheme 11.



Scheme 11. Synthesis of Pd(II)@PS-NHC@Co/C **22**.)) = ultrasound.

Besides the calculations based on elemental analysis and ICP-OES, the synthesis of Pd(II)@PS-NHC@Co/C **22** was further pursued by attenuated total reflection infrared (ATR-IR) spectroscopy in Figure 26. The conversion of poly(benzyl chloride) styrene nanoparticles **20** to **21** was confirmed by the vanishing of the characteristic benzyl chloride peak at 1264 cm^{-1} as well as the definite appearance of peaks at 1156 cm^{-1} (C-N) and $3500\text{-}3200 \text{ cm}^{-1}$ (O-H, caused by the hygroscopic ionic liquid). The

absence of the H₂O-band in the spectra of **22** further verified the successful formation of Pd-NHC complexes. XPS studies indeed revealed Pd(II) as predominant oxidation state.

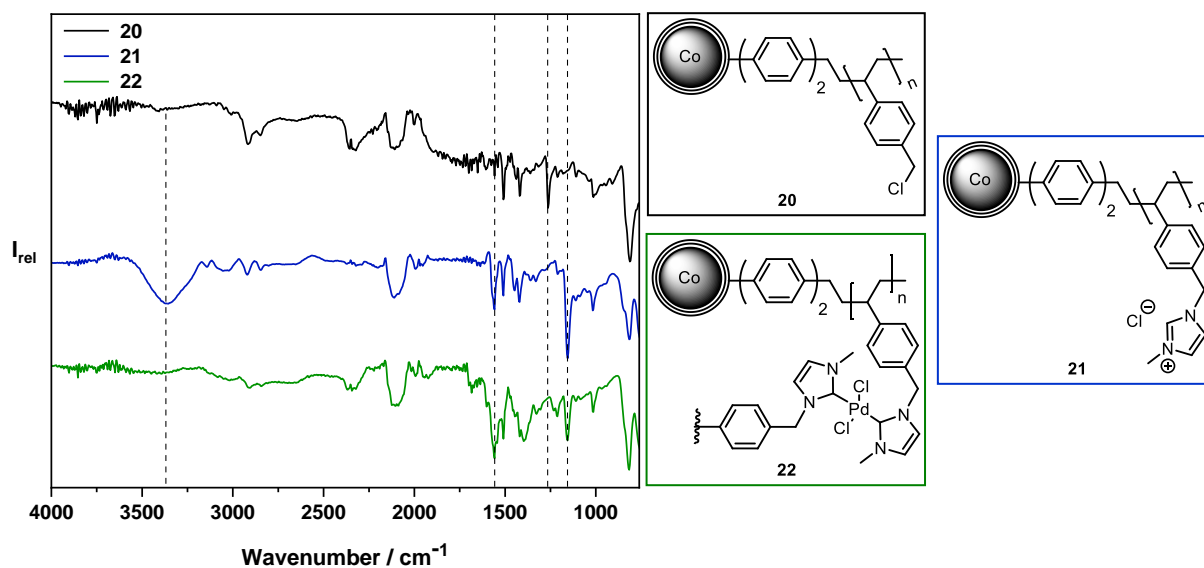


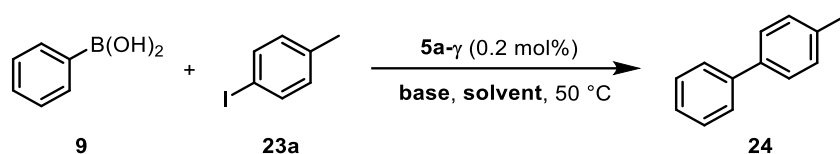
Figure 26. Comparison of ATR-IR spectra of **20** (top), **21** (middle), and **22** (bottom).

2.3. Application of the magnetic Co/C nanocatalysts in the Suzuki-Miyaura coupling

2.3.1. Screening of reaction conditions for the Pd-catalyzed cross-coupling

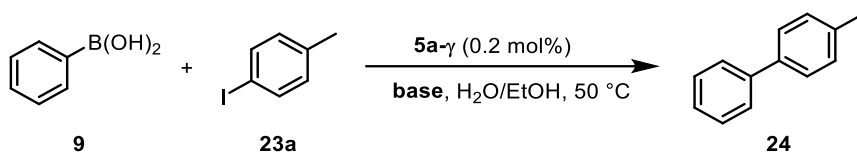
Based on the publications of Ding,^[136] Paegel,^[137] and Satz^[138] concerning DNA-compatible reaction conditions and in consultation with Dr. Brunschweiler (TU Dortmund), temperatures up to 50 °C as well as the listed aqueous solvent mixtures and bases in Table 8 were considered to be tolerable for the preliminary screening experiments.

Having settled for water/ethanol (1:1) as solvent (entry 4), suitable bases like carbonates and organic bases were tested. Potassium carbonate and *N,N*-diisopropylethylamine (DIPEA) gave the best results with a slightly higher yield using potassium carbonate (entries 9 and 10). To further evaluate this investigation, recycling studies were carried out to give an insight into the differences in activity and metal leaching. During the recycling in Table 9, potassium carbonate was clearly superior to DIPEA by means of activity in the first cycle (entries 1 and 6) as well as its reusing potential (entries 1-5 and 6-7). This was further confirmed by ICP-OES analysis, showing a high loss of palladium of 33% within only two cycles using DIPEA. However, also in the case of potassium carbonate the activity dropped after the first cycle from 81% to 49% yield. Within the next runs, the yield further decreased to roughly 20% yield, along with an overall high Pd loss of 31% (entries 1-5), which might be the reason for the decrease.

Table 8. Solvent and base screening of the Suzuki-Miyaura coupling with catalyst **5a-γ**.

| Entry | Solvent | Base | Time [min] | Yield [%] |
|-------|-----------------------|---------------------------------|------------|-----------|
| 1 | H ₂ O | Na ₂ CO ₃ | 30 | 4 |
| 2 | H ₂ O/NMP | Na ₂ CO ₃ | 30 | traces |
| 3 | H ₂ O/MeCN | Na ₂ CO ₃ | 30 | 28 |
| 4 | H ₂ O/EtOH | Na ₂ CO ₃ | 30 | 34 |
| 5 | H ₂ O/EtOH | NaHCO ₃ | 15 | 2 |
| 6 | H ₂ O/EtOH | K ₂ HPO ₄ | 15 | 5 |
| 7 | H ₂ O/EtOH | NEt ₃ | 15 | 18 |
| 8 | H ₂ O/EtOH | Na ₂ CO ₃ | 15 | 25 |
| 9 | H ₂ O/EtOH | K ₂ CO ₃ | 15 | 30 |
| 10 | H ₂ O/EtOH | DIPEA | 15 | 27 |

Reaction conditions: 0.50 mmol 4-iodotoluene **23a**, 0.75 mmol phenylboronic acid **9**, 1.0 mmol base and **5a-γ** with L(Pd)=2.3 wt% Pd (0.2 mol%, 5.6 mg, 1 μmol) at 50 °C in 4 mL solvent (1:1).

Table 9. Recycling studies of catalyst **5a-γ** using DIPEA or potassium carbonate as base.

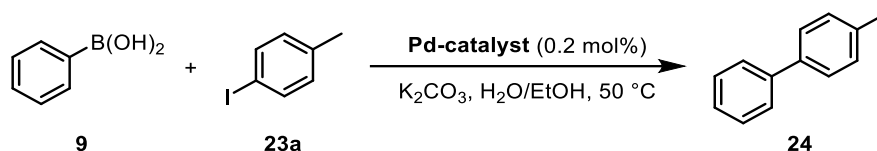
| Entry | Cycle | Base | Time [min] | Yield [%] | Pd [ppm] | Co [ppm] |
|-------|-------|--------------------------------|------------|-----------|----------|----------|
| 1 | 1 | K ₂ CO ₃ | 80 | 81 | 80 | 145 |
| 2 | 2 | K ₂ CO ₃ | 80 | 49 | 76 | 32 |
| 3 | 3 | K ₂ CO ₃ | 80 | 36 | 32 | 155 |
| 4 | 4 | K ₂ CO ₃ | 80 | 18 | 14 | 60 |
| 5 | 5 | K ₂ CO ₃ | 80 | 23 | 77 | 105 |
| 6 | 1 | DIPEA | 120 | 58 | 109 | 21 |
| 7 | 2 | DIPEA | 120 | 34 | 149 | 698 |

Reaction conditions: 0.50 mmol 4-iodotoluene **23a**, 0.75 mmol phenylboronic acid **9**, 1.0 mmol base and **5a-γ** with L(Pd)=2.3 wt% Pd (0.2 mol%, 5.6 mg, 1 μmol) at 50 °C in 4 mL H₂O/EtOH (1:1).

Based on the recycling and metal leaching in Table 9, catalyst **5a-γ** was considered to be not suitable for the recycling in the Suzuki-Miyaura cross-coupling, thus the aforementioned palladium systems Pd@PEI@Co/C **11** and Pd(II)@PS-NHC@Co/C **22** were explored in the cross-coupling of phenylboronic acid **9** with 4-iodotoluene **23a** (Table 10). In order to make a statement on the impact of the applied catalysts on the activity, the reaction time was reduced to 40 minutes for all catalysts. Applying catalyst

22, almost full conversion could be achieved with a low palladium loss (< 3% Pd) and moderate cobalt contamination of 29 ppm (entry 2). Due to the high Pd loading of 6.6 wt% Pd for **22**, only 3.3 mg catalyst were required for 0.2 mol% compared to 11 mg of **5a-γ**. Surprisingly, Pd@PEI@Co/C **11** with a good water dispersibility, as a result of the high amino-functionalization degree, showed almost no activity in the cross-coupling reaction under these mild conditions. Since the yield was below 5%, the metal contamination was not determined.

Table 10. Screening of the Suzuki-Miyaura coupling with catalysts **5a-γ**, **22**, and **11**.



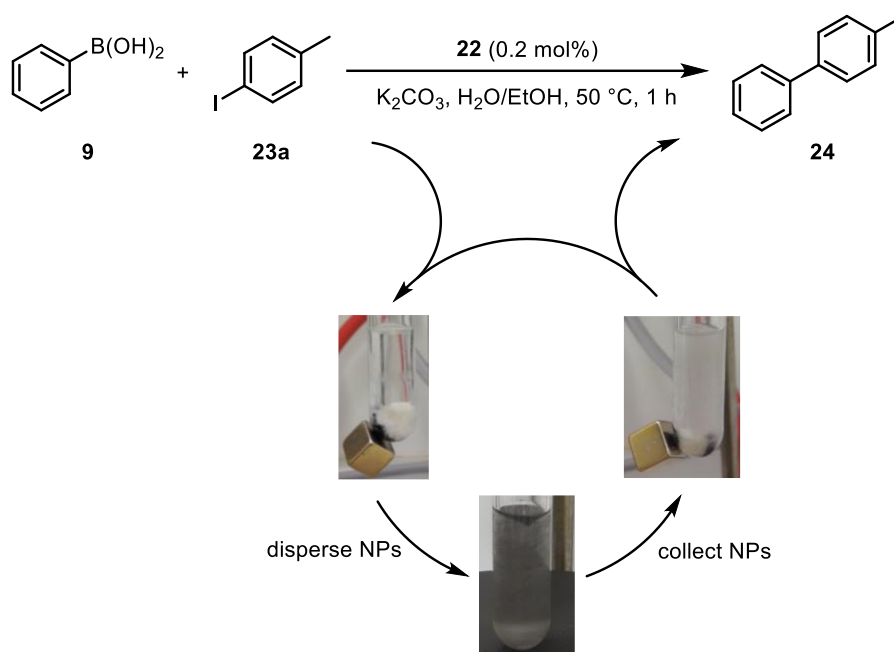
| Entry | Catalyst | Time [min] | Yield [%] | Pd [ppm] | Pd [%] | Co [ppm] |
|-------|---------------------------------|------------|-----------|-------------|-------------|-------------|
| 1 | 5a-γ (1.9 wt% Pd), 11 mg | 40 | 44 | 121 | 13 | 274 |
| 2 | 22 (6.6 wt% Pd), 3.3 mg | 40 | 83 | 24 | 2.6 | 29 |
| 3 | 11 (4.5 wt% Pd), 4.4 mg | 40 | 4 | <i>n.d.</i> | <i>n.d.</i> | <i>n.d.</i> |

Reaction conditions: 1.0 mmol 4-iodotoluene **23a**, 1.5 mmol phenylboronic acid **9**, 2.0 mmol K_2CO_3 and Pd-catalyst (0.2 mol%, 2 μmol) at 50 °C in 4 mL $\text{H}_2\text{O/EtOH}$ (1:1); *n.d.*: not determined.

2.3.2. Recycling studies with Pd(II)@PS-NHC@Co/C **22**^{§§}

With the optimized reaction conditions and the most promising catalyst **22** in hands, the focus turned to its recyclability. Therefore, **22** was recycled six times using 4-iodotoluene **23a** and phenylboronic acid **9** according to the protocol depicted in Table 11. The catalyst showed no loss in activity within two runs, however, during the next four cycles, the yield dropped to an average of 50%. Having a closer look at the ICP-OES values, the low palladium leaching of overall 7% within the six runs suggested a good palladium stabilization and trapping effect from the polymer. Thus, rather a deactivation of the palladium or a decline in diffusion and mass transfer of the polymer were considered to be the reason for the diminished recyclability.

^{§§} Results are partially taken from the Bachelor thesis of M. A. Pertl (supervised by L. Stadler).

Table 11. Recycling studies of Pd-catalyst **22** at 50 °C.

| Cycle | Conversion [%] | Yield [%] | TOF [h^{-1}] | Pd [ppm] | Co [ppm] |
|-------|----------------|-----------|------------------|----------|----------|
| 1 | 93 | 91 | 455 | 18 | 6 |
| 2 | 100 | 99 | 495 | 7 | 3 |
| 3 | 72 | 58 | 290 | 4 | 3 |
| 4 | 57 | 42 | 210 | 3 | 3 |
| 5 | 56 | 42 | 210 | 17 | 5 |
| 6 | 72 | 60 | 300 | 3 | 3 |

Reaction conditions: 0.50 mmol 4-iodotoluene **23a**, 0.75 mmol phenylboronic acid **9**, 1.0 mmol K_2CO_3 and **22** with $L(Pd)=6.6$ wt% Pd (0.2 mol%, 3.3 mg, 2 μ mol) at 50 °C in 4 mL $H_2O/EtOH$ (1:1) for 60 minutes.

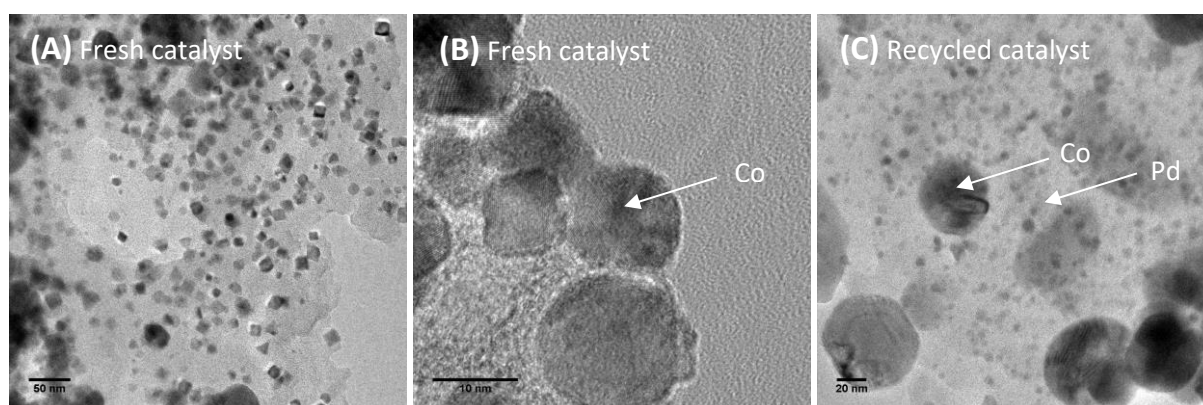


Figure 27. TEM images of the catalyst **22**: (A),(B) before (fresh catalyst: showing Co/C NPs with polymer) and (C) after four recycling runs at 50 °C. Palladium nanoparticles are formed with an average size of 5 nm in the right image (C).

Taking into account that the magnetically Pd-NHC-pincer complex **17** in chapter 2.2.1 showed a uniform Pd nanoparticle formation without loss in activity during the recycling (Figure 25), TEM

analysis of the recycled catalyst **22** was carried out. Indeed, Figure 27 revealed Pd nanoparticles with an average size of 5 nm being in accordance with the before discussed investigations of Reiser *et al.*^[47] Bearing in mind, that the palladium nanoparticle formation from NHC complexes is a thermodynamically driven reaction, the reactivity and behavior of the catalyst were tested for the recycling at room temperature (22 °C to 33 °C, depending on each the cycle). However, even prolonging the reaction time to 22 hours did not achieve full conversion of the starting material, resulting in moderate yields of 51±4% for **24** (Table 12). The combined palladium leaching over the ten cycles was only 2% as determined by ICP-OES. Again TEM micrographs of the recycled catalyst **22** were recorded (Figure 28). This time, the number of Pd nanoparticles was apparently less, even after the ten cycles, confirming the presumption.

Table 12. Recycling of catalyst **22** in the Suzuki-Miyaura coupling of **23a** with **9** at room temperature.

| Cycle | Yield [%] | TOF [h ⁻¹] | Pd [ppm] | Co [ppm] |
|-------|-----------|------------------------|----------|----------|
| 1 | 56 | 13 | 2 | 2 |
| 2 | 54 | 12 | 4 | 1 |
| 3 | 50 | 11 | 3 | 1 |
| 4 | 50 | 11 | 3 | 1 |
| 5 | 51 | 12 | 1 | 1 |
| 6 | 47 | 11 | 2 | 1 |
| 7 | 45 | 10 | 6 | 1 |
| 8 | 56 | 13 | 5 | 1 |
| 9 | 51 | 12 | 3 | 2 |
| 10 | 45 | 10 | 4 | 1 |

Reaction conditions: 0.50 mmol 4-iodotoluene **23a**, 0.75 mmol phenylboronic acid **9**, 1.0 mmol K₂CO₃ and **22** with L(Pd)=6.6 wt% Pd (0.2 mol%, 3.3 mg, 2 μmol) at room temperature (22-33 °C) in 4 mL H₂O/EtOH (1:1) for 22 hours.

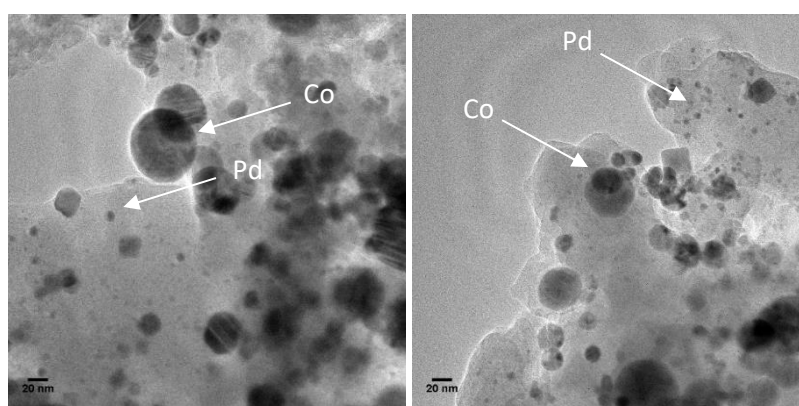
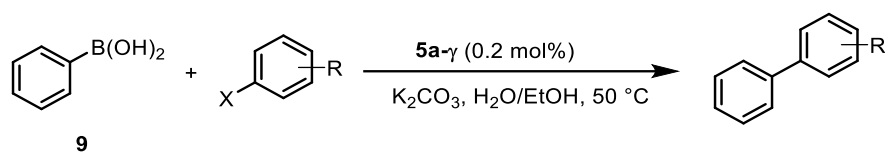


Figure 28. TEM images of the catalyst **22** after ten cycles at room temperature. A moderate quantity of palladium nanoparticles is apparent with an average size of 5 nm.

However, considering the higher turnover frequencies at 50 °C combined with a complete conversion of the starting materials in the first cycles as more important than steady recyclability, the substrate scope was evaluated at the enhanced temperature of 50 °C. To benefit from the purpose of an easily separable catalyst by magnetic decantation, these substrates were examined during the recycling, too. As a reference, the last substrate was 4-iodotoluene **23a** to guarantee better comparability with the above-described recycling. In Table 13, aryl iodides (**14a**, **25a**, **27a**, **23a**) and the corresponding aryl bromides (**14b**, **25b**, **27b**, **23b**) were investigated with representative examples for an electron-withdrawing (entry 1), electron-deficient (entry 2), and sterically more demanding substrate (entry 3). Within 60 minutes and 3 hours, respectively, 4-iodoanisole **14a** and 4-bromoanisole **14b** could be successfully coupled with phenylboronic acid **9** to yield **16** in excellent yields up to 97%. In the second cycle, again 1-iodo-4-nitrobenzene **25a** and **25b** gave almost the same high yields, showing that the catalyst **22** is suitable for electron-withdrawing (cycle 1) as well as electron-donating substrates (cycle 2). However, applying 1-iodonaphthalene **27a** in the third cycle, resulted in a moderate yield of 54% of **28** compared to 17% using the bromide-analog **27b**. To examine if this difference in yield is reasoned by a possible deactivation caused by the aryl bromides, the fourth cycle was carried out aiming for 4-methyl-1,1'-biphenyl **24**, which was extensively investigated previously in the recycling studies. Since the expected yields of 50 to 60% were achieved with the four times recycled catalyst, a possible deactivation by aryl bromides was excluded. Overall, three to ten times higher turnover-frequencies could be achieved for the aryl iodides compared to the bromide-analogs, which is in accordance with the literature. However, **22** was capable to couple the aryl bromides with prolonged reaction times without the need for harsher reaction conditions like higher temperatures.

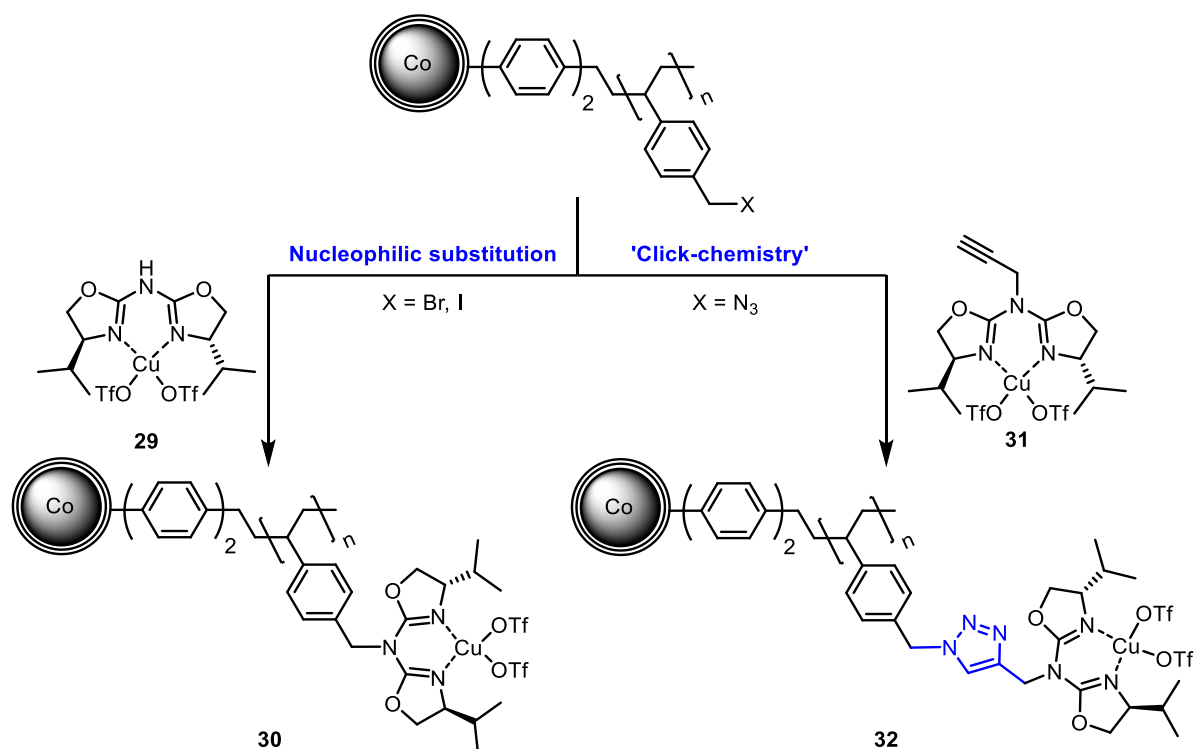
Table 13. Exploring the substrate scope during recycling of catalyst **22** at 50 °C.

| Cycle | Aryl halide | Product | Yield [%] | | TOF [h ⁻¹] | |
|-------|-----------------------------------------|---------------|-----------|--------|------------------------|--------|
| | | | X = I | X = Br | X = I | X = Br |
| 1 | 14a: X=I 14b: X=Br | 16 | 97 | 96 | 485 | 160 |
| 2 | 25a: X=I 25b: X=Br | 26 | 94 | 93 | 470 | 155 |
| 3 | 27a: X=I 27b: X=Br | 28 | 56 | 17 | 280 | 28 |
| 4 | 23a: X=I 23b: X=Br | 24 | 52 | 61 | 260 | 102 |

Reaction conditions: 1.0 mmol aryl halide, 1.1 mmol phenylboronic acid **9**, 2.0 mmol K₂CO₃ and **22** with L(Pd)=6.6 wt% Pd (0.2 mol%, 3.3 mg, 2 μmol) at 50 °C in 4 mL H₂O/EtOH (1:1) for 60 minutes (X=I) or 3 hours (X=Br).

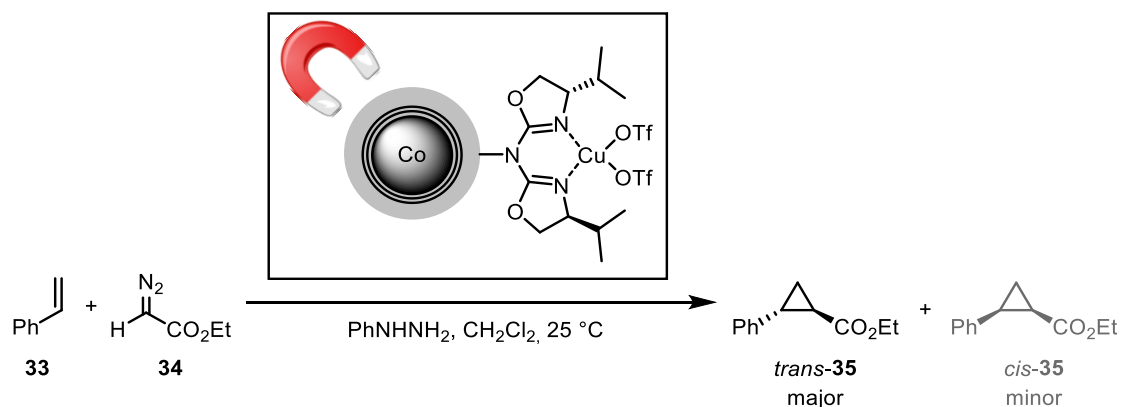
In summary, preliminary studies revealed an efficient magnetically recoverable Pd(II)-catalyst for the Suzuki-Miyaura cross-coupling at low temperatures. In particular, it was shown that also aryl bromides could be employed as substrates without the demand for harsher reaction conditions. Thus, palladium(II) NHC-functionalized catalyst Pd(II)@PS-NHC@Co/C **22** was considered to be worthwhile for further investigation in its application towards generating a genetically-tagged small molecule libraries, conducted by the working group of Dr. Brunschweiler at the TU Dortmund.

3. Recyclable aza-bis(oxazoline) ligands for the asymmetric cyclopropanation



Scheme 12. General overview of the synthesis of recyclable aza-bis(oxazoline) ligands *via* the two applied linking strategies.

Chiral copper(II)-aza-bis(oxazoline) complexes were immobilized onto polystyrene-functionalized magnetic Co/C nanobeads *via* two different linking strategies. On the one hand, a nucleophilic substitution achieved direct linking of the ligands to the polystyrene system, on the other hand, azide-functionalized nanoparticles were investigated for the grafting *via* a copper(I)-catalyzed azide-alkyne cycloaddition (CuAAC), resulting in triazole units as a linker. In addition, the effect of a high polymer loading in relation to a low functionalization degree of the synthesized materials was compared regarding its recyclability and selectivity using styrene and ethyl diazoacetate as cost-efficient starting materials with a straightforward analysis by gas chromatography.



Scheme 13. Recyclable aza-bis(oxazoline) ligands for the application in asymmetric copper-catalyzed cyclopropanations.

3.1. Immobilization of aza-bis(oxazoline) ligands for the Cu(I)-catalyzed cyclopropanation

The copper-catalyzed generation of optically active cyclopropane derivatives from achiral olefins and diazo compounds represents the first enantioselective, intermolecular cyclopropanation, published back in 1966 by Nozaki and co-workers.^[139] Even though the observed enantioselectivity was low, these results underlined that a homogenous metal catalyst can provide enantioselectivity by the complexation to a chiral ligand. Based on this general concept, an extensive effort was undertaken to enhance the enantioselectivity of this reaction. Among the most essential achievements for the asymmetric copper-catalyzed cyclopropanation was the development of the semicorrin **36**^[140] and aza-semicorrin **37**^[141] ligands by Pfaltz *et al.* and the bis(oxazolines) (BOX) **38** by Masamune *et al.*^[142] and Evans *et al.*^[143] (Figure 29). Worth to mention, the basis for the development of the BOX ligands **38** was made by Brunner *et al.*^[144] in 1989, who disclosed chiral oxazolines, namely pyridinyloxazoline, for the asymmetric catalysis.

In the Reiser group, chiral aza-bis(oxazoline) (azaBOX) **39**^{[145],[146]} ligands have been established as a reasonable alternative to the related C₂-symmetrical semicorrins **36**, aza-semicorrins **37**, and bis(oxazolines) **38**. A variety of successful approaches utilizing **39** ligands for the asymmetric Cu(I)-cyclopropanation were examined.^{[147],[148]–[150]} **39**-Type ligands combine the advantage of an easy preparation from readily available amino alcohols, analogous to **38**, with a high degree of diversity due to the central nitrogen atom, which can be readily functionalized similar to **37**, making them attractive for the immobilization on various supports.^{[72],[151],[152],[153]} Additionally, theoretical calculations and appropriate catalytic experiments showed a higher coordination ability of azaBOX **39** ligands than their corresponding BOX **38** analogs and thus a reduced tendency for metal leaching, which in turn enhances the potential for a suitable immobilization.^[154]

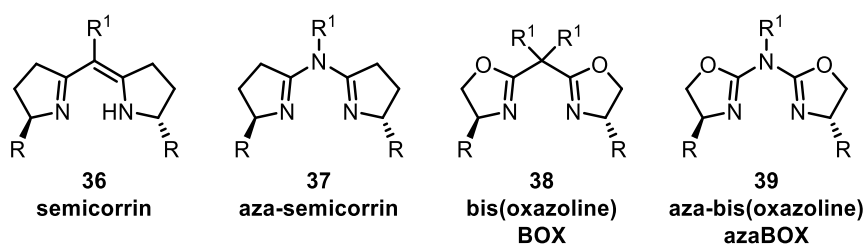


Figure 29. General chemical structures of different ligands **36–39** for the asymmetric catalysis.

Together with the implementation of azaBOX as a new class of chiral ligands for the enantioselective copper(I)-catalyzed cyclopropanation in 2000, Glos and Reiser^[145] also published a polymer-bound version of **39**. This demonstrates the high functionalization potential of these types of ligands. Methoxypoly(ethylene glycol) (MeOPEG 5000) was chosen as semi-homogeneous support for the immobilization of *tert*-butyl azaBOX ligand ^tBu-**39**. To achieve the desired attachment to the polymer, MeOPEG needed to be modified with benzylidene as a spacer to result in **43** (Figure 30). The

performance of this newly synthesized, immobilized version of ^tBu-azaBOX **43** was evaluated in the asymmetric cyclopropanation and compared to the homogeneous ligands **37**, **38**, **40**, **41**, and **42**.

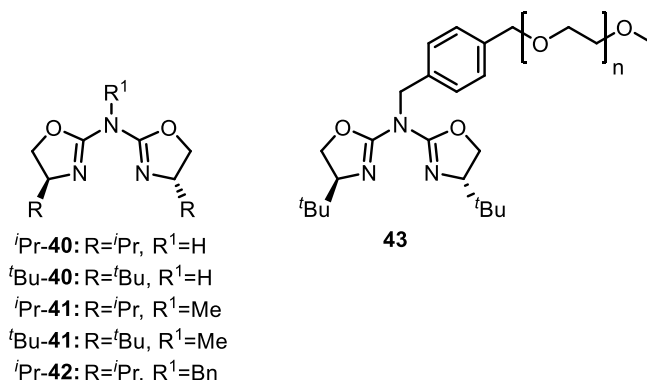
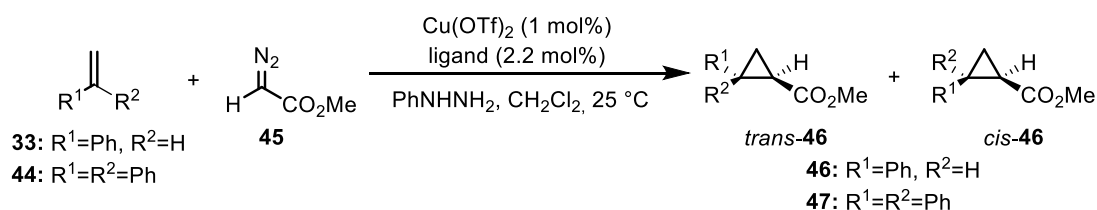


Figure 30. Homogeneous and immobilized chiral azaBOX ligands **40-43** employed in the enantioselective Cu(I)-catalyzed cyclopropanation reported by Glos and Reiser in 2000.^[145]

In the enantioselective cyclopropanation of styrene **33**, the best results could be obtained with ^tBu-**41** with 82% yield and 92% *ee* for *trans*-**46** and 87% *ee* for *cis*-**46** (Scheme 14). Noteworthy, the polymer-bound ligand **43** achieved similar results with 69% yield and an enantiomeric excess of 91% and 87%, respectively, proving that the support did not affect the selectivity of the catalyst. The recyclability of the immobilized catalyst was demonstrated over thirteen cycles with steady 87-90% *ee* for *trans*-**46**. Surprisingly, in the cyclopropanation of 1,1-diphenylethylene **44**, the polymer-bound catalyst **43** was significantly superior to the alkylated ligands **41** in both, yield and enantioselectivity (**47**: 78% yield, 90% *ee*).^{***} In this case, **43** could be reused for six cycles. While the enantioselectivity was good throughout the recycling (83 to 90% *ee*), the yield fluctuated considerably, with values between 36% and 80% for **47**. The comparable homogeneous ligand ^tBu-**38** (R = ^tBu, R¹ = Me) showed a slightly higher selectivity of 99% *ee* for **47** with a diminished yield of 70%. This time, however, reactivation of the catalyst **43** with phenylhydrazine was necessary for the recycling process before each cycle.

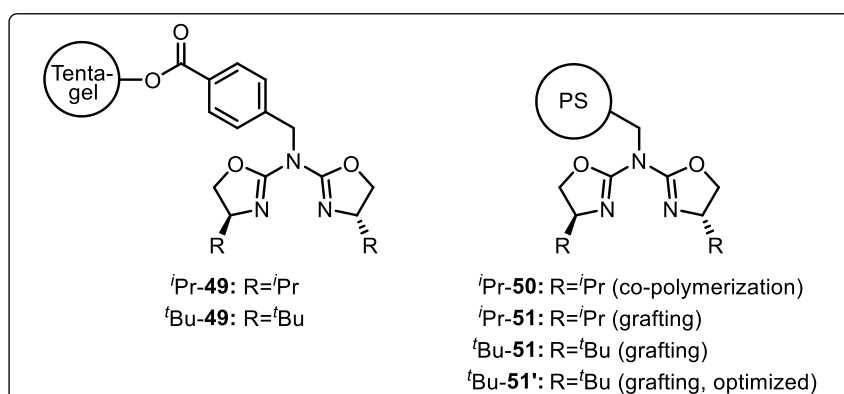
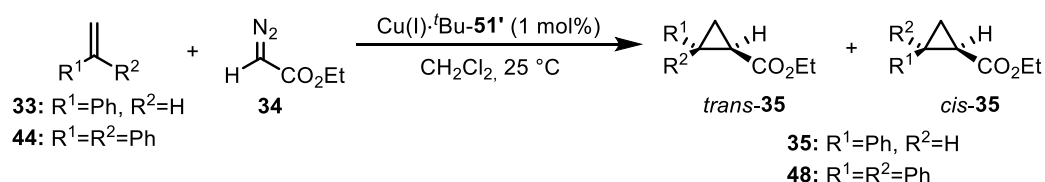


Scheme 14. Enantioselective Cu(I)-catalyzed cyclopropanation of styrene **33** and 1,1-diphenylethylene **44** with methyl diazoacetate **45**.

To improve the low ligand loading of **43** (0.05-0.1 mmol ligand per gram of polymer) and the necessity of an additional precipitation step to recover the catalyst, further investigations into insoluble supports

^{***} In this example, the homogeneous, non-alkylated ligand **40** was indeed superior to the alkylated **41**. This makes the best catalytic performance of the immobilized version **43** even more remarkable.

were conducted. An example of these efforts is shown in the joint publication of Mayoral and Reiser in 2006,^[152] where two different polymer-supports were examined. On the one hand, TentagelTM was utilized, obtaining the immobilized ligand **49**, depicted in Scheme 15, and on the other hand, a polystyrene network was functionalized *via* two different immobilization strategies. While the co-polymerization of a styryl-functionalized azaBOX ligand with styrene and divinylbenzene resulted in **50**, the grafting of the azaBOX ligand to a modified Merrifield resin gave **51** as immobilized polystyrene version. The prepared heterogeneous azaBOX-based ligands were compared regarding their efficiency in the copper-catalyzed enantioselective cyclopropanation of **33** and **44** to give *cis*-/*trans*-**46** and **47** (Scheme 14) and *cis*-/*trans*-**35** and **48** (Scheme 15), respectively. While the TentagelTM-based catalyst Cu(I)-**49** gave higher yields, the application of Cu(I)-**51** resulted in significantly improved enantioselectivities. The catalyst synthesized using the co-polymerization approach, Cu(I)-**50**, revealed inferior results compared to the grafting-method. Building upon the superior enantioselectivities derived with the ligand **51**, this Merrifield-based ligand was further developed to achieve a higher activity. So, the optimized catalyst Cu(I)-*t*Bu-**51'**, with a high ligand loading of 0.99 mmol·g⁻¹, subsequently demonstrated the best overall performance for the formation of **35** and **48** and further confirmed good recyclability. This immobilized azaBOX version even exceeded the best results obtained with homogeneous azaBOX ligands for the cyclopropanation of styrene **33** with ethyl diazoacetate **34** with yields up to 94% and 99% *ee* for *trans*-cyclopropane **35**, proving a beneficial effect of the immobilization.

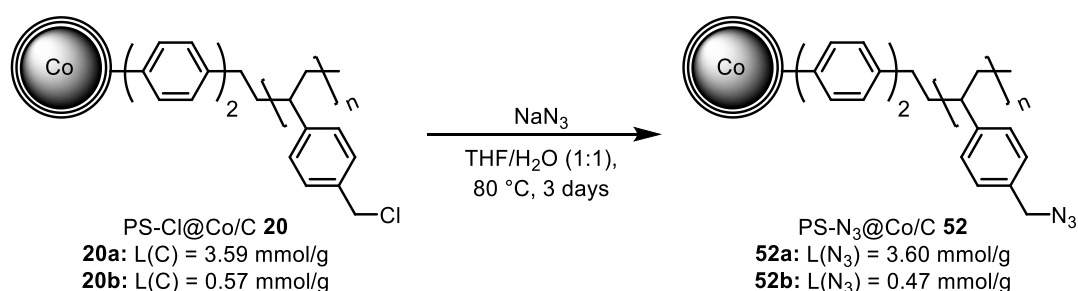


Scheme 15. Enantioselective Cu(I)-catalyzed cyclopropanation of styrene **33** and 1,1-diphenylethylene **44** with ethyl diazoacetate **34**.

3.2. Immobilization of aza-bis(oxazolines) onto magnetic Co/C nanoparticles

3.2.1. Synthesis via 'Click-chemistry'

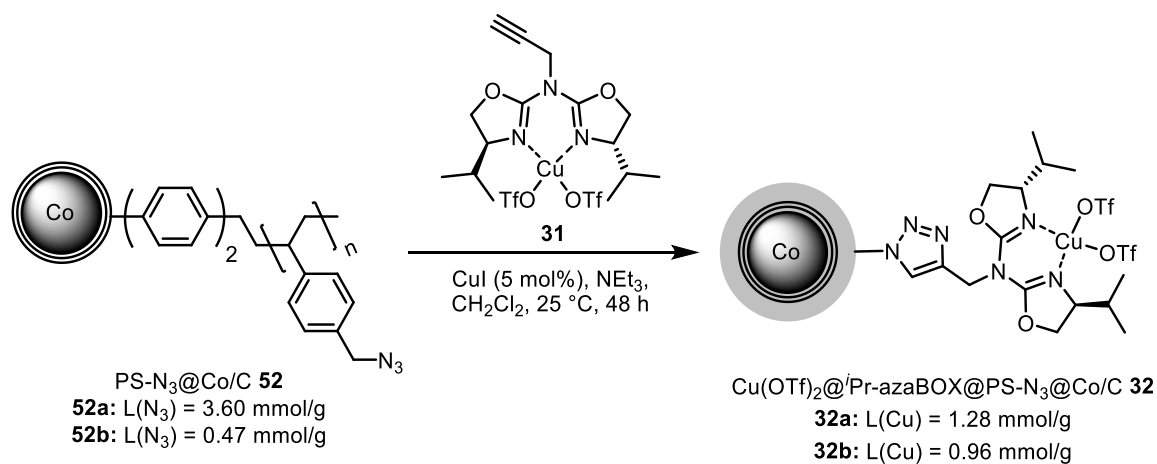
The idea of synthesizing a magnetic variation of chiral aza-bis(oxazoline) ligands for the copper-catalyzed cyclopropanation was based on the growing potential of cyclopropanated products,^[155] the ease of recyclability implicated by the Co/C nanoparticles, and the preceding successful application of magnetic azaBOX ligands for the kinetic resolution of 1,2-diols (Figure 10).^{[72],[151]} However, the ligand loading for the known magnetic azaBOX@Co/C NPs was quite low with $0.1 \text{ mmol}\cdot\text{g}^{-1}$, requiring 100 mg catalyst for a reaction with 1 mol% Cu on a 1 mmol scale. With regard to the model substrate (\pm)-1,2-diphenylethane-1,2-diol, almost 50 wt% of the nanocatalyst were necessary for 1 mol%. Thus, polystyrene-functionalized nanoparticles PS-Cl@Co/C **20** were used for preliminary studies to increase the maximum binding capacity. By using different reaction times for the polymerization of PS-Cl@Co/C **20**, two different carbon loadings (L (C)) could be achieved: **20a** with $3.59 \text{ mmol}\cdot\text{g}^{-1}$ (48 hours) and **20b** with $0.57 \text{ mmol}\cdot\text{g}^{-1}$ (18 hours). Having these polymers in hand, two common linking strategies for attaching ligands to the heterogeneous support were tested and compared regarding their effectiveness. Both methods were performed with high and low polymer loadings, respectively. For the copper-catalyzed azide-alkyne cycloaddition, an azide functionalized nanoparticle system needed to be synthesized first. Therefore, a literature-known strategy by Reiser *et al.*^[156] for the exchange of chloride for azide was used. With an excess of sodium azide a quantitative conversion to PS-N₃@Co/C **52a** with an azide loading calculated from the nitrogen elemental analysis of $L(\text{N}_3) = 3.60 \text{ mmol}\cdot\text{g}^{-1}$ and **52b** with $0.47 \text{ mmol}\cdot\text{g}^{-1}$ were obtained (Scheme 16).



Scheme 16. Conversion of PS-Cl@Co/C **20** to PS-N₃@Co/C **52**.

To 'click' the azide nanoparticles PS-N₃@Co/C **52a** and **52b** with an azaBOX ligand, (*S,S*)-Bis-(4-isopropyl-4,5-dihydrooxazol-2-yl)-prop-2-ynyl-amine **31** needed to be synthesized first. *i*Pr-**40** was deprotonated at $-78 \text{ }^\circ\text{C}$ with *n*-butyllithium, before adding propargylbromide to achieve the alkyne-tagged-azaBOX ligand in almost quantitative yield.^{[148],[151]} Then, the propargylated aza-bis(oxazoline) was complexed with copper(II) triflate to avoid undesired complexation of copper(I) iodide during the cycloaddition, obtaining ligand **31**. Additionally, this step was carried out due to the known beneficial effect of triflate as counterion^{[157],[158]} and, in turn, for better comparability with the catalysts

synthesized *via* the second route (direct nucleophilic substitution). PS-N₃@Co/C **52** was stirred with **31** and 5 mol% copper(I) iodide at ambient temperature to give rise to 1,2,3-triazoles substituted with the chiral catalysts and copper loadings of 1.28 mmol·g⁻¹ for **32a** and 0.96 mmol·g⁻¹ for **32b** (Scheme 17). Based on the metal contents determined by ICP-OES, 23% of the copper complex **31** were attached in the case of **32a** and 105% for **32b**. The too high value of 105% suggests undesired incorporation of copper(I) iodide, however, the linking worked excellent with 98% referring to the nitrogen elemental analysis of 0.46 mmol·g⁻¹. Additionally, the discrepancy of the high copper loading of 0.96 mmol·g⁻¹ in relation to a nitrogen loading of 0.46 mmol·g⁻¹ indicates that almost half of the copper was incorporated within the polymer and most likely coordinated at the 1,2,3-triazole units. For material **32a**, the loading of the chiral ligand of 1.20 mmol·g⁻¹ (33% occupancy) was in good agreement with the copper loading of 1.28 mmol·g⁻¹, considering the azaBOX ligand as predominant coordination center.



Scheme 17. CuAAC of PS-N₃@Co/C **52** with **31** to Cu(OTf)₂@ⁱPr-azaBOX@PS-N₃@Co/C **32**. The gray shell indicates the polystyrene polymer depicted on the left side.

The success of the reaction was further confirmed by ATR-IR spectroscopy in Figure 31. For the ease of recording and measuring, the materials **52a** and **32a** with high polymer and consequently high azide loadings are compared. Most prominent is the characteristic azide vibration at 2087 cm⁻¹ for **52a**, which is replaced by the predominant vibration at 1670 cm⁻¹ caused by the attached aza-bis(oxazoline) ligand of **32a**.

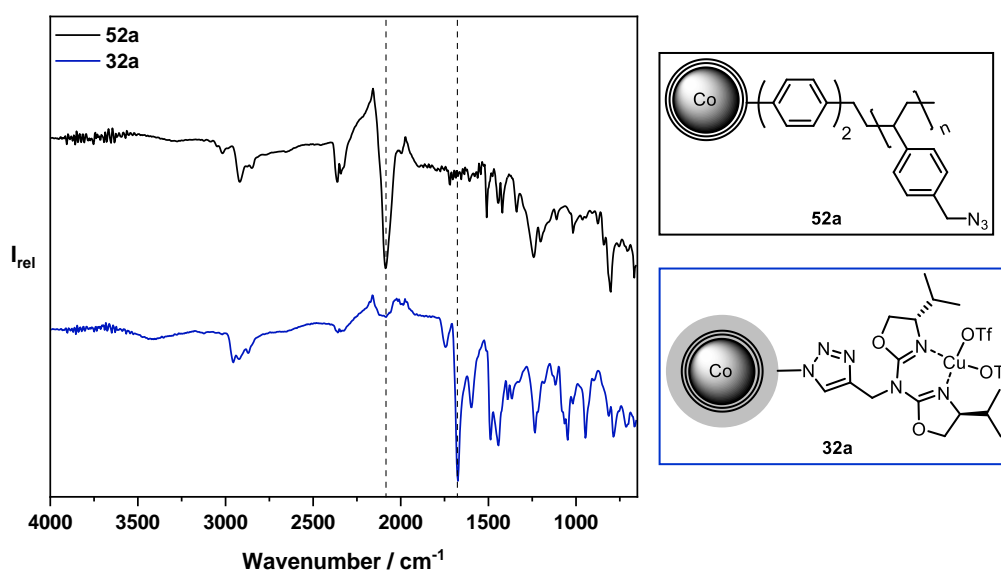
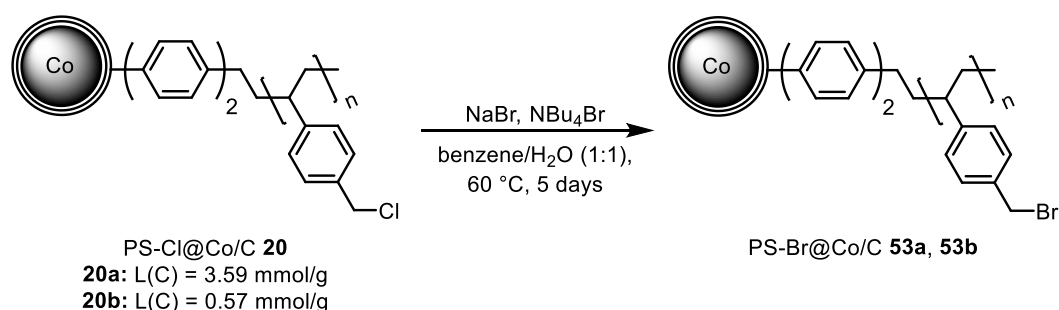


Figure 31. Comparison of ATR-IR spectra of **52a** (top) and **32a** (bottom).

3.2.2. Synthesis via nucleophilic substitution

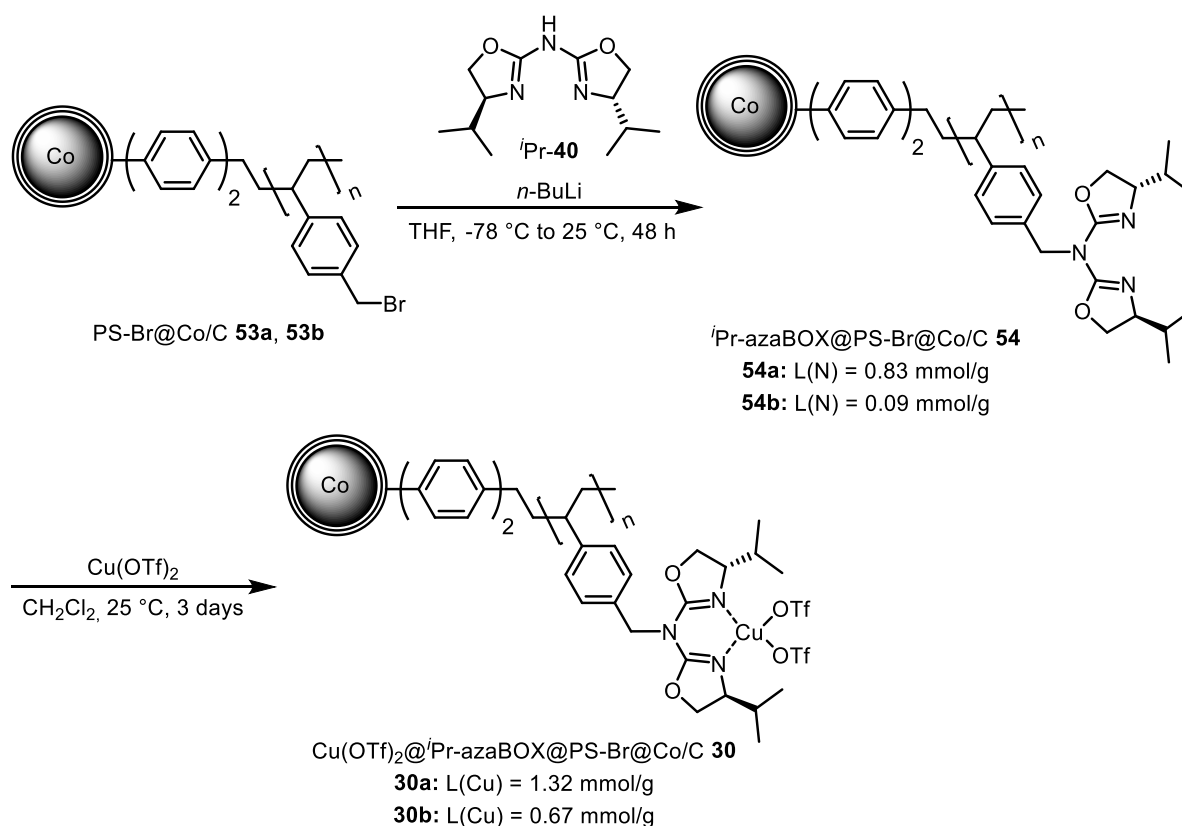
For the ⁱPr-azaBOX nanoparticles **30** which are directly linked to the polystyrene network *via* a nucleophilic substitution, the PS-Cl@Co/C **20** needed to be modified with better leaving groups. Therefore, the investigations of Reiser *et al.*^{[152],[159]} were explored for the initial studies. Werner demonstrated the need for a pre-activation of a Merrifield resin by the exchange to the bromide-analog, since benzylchloride itself showed no conversion for the substitution with ⁱPr-azaBOX **40**. Changing the chloride to bromide by a large excess of sodium bromide and tetra-*n*-butylammonium bromide (TBAB) in a suspension of water and benzene, offered the effective grafting of the chiral ligand to the polystyrene support. Following this procedure, PS-Cl@Co/C **20** was reacted with the aforementioned reagents at 60 °C for 5 days to obtain PS-Br@Co/C **53** (Scheme 18).



Scheme 18. Conversion of PS-Cl@Co/C **52** to PS-Br@Co/C **53**.

The monitoring of the reaction progress by the change of halide was not possible by elemental analysis at this time, so the received nanoparticles **53a** with a carbon loading of the precursor NPs of

3.56 mmol·g⁻¹ and a precursor loading of 0.57 mmol·g⁻¹ for **53b** were directly used for the next step. In Scheme 19, the nucleophilic substitution of PS-Br@Co/C **53a** and **53b** with ⁱPr-**40** to obtain the polystyrene-bound aza-bis(oxazolines) (ⁱPr-azaBOX@PS-Br@Co/C) **54a** and **54b** is depicted in the first step. The azaBOX-loadings were calculated based on the nitrogen amount of the elemental analysis. **54a** was obtained with a moderate linking rate of 23%, corresponding to 0.83 mmol·g⁻¹. In case of the bromide-precursor **53b** with an estimated low polymer loading, 0.09 mmol ligand were bound per gram of nanomaterial **54b** (19% conversion). Next, these polymers were complexed in a second step with copper(II) triflate to achieve **30a** with a copper loading of 1.32 mmol·g⁻¹ and **30b** with 0.67 mmol·g⁻¹ (Scheme 19).



Scheme 19. Nucleophilic substitution of PS-Br@Co/C **53** with ⁱPr-azaBOX **40** and subsequent complexation to yield Cu(OTf)₂@ⁱPr-azaBOX@PS-Br@Co/C **30**.

Again, the ATR-IR spectra in Figure 32 were taken comparing the high polymer loadings. **54a** shows various new signals between 800 and 1632 cm⁻¹ related to ⁱPr-azaBOX ligand **40** linked to the magnetic nanoparticles. Consequently, this approach worked as well, giving rise to chiral copper-complexed ligands directly attached to the magnetic polystyrene polymer without the need for any additional functional linking groups like triazole-moieties.

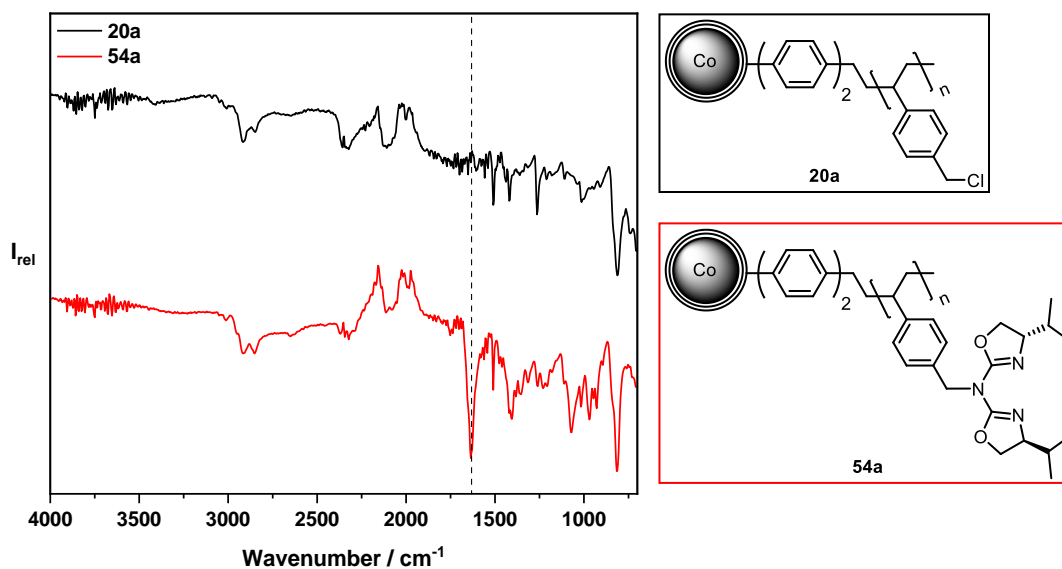
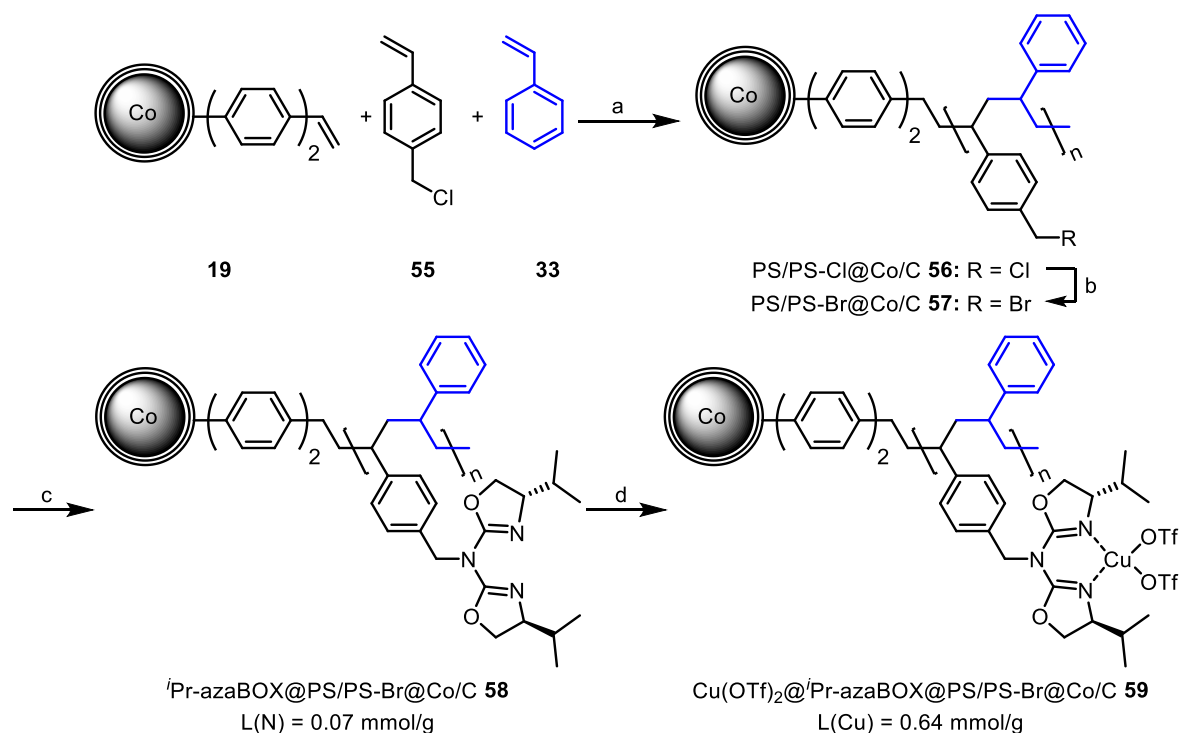


Figure 32. Comparison of ATR-IR spectra of **20a** (top) and **54a** (bottom).

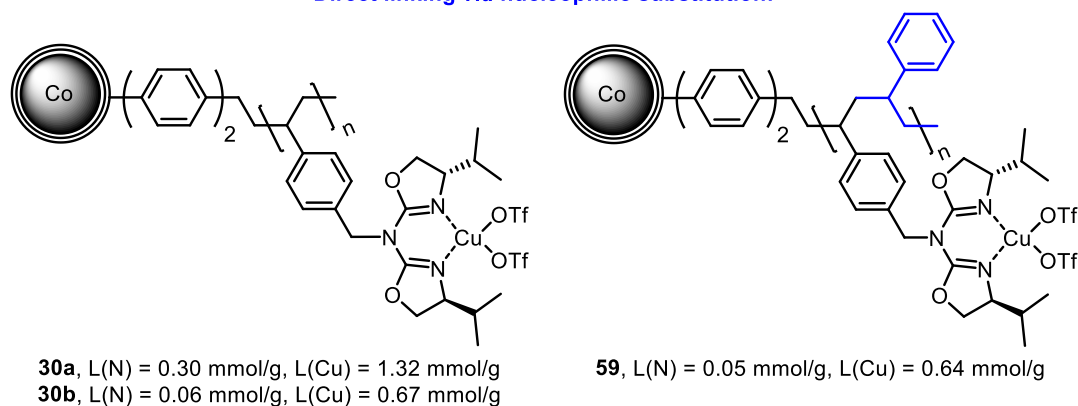
Based on the synthesis route *via* the nucleophilic substitution of benzylbromide, a polymerization reaction using 4-(chloromethyl)styrene **55** and styrene **33** with a ratio of 1 to 0.7 was performed, aiming for a polystyrene/benzylchloride co-polymer. In this manner, PS/PS-Cl@Co/C **56** could be synthesized with a carbon loading of 0.60 mmol·g⁻¹. The remaining steps up to the final copper-complexed **59** were carried out in a similar way to material **30** (Scheme 20).

For the sake of clarity, an overview of the final copper-complexed azaBOX ligands immobilized onto the magnetic polymers synthesized in this chapter is depicted in Figure 33, including the corresponding ligand loadings L(N) and copper loadings L(Cu) (calculated by elemental microanalysis and ICP-OES).



Scheme 20. Co-polymerization of vinylbiphenyl-coated Co/C nanoparticles **19** with subsequent conversion and complexation to **59**. *Reagents and conditions:* a) AIBN (5 mol%), DMF, 85 °C, 16 h; b) NaBr, NBu_4Br , benzene/ H_2O (1:1), 60 °C, 5 days; c) $i\text{Pr-azaBOX}$ **40**, $n\text{-BuLi}$, THF, -78 °C to 25 °C, 48 h; d) Cu(OTf)_2 , CH_2Cl_2 , 25 °C, 3 days.

Direct linking via nucleophilic substitution:



Linking via Click-chemistry (CuAAC):

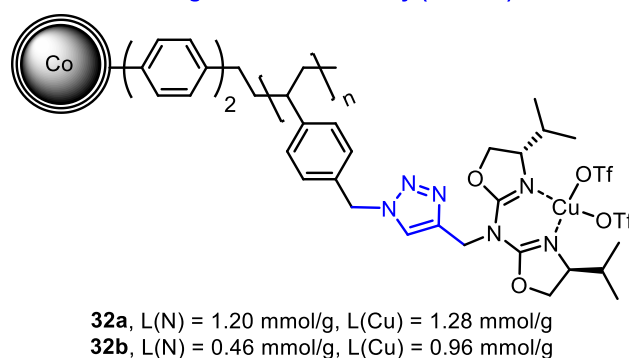


Figure 33. Overview of the synthesized copper-complexed nanomaterials.

3.3. Application of magnetic aza-bis(oxazolines) in the asymmetric cyclopropanation

The focus then turned to the application of the synthesized nanomaterials in the enantioselective cyclopropanation using styrene and ethyl diazoacetate as readily available and cheap starting materials. Additionally, the application of these starting materials allowed the utilization of gas chromatography as well as chiral gas chromatography as a straightforward analytical method. The availability of a well practicable monitoring of the reaction progress allowed to receive information about the conversion, yield, diastereomeric ratio, and enantioselectivity, and consequently offered a suitable opportunity to compare the variety of the applied catalysts with regards to all factors.

In Table 14, the results of the cyclopropanation of styrene **33** with ethyl diazoacetate **34** are summarized. To achieve meaningful results for an appropriate comparison of the diverse polymer loadings and synthesis methods, each nanomaterial was recycled at least three times or until a decline in catalytic activity or enantioselectivity was apparent, whereby the ratio of *trans*-**35** to *cis*-**35** was always in the range between 60/40 to 70/30. The number of performed cycles already indicates a trend towards the lack of recyclability of the catalysts with a low polymer- and, consequently, low ligand loading. Especially in entry 4, using **30b**, almost no selectivity could be detected. The attempt of recycling this catalyst for a second cycle confirmed the inactivity of **30b** with traces of product. For **32b** entry 2, the first run showed promising high enantioselectivities of 67% *ee* for *trans*-**35** and 55% *ee* for *cis*-**35**. However, also this catalyst was not recyclable without losses in both, yield and selectivity. The most likely reasons, therefore, are catalyst poisoning by inactivation, catalyst leaching, or polymer clogging. Comparing these results explicit to the corresponding materials with a higher degree of polymerization, entry 1, verified the beneficial effect of a higher polymer loading for the yield. **32a** only decreased to yields as low as 9% at run three, corresponding to at least a small improvement compared to **32b**. Although the higher loading was advantageous for the activity, the selectivity was negatively influenced by the potential interference of the chiral ligands packed too closely, being perceptible in a decline of enantiomeric excess from 67% to 57%. The synthesized co-polymer **59** includes styrene as a kind of spacer and, thus, enlarging the distance between the attached catalytically active units onto the benzyl chloride positions. Indeed, this methodology served the purpose by balancing high selectivities with moderate recycling of three runs (entry 5). However, the comparably low degree of polymerization achieved *via* the co-polymerization for PS/PS-Cl@Co/C **56** ($L(C) = 0.60 \text{ mmol}\cdot\text{g}^{-1}$), in turn, diminished the recyclability. The directly linked catalyst **30a** (entry 3) showed the best performance of all applied materials with solely minor variations in yield throughout the four cycles and a maximum in selectivity with 84% *ee* of *trans*-**35** and 66% *ee* of *cis*-**35**. In agreement with the already stated investigations, **30a** fits the requirements of a high polymer loading ($L(C) = 3.59 \text{ mmol}\cdot\text{g}^{-1}$ of **20a**) with an intermediate ligand loading ($L(N) = 0.83 \text{ mmol}\cdot\text{g}^{-1}$ of **54a**), corresponding to roughly

23% occupancy. Noteworthy, unlike the entries 1, 2, and 4, the enantioselectivity and yield even increased after the first run (run 1: 43% yield, 19% *ee trans*-**35**) to the presented values, explained by the loss of non-complexed or worse complexed copper and eventually an enhanced dispersibility during the recycling process.

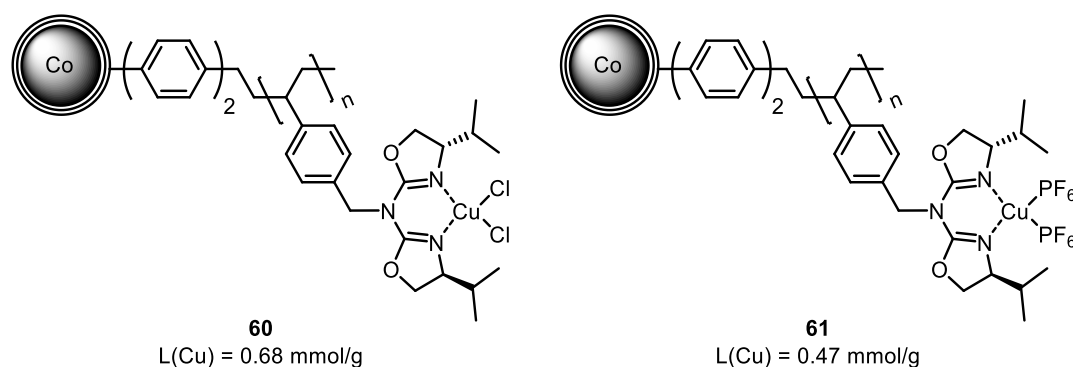
Table 14. Results of the cyclopropanation of styrene with the nanocatalysts **30a**, **30b**, **32a**, **32b**, and **59**.

Reaction scheme: Styrene (**33**) + Ethyl diazoacetate (**34**) $\xrightarrow[\text{PhNHNH}_2, \text{CH}_2\text{Cl}_2, 25^\circ\text{C}]{\text{Cu(II)-catalyst (20 mg)}}$ *trans*-**35** + *cis*-**35**

| Entry | Catalyst | Cycle | Yield [%] | <i>trans/cis</i> | <i>ee trans</i> [%] | <i>ee cis</i> [%] |
|-------|------------|-------|-----------|------------------|---------------------|-------------------|
| 1 | 32a | 1 | 36 | 67/33 | 57 | 48 |
| | | 2 | 15 | 71/29 | 48 | 42 |
| | | 3 | 9 | 66/34 | 46 | 40 |
| 2 | 32b | 1 | 31 | 67/33 | 67 | 55 |
| | | 2 | 6 | 67/33 | 52 | 44 |
| 3 | 30a | 1 | 43 | 61/39 | 19 | 14 |
| | | 2 | 51 | 65/35 | 84 | 66 |
| | | 3 | 49 | 68/32 | 75 | 63 |
| | | 4 | 44 | 62/38 | 73 | 64 |
| 4 | 30b | 1 | 32 | 65/35 | 1 | <1 |
| | | 2 | 1 | <i>n.d.</i> | <i>n.d.</i> | <i>n.d.</i> |
| 5 | 59 | 1 | 35 | 66/34 | 13 | 11 |
| | | 2 | 26 | 68/32 | 68 | 59 |
| | | 3 | 9 | 64/36 | 56 | 48 |

Conditions: 1.00 mmol styrene **33**, 20 mg Cu(II)-catalyst (2-3 mol%) with 4 mL solvent for 22 hours; *n.d.*: not determined.

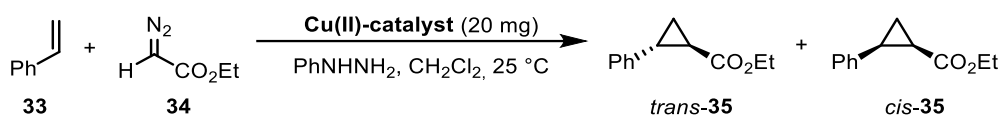
With the suitable nanocatalyst **30a** in hands, the impact of the counterions was studied. To begin these studies, the investigations of Zhou *et al.*^[160] and the group of Maguire^[157] were considered. They demonstrated that hexafluorophosphate was superior to triflate as counterion, which in turn obtained higher selectivities than chloride for the C-H insertion. Therefore, the precursor ⁱPr-azaBOX@PS-Br@Co/C **54a** was used for the complexation of the copper-complexes, following an adapted literature procedure of Maguire *et al.*^[157] Stirring the magnetic precursor with CuCl₂ at ambient temperature resulted in CuCl₂@ⁱPr-azaBOX@PS-Br@Co/C **60** with a copper loading of 0.68 mmol·g⁻¹ and subsequent exchange with the aid of an excess of potassium hexafluorophosphate led to Cu(PF₆)₂@ⁱPr-azaBOX@PS-Br@Co/C **61** with a copper loading of 0.47 mmol·g⁻¹ (Scheme 21).



Scheme 21. Copper(II) complexed ^tPr-azaBOX-immobilized Co/C NPs **60** and **61**.

Applying these nanocatalysts in the benchmark cyclopropanation of styrene **33** showed no beneficial contribution of the exchanged counterions over triflate. As expected, the replacement of triflate to chloride resulted in the formation of almost racemic products *trans*- and *cis*-**35**, without effecting the diastereomeric ratio (Table 15, entry 1-2). Contrary to the literature reports using homogeneous catalysts, the desired increase of enantioselectivity using PF₆⁻ was not observed for the heterogeneous nanocatalyst **61** with an optimum of 25% *ee* for *trans*-**35** in the second cycle (entry 4).

Table 15. Results of the cyclopropanation of styrene **33** with the nanocatalysts **60** and **61**, comparing the effect of the counterions.

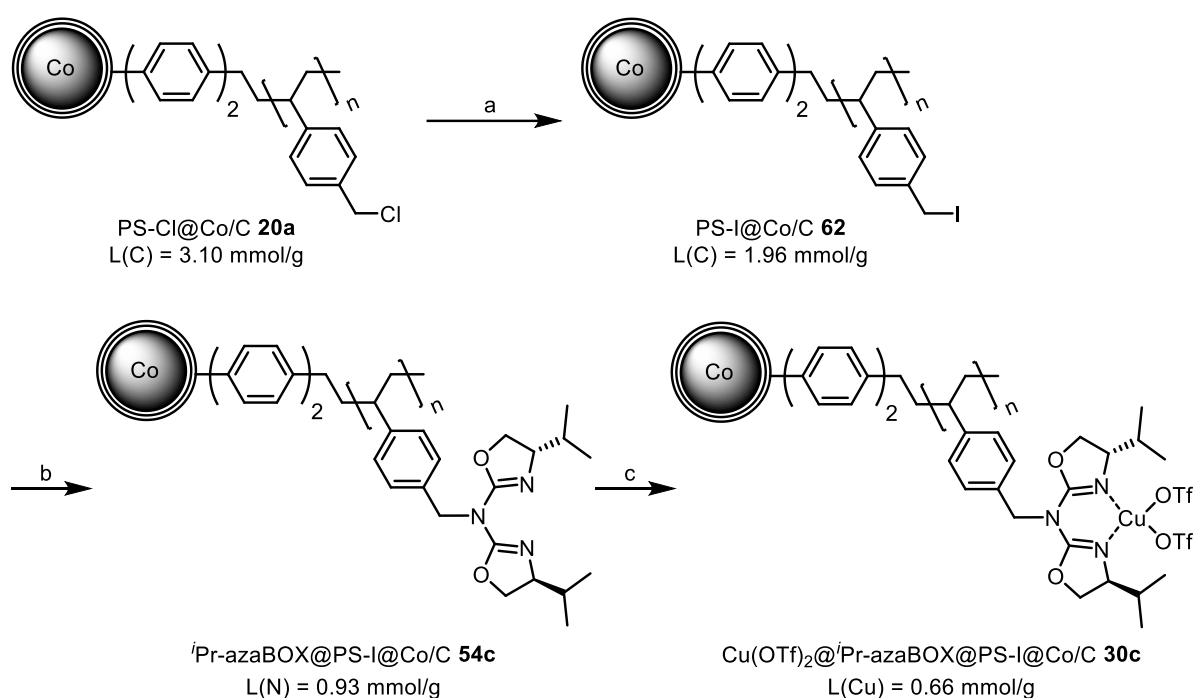


| Entry | Catalyst | Cycle | Yield [%] | <i>trans/cis</i> | <i>ee trans-35</i> [%] | <i>ee cis-35</i> [%] |
|-------|-----------|-------|-----------|------------------|------------------------|----------------------|
| 1 | 60 | 1 | 25 | 69/31 | <1 | <1 |
| 2 | 60 | 2 | 4 | <i>n.d.</i> | 2 | <i>n.d.</i> |
| 3 | 61 | 1 | 14 | 68/32 | 13 | 13 |
| 4 | 61 | 2 | 5 | 71/29 | 25 | 24 |
| 5 | 61 | 3 | 5 | 70/30 | 19 | 21 |

Conditions: 1.00 mmol styrene **33**, 20 mg Cu(II)-catalyst (1-2 mol%) with 4 mL solvent for 22 hours; *n.d.*: not determined.

Having settled **30a** as an appropriate nanocatalyst with decent recycling potential and high selectivities, the focus was moved to the up-scaling of the synthesis. While doing so, the conversion of PS-Cl@Co/C **20a** to the bromide-analog **53a** turned out to be the most critical step, with a loss of material by roughly half. Employing 900 mg **20a** solely yielded 480 mg of **53a** despite a calculated higher molecular weight of the product. Further proceeding with the immobilization of the ^tPr-azaBOX ligand **40**, revealed the apparent decrease and damage of the polymer, confirmed by the elemental analysis. Starting with a carbon content of 45% for **20a**, terminated in 22% carbon for **54a** with a ligand loading of 0.05 mmol·g⁻¹ based on the nitrogen content. A way to circumvent this issue was the

development of a new synthesis route to obtain a polystyrene-based network with high loadings with simultaneously suitable leaving groups for the nucleophilic substitution without the need for the harsh reaction conditions and long reaction times (5 days) used so far. A heterogeneous approach of the Finkelstein reaction seemed to be a promising alternative, exchanging the chloride to iodide.^{†††} Therefore, PS-Cl@Co/C **20a** ($L(C) = 3.10 \text{ mmol}\cdot\text{g}^{-1}$) were dispersed in acetone with sodium iodide at 50 °C for two hours. Decanting the supernatant and washing the nanoparticles with diethyl ether, visualized the precipitation of sodium chloride. This time, the mass balance achieved the logical gain of material **62** (Scheme 22). Attaching the chiral ligand *i*Pr-**40** to yield **54c** ($L(N) = 0.93 \text{ mmol}\cdot\text{g}^{-1}$) and complexing copper(II) triflate, accordingly, resulted in the final catalyst Cu(OTf)₂@*i*Pr-azaBOX@PS-I@Co/C **30c** with a copper loading of 0.66 mmol·g⁻¹.



Scheme 22. Synthesis of Cu(OTf)₂@*i*Pr-azaBOX@PS-I@Co/C **30c** via PS-I@Co/C **62**. Reagents and conditions: a) NaI, acetone, 50 °C, 2 h; b) *i*Pr-azaBOX **40**, *n*-BuLi, THF, -78 °C to 25 °C, 48 h; c) Cu(OTf)₂, CH₂Cl₂, 25 °C, 3 days.

In Figure 34, a closer look was taken at the recycling and effectiveness of the newly synthesized nanomaterial **30c**. To begin with the benchmark reaction, the cyclopropanation of styrene was examined once more with 1.4 mol% catalyst. Upon six cycles, the catalyst **30c** proved to be active with a reasonably stable yield of *trans*-**35** and *cis*-**35** between 54% and 63%. Moreover, besides the moderate enantioselectivity in the first cycle (51% *ee trans*-**35**), an increased selectivity up to 76% *ee trans*-**35** could be detected within the recycling process. The activity dropped after the sixth cycle with a steady decline to 21% yield and 59% *ee trans*-**35** in the eighth cycle. The reason, therefore, was

^{†††} Attempts using 4-(bromomethyl)styrene or 4-(iodomethyl)styrene as precursor for the synthesis of materials **53** or **62** achieved only insufficient polymer loadings.

indeed the loss of copper, corresponding to 88% within six cycles. Overall, 95% of the initially applied copper could be detected in the combined solutions of all runs with the majority of 36% in the first one. The loss of uncomplexed copper is also apparent in the increasing enantioselectivity over the repetitive cycles. However, the decrease of copper did not affect the activity up to six cycles. To examine the impact of material loss caused by an incomplete magnetic recovering, the catalyst was regained and dried. Thus, 9.3 mg of **30c** were achieved, being equivalent to barely half of the employed nanocatalyst (17 mg). Derived from that result, the moderate calculated magnetic recovery rate of the catalyst of 55% explained the decline in reactivity, as well.

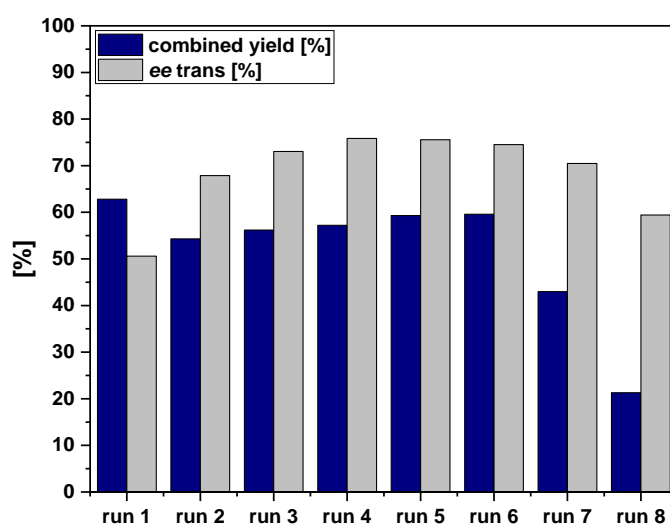


Figure 34. Recycling **30c** in the cyclopropanation of styrene **33** with ethyl diazoacetate **34**.

To broaden the scope of application, the cyclopropanation of the more challenging substrate methyl furan-2-carboxylate **63** was investigated. Therefore, *tert*-butyl diazoacetate **65** was used to form (1*S*,5*S*,6*S*)-(–)-2-Oxabicyclo[3.1.0]hex-3-ene-3,6-dicarboxylic 6-*tert*-butyl ester 3-methyl ester **66** aiming for a higher enantiomeric excess than the corresponding derivatives received from the methyl or ethyl diazoacetate according to literature.^[150]

The results of the repetitive cyclopropanation of the aforementioned alkene **63** and *N*-Boc-pyrrole **64** with the *tert*-butyl diazoacetate **65** are summarized in Table 16. The reuse of **30c** obtained moderate yields within four cycles up to 21% isolated **66**. According to literature, the yields for these challenging substrates were expected to be moderate with 38% yield and 95% *ee* for **66** using *i*Pr-BOX **38** as best ligand and 37% yield and 93% *ee* for **67**, respectively.^{[149],[150]} However, for the literature value of **67** the *t*Bu-azaBOX ligand **39** was necessary to achieve the good enantiomeric excess. Based on the outcome in Figure 34 combined with the knowledge of a nearly complete loss of copper, an approach

regarding the reactivation of the catalyst **30c** was examined. Therefore, new copper(II) triflate was added to the recovered catalyst and dispersed in CH₂Cl₂ for three days to again obtain the coordinated copper. After careful washing, the catalyst was reused for the cyclopropanation of **63**. Unfortunately, this effort failed as already the second run after the reactivation attempt (cycle 7, Table 16) only obtained traces of **66**. This finding suggests that the deactivation is not only caused by the absence of copper, but rather the combination of various possible factors including polymer clogging, ligand leaching, or the formation of an oxidized, inactive copper species.

Table 16. Repetitive cyclopropanation of methyl furan-2-carboxylate **63** and *N*-Boc-pyrrole **64** with *tert*-butyl diazoacetate **65** and **30c** as catalyst.

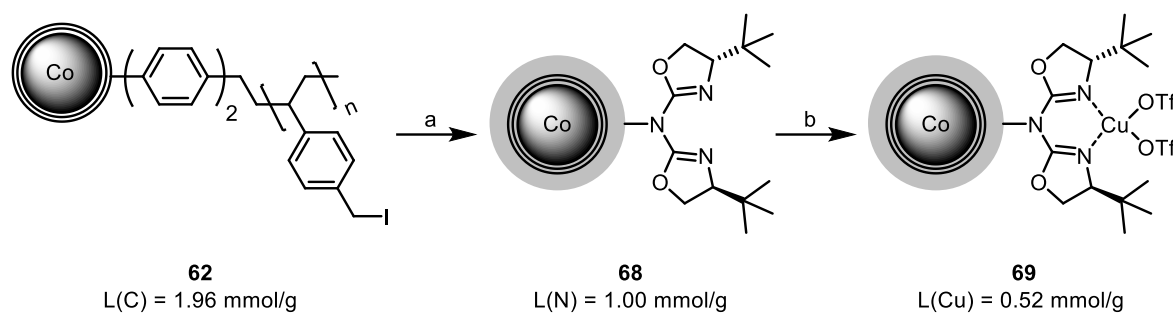
63: R = CO₂Me, X = O
64: R = H, X = NBoc

66: R = CO₂Me, X = O
67: R = H, X = NBoc

| Cycle | Alkene | Product | Yield ^a [%] | <i>ee</i> [%] |
|----------------|-----------|-----------|------------------------|----------------------|
| 1 | 63 | 66 | 17 | 40 |
| 2 | 63 | 66 | 21 | 71 (87) ^b |
| 3 | 63 | 66 | 10 | 68 |
| 4 | 63 | 66 | 10 | 74 |
| 5 | 64 | 67 | 32 | 27 |
| 6 ^c | 63 | 66 | <i>n.d.</i> | <i>n.d.</i> |
| 7 | 63 | 66 | <4 | <i>n.d.</i> |

[a] Isolated yield based on initial alkene; [b] After single recrystallization from hexanes; [c] New Cu(OTf)₂ was added. Conditions: 1.00 mmol alkene, 1.50 mmol **65**, 20 mg **30c** (1.4 mol%) with 4 mL solvent; *n.d.*: not determined.

Aiming for an improved enantiomeric excess, especially in case of the cyclopropanated product **67**, the synthesis of an immobilized version of the ^tBu-azaBOX ligand **40** was considered to be worthwhile. Following the optimized procedure of **30c**, Cu(OTf)₂@^tBu-azaBOX@PS-I@Co/C **69** was prepared as illustrated in Scheme 23. The *tert*-butyl substituted azaBOX ligand ^tBu-**40** could be attached with a calculated loading of 1.00 mmol·g⁻¹ based on the nitrogen content. After the complexation of the copper(II) triflate, 0.52 mmol·g⁻¹ Cu were determined *via* ICP-OES measurements. This indicated the successful synthesis of **69**, being in good agreement with the ligand and copper loadings achieved for **30c**.

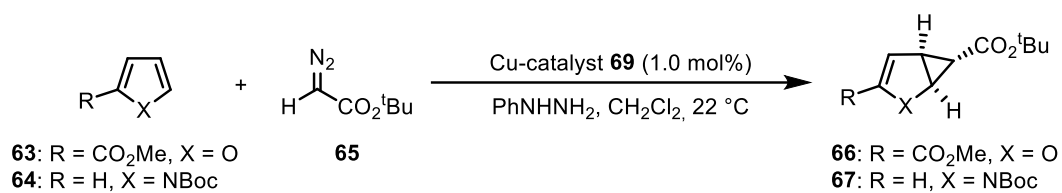


Scheme 23. Synthesis of $\text{Cu}(\text{OTf})_2@t\text{Bu-azaBOX@PS-I@Co/C}$ **69** via PS-I@Co/C **62**. Reagents and conditions: a) $t\text{Bu-40}^{***}$, $n\text{-BuLi}$, THF, $-78\text{ }^\circ\text{C}$ to $25\text{ }^\circ\text{C}$, 48 h; b) $\text{Cu}(\text{OTf})_2$, CH_2Cl_2 , $25\text{ }^\circ\text{C}$, 3 days. The gray shell indicates the polystyrene polymer depicted on the left side.

This catalyst was then employed in the cyclopropanation of *N*-Boc-pyrrole **64**. Since previous results showed a trend towards increased enantioselectivity for the recycled catalytic systems, **69** was reused as well. In contrast to the expected beneficial effect of the *tert*-butyl azaBOX functionalized nanoparticles, **67** was obtained as racemic mixture within the first two cycles. Even after the fourth cycle, only a poor selectivity of 18% *ee* could be observed accompanied by a diminished yield. Changing the substrate to **63**, demonstrated the utter inactivity of **69**. The explanation for this insufficient performance might already originate from the employed *tert*-butyl azaBOX ligand **40**. Having a closer look at the synthesis of $t\text{Bu-40}$ combined with the supposed narrow binding sites of the polymer **62**, suggests that either the aminooxazoline (*S*)-4-(*tert*-butyl)-4,5-dihydrooxazol-2-amine (precursor of $t\text{Bu-40}$) was immobilized onto the nanoparticles due to incomplete conversion during the ligand synthesis itself, or the sterically demanding *tert*-butyl groups are disturbed by a too high loading, bringing the functional sites too close to each other.

In summary, a feasible magnetic polystyrene polymer was developed which can be functionalized *via* two common linking strategies with the potential for the attachment of a variety of catalysts for the enantioselective cyclopropanation. While the copper-functionalized nanomaterials were not deemed worthwhile to pursue due to the low costs of copper, the corresponding rhodium derivatives are currently under investigation in the working group of Prof. Dr. Huw M. L. Davies (Emory University, Atlanta), exploring **52a** and **52b** for their suitability regarding the attachment of chiral rhodium catalysts.

^{***} $t\text{Bu-azaBOX}$ $t\text{Bu-40}$ was kindly provided by Urszula Klimczak.

Table 17. Repetitive cyclopropanation of *N*-Boc-pyrrole **64** and methyl furan-2-carboxylate **63** with *tert*-butyl diazoacetate **65** and **69** as the catalyst.

| Cycle | Alkene | Product | Yield ^a [%] | <i>ee</i> [%] |
|-------|-----------|-----------|------------------------|---------------|
| 1 | 64 | 67 | 32 | <i>rac.</i> |
| 2 | 64 | 67 | 37 | <i>rac.</i> |
| 3 | 64 | 67 | 18 | 11 |
| 4 | 64 | 67 | 11 | 18 |
| 5 | 63 | 66 | <1 | <i>n.d.</i> |

[a] Isolated yield based on initial alkene; *Conditions*: 1.00 mmol alkene, 1.50 mmol **65**, 20 mg **69** (1.0 mol%) with 4 mL solvent; *n.d.*: not determined; *rac.*: racemic.

4. Reversible extraction of toxic heavy metals from water

Microporous organic polymers (MOPs) based on magnetic carbon-coated cobalt nanoparticles (Co/C NPs) have been investigated as recyclable high capacity adsorbents for toxic heavy metal ions. The herein reported material enables an easy and straightforward extraction method for a broad variety of heavy metals, with special attention to lead and mercury. Especially desirable is the high selectivity towards mercury ions against other metal ions. The nanoadsorbents are prepared *via* a two-step synthesis route, using readily available starting materials to design microporous polymers with enlarged surface areas and diverse functional groups for enhanced metal binding affinities. Applying hyper-cross-linked 2,2'-biphenol as polymer structure, adsorption capacities as high as 273 mg Pb²⁺ and outstanding 810 mg Hg²⁺ per gram of nanoparticles can be achieved. The easy recycling procedure enables efficient decontamination of water polluted with lead, chromium, and copper ions with the aid of an external magnet up to nine cycles.

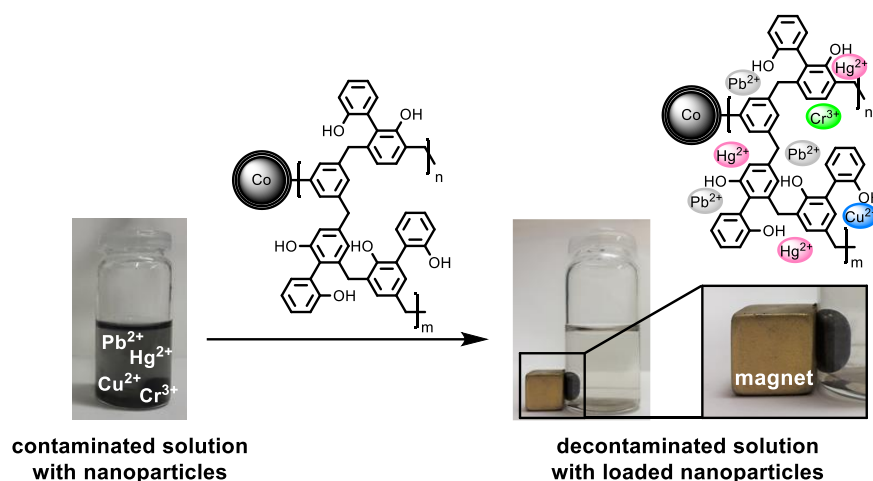


Figure 35. Decontamination of an aqueous solution polluted with lead, mercury, copper, and chromium ions by the aid of the nanoscavenger, showing the facile recovery of the nanoadsorbent *via* an external magnet.

4.1. Introduction

The release of toxic heavy metal ions into the ecosystem and the emerging threats to human health have become a critical issue of worldwide concern. Unlike organic pollutants, most heavy metals are non-biodegradable and consequently tend to accumulate in the environment and living organisms. Thereby, the major sources of contamination are caused by anthropogenic activities including wastewaters from agriculture, industry, urban areas, mining, hazardous solid waste disposal sites, coal, and fossil fuel combustion.^{[161],[162]} The pollution of the air, soil, fresh- and groundwater, in turn, redistributes and spreads the heavy metals up to bioaccumulation (see Figure 36 for a graphical representation).

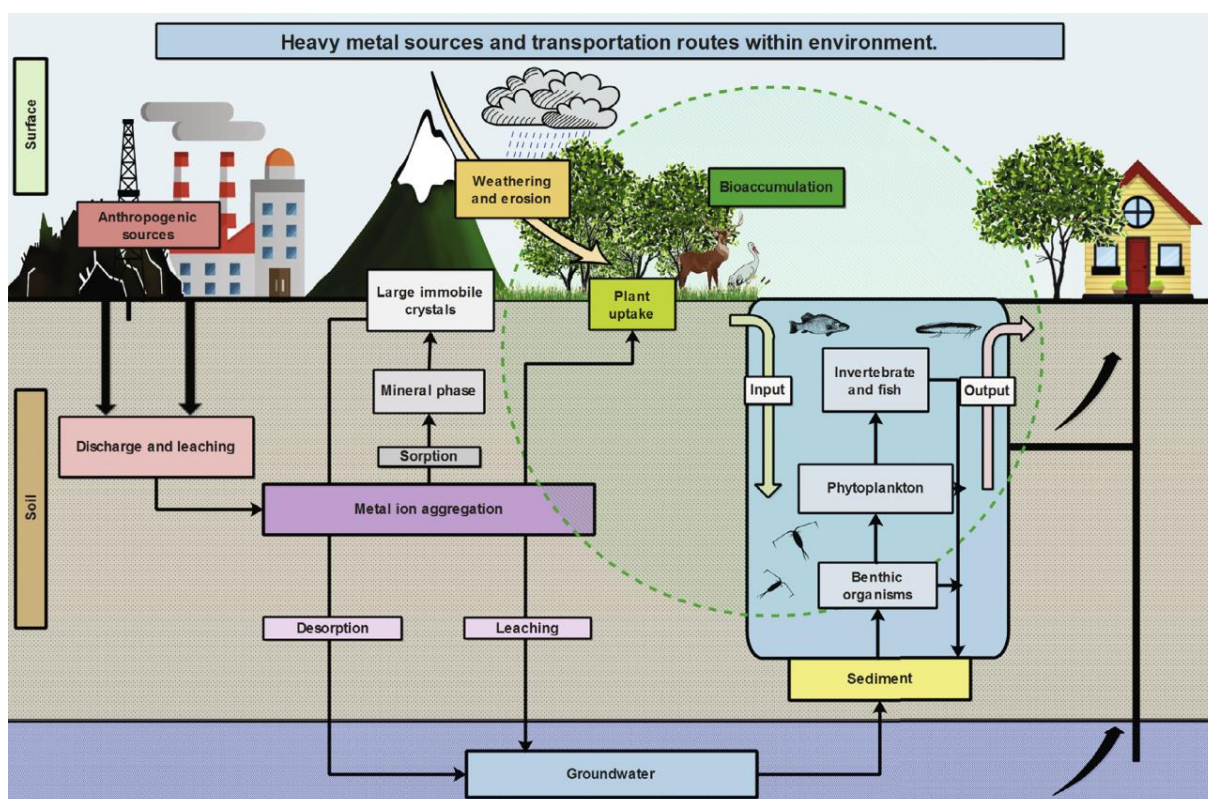


Figure 36. Flowchart illustrating the redistribution and bioaccumulation of heavy metals from anthropogenic origin by soil, fresh- and groundwater systems. Reprinted with permission from [162]. Copyright © 2017, Elsevier.

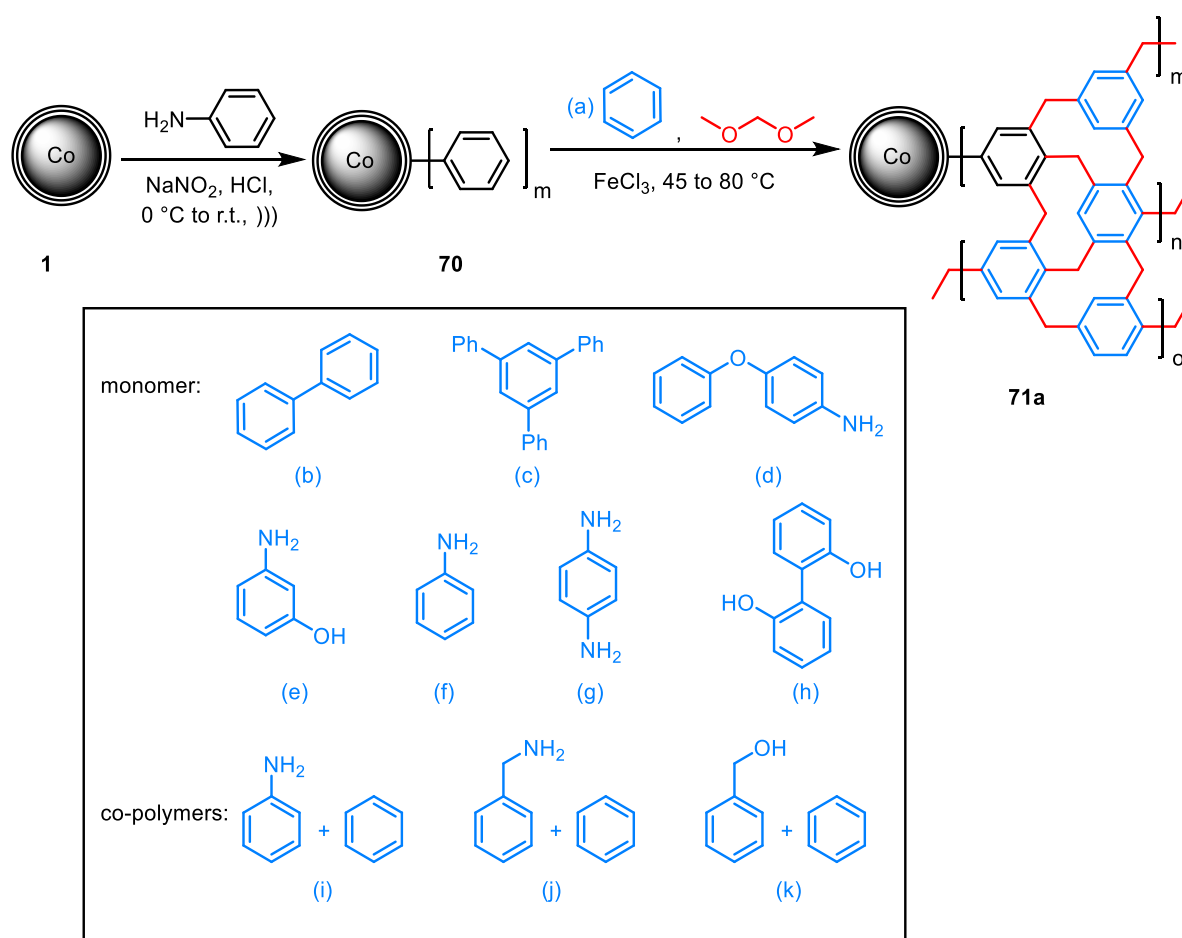
Besides nutritionally essential metals like cobalt, chromium(III), copper, iron, manganese, molybdenum, selenium and zinc, other metals like arsenic, cadmium, chromium(VI), lead and mercury do not hold any known beneficial effects for the human health and are ranked among the most toxic metals in the environment.^[163] Therefore, the necessity for efficient decontamination methods emerged, revealing diverse chemical and physical processes such as chemical precipitation, ion exchange, ultrafiltration, electrochemical treatment, sedimentation, membrane filtration, and adsorption. Adsorption has been proven as one of the most economical and efficient methods, opening the opportunity of regenerating the adsorbent with a suitable desorption process.^[164] Widely applied

adsorbents are porous materials, which possess a high surface area and large pore volume such as activated carbon, zeolite, or biomass. To enhance the adsorption affinities, micropores with a size below 2 nm seem theoretically advantageous based on the ionic radii of the metal ions.^[90] Introducing microporous organic polymers (MOPs) as comparably soft adsorbents, further advantages can be achieved. The use of diverse monomers enables a tunable pore structure, the introduction of functional groups for improved binding affinities, an adjustable dispersibility in various solvents, and may influence the selectivity.^[90] Due to their unique properties, these kinds of polymers gained the interest of researchers and a variety of hyper-cross-linked materials was developed with limited reports examining their ability to adsorb toxic metal ions.^[162] Highlighting a recent publication of Ji *et al.*,^[165] hyper-cross-linked polystyrene modified with thiourea was used for the removal of either cadmium, copper, or lead ions, respectively, from aqueous solutions. Almost quantitative desorption of Cd^{2+} , Cu^{2+} , and Pb^{2+} was achieved by an aqueous EDTA solution, regenerating the adsorbent for at least five cycles. In competitive adsorption studies, the porous material showed a high affinity towards Pb^{2+} and could be extracted almost selectively in the presence of the cadmium or copper ions. However, more complex metal solutions or a more detailed recycling protocol were not reported.

For the ease of handling, other approaches focused on magnetic nanomaterials, combining the simplicity with a high surface-area-to-volume ratio and high extraction capacities.^[166] Thereof, the publication of Reiser *et al.*,^[55] utilizing PEI-coated Co/C nanobeads (PEI@Co/C) for the selective extraction of mercury(II) from aqueous solutions, is among the most promising applications. This material proved to be efficient for relevant mercury concentrations ($\text{mg}\cdot\text{L}^{-1}$ as well as $\mu\text{g}\cdot\text{L}^{-1}$) within short extraction times and an easy recycling protocol, benefiting from the magnetic properties of the Co/C nanobeads. Further relevance was demonstrated by a large-scale experiment, where 20 L of an aqueous mercury-containing solution ($30\ \mu\text{g}\cdot\text{L}^{-1}\ \text{Hg}^{2+}$) were decontaminated by using only 60 mg of PEI@Co/C. Even though a great effort has been devoted to the investigation of new adsorbents, there are still several restrictions left combining readily synthesizable materials, metal selectivity, and high metal capacities with a wide operating area without the necessity for a complex regeneration process, potentially limiting their further applications. In this study, microporous organic polymers based on magnetic carbon-coated cobalt nanoparticles are investigated for the efficient extraction of chromium, lead, and mercury from water with high metal adsorption capacities up to 273 mg Pb^{2+} and 810 mg Hg^{2+} per gram of nanoascavenger. The combination of MOPs with the magnetic support allowed the successful application at several concentrations, as well as an easy recycling process and material synthesis from readily available starting materials, which offers great potential for industrial purposes.

4.2. Results and Discussion

As previously established, carbon-coated cobalt (Co/C) nanomagnets **1** were considered to be an appropriate support, based on their high chemical and thermal stability as well as their high saturation magnetization ($158 \text{ emu}\cdot\text{g}^{-1}$).^[37] A large number of applications resulted from these advantages, demonstrating their successful use as reagents and catalysts.^[38] Further, magnetic scavengers were reported for the removal of organic pollutants,^[59] cadmium,^[167] copper,^[167] lead,^[167] mercury,^[55] gold,^{[168],[169]} and platinum^[169] metal ions. The industrial relevance of magnetic filtration and extraction of carbon-coated metal nanoparticles was also proven by Stark *et al.*^[170] on a 'ton per hour' scale for the treatment of large volumes. However, the studies were either non-selective or only applicable for the removal of one metal species, without adsorption capacity for other toxic metal ions. In order to design a scavenger that can efficiently and selectively extract mercury from an aqueous solution, but also has binding affinities towards other crucial metal contaminants, pristine Co/C nanobeads **1** were covalently functionalized with microporous organic polymers (Scheme 24). The suitability of Co/C-based microporous organic polymers was already proven for the encapsulation of palladium nanoparticles catalyzing hydrogenation reactions with good recyclability (chapter 1).^[171]



Scheme 24. Synthesis of benzene@Co/C **71a**. Analogous to **71a**, MOPs@Co/C **71b-71k** were synthesized using monomers b-k.))) = ultrasound.

Encouraged by the promising simplicity of the synthesis of these materials and their high chemical stability (chapter 1), the expansion of their application area was considered. However, this time, benzene-tagged Co/C **70** were utilized as the simplest arene-functionalized magnetic anchoring point for the formation of the MOPs@Co/C **71a-k** (Scheme 24). To synthesize the hyper-cross-linked networks, again, the polymerization strategy reported by Tan *et al.*^[98] was used, with formaldehyde dimethyl acetal (FDA) as an external cross-linker for “knitting” rigid aromatic monomers. In order to overcome the strongly hydrophobic character of the carbon-based polymers, amino- and hydroxyl-groups were introduced during the polymerization with a simultaneous effect onto the pore sizes and surface areas, as addressed in chapter 1.2, comparing a toluene-based network **4a-y** with 2,2'-biphenol **4d** ($V_{0.1/\text{tot}} = 0.37$, $S_{\text{BET}} = 277 \text{ m}^2 \cdot \text{g}^{-1}$ compared to $V_{0.1/\text{tot}} = 0.63$, $S_{\text{BET}} = 389 \text{ m}^2 \cdot \text{g}^{-1}$).^[171] For the synthesis of **71i-k**, a co-polymerization strategy was employed, combining the monomers (i)-(k) with benzene, since benzene is known to form highly microporous polymeric structures and has a beneficial influence onto the surface area and porosity of co-polymers.^[93]

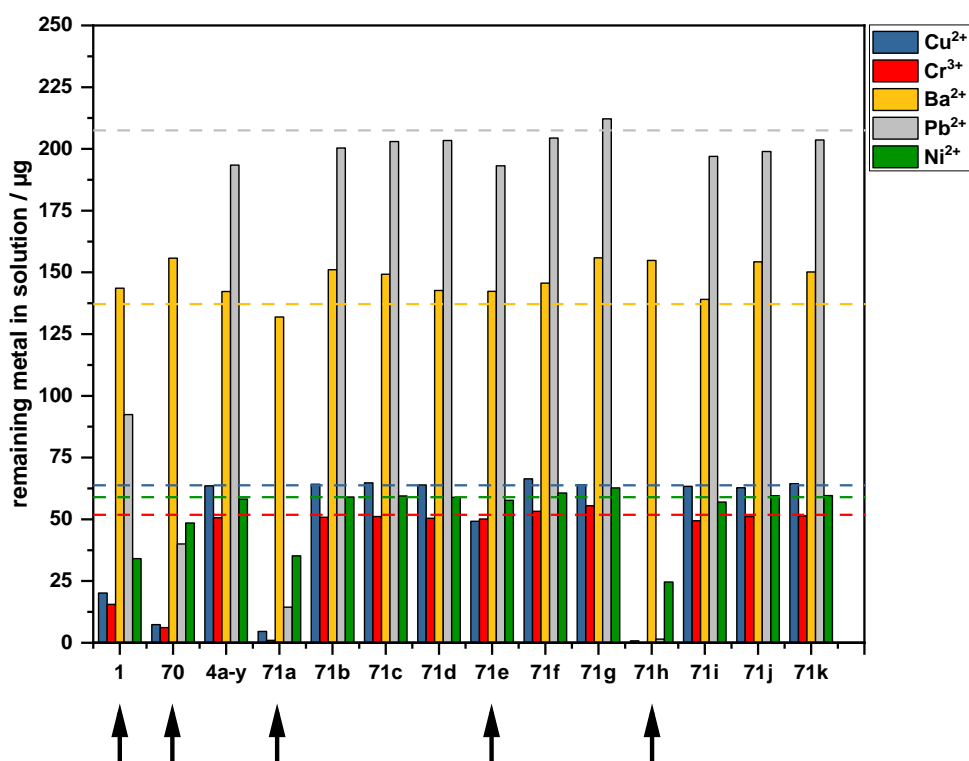


Figure 37. Comparison of the extraction capacity of nanomagnets **1**, **70**, and MOPs@CoC **4a-y**, **71a** to **71k**. 10 mg of the nanoparticles were stirred in 10 mL (100 µM) heavy metal solution for 20 hours. The dashed line indicates the initial metal amounts. The arrows highlight nanoparticles which extracted heavy metals to some extent. For the best adsorption capacities, a zoom is given in Figure 38.

For an overview of the dispersibility and adsorption capacities, polymers **71a-71k** were compared with pristine Co/C nanobeads **1**, the starting unit **70**, and the microporous polymer **4a-y** in an aqueous

solution of barium, copper, chromium, nickel, and lead ions (100 μM) with 10 mg of the nanomaterial in each case (Figure 37). Solely polymers **71a** and **71h** showed an appreciable metal removal (Figure 37, zoomed graph in Figure 38), **71e** could extract copper partially (23%), whereby the other polymers **4a-y**, **71b-d**, **71f-g**, and **71i-k** did not extract any metal ions. Benzene-functionalized **71a** and 2,2'-biphenol-functionalized **71h** could almost quantitatively extract copper, chromium and lead ions (**71a**: 93% Cu^{2+} , 98% Cr^{3+} , 93% Pb^{2+} ; **71h**: 99% Cu^{2+} , 100% Cr^{3+} , 99% Pb^{2+}). Despite the theoretically high hydrophobic character of **71a**, the extraction worked surprisingly well. This could be explained by the outstanding properties benzene-based MOPs contribute to the microporosity and surface area,^{[93],[98]} which in turn influence the mass transfer and diffusion rates. However, amine-functionalized polymers and co-polymers using benzene **71i-71k** gave no rise to enhanced binding affinities for any metal ions. Reducing the applied amount of the MOPs@Co/C to 2.0 mg, revealed up to five times higher adsorption capacities for the porous polymers **71a** (18 $\text{mg}\cdot\text{g}^{-1}$ Cu^{2+} , 15 $\text{mg}\cdot\text{g}^{-1}$ Cr^{3+} , 41 $\text{mg}\cdot\text{g}^{-1}$ Pb^{2+}) and **71h** (19 $\text{mg}\cdot\text{g}^{-1}$ Cu^{2+} , 15 $\text{mg}\cdot\text{g}^{-1}$ Cr^{3+} , 57 $\text{mg}\cdot\text{g}^{-1}$ Pb^{2+}) compared to relatively low extraction capacities of the pristine nanobeads **1** (4 $\text{mg}\cdot\text{g}^{-1}$ Cu^{2+} , 4 $\text{mg}\cdot\text{g}^{-1}$ Cr^{3+} , 11 $\text{mg}\cdot\text{g}^{-1}$ Pb^{2+}) and benzene-tagged **70** (5 $\text{mg}\cdot\text{g}^{-1}$ Cu^{2+} , 5 $\text{mg}\cdot\text{g}^{-1}$ Cr^{3+} , 16 $\text{mg}\cdot\text{g}^{-1}$ Pb^{2+} , see Figure 59 in Experimental Part).

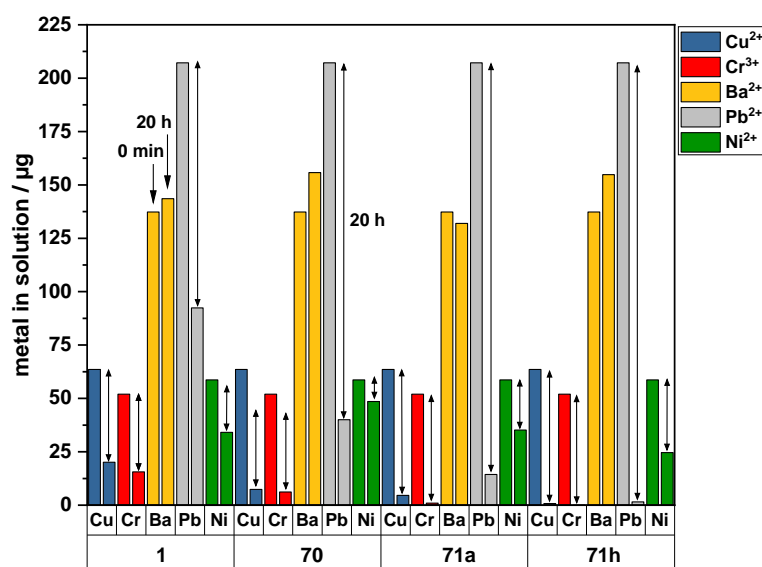


Figure 38. Zoom of the best extraction capacities from Figure 37, showing **1**, **70**, **71a**, and **71h** (10 mg NPs were stirred in 10 mL (100 μM) heavy metal solution for 20 hours). The left bar represents the initial metal in solution at $t = 0$ min.

Further benchmarking the nanoadsorbent **71h** with the so-far best performance regarding its mercury(II) selectivity showed a complete and exclusive extraction of Hg^{2+} in presence of barium, copper, chromium, nickel, and lead ions within short reaction times (Figure 39A).

Increasing the metal ions concentrations ten times and further enlarging the volume of the aqueous solution, 15 μmol of each metal were stirred with 2.0 mg **71h**. Even after four days, only the mercury

ions were notably diminished by 1.6 mg Hg²⁺, corresponding to an excellent adsorption capacity of 810 mg Hg²⁺ per gram of nanoparticles (Figure 39B). Comparing this to unfunctionalized Co/C nanobeads **1**, the extraction capacity was limited to 13 mg Hg²⁺ per g NPs, with the major drawback that an efficient release of the mercury and, therefore, recycling was not possible, even under harsh reaction conditions like heating in *aqua regia*.^[55]

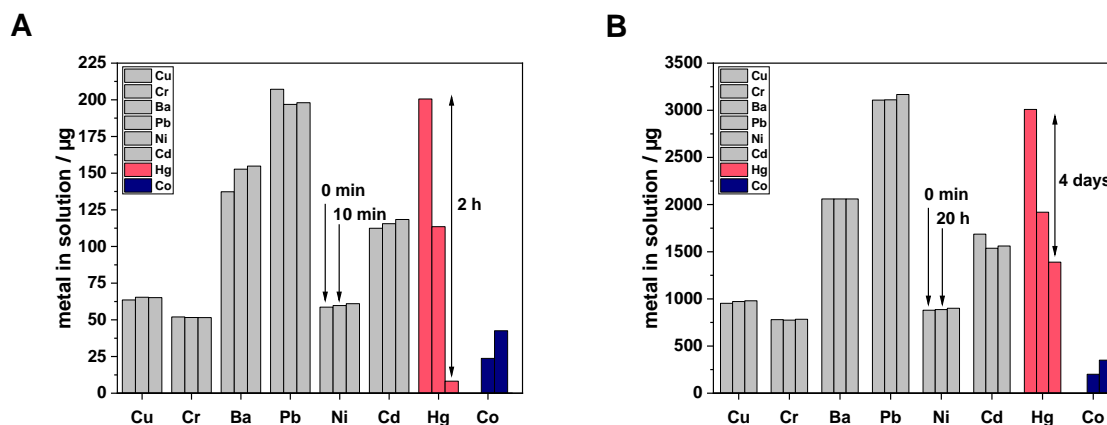


Figure 39. Selectivity of **71h** (A) Comparing 1 µmol of each metal at t = 0 min, 10 min, and 2 hours. (2 mg **71h** in 10 mL (100 µM) metal solution). (B) Comparing 15 µmol of each metal at t = 0 min, 20 hours, and 4 days. (2 mg **71h** in 15 mL (1 mM) metal solution).

Considering the previous investigations that **71h** is capable to scavenge copper, chromium and lead ions, as well as its selectivity for mercury(II) ions in competitive studies, a combined approach for the extraction of all heavy metal ions was investigated. Therefore, the amount of the nanoadsorbent was adjusted to increase the overall adsorption capacity, aiming for the complete decontamination of the mercury ions, followed by the subsequent extraction of the residual metal ions. Indeed, the calculated amount of only 6.5 mg of **71h** was capable to efficiently detoxify a solution of copper, chromium, lead, and mercury ions (100 µM; 5.3 mg·L⁻¹ Cu²⁺, 5.3 mg·L⁻¹ Cr³⁺, 22 mg·L⁻¹ Pb²⁺, 18 mg·L⁻¹ Hg²⁺) at the same time (Figure 40). Within the 20 hours extraction time, a cobalt contamination of 23 mg·L⁻¹ could be observed from the Co/C support. However, it is particularly noteworthy that the utilized nanoparticles were able to remove both highly toxic metal ions, lead and mercury, which are included on the list of the ‘ten chemicals of major public health concern’ from the World Health Organization WHO.^[172]

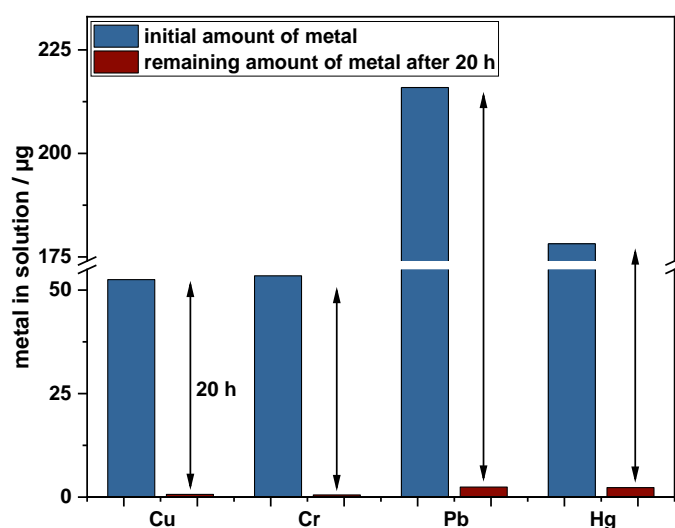


Figure 40. Complete decontamination of 10 mL of an aqueous solution containing 5.3 mg·L⁻¹ Cu²⁺, 5.3 mg·L⁻¹ Cr³⁺, 21.6 mg·L⁻¹ Pb²⁺, 17.8 mg·L⁻¹ Hg²⁺ (100 µM) within 20 hours using 6.5 mg **71h**.

Besides the above described heavy metals, further metal affinities and adsorption capacities of **71h** were examined (Table 18). Zinc ions were investigated as a single metal solution, resulting in a moderate adsorption capacity of 14 mg Zn²⁺ per gramm of **71h**. Cadmium, iron, and cobalt ions were explored as a combined solution. The solution could be almost completely decontaminated from iron ions, however, solely 30% could be released from the support itself, determining a notable amount being deposited on the glass wall over the extraction process. Over this period of time, an increase of the cobalt concentration in the solution was detected, suggesting no adsorption or complexation of the cobalt ions from the solution into the support.

Table 18. Additional metal affinities and adsorption capacities of **71h**.

| Entry | Metal ion | Adsorbed metal [%] | Adsorption capacity [mg·g ⁻¹ NP] |
|-------|------------------|--------------------|---------------------------------------------|
| 1 | Zn ²⁺ | 42 | 14 |
| 2 | Cd ²⁺ | 20 | 9 |
| 3 | Fe ²⁺ | 91 ^a | 9 ^b |
| 4 | Co ²⁺ | - ^c | - ^c |

Extraction conditions: 2.0 mg **71h** were stirred in 10 mL of a 100 µM solution of the corresponding metal for 20 hours. Zn²⁺ was tested as single metal solution, Cd²⁺, Co²⁺, and Fe²⁺ were combined. [a] only 30% were determined in the NPs, the rest (41%) were deposited on the glass wall; [b] Corresponding to the amount detected onto the NPs; c) No decrease in the cobalt concentration was observed, solely an increase.

Having proven the feasibility of the nanomagnets for extracting metal ions that are causing extensive environmental contamination and health problems, their applicability in real water samples had to be explored. Therefore, drinking water, containing natural amounts of anions and cations, was spiked with Cu²⁺, Cr³⁺, Pb²⁺, Hg²⁺ (10 µM) and the heavy metal contamination was measured before and after

the treatment with **71h** (Table 19). The results proved, that the toxic metal ions could also be removed from the spiked real water samples within 20 hours without being disturbed by the other ions present in the solution. This was further verified by recycling experiments with **71h**, achieving similar results.

Table 19. Extraction of metal ions with **71h** from spiked mineral water (10 μM heavy metal ions).

| | Metal ions before and after extraction [$\text{mg}\cdot\text{L}^{-1}$] | | | |
|--------------------|--------------------------------------------------------------------------|------------------|------------------|------------------|
| | Cu^{2+} | Cr^{3+} | Pb^{2+} | Hg^{2+} |
| Initial amount | 0.66 | 0.58 | 2.24 | 1.86 |
| Run 1 ^a | 0.07 | 0.09 | 0.15 | 0.26 |
| Run 2 ^a | 0.05 | 0.09 | 0.14 | 0.24 |

[a] Extraction conditions: 2.3 mg **71h** were used at 30 °C to decontaminate 10 mL mineral water spiked with Cu^{2+} , Cr^{3+} , Pb^{2+} , Hg^{2+} (10 μM) containing approximately sodium 20 $\text{mg}\cdot\text{L}^{-1}$, potassium 2 $\text{mg}\cdot\text{L}^{-1}$, magnesium 18 $\text{mg}\cdot\text{L}^{-1}$, calcium 97 $\text{mg}\cdot\text{L}^{-1}$, chloride 5 $\text{mg}\cdot\text{L}^{-1}$, sulfate 14 $\text{mg}\cdot\text{L}^{-1}$, hydrogencarbonate 415 $\text{mg}\cdot\text{L}^{-1}$ ($\text{pH} \approx 8$) within 20 hours.

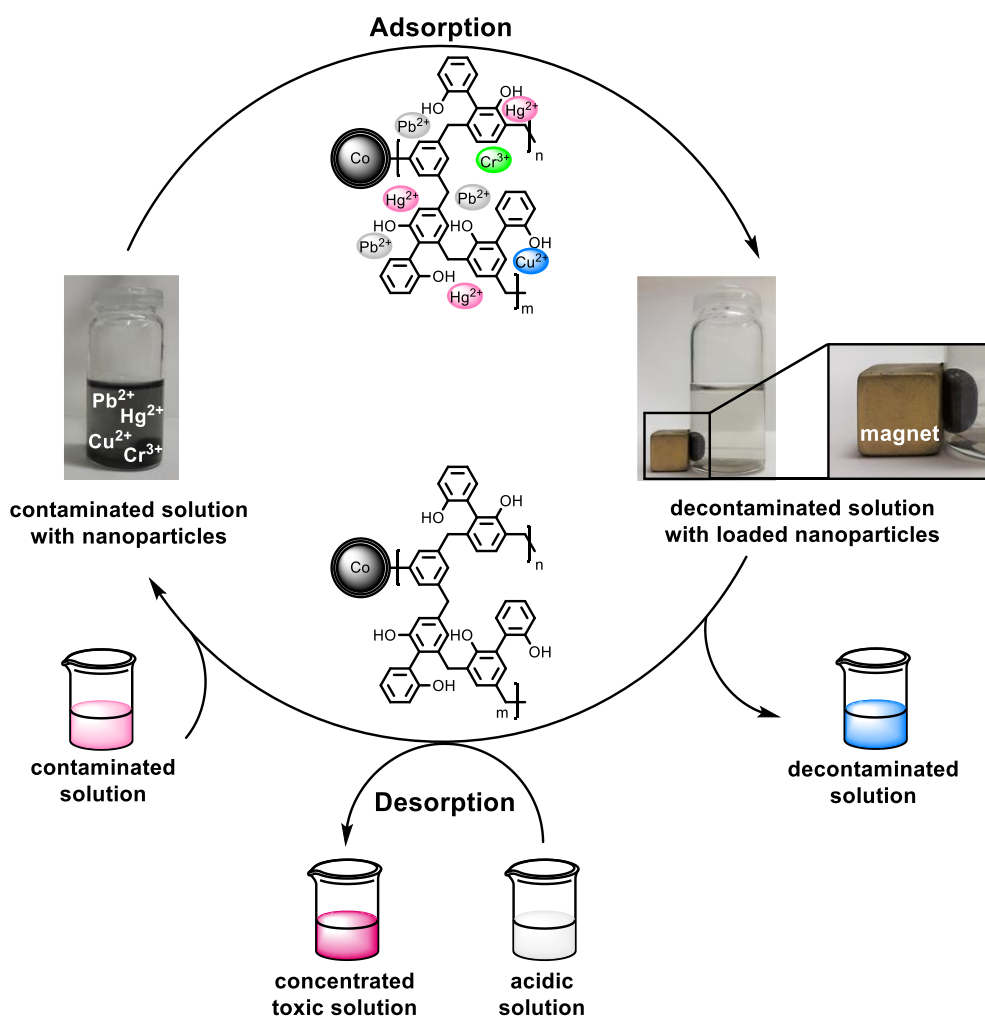


Figure 41. Recycling protocol for the extraction of toxic heavy metals from aqueous solutions with **71h**.

For retrieving the nanoadsorbent from the aqueous solution, a multicycle extraction/recycling protocol was established, as depicted in Figure 41. An external magnet collected the dispersed nanoparticles

71h within seconds and the decontaminated aqueous solution was decanted. The nanoparticles with the adsorbed heavy metals were redispersed in an aqueous acidic solution to release and concentrate the heavy metals and regain **71h**.

To evaluate the potentially most important advantage of the magnetic support besides retrieval from the solution, regeneration and recycling needed to be examined next. These parameters have been tested for low concentrations (10 μM , Table 20) as well as higher metal concentration (100 μM , Table 21) to cover the widest possible range of applications. Table 20 illustrates the adsorption efficiency of **71h** over nine cycles, with only a minor decrease in capacity of 3%. After every third cycle, the metal ions were desorbed (desorption value see Table 20 in brackets) with an acidic solution for 30 minutes, before regenerating it with an aqueous sodium carbonate solution. With this recycling procedure, all metal ions were almost quantitatively extracted from the solution over nine cycles (89 to 94% extracted), corresponding to overall 56 $\mu\text{g Cu}^{2+}$, 43 $\mu\text{g Cr}^{3+}$, and 169 $\mu\text{g Pb}^{2+}$ by 2 mg of **71h**.

Table 20. Recycling of **71h** to detoxify an aqueous solution with low heavy metal concentrations (10 μM).^a

| Cycle | Cu [%] | Cr [%] | Pb [%] | Co [$\text{mg}\cdot\text{L}^{-1}$] |
|-------|---------|---------|----------|--------------------------------------|
| Run 1 | 94 | 90 | 94 | 2.21 |
| Run 2 | 94 | 91 | 94 | 2.57 |
| Run 3 | 94 (97) | 91 (95) | 93 (105) | 2.49 |
| Run 4 | 91 | 89 | 92 | 2.26 |
| Run 5 | 93 | 91 | 92 | 2.80 |
| Run 6 | 92 (94) | 88 (88) | 93 (99) | 2.96 |
| Run 7 | 91 | 90 | 93 | 2.38 |
| Run 8 | 92 | 92 | 92 | 2.75 |
| Run 9 | 93 (90) | 91 (82) | 91 (82) | 3.00 |

Metal adsorbed based on concentration of the remained solution. In brackets: metal released referring to adsorbed metal of previous 3 runs. [a] *Extraction conditions:* 2 mg **71h** were used at 30 °C to decontaminate 10 mL of a 10 μM metal solution (corresponding to 5.2 $\mu\text{g Cr}^{3+}$, 6.4 $\mu\text{g Cu}^{2+}$, 21 $\mu\text{g Pb}^{2+}$ per run) within 4 hours. Desorption was carried out after every third cycle with 5 mL of 0.1 M HCl solution.

Recycling the nanoadsorbent **71h** at the maximal calculated capacity for 4 mg nanomaterial with 1 μmol of Cu^{2+} , Cr^{3+} , and Pb^{2+} (100 μM) within 20 hours, showed an excellent extraction and desorption performance for four cycles (Table 21). However, after the fourth run a sharp decline could be observed for the extraction of copper and lead (run 5 and 6). The extraction potential of chromium was only slightly influenced by the general trend. Summarizing the overall adsorbed metal ions over the six runs, 258 $\mu\text{g Cu}^{2+}$, 265 $\mu\text{g Cr}^{3+}$, and 787 $\mu\text{g Pb}^{2+}$ were extracted with 4 mg of **71h**.

Table 21. Recycling of **71h** to detoxify an aqueous solution with higher heavy metal concentrations (100 μM).^a

| Cycle | Cu [%] | Cr [%] | Pb [%] | Co [$\text{mg}\cdot\text{L}^{-1}$] |
|-------|----------|---------|---------|--------------------------------------|
| Run 1 | 98 (100) | 98 (97) | 96 (98) | 17.4 |
| Run 2 | 98 (101) | 98 (88) | 86 (91) | 19.5 |
| Run 3 | 98 (101) | 98 (96) | 89 (93) | 16.7 |
| Run 4 | 98 (100) | 98 (94) | 97 (98) | 13.9 |
| Run 5 | 50 (86) | 87 (83) | 43 (81) | 8.43 |
| Run 6 | 32 (71) | 71 (80) | 31 (68) | 5.61 |

Metal adsorbed based on concentration of the remained solution. In brackets: metal released referring to adsorbed metal. [a] *Extraction conditions:* 4 mg **71h** were used at 30 °C to decontaminate 10 mL of a 100 μM metal solution (corresponding to 52 μg Cr^{3+} , 64 μg Cu^{2+} , 207 μg Pb^{2+} per run) within 20 hours. Desorption was carried out after every cycle with 5 mL of 0.1 M HCl solution.

Further evaluating the decontamination efficiency of mercury under very short reaction times of 10 minutes, 2 mg of **71h** were used to detoxify a solution containing 10 μM Hg^{2+} (Table 22). Thereby, good adsorption and desorption of mercury with a low cobalt leaching ($< 1.1 \text{ mg}\cdot\text{L}^{-1}$) could be obtained. However, initial studies showed that this time the previously applied acidic solution (0.1 M HCl) was not sufficient for a complete release of mercury. Thus, different acids and concentrations were investigated, revealing 2 M HCl as most potent acid with a moderate cobalt leaching on the one hand and complete desorption of Hg^{2+} on the other hand (for further details see Figure 60, Experimental Part).

Table 22. Recycling of **71h** to detoxify a mercury containing solution with low (left) and higher (right) metal concentrations.

| Cycle | 10 μM Hg^{2+} , 10 min ^a | | 100 μM Hg^{2+} , 2 hours ^b | |
|-------|---------------------------------------------------------|--------------------------------------|-----------------------------------------------------------|--------------------------------------|
| | Hg [%] | Co [$\text{mg}\cdot\text{L}^{-1}$] | Hg [%] | Co [$\text{mg}\cdot\text{L}^{-1}$] |
| Run 1 | 88 | 1.12 | 84 (78) | 3.08 |
| Run 2 | 89 | 1.07 | 83 (85) | 2.29 |
| Run 3 | 80 (97) | 0.87 | 34 (67) | 1.33 |
| Run 4 | 28 ^c | 0.05 | 44 (68) | 0.77 |
| Run 5 | 88 | 0.56 | 31 (64) | 1.39 |
| Run 6 | 88 (99) | 0.62 | 33 (57) | 0.35 |
| Run 7 | 89 | 0.73 | | |
| Run 8 | 72 | 0.53 | | |
| Run 9 | 41 (87) | 0.20 | | |

Metal adsorbed based on concentration of the remained solution. In brackets: metal released referring to adsorbed metal. [a] *Extraction conditions:* 2 mg **71h** were used at 30 °C to decontaminate 10 mL of a 10 μM mercury solution (20 μg Hg^{2+}) in 10 minutes. Desorption was carried out after every third cycle with 5 mL of a 2M HCl solution; [b] Conditions: 2 mg **71h** were used at 30 °C to decontaminate 10 mL of a 100 μM mercury solution (201 μg Hg^{2+}) in 2 hours. Desorption was carried out after every cycle with 5 mL of a 2M HCl solution; [c] This run is considered to be an outlier, caused by insufficient dispersion.

Investigating the recyclability of the nanoscavenger at low mercury ion concentrations (10 μM , Table 22) showed a good to excellent adsorption of mercury ions with complete desorption. Only after eight

runs, a drop in the adsorption capacity to 41% was observed. Applying higher initial mercury concentrations of 100 μM , an extended extraction time of 2 hours was necessary to detoxify the solution with the same low amount of 2 mg of **71h**. The prolonged adsorption time increased the Co leaching only to a small extent ($3.1 \text{ mg}\cdot\text{L}^{-1} \text{ Co}$), while removing $16.9 \text{ mg}\cdot\text{L}^{-1} \text{ Hg}^{2+}$ in the first cycle. Although the capacity dropped after the second cycle, the nanoadsorbent was still able to capture at least $6.2 \text{ mg}\cdot\text{L}^{-1}$ mercury for further four consecutive cycles, corresponding to overall 781 μg of adsorbed mercury ions per 2 mg of **71h**.

Encouraged by the simple recycling protocol depicted in Figure 41, the adsorption capacities of the single metal ions were analyzed with regard to their desorption properties and impact on the recoverability (Table 23). Therefore, 2 mg **71h** were used for the decontamination of three times each 10 mL of a 200 μM solution of lead. Gratifyingly, overall 93% lead were extracted within the three runs, corresponding to an excellent adsorption capacity of 273 mg Pb^{2+} per gram of **71h**. After desorbing Pb^{2+} from the latter with an acidic solution, the next metal solution, chromium, was examined. Accordingly, 40 mg Cr^{3+} , 54 mg Cu^{2+} , and 94 mg Hg^{2+} per gram of scavenger could be extracted by the nanoadsorbent **71h** within the recycling procedure, further demonstrating its reusability and capability for diverse metal ions.

Table 23. Testing the maximal adsorption capacities of single metal solutions during the recycling of **71h**.

| | | Adsorbed metal [%] | Desorbed metal [%] | Adsorption capacity [$\text{mg}\cdot\text{g}^{-1}$] |
|-----------|----|--------------------|--------------------|-------------------------------------------------------|
| Run 1-3 | Pb | 93 | 93 | 273 |
| Run 4-6 | Cr | 52 | 43 | 40 |
| Run 7-9 | Cu | 71 | 75 | 54 |
| Run 10-12 | Hg | 33 | 44 | 94 |

Extraction conditions: 2.1 mg **71h** were stirred three consecutive times in 10 mL of a 200 μM solution of the corresponding metal for 20 hours, afterwards the metals were released with acid. Subsequently, **71h** was regenerated with a Na_2CO_3 solution and reused for the next metal. The desorbed metal is calculated based on the adsorbed amount.

In summary, a hyper-cross-linked magnetic polymer based on 2,2'-biphenol achieved high extraction capacities with unique selectivity for mercury ions. The affinity to other toxic heavy metal ions, especially lead and mercury, is particularly interesting, since the described nanoadsorbent was further able to detoxify a solution containing copper, chromium, lead, and mercury ions in 100 μM . The recyclability was ensured for up to eight cycles without a loss in efficiency for low heavy metal concentrations and four cycles for higher concentrations. The facile magnetic retrieval of the scavenger, as well as the simple regeneration process, may provide a designated alternative for industrial purposes.

C. Summary

The application of magnetic nanobeads as semi-heterogeneous supports has gained considerable attention over the last century, allowing a facile recovery and sustainable recyclability of the immobilized reagents, scavengers, or catalysts.

The first chapter of this thesis compares the influence of different monomers for the synthesis of microporous organic polymers and their resulting capability to encapsulate palladium nanoparticles (Figure 42). Starting with toluene-based polymers, the impact of the external cross-linker FDA was investigated. The highest surface area was achieved for polymer **4a-γ** with 2.5 equivalents of the cross-linker. Incorporating palladium nanoparticles further demonstrated the beneficial effect of the high cross-linker content by means of the highest catalytic activity for the Pd-catalyst **5a-γ**. Thus, high turnover frequencies of up to 3000 h^{-1} were achieved for the hydrogenation of alkenes, alkynes, and nitro arenes, whereby the magnetic core of the nanobeads ensured an easy and fast recyclability for at least six consecutive runs. Introducing hydroxyl groups into the MOP *via* 2,2'-biphenol as monomer reduced the metal leaching from the catalyst (**5d**) to a minimum, while maintaining a high catalytic activity and recyclability in the hydrogenation reaction.

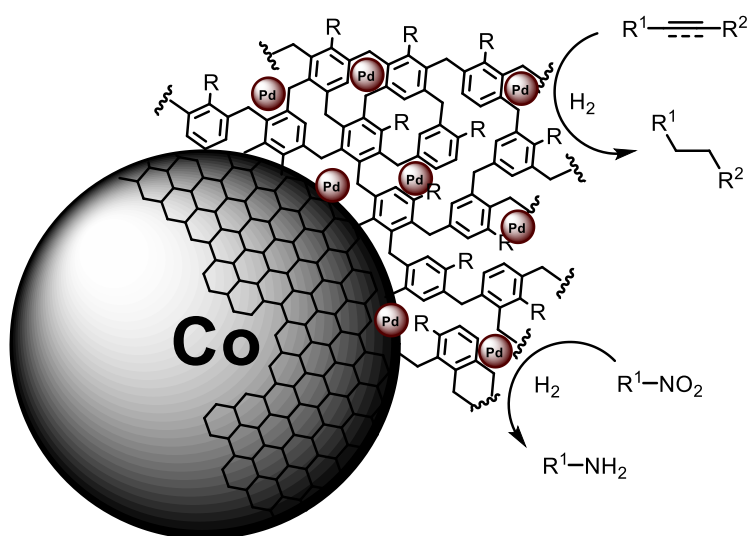


Figure 42. Hydrogenation of alkenes, alkynes, and nitro arenes using Pd@MOPs@Co/C as recyclable catalysts.

In the second chapter, a palladium-based nanocatalyst is described for the use in the Suzuki-Miyaura coupling with focus on mild reaction conditions with low temperatures up to $50 \text{ }^\circ\text{C}$. An immobilized *N*-heterocyclic carbene palladium(II) complex enabled the efficient coupling of aryl iodides as well as aryl bromides with boronic acids for up to six cycles (Figure 43). The linking of this complex to polystyrene-functionalized Co/C nanobeads facilitated the recycling protocol by simple magnetic decantation combined with an overall low metal leaching. Thus, palladium(II) NHC-functionalized catalyst

Pd(II)@PS-NHC@Co/C **22** was considered to be worthwhile for further investigation in its application towards genetically-tagged small molecule libraries. Currently conducted in the working group of Dr. Brunschweiler at the TU Dortmund.

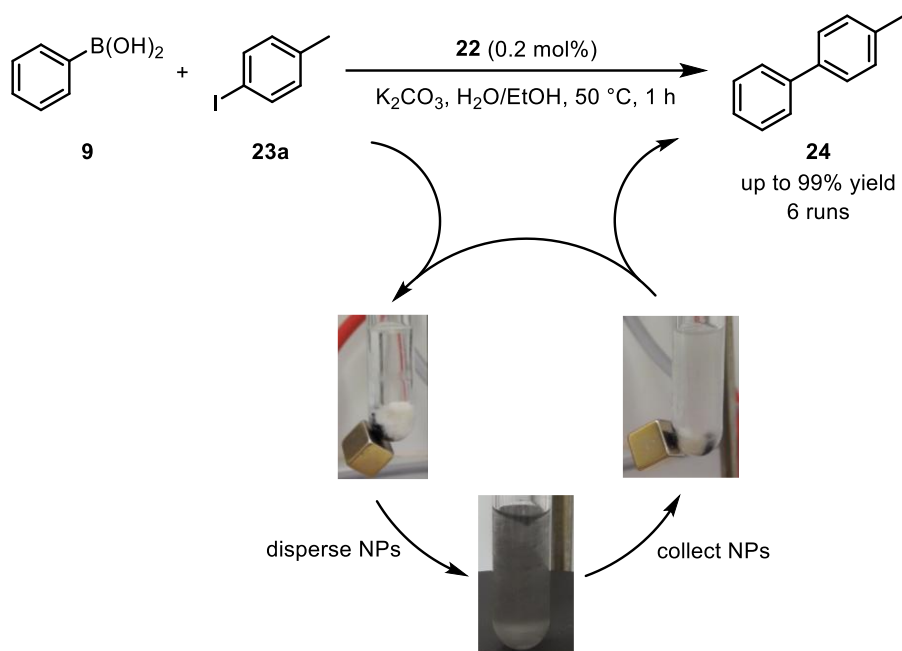
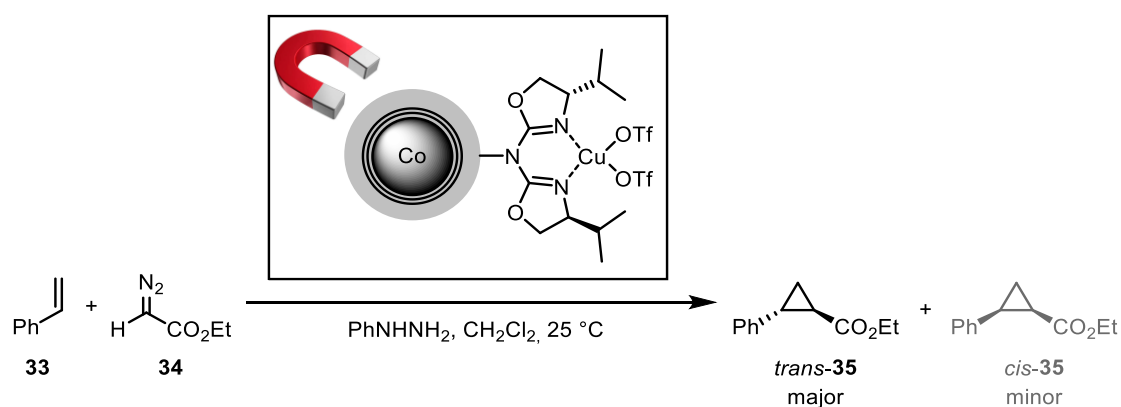


Figure 43. Suzuki-Miyaura coupling under mild reaction conditions catalyzed by Pd(II)@PS-NHC@Co/C **22** for a facile recovery.

The third chapter describes the immobilization of chiral copper(II)-aza-bis(oxazoline) complexes onto polystyrene-functionalized magnetic Co/C nanobeads *via* two common linking strategies. As model reaction, the asymmetric copper-catalyzed cyclopropanation of styrene **33** was chosen, revealing a distinct advantage of the directly linked catalyst **30c** with a high ligand loading (Scheme 25). Low ligand loadings and the grafting to azide-functionalized nanoparticles **52** *via* 'click-chemistry' showed a decreased enantioselectivity and lack of recyclability. Applying catalyst **30c**, six consecutive cyclopropanation cycles were performed with up to 63% yield of **35** and 76% *ee* for *trans*-**35**.



Scheme 25. Enantioselective cyclopropanation of **33** using Cu(II)@azaBOX@PS@Co/Cs as recyclable catalysts.

The final chapter investigates MOPs immobilized on Co/C nanobeads as recyclable high capacity adsorbents for toxic heavy metal ions with special attention to lead and mercury. Again, different monomers were utilized for the synthesis of a broad variety of nanomaterials. Comparing these in the competitive extraction of mercury, lead, copper, and chromium ions revealed a high adsorption potential for all of these metal ions using 2,2'-biphenol@Co/C **71h** as polymer (Figure 44). Further, this nanoscavenger showed an excellent selectivity towards mercury ions with an outstanding adsorption capacity up to 810 mg Hg²⁺ per gram of nanoparticles. The facile recycling procedure enabled an efficient decontamination of water polluted with lead, chromium, and copper ions with the aid of an external magnet for up to nine cycles. Adjusting the applied amount of nanoscavenger allowed either the selective extraction of mercury ions or the purification of the water from all metal ions.

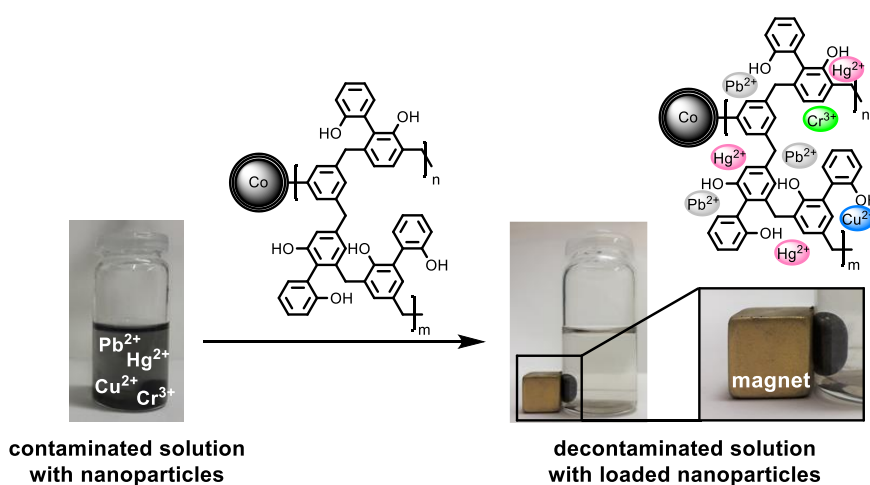


Figure 44. Decontamination of an aqueous solution polluted with lead, mercury, copper, and chromium ions by the aid of the nanoscavenger **71h**, showing the facile recovery of the nanoparticles by an external magnet within seconds.

D. Zusammenfassung

Die Verwendung magnetischer Nanopartikel als semi-heterogene Trägermaterialien hat innerhalb des letzten Jahrhunderts beträchtliche Aufmerksamkeit auf sich gezogen. Diese ermöglichen eine einfache Rückgewinnung und nachhaltige Recyclingfähigkeit von den immobilisierten Reagenzien, Scavengern oder Katalysatoren.

Das erste Kapitel dieser Dissertation vergleicht den Einfluss verschiedener Monomere auf die Synthese von mikroporösen organischen Polymeren und ihre daraus resultierende Fähigkeit, Palladium-Nanopartikel einzulagern (Abbildung 1). Ausgehend von Polymeren basierend auf dem Monomer Toluol wurde die Auswirkung des externen Quervernetzers FDA untersucht. Die höchste Oberfläche konnte für das Polymer **4a-y**, unter Verwendung von 2,5 Äquivalenten des Quervernetzers, erreicht werden. Die vorteilhafte Wirkung eines hohen Quervernetzer-Anteils wurde ferner durch die Einlagerung von Palladium-Nanopartikeln gezeigt, da mit dem Pd-Katalysator **5a-y** die höchste katalytische Aktivität erhalten wurde. Auf diese Weise konnten hohe TOFs bis zu 3000 h^{-1} für die Hydrierung von Alkenen, Alkinen und Nitroaromaten erzielt werden, wobei der magnetische Kern der Nanopartikel eine einfache und schnelle Recyclingfähigkeit für mindestens sechs aufeinanderfolgende Zyklen sicherstellte. Das Einführen von Hydroxylgruppen in das MOP durch das Monomer 2,2'-Biphenol reduzierte das Metall-Leaching des Katalysators (**5d**) auf ein Minimum. Gleichzeitig konnte dabei die hohe katalytische Aktivität in der Hydrierungsreaktion sowie die Recyclingfähigkeit des Katalysators aufrechterhalten werden.

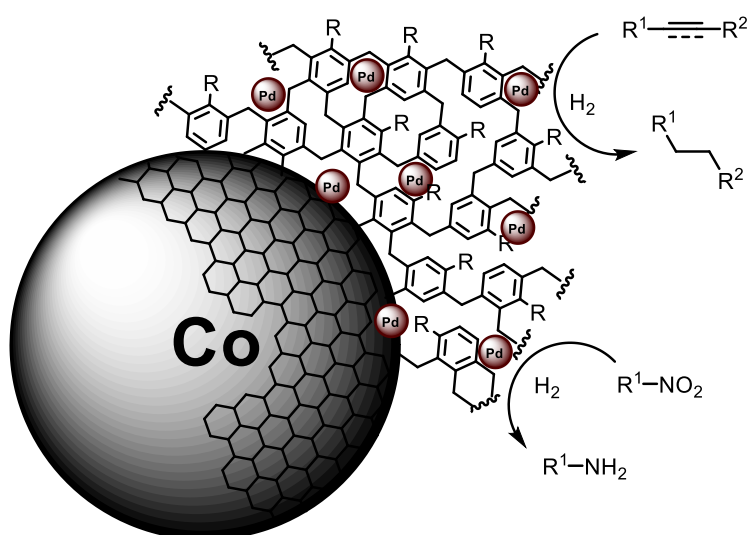


Abbildung 1. Hydrierung von Alkenen, Alkinen und Nitroaromaten unter Verwendung von Pd@MOPs@Co/C als wiederverwendbare Katalysatoren.

Im zweiten Kapitel wird ein Palladium-basierter Nanokatalysator für die Verwendung in der Suzuki-Miyaura Kupplung beschrieben. Der Schwerpunkt wurde hierbei auf milde Reaktionsbedingungen mit

niedrigen Temperaturen von bis zu 50 °C gelegt. Ein immobilisierter *N*-heterocyclischer Palladium(II)-Carben-Komplex ermöglichte sowohl die effiziente Kupplung von Boronsäuren mit Aryliodiden als auch mit Arylbromiden für bis zu sechs Zyklen (Abbildung 2). Die Verknüpfung dieses Komplexes mit Polystyrol-funktionalisierten Co/C Nanopartikeln erleichterte das Recycling-Protokoll durch eine einfache magnetische Dekantation in Kombination mit einem insgesamt niedrigen Metall-Leaching. Daher wurde der Palladium(II)-NHC-funktionalisierte Katalysator Pd(II)@PS-NHC@Co/C **22** als geeignet angesehen, um ihn für weitere Untersuchungen zur Erstellung einer Bibliothek von genetisch markierten kleinen Molekülen zu verwenden. Diese werden derzeit in der Arbeitsgruppe von Dr. Brunschweiler in der TU Dortmund durchgeführt.

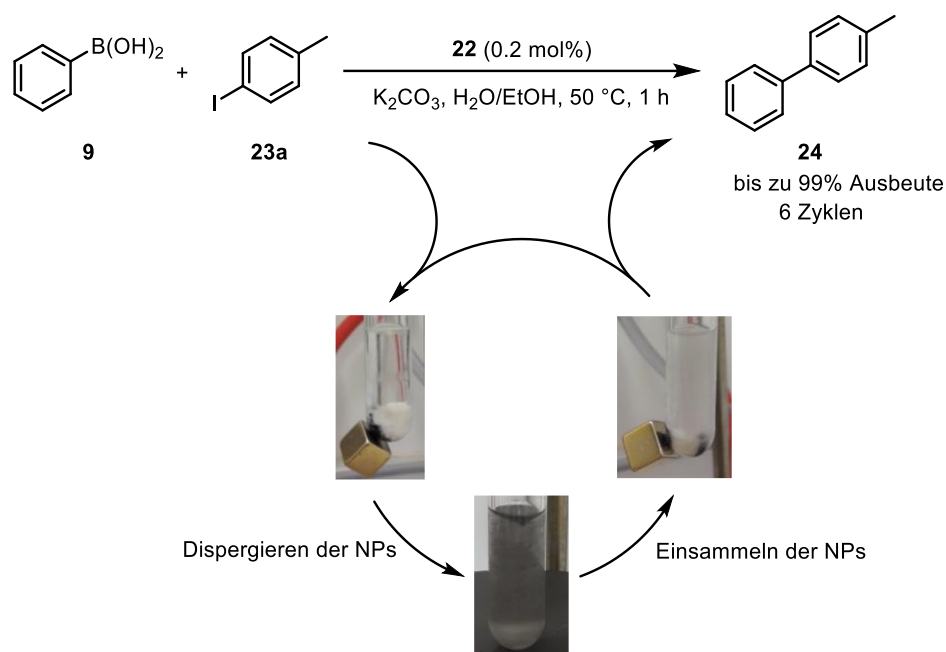
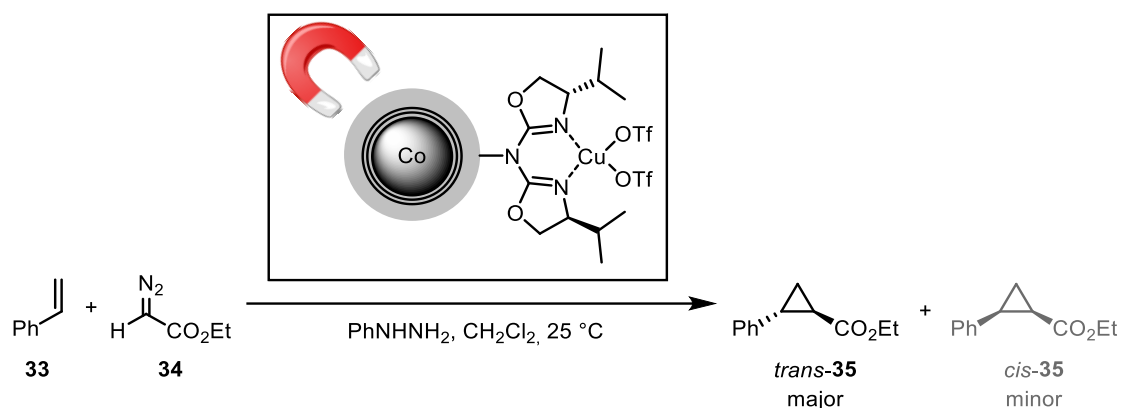


Abbildung 2. Suzuki-Miyaura Kupplung unter milden Reaktionsbedingungen, katalysiert mit Pd(II)@PS-NHC@Co/C **22** für eine einfache Rückgewinnung.

Das dritte Kapitel beschreibt die Immobilisierung von chiralen Kupfer(II)-aza-bis(oxazolin)-Komplexen auf Polystyrol-funktionalisierten magnetischen Co/C Nanopartikeln über zwei gängige Verknüpfungsstrategien. Als Modellreaktion wurde die asymmetrische Cyclopropanierung von Styrol **33** ausgewählt, die einen deutlichen Vorteil des direkt verknüpften Katalysators **30c** mit einer hohen Ligandenbeladung aufzeigte (Schema 1). Nicht nur niedrige Ligandenbeladungen, sondern auch die Ligandenanbindung an Azid-funktionalisierte Nanopartikel **52** durch „Click-Chemie“ resultierten beide in verminderten Enantioselektivitäten und einer reduzierten Recyclingfähigkeit. Unter Verwendung des Katalysators **30c** konnten sechs aufeinanderfolgende Cyclopropanierungs-Zyklen mit einer Ausbeute von bis zu 63% für das Produkt **35** und 76% *ee* für *trans*-**35** durchgeführt werden.



Schema 1. Enantioselektive Cyclopropanierung von **33** unter Verwendung von Cu(II)@azaBOX@PS@Co/Cs als wiederverwendbare Katalysatoren.

Das letzte Kapitel untersucht MOPs, die auf Co/C Nanopartikeln immobilisiert wurden, in Hinsicht auf ihre Fähigkeit als wiederverwendbare Nanoadsorber mit hohen Kapazitäten für toxische Schwermetallionen. Hierbei wurden insbesondere Blei- und Quecksilberionen berücksichtigt. Auch hier wurden verschiedene Monomere zur Synthese verwendet, um eine breite Vielfalt an Nanomaterialien herzustellen. Ein Vergleich dieser in der kompetitiven Extraktion von Quecksilber-, Blei-, Kupfer- und Chromionen demonstrierte ein hohes Adsorptionspotential von Polymer 2,2'-Biphenol@Co/C **71h** für all diese Metallionen (Abbildung 3). Ferner zeigte dieser Nanoadsorber eine ausgezeichnete Selektivität gegenüber Quecksilberionen mit einer hervorragenden Adsorptionskapazität von bis zu 810 mg Hg²⁺ pro Gramm der Nanopartikel. Das einfache Recyclingverfahren unter Verwendung eines externen Magneten, ermöglichte eine effiziente Dekontamination von einer mit Blei-, Chrom- und Kupferionen belasteten Wasserprobe für bis zu neun Zyklen. Die Anpassung der eingesetzten Menge der Adsorberpartikel ermöglichte entweder die selektive Extraktion von Quecksilberionen oder die Entfernung aller Metallionen aus dem Wasser.

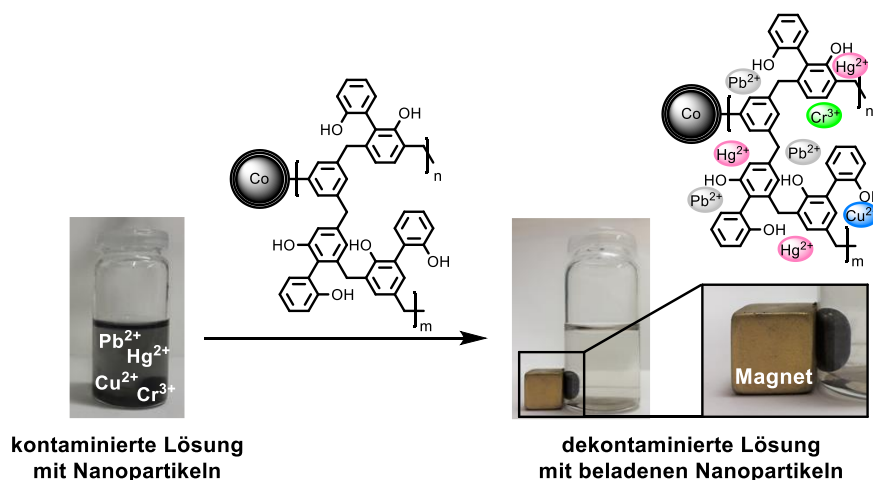


Abbildung 3. Dekontaminierung einer mit Blei-, Quecksilber-, Kupfer- und Chromionen verunreinigten wässrigen Lösung mit Hilfe des Nanoadsorbers **71h**. Die Rückgewinnung der Nanopartikel erfolgt innerhalb von Sekunden durch einen externen Magneten.

E. Experimental Part

1. General Information

Chemicals and solvents

All commercially available chemicals were obtained in high quality and used without further purification, unless otherwise noted. Hexanes (60/40) and ethyl acetate were freshly distilled before usage. Anhydrous solvents were prepared by the technicians applying established procedures.^[173]

Heavy-wall glass tubes or heavy-wall Schlenk flasks are borosilicate glass tubes which are stable up to 5 bar.

All products were literature known and in accordance with the analytical data. Carbon-coated cobalt nanoparticles (Co/C) were analyzed in accordance with the analytical possibilities, whereby the elemental analysis and cobalt leaching may differ slightly depending on the applied Co/C batch.

Co/C nanoparticles **1** were obtained from Prof. W. J. Stark from the ETH Zurich, Switzerland. Prior to use, they were washed according to the general procedure **GP-1**. They were dispersed by the aid of an ultrasound bath (Sonorex RK 255 H-R, Bandelin) and recovered with the help of a commercially available neodymium based magnet (12 x 12 mm or 15 x 30 mm).

NMR-Spectroscopy

¹H NMR spectra were recorded on a BRUKER Avance 300 (300 MHz) and a BRUKER Avance III 400 "Nanobay" (400 MHz) spectrometer. ¹³C NMR spectra were recorded on a BRUKER Avance 300 (75 MHz) and a BRUKER Avance III 400 "Nanobay" (101 MHz) spectrometer. All spectra were recorded at ambient temperature in CDCl₃ or CD₃OD. Chemical shifts for ¹H NMR spectra are reported as δ , parts per million [ppm], calibrated to the signal of the solvent: CDCl₃ = 7.26 or CD₃OD = 3.31 ppm. Chemical shifts for ¹³C NMR spectra are calibrated to the signal of the solvent: CDCl₃ = 77.16 or CD₃OD = 49.00 ppm. The coupling constants *J* are in Hertz [Hz]. Splitting patterns for the spin multiplicity in the ¹H NMR spectra are denoted as follows: s = singlet, d = doublet, t = triplet, q = quartet, dt = doublet of a triplet, dd = doublet of a doublet, m = multiplet.

Quantitative NMR analysis (qNMR)

Quantitative ¹H NMR analysis was carried out using an internal standard (1,3,5-trimethoxybenzene (singlet at 6.09 ppm (3H) and 3.77 ppm (9H)). The integral of a peak in the ¹H NMR spectra is proportional to the number of nuclei creating this resonance. The amount of product was quantified by the following equation:

$$\frac{n(\text{product})}{n(\text{standard})} = \frac{Int^0(\text{product})}{Int^0(\text{standard})} \text{ with } Int^0 = \frac{Int}{N(\text{protons})}$$

Int^0 = normalized integral; peak integral (Int) divided through the number of protons (N(protons))

Elemental microanalysis (EA)

Elemental microanalysis was performed by the Micro Analytical Laboratory of the University of Regensburg using a Vario MICRO cube. The loading of the element X can be calculated *via* the following equation.

$$loading(X) = \frac{\Delta w(X) \cdot 10}{M(X) \cdot N(X)}$$

$\Delta w(X)$ = mass fraction difference before and after functionalization according to the element X

$M(X)$ = molecular weight ($\text{g} \cdot \text{mol}^{-1}$) of the element X

$N(X)$ = number of added atoms of the element X

10 = conversion factor for units

Thin-layer chromatography (TLC)

Thin-layer chromatography was performed with TLC pre-coated aluminum sheets (Merck Silica gel 60 F254, 0.2 mm layer thickness). Visualization was obtained by irradiation with UV light ($\lambda = 254$ nm and 366 nm) and through the use of TLC stains, e.g. KMnO_4 , vanillin/sulfuric acid, and ninhydrin solutions, followed by heating.

Column chromatography

(Flash-) Column chromatography was performed using Merck Gerduran 60 (0.063 – 0.200 mm) or Merck flash (0.040 – 0.063 mm) silica gel.

Infrared spectroscopy (IR)

Infrared spectra were recorded on an Agilent Cary 630 FT-IR spectrometer. The wavenumbers are reported as cm^{-1} . Nanoparticles were measured neat. Meaningful IR spectra were not possible at low polymer loadings and for all functionalized nanoparticles and are thus only mentioned where necessary.

Chiral high performance liquid chromatography (chiral HPLC)

Chiral HPLC was performed on a Varian LC-902 Liquid Chromatograph using a Chiralpak AS-H column (4.6×250 mm, $10 \mu\text{m}$), as well as Phenomenex Lux Cellulose-1 and Cellulose-2 columns (4.6×250 mm, $5 \mu\text{m}$). Absolute configuration of the product was determined by comparison with literature values.

Gas chromatography (GC)

Gas chromatography was carried out on a Fisons Instruments GC8000 equipped with a capillary column (DB-1 100% dimethylpolysiloxane, 30 m x 250 μm x 0.25 μm) and flame ionization detector (temperature: 300 °C detector, 250 °C injector). Chiral gas chromatography was carried out on a Fisons Instruments GC8000 equipped with a Cyclodex- β column (CP-chirasil-DexCB; 25 m x 250 μm x 0.25 μm) and flame ionization detector (temperature: 250 °C detector, 250 °C injector). Gas chromatography coupled with mass spectrometry (GC-MS) was carried out on a Shimadzu GCMS-QP2010 SE equipped with a quadrupole mass analyzer.

Transmission electron microscopy (TEM) and element mapping

Transmission electron microscopy was performed on a FEI TecnaiF30 using standard TEM plates (carbon film on 400 mesh grids copper) with 3.05 mm diameter at the Department of Physics of the University of Regensburg Italian Institute of Technology, Genoa. For HRTEM analysis the sample was dispersed in ethanol with the aid of an ultrasonic bath for 5 min and a drop of the solution was placed on a copper grid with holey carbon film. Element mapping (STEM energy-dispersive X-ray spectroscopy (EDS)) was acquired by high-resolution transmission electron microscopy on FEI Model: Tecnai G2, F30 Resolution point: 2.0 Angstrom Line: 1.0 a Magnification: 58 \times to 1000000 \times at potential 300 kV at the RCPTM, Palacky University, Czech Republic. These measurements were performed at RCPTM, Palacky University, Czech Republic.

X-ray photoelectron spectroscopy (XPS)

X-ray photoelectron spectroscopy was carried out on a Perkin-Elmer Physical Electronics PHI5700 ESCA System at the Department of Physics of the University of Regensburg. Furthermore, XPS was performed on a PHI 5000 VersaProbe II XPS system (Physical Electronics) with monochromatic Al-K α source (15 kV, 50 W) and photon energy of 1486.7 eV at the Palacky University, Czech Republic. Dual beam charge compensation was used for all XPS measurements. All the spectra were measured in the vacuum of 1.3×10^{-7} Pa and at the room temperature of 21 °C. The analyzed area on each sample was spot of 100 μm in diameter. The survey spectra were measured with pass energy of 187.850 eV and electronvolt step of 0.8 eV while for the high-resolution spectra pass energy of 23.500 eV and electronvolt step of 0.2 eV were used. The spectra were evaluated with the MultiPak (Ulvac - PHI, Inc.) software. All binding energy (BE) values were referenced to the carbon peak C 1s at 284.80 eV.

Nitrogen sorption measurements

Nitrogen sorption measurements were conducted at 77 K using an Autosorb iQ instrument at the Italian Institute of Technology, Genoa. The samples were degassed at 200 °C for 3 h under vacuum

prior to measurement. Surface areas and pore volumes were calculated by multi-point Brunauer-Emmett-Teller (BET) method, pore size distribution calculated by the Barrett-Joyner-Halenda (BJH) method, and micropore size distribution was obtained by the Horvath-Kawazoe (HK) method at the Italian Institute of Technology, Genoa.

Thermo-gravimetric analysis (TGA)

Thermo-gravimetric analysis was performed from 30 to 1000 °C at a heating rate of 10 °C/min by the Institute of Physical and Theoretical Chemistry of the University of Regensburg on a Perkin-Elmer TGA7.

UV-vis spectrophotometry

UV-vis spectra were recorded by a Specord® Plus 200 spectrophotometer in a scanning range of 200 – 600 nm at room temperature of 25 °C using standard quartz cuvettes.

Inductively coupled plasma-optical emission spectrometry (ICP-OES)

Samples for the inductively coupled plasma optical emission spectrometry (ICP-OES) were measured with a Spectro Analytical Instruments ICP Modula EOP (November 2016 to November 2018) or Spectroblue FMX36 (March 2019 to December 2020) in an acidic medium (32% *aqua regia*, v/v) after prior standardization and calibration. The metals were determined at the following wavelengths: Spectro Analytical Instruments ICP Modula EOP: Co $\lambda = 228.616$ nm, Cu $\lambda = 221.810$ nm, Fe $\lambda = 239.562$ nm, Pd $\lambda = 340.458$ nm. Spectroblue FMX36: Co $\lambda = 228.616$ nm, Cu $\lambda = 324.754$ nm, Fe $\lambda = 259.941$ nm, Pd $\lambda = 340.458$ nm (360.955 nm additional).

Inductively coupled plasma-mass spectrometry (ICP-MS)

Samples for the inductively coupled plasma mass spectrometry (ICP-MS) were measured with a Perkin Elmer Elan 9000, P0890211 (January to March 2019) in an acidic medium (5% HNO₃, v/v) after prior standardization and calibration. The inspected ions were detected at a mass-to-charge (*m/z*) ratio of Co 58.9 and Cu 62.9 with Sc as an internal standard at 45.0.

The samples were prepared according to the sample preparation ICP-OES resulting in 32% *aqua regia* solution (v/v). Then, this solution was filtered through a syringe filter (hydrophilic PTFE 0.2 μm) and diluted with 5% HNO₃ (ultrapure grade) (v/v) to 10 mL (leaching sample: 1/20 dilution, catalyst sample: 1/200). Finally, a defined volume of a Sc solution was added as internal standard.

General sample preparation for ICP-OES

5.0 mg of the functionalized Co/C nanoparticles were heated in 1.6 mL *aqua regia* at 100 °C for 10 minutes. The particles were collected by an external magnet and the solution was transferred to a 10 mL volumetric flask. This process was repeated and the combined solution was filled up with H₂O (millipore grade) to 10 mL. Subsequently, the solution was filtered through a syringe filter (hydrophilic PTFE 0.2 μm) resulting in a 32% *aqua regia* solution (v/v).

General sample preparation for leaching experiments for ICP-OES

The reaction and washing solutions were combined in a round bottom flask, filtered through a syringe filter (hydrophobic PTFE 0.2 μm), the solvent was evaporated and the dried product was treated with 2.4 mL HCl_{conc.} and 0.8 mL HNO_{3 conc.} and heated at 100 °C for 10 minutes. Upon cooling to room temperature, the mixture was washed with millipore water and the aqueous phase was transferred to a volumetric flask with simultaneous filtering through a syringe filter (hydrophilic PTFE 0.2 μm) resulting in 32% *aqua regia* solution (v/v).

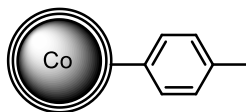
General procedure for washing pristine Co/C NPs (1) (GP-1)

Prior to use, the received carbon-coated cobalt nanoparticles (Co/C) **1** were washed five times for 24 hours in a HCl_{conc.}/H₂O_{millipore} mixture (1:1). Subsequently, the particles were collected by the help of an external magnet and washed with millipore water until the pH of the decanted solution was neutral to remove any acid residuals. Finally, the particles were washed with acetone (3x) and diethyl ether (2x) and dried at 50 °C under vacuum.^[37]

Elemental microanalysis [%]: 4.50 C, traces H, 0 N.

2. Hydrogenation reactions using microporous organic polymers

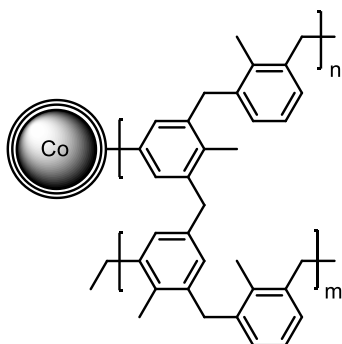
2.1. Synthesis of catalyst and starting materials



Toluene-functionalized Co/C NPs (**3**)

According to literature procedure,^[37] unfunctionalized Co/C NPs **1** (1.00 g, 4.50% C, traces H), 4-toluidine (161 mg, 1.50 mmol, 1.0 equiv.) and concentrated HCl (0.6 mL) were suspended in H₂O_{millipore} (25 mL) with the aid of an ultrasonic bath. A pre-cooled solution of sodium nitrite (158 mg, 2.29 mmol, 1.5 equiv.) in H₂O_{millipore} (12 mL) was added dropwise at 0 °C to *in-situ* generate the diazonium species. The slurry was stirred for another 30 minutes in the ice bath and subsequently sonicated at ambient temperature for 30 minutes. The nanobeads were retracted by magnetic decantation and washed with NaOH (1 M, 3x), water (3x), acetone (6x), diethylether (2x), and dried under vacuum to afford 1.00 g of **3**.

Elemental microanalysis [%]: 4.96 C, 0.06 H, 0 N; **Loading (C):** 0.05 mmol/g.



General procedure for toluene@Co/C (**4a-γ**) (GP-2)

To a round bottom flask 500 mg toluene-functionalized Co/C NPs **3** anhydrous toluene (266 μL, 230 mg, 2.50 mmol, 1.0 equiv.), formaldehyde dimethyl acetal (555 μL, 476 mg, 6.25 mmol, 2.5 equiv.), anhydrous iron (III) chloride (1.01 g, 6.25 mmol, 2.5 equiv.), and 1,2-dichloroethane (45 mL) were introduced. The slurry was sonicated for 10 minutes and heated for five hours at 45 °C to form the network and then 19 hours at 80 °C to produce the microporous network. Upon cooling, the polymer was washed with ethanol and diethyl ether until the decanted solution was clear. The particles were dried *in vacuo* at 60 °C to afford 686 mg of **4a-γ**.

Elemental microanalysis [%]: 29.7 C, 2.12 H, 0 N.

Toluene@Co/C (4a-β)

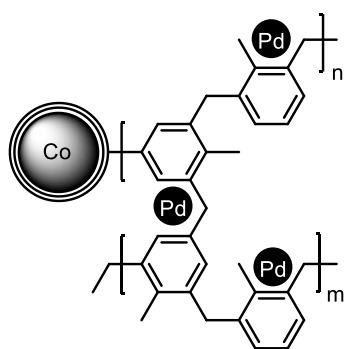
4a-β was synthesized according to **GP-2**, using 200 mg of NPs **3**, anhydrous toluene (106 μL, 92.1 mg, 1.00 mmol, 1.0 equiv.), formaldehyde dimethyl acetal (178 μL, 152 mg, 2.00 mmol, 2.0 equiv.), anhydrous iron (III) chloride (324 mg, 2.00 mmol, 2.0 equiv.), and 1,2-dichloroethane (18 mL) to afford 239 mg of **4a-β**.

Elemental microanalysis [%]: 21.8 C, 1.30 H, 0 N.

Toluene@Co/C (4a-α)

4a-α was synthesized according to **GP-2**, using 200 mg of NPs **3**, anhydrous toluene (106 μL, 92.1 mg, 1.00 mmol, 1.00 equiv.), formaldehyde dimethyl acetal (111 μL, 95.1 mg, 1.25 mmol, 1.25 equiv.), anhydrous iron (III) chloride (203 mg, 1.25 mmol, 1.25 equiv.), and 1,2-dichloroethane (18 mL) to afford 194 mg of **4a-α**.

Elemental microanalysis [%]: 11.8 C, 0.55 H, 0 N.



General procedure for Pd@toluene@Co/C (5a-γ, 1.9 wt% Pd) (GP-3)

A microwave vial was charged with toluene@Co/C nanoparticles **4a-γ** (0.50 g), Pd₂dba₃·CHCl₃ (52 mg, 50 μmol) and anhydrous toluene (15 mL) with subsequent nitrogen bubbling for 5 minutes. The reaction mixture was sonicated for 10 minutes and then heated in a focused microwave oven to 110 °C for 2 minutes. The resulting catalyst was recovered *via* magnetic decantation and washed with CH₂Cl₂ (6x). After drying the particles **5a-γ** at 60 °C *in vacuo*, 0.51 g were obtained with a loading of 0.18 mmol/g (89%) and 1.9 wt% Pd.

Elemental microanalysis [%]: 25.2 C, 1.75 H, 0 N; **Loading (Pd):** 0.18 mmol/g, 1.9 wt%.

Synthesis of 4b-4e and 5b-5e (2.5 equiv. FDA)

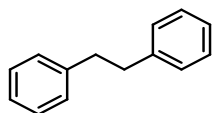
Polymers **4b-4e** and Pd-catalysts **5b-5e** were synthesized by Maryam Homafar according to **GP-2** and **GP-3**, respectively. Further details and characterization of these materials was published by Reiser *et al.*^[116] and is available online.

2.2. Catalysis**General procedure for hydrogenation reaction using Pd@toluene@Co/C (5a-γ, 1.9 wt% Pd) (GP-4)**

A Schlenk flask was charged with substrate (500 μmol, 1.0 equiv.), 2-PrOH (10 mL) and palladium catalyst **5a-γ** (1.9 wt% Pd) (5.7 mg, 1.0 μmol, 0.2 mol%). Then a substrate-dependent internal standard (dodecane (125 μL, 93.7 mg, 550 μmol, 1.1 equiv.) or ethylbenzene (0.067 mL, 58.4 mg, 550 μmol, 1.1 equiv.)) was added, and the mixture was stirred for 10 minutes. Subsequently, the flask was evaporated and flushed with H₂ for several times followed by vigorous stirring under 1 atm H₂. The reaction progress was monitored by GC analysis after collecting the nanoparticles by an external magnet and filtering the resulting solution through a syringe filter (hydrophobic PTFE 0.2 μm) before injection to GC.

General procedure for the recycling of Pd@toluene@Co/C (5a-γ, 1.9 wt% Pd) (GP-5)

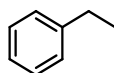
For recycling experiments, diphenylacetylene was chosen as a model substrate. Therefore, diphenylacetylene **8** (178 mg, 1.00 mmol, 1.0 equiv.) was hydrogenated in 20 mL 2-PrOH with Pd@toluene@Co/C **5a-γ** (1.9 wt% Pd) (12 mg, 2.0 μmol, 0.2 mol%) according to the **GP-4**. The reaction progress was monitored by GC analysis after collecting the nanoparticles by an external magnet and filtering the resulting solution through a syringe filter (hydrophobic PTFE 0.2 μm) before injection to GC. After the full conversion was reached, the particles were separated from the solution *via* magnetic decantation and washed with 2-PrOH (2x), CH₂Cl₂ (2x), dried under vacuum, and reused for the next run. After six consecutive runs, 88% of the original catalyst Pd@toluene@Co/C **5a-γ** (10 mg, 1.8 μmol) were regained.



1,2-Diphenylethane (7)

1,2-Diphenylethane **7** was prepared from 1,2-diphenylethyne **8** (90.0 μL , 89.1 mg, 500 μmol) according to general procedure **GP-4** using dodecane as internal standard. GC conditions: 3 min at 140 $^{\circ}\text{C}$, 16 $^{\circ}\text{C}/\text{min}$ to 300 $^{\circ}\text{C}$; retention time: dodecane (3.24 min), 1,2-diphenylethane (6.27 min), 1,2-diphenylethyne (7.50 min).

Further, 1,2-diphenylethane **7** was prepared from (*E*)-1,2-diphenylethene **6** (90.1 mg, 500 μmol) according to general procedure using dodecane as internal standard. GC conditions: 3 min at 140 $^{\circ}\text{C}$, 16 $^{\circ}\text{C}/\text{min}$ to 300 $^{\circ}\text{C}$; retention time: dodecane (3.18 min), 1,2-diphenylethane (6.23 min), (*E*)-1,2-diphenylethene (7.91 min).



Ethylbenzene

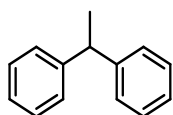
Ethylbenzene was prepared from styrene (57.3 μL , 52.1 mg, 500 μmol) according to general procedure **GP-4** using dodecane as internal standard. GC conditions: 3 min at 50 $^{\circ}\text{C}$, 10 $^{\circ}\text{C}/\text{min}$ to 250 $^{\circ}\text{C}$; retention time: ethylbenzene (5.01 min), styrene (5.55 min), dodecane (11.63 min).

Further, ethylbenzene was prepared from ethynylbenzene (54.9 μL , 51.1 mg, 500 μmol) according to general procedure using dodecane as internal standard. GC conditions: 1 min at 50 $^{\circ}\text{C}$, 1 $^{\circ}\text{C}/\text{min}$ to 60 $^{\circ}\text{C}$ (0 min), 20 $^{\circ}\text{C}/\text{min}$ to 250 $^{\circ}\text{C}$; retention time: ethylbenzene (5.45 min), ethynylbenzene (5.81 min), styrene (6.37 min), dodecane (15.85 min).



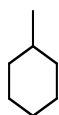
Bicyclo[2.2.1]heptane

Bicyclo[2.2.1]heptane was prepared from bicyclo[2.2.1]hept-2-ene (47.1 mg, 500 μmol) according to general procedure **GP-4** using dodecane as internal standard. GC conditions: 3 min at 50 $^{\circ}\text{C}$, 10 $^{\circ}\text{C}/\text{min}$ to 200 $^{\circ}\text{C}$; retention time: bicyclo[2.2.1]hept-2-ene (2.59 min), bicyclo[2.2.1]heptane (3.04 min), dodecane (11.65 min).



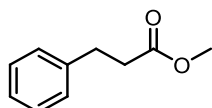
Ethane-1,1-diyldibenzene

Ethane-1,1-diyldibenzene was prepared from ethene-1,1-diyldibenzene (88.4 μL , 90.1 mg, 500 μmol) according to general procedure **GP-4** using dodecane as internal standard. GC conditions: 3 min at 140 $^{\circ}\text{C}$, 16 $^{\circ}\text{C}/\text{min}$ to 300 $^{\circ}\text{C}$; retention time: dodecane (3.23 min), ethene-1,1-diyldibenzene (5.95 min), ethane-1,1-diyldibenzene (6.17 min).



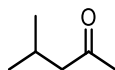
Methylcyclohexane

Methylcyclohexane was prepared from 1-methylcyclohex-1-ene (59.3 μL , 48.1 mg, 500 μmol) according to general procedure **GP-4** using dodecane as internal standard. GC conditions: 3 min at 50 $^{\circ}\text{C}$, 10 $^{\circ}\text{C}/\text{min}$ to 200 $^{\circ}\text{C}$; retention time: methylcyclohexane (2.71 min), 1-methylcyclohex-1-ene (3.38 min), dodecane (11.54 min).



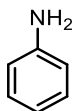
Methyl 3-phenylpropanoate

Methyl 3-phenylpropanoate was prepared from methyl cinnamate (81.1 mg, 500 μmol) according to general procedure **GP-4** using dodecane as internal standard. GC conditions: 3 min at 100 $^{\circ}\text{C}$, 20 $^{\circ}\text{C}/\text{min}$ to 300 $^{\circ}\text{C}$; retention time: dodecane (5.70 min), methyl 3-phenylpropanoate (6.15 min), methyl cinnamate (7.15 min).



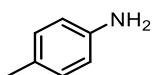
4-Methylpentan-2-one

4-Methylpentan-2-one was prepared from 4-methylpent-3-en-2-one (57.2 μL , 49.1 mg, 500 μmol) according to general procedure **GP-4** using dodecane as internal standard. GC conditions: 3 min at 50 $^{\circ}\text{C}$, 10 $^{\circ}\text{C}/\text{min}$ to 75 $^{\circ}\text{C}$ (0 min), 20 $^{\circ}\text{C}/\text{min}$ to 200 $^{\circ}\text{C}$; retention time: 4-methylpent-3-en-2-one (2.78 min), 4-methylpentan-2-one (3.70 min), dodecane (9.87 min).



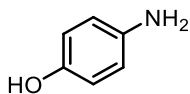
Aniline

Aniline was prepared from nitrobenzene (51.3 μL , 61.6 mg, 500 μmol) according to general procedure **GP-4** using ethylbenzene as internal standard. GC conditions: 3 min at 50 $^{\circ}\text{C}$, 10 $^{\circ}\text{C}/\text{min}$ to 200 $^{\circ}\text{C}$; retention time: ethylbenzene (5.00 min), aniline (7.05 min), nitrobenzene (9.04 min).



4-Aminotoluene

4-Aminotoluene was prepared from 4-nitrotoluene (68.6 mg, 500 μmol) according to general procedure using **GP-4** dodecane as internal standard. GC conditions: 3 min at 50 $^{\circ}\text{C}$, 10 $^{\circ}\text{C}/\text{min}$ to 200 $^{\circ}\text{C}$; retention time: 4-aminotoluene (8.95 min), 4-nitrotoluene (11.33 min), dodecane (11.62 min).



4-Aminophenol

A Schlenk flask was charged with 4-nitrophenol (69.6 mg, 500 μmol , 1.0 equiv.), 2-PrOH (10 mL), palladium catalyst **5a- γ** (1.9 wt% Pd) (27 mg, 4.8 μmol , 1 mol%), and a septum. The mixture was stirred at room temperature until good dispersion was achieved. Subsequently, the flask was evaporated and flushed with H_2 for several times followed by vigorous stirring under 1 atm H_2 at 50 $^{\circ}\text{C}$. Kinetic studies were carried out by UV-vis spectroscopy. Therefore, samples were taken every 10 minutes by collecting the catalyst with an external magnet, taking 0.10 mL of the reaction mixture with a syringe, and filtering through a syringe filter (hydrophobic PTFE 0.2 μm). The resulting solution was diluted with 2-PrOH to

yield a concentration of 0.050 mM. Afterwards, UV-vis spectra were recorded in a standard quartz cuvette with an approximate volume of 3 mL in a range of 200 to 600 nm.

$^1\text{H NMR}$ (400 MHz, MeOD): $\delta_{\text{H}} = 6.64$ (dt, $J = 5.1, 2.7$ Hz, 2H), 6.59 (dt, $J = 5.1, 2.7$ Hz, 2H).

$^{13}\text{C NMR}$ (101 MHz, MeOD): $\delta_{\text{C}} = 149.9, 138.9, 117.1, 115.3$.

2.3. Sample preparation and miscellaneous

Nitrogen sorption data

Table 24. Nitrogen sorption data of toluene@Co/C **4a- α** to **4a- γ** and 2,2'-biphenol@Co/C **4d** polymers.

| No. | FDA | | surface area ^a | | multi-point BET plot |
|-------------------------------|----------|----------|------------------------------------|-----------------------------------------------------------------------|-------------------------|
| | [equiv.] | mass [g] | [m ² ·g ⁻¹] | $V_{0.1/\text{tot}}$ ^b [cm ³ ·g ⁻¹] | considering |
| 4a-α | 1.25 | 0.1606 | 43 | 0.14 | 0.075 < P/P_0 < 0.225 |
| 4a-β | 2.00 | 0.2057 | 85 | 0.23 | 0.05 < P/P_0 < 0.200 |
| 4a-γ | 2.50 | 0.1218 | 277 | 0.37 | 0.05 < P/P_0 < 0.126 |
| 4d | 2.50 | 0.0850 | 389 | 0.63 | 0.002 < P/P_0 < 0.076 |

[a] Surface area calculated by multi-point BET plot. [b] Ratio of micropore volume over the total pore volume at 77.3 K.

UV-vis spectra

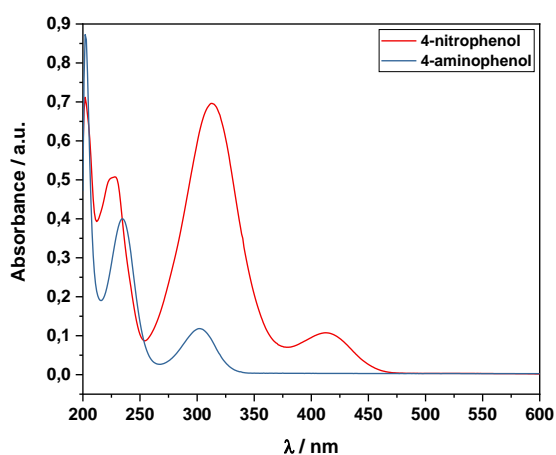


Figure 45. UV-vis spectra of 4-nitrophenol and 4-aminophenol.

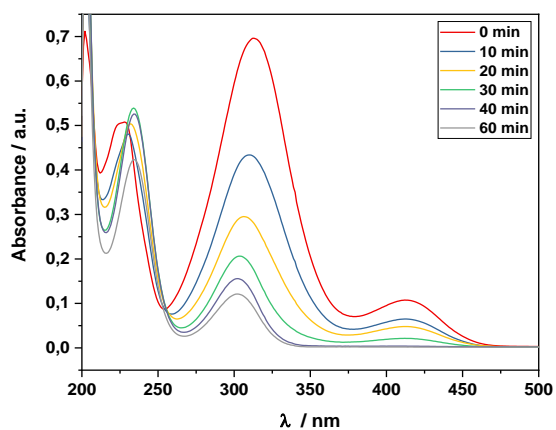


Figure 46. UV-vis spectra of the hydrogenation of 4-nitrophenol to 4-aminophenol applying **5a-γ** (1.9 wt%).

TEM images and Pd nanoparticles size distributions

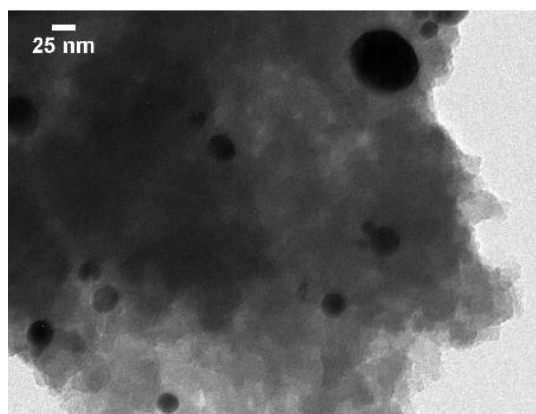


Figure 47. TEM image of **5a-γ** with 0.2 wt% Pd (no unambiguous determination of size distribution possible).

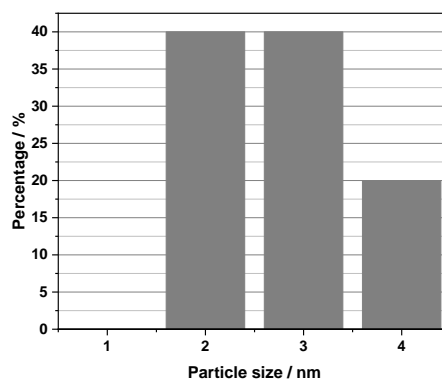
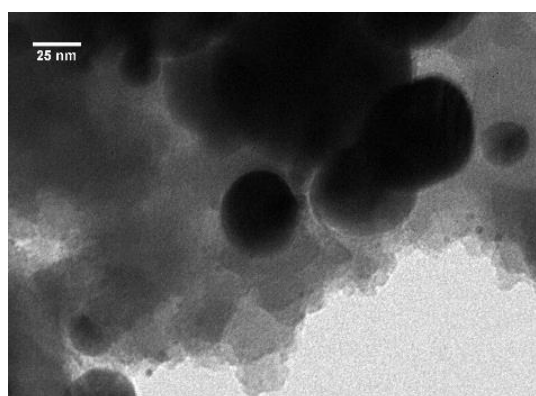


Figure 48. TEM image of **5a-γ** with 0.4 wt% Pd.

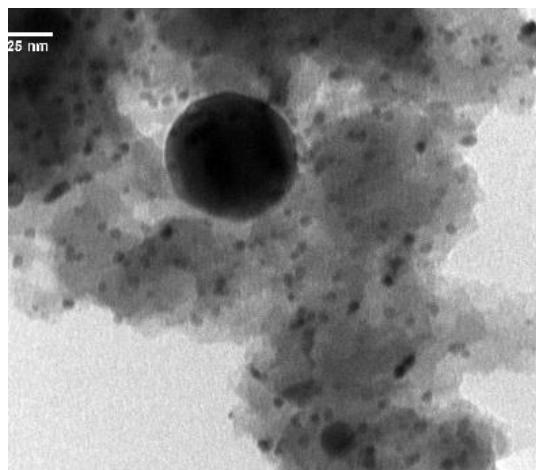


Figure 49. TEM image of 5a- γ with 1.0 wt% Pd.

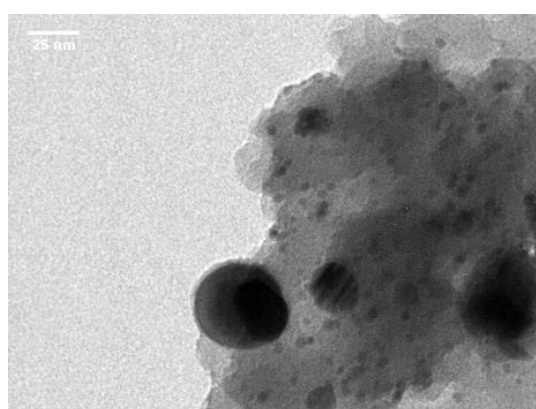
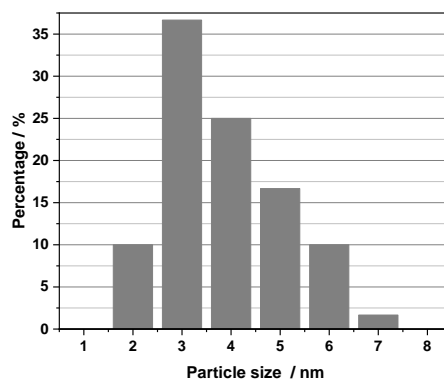


Figure 50. TEM image of 5a- γ with 1.7 wt% Pd.

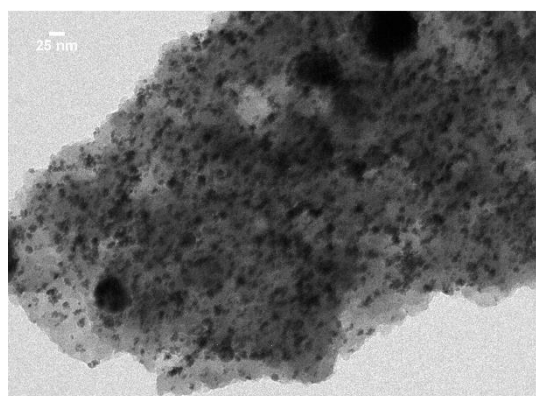
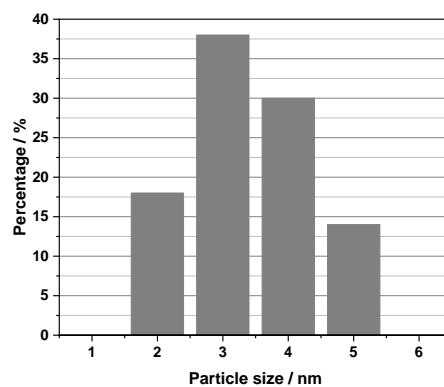
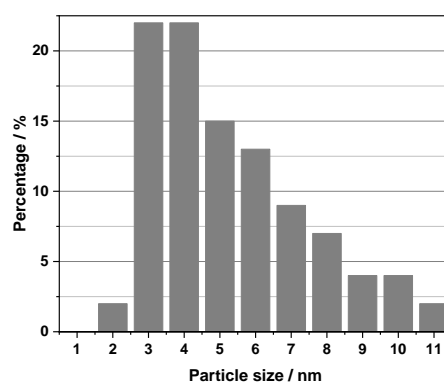


Figure 51. TEM image of 5a- γ with 3.9 wt% Pd.



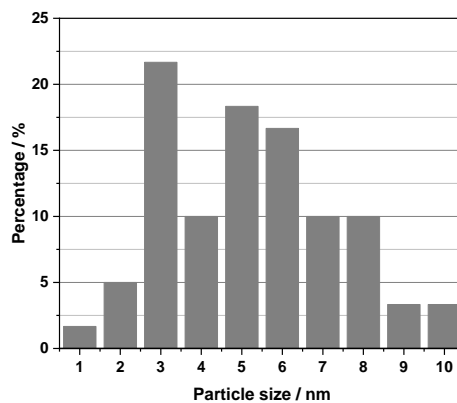
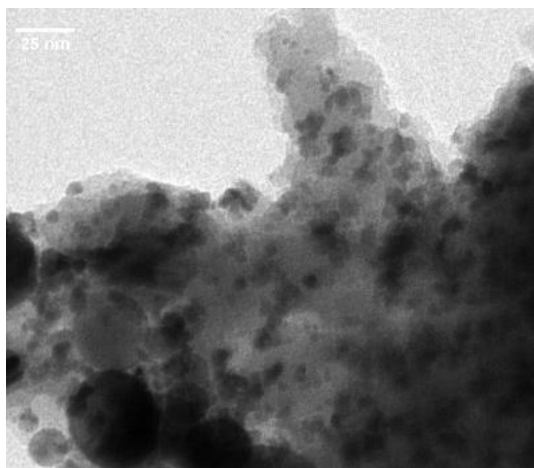


Figure 52. TEM image of 5a- γ with 14 wt% Pd.

XPS spectra

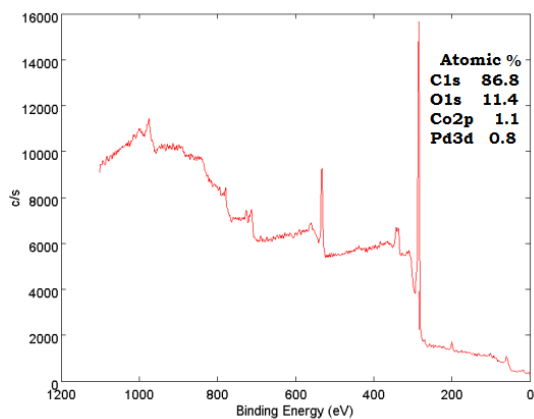


Figure 53. XPS survey spectrum of the catalyst 5a- γ (1.9 wt%).

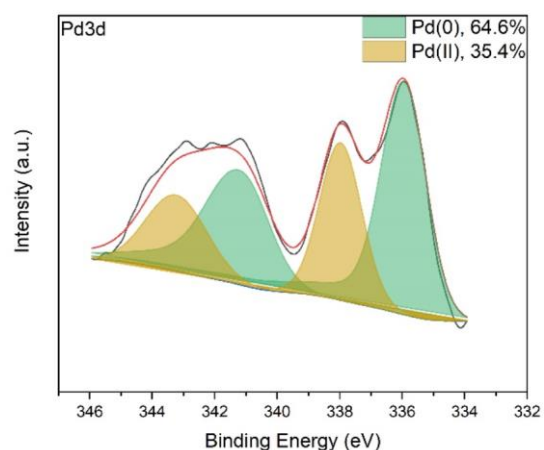


Figure 54. XPS spectrum of Pd3d of the catalyst 5a- γ (1.9 wt% Pd) after pre-treatment with hydrogen at atmospheric pressure before measurement.

Thermogravimetric analysis

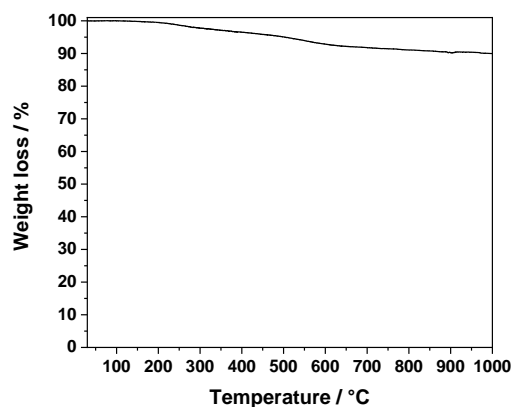


Figure 55. TGA measurement of **5a- γ** (1.9 wt%).

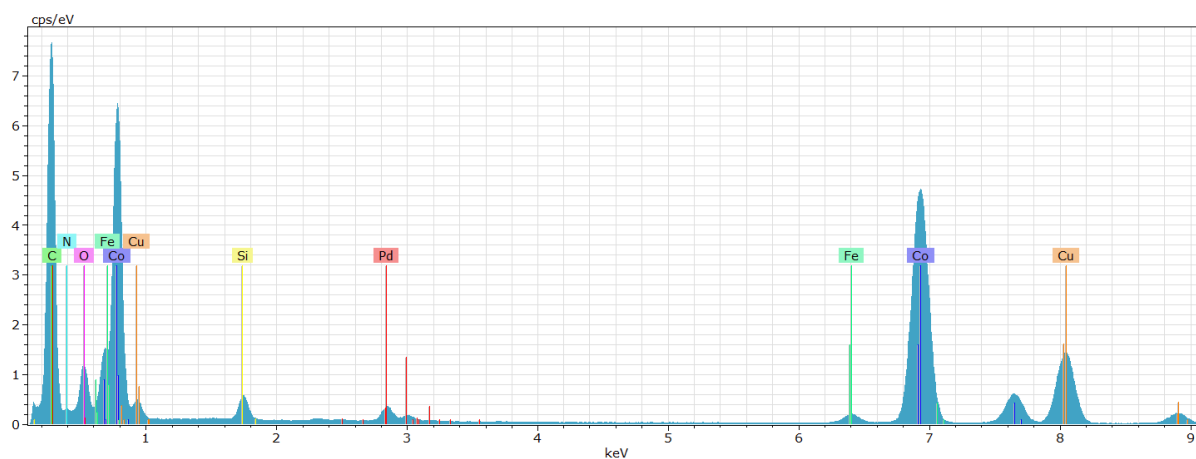


Figure 56. EDS survey spectrum of **5a- γ** (1.9 wt%).

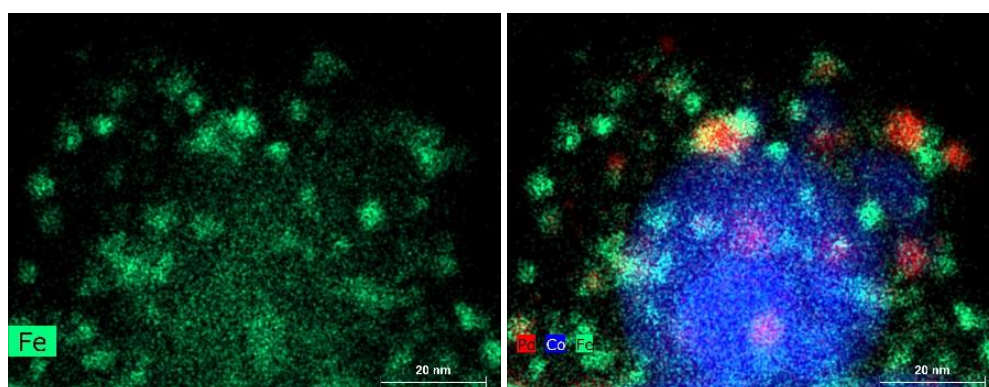
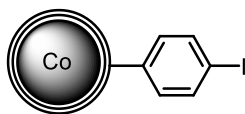


Figure 57. HAADF images and EDS chemical mapping of **5a- γ** (1.9 wt%) showing elemental mapping of Fe and Pd-Co-Fe together.

3. Suzuki-Miyaura coupling under mild reaction conditions

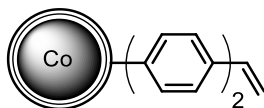
3.1. Synthesis of catalyst and starting materials



4-Iodobenzene-functionalized Co/C nanobeads iodobenzene@Co/C (**18**)

According to literature procedure,^[134] unfunctionalized Co/C NPs **1** (1.00 g, 3.43% C, 0.03% H), 4-iodoaniline (329 mg, 1.50 mmol, 1.0 equiv.) and concentrated HCl (0.6 mL) were suspended in H₂O_{millipore} (3 mL) with the aid of an ultrasonic bath. A pre-cooled solution of sodium nitrite (158 mg, 2.29 mmol, 1.5 equiv.) in H₂O_{millipore} (7 mL) was added dropwise at 0 °C to *in-situ* generate the diazonium species. The slurry was stirred for another 30 minutes in the ice bath and subsequently sonicated at ambient temperature for 30 minutes. The nanobeads were retracted by magnetic decantation and washed with NaOH (1 M, 3x), water (3x), acetone (6x), diethylether (2x), and dried under vacuum to afford 1.01 g of **18**.

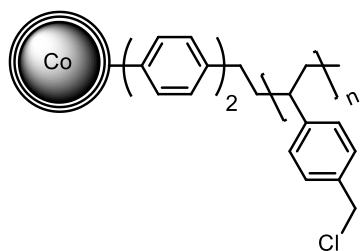
Elemental microanalysis [%]: 4.63 C, 0.22 H, 0.12 N; **Loading (C):** 0.098 mmol/g.



Vinylbiphenyl-functionalized Co/C nanobeads vinylbiphenyl@Co/C (**19**)

According to literature procedure,^[134] a Schlenk flask was charged with iodobenzene@Co/C **18** (500 mg, 0.049 mmol, 1.0 equiv.), 4-vinylphenylboronic acid (109 mg, 737 μmol, 15.0 equiv.), Pd(OAc)₂ (8.49 mg, 37.8 μmol, 0.77 equiv.), triphenylphosphine (27.4 mg, 105 μmol, 2.1 equiv.), and Na₂CO₃ (86.1 mg, 813 μmol, 16.6 equiv.) under nitrogen atmosphere. Degassed H₂O_{millipore} (3 mL) and degassed 1-propanol (3 mL) were added and the mixture was refluxed at 95 °C for 19 hours. Upon cooling, the nanoparticles were collected by an external magnet and the supernatant was decanted. The nanobeads were washed with H₂O_{millipore} (3x), MeOH (2x), acetone (6x), and dried *in vacuo* at 50 °C to obtain **19** in 505 mg.

Elemental microanalysis [%]: 7.50 C, 0.31 H, 0.10 N; **Loading (C):** 0.21 mmol/g.



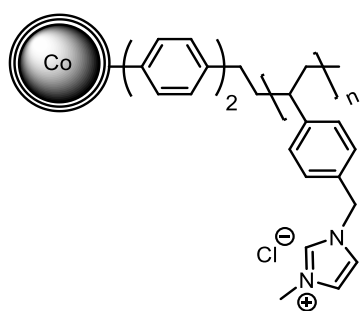
L (C) = 3.10 mmol/g.

Poly(benzyl chloride)styrene-functionalized Co/C nanobeads PS-Cl@Co/C (20)

According to an adapted literature procedure,^[46] freshly distilled 4-(chloromethyl)styrene (2.09 mL, 2.03 g, 13.3 mmol, 1.0 equiv.), vinylbiphenyl@Co/C **19** (1.00 g, L(C) = 0.21 mmol/g, 213 μ mol, 0.02 equiv.), and anhydrous DMF (2.5 mL) were introduced to a flame-dried Schlenk flask and degassed *via* three consecutive freeze-pump-thaw cycles. Subsequently, a solution of AIBN (65.7 mg, 400 μ mol, 3 mol%) in degassed, anhydrous DMF (1.5 mL) was added dropwise and the slurry stirred at ambient temperature for 20 minutes. The resulting mixture was slowly heated to 100 °C and allowed to stir for 48 hours. Afterwards, the nanoparticles were collected, washed with acetone until the supernatant was clear (10 to 20x), and dried *in vacuo*. The particles were crushed with a pestle and washed again with acetone until the solution was clear (10x), CH₂Cl₂ (5x), and dried *in vacuo* at 50 °C to yield **20** with 2.28 g.

Elemental microanalysis [%]: 44.4 C, 3.62 H, 0.19 N; **Loading (C):** 3.10 mmol/g.

IR [cm⁻¹]: 2915, 2117, 1607, 1510, 1439, 1420, 1264, 1014, 813, 667.



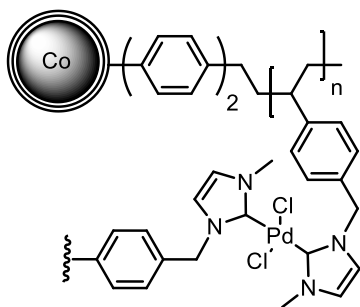
Poly(benzyl-methyl imidazolium chloride)styrene functionalized Co/C nanobeads PS-IL@Co/C (21)

According to an adapted literature procedure,^{[69],[174]} PS-Cl@Co/C NPs **20** (300 mg, L (C) = 3.10 mmol/g, 930 μ mol, 1.0 equiv.) were introduced to a microwave vial together with 3 mL anhydrous toluene. Subsequently, the solution was saturated with N₂ and the suspension was sonicated in an ultrasonic bath for 10 minutes until good dispersion was reached. Under nitrogen atmosphere, *N*-methyl-

imidazole (185 μL , 191 mg, 2.32 mmol, 2.5 equiv.) was added and the mixture heated to 150 $^{\circ}\text{C}$ in a microwave oven. After 60 minutes, the particles were collected by an external magnet, washed with toluene (5x), CH_2Cl_2 (3x), and dried under vacuum at 80 $^{\circ}\text{C}$ to yield 388 mg of **21**.

Elemental microanalysis [%]: 46.4 C, 4.19 H, 6.11 N; **Loading (N):** 2.15 mmol/g.

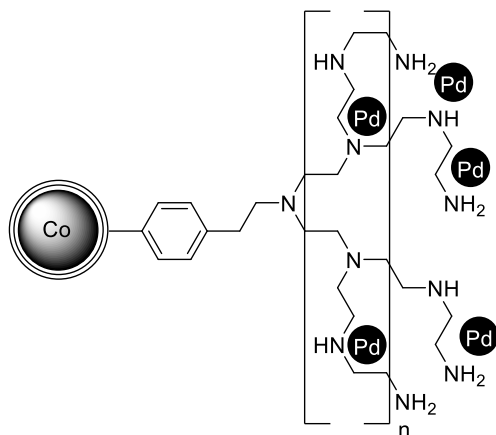
IR [cm^{-1}]: 3500-3200, 3060, 2930, 2117, 2091, 1558, 1510, 1446, 1424, 1156, 1018, 816, 708.



Palladium(II) NHC-functionalized catalyst Pd(II)@PS-NHC@Co/C (22)

According to an adapted literature procedure,^[133] a round bottom flask was charged with PS-IL@Co/C NPs **21** (200 mg, L (N) =2.15 mmol/g, 430 μmol , 1.0 equiv.), 2 mL DMF, and 2 mL of a 1 wt% Na_2CO_3 solution. After good dispersion was reached, $\text{Pd}(\text{OAc})_2$ (76.6 mg, 341 μmol , 0.79 equiv.) was added and the mixture was stirred at 50 $^{\circ}\text{C}$ for 24 hours. After the reaction was cooled to room temperature, the particles were washed with water (5x), methanol (5x), diethylether (3x), and dried under vacuum to yield 164 mg of **22**.

Elemental microanalysis [%]: 33.5 C, 3.13 H, 4.07 N; **Loading (Pd):** 0.74 mmol/g, 7.9 wt% (43% Pd of used Pd incorporated; 69% Pd of possible Pd incorporated referring to two equiv. PS-IL@Co/C per Pd).



Polyethyleneimine functionalized palladium catalyst Pd@PEI@Co/C (**11**)

Pd@PEI@Co/C **11** was synthesized by Dr. Benjamin Kastl according to an adapted literature procedure.^{[37],[81],[132]} Therefore, PEI functionalized Co/C NPs (50 mg) were dispersed in 2 mL H₂O_{millipore} by the aid of an ultrasonic bath for 10 minutes. The pH was adjusted to 6 with 1 M HCl (50 μ L) and a solution of sodium tetrachloropalladate (5 mL, 0.047 M) was added dropwise. After 1 hour, a solution of sodium borohydride in water (0.094 M) was added and stirred for 30 minutes. Subsequently, the Pd@PEI@Co/C NPs **11** were collected by an external magnet and washed with water (4x) and isopropanol (4x). After drying under vacuum, the particles were determined with 91% and a Pd loading of 0.8 mmol/g, 8.5 wt%.

3.2. Catalysis

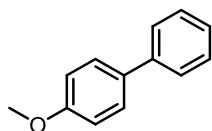
General procedure for the recycling of the Suzuki coupling (GP-6)

For recycling experiments, 4-iodotoluene **23a** and phenylboronic acid **9** were chosen as model substrates. Therefore, a pressure tube was charged with 4-iodotoluene **23a** (218 mg, 1.00 mmol, 1.0 equiv.), phenylboronic acid **9** (183 mg, 1.10 mmol, 1.1 equiv.), potassium carbonate (276 mg, 2.00 mmol, 2.0 equiv.), palladium catalyst **22** (3 mg, 2 μ mol, 0.2 mol%), and 4 mL solvent (EtOH/H₂O_{millipore} 1/1). Subsequently, the reaction mixture was stirred vigorously under room temperature and the reaction progress was monitored with TLC analysis (hexanes, R_f = 0.63). After 22 hours, the nanoparticles were collected by an external magnet, the resulting solution decanted into a separating funnel, and the catalyst washed thoroughly with distilled water and ethyl acetate. The washing solutions were extracted together with the reaction solution (3x ethyl acetate). In case of difficult phase separation, saturated brine was added. The organic phases were combined and dried over Na₂SO₄. In the end, the drying agent was filtered off, the solvent was evaporated, and the crude yield determined with an internal standard (1,3,5-trimethoxybenzene, 25.0 mg, 149 μ mol, 0.15 equiv.)

by NMR analysis. For the next run, the catalyst was directly reused without prior drying. Therefore, the reaction vessel including the nanoparticles was loaded with 4-iodotoluene **23a**, phenyl boronic acid **9**, potassium carbonate, solvent, and the reaction again run at room temperature for 22 hours.

General procedure for the substrate scope of the Suzuki coupling (GP-7)

A pressure tube was charged with aryl halide (1.00 mmol, 1.0 equiv.), boronic acid **9** (134 mg, 1.10 mmol, 1.1 equiv.), potassium carbonate (276 mg, 2.00 mmol, 2.0 equiv.), 4 mL solvent (EtOH/H₂O_{millipore} 1/1), and palladium catalyst **22** (3 mg, 2 μmol, 0.2 mol%). Subsequently, the reaction mixture was stirred at 50 °C, whereby the reaction progress was monitored by TLC analysis. After a given time, the nanoparticles were collected by an external magnet, the resulting solution decanted into a separating funnel, and the catalyst washed thoroughly with distilled water and ethyl acetate. The washing solutions were extracted together with the reaction solution (3x ethyl acetate). In case of difficult phase separation, saturated brine (5 mL) was added. The organic phases were combined and dried over Na₂SO₄. In the end, the drying agent was filtered off, the solvent was evaporated, and the product was isolated by column chromatography (SiO₂, hexanes/ethyl acetate). The magnetic catalyst **22** was dried in the pressure tube and directly reused for the next run and substrate.



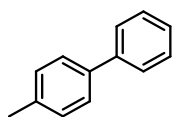
4-Methoxy-1,1'-biphenyl (**16**)

4-Methoxy-1,1'-biphenyl **16** was synthesized according to general procedure **GP-7** using 1-iodo-4-methoxybenzene **14a** (234 mg, 1.00 mmol, 1.0 equiv.) or 1-bromo-4-methoxybenzene **14b** (125 μL, 187 mg, 1.00 mmol, 1.0 equiv.), respectively, phenylboronic acid **9** (134 mg, 1.10 mmol, 1.1 equiv.), potassium carbonate (276 mg, 2.00 mmol, 2.0 equiv.), and 4 mL solvent (EtOH/H₂O_{millipore} 1/1) with palladium catalyst **22** (3 mg, 2 μmol, 0.2 mol%) at 50 °C. The crude product was purified by column chromatography (SiO₂, hexanes/ethyl acetate, 24:1) to afford a white to pale yellow solid (179 mg, 0.970 mmol, 97% or 176 mg, 0.960 mmol, 96%, respectively).

R_f = 0.50 (hexanes/ethyl acetate 24:1).

¹H NMR (300 MHz, CDCl₃): δ_H (ppm) = 7.61–7.50 (m, 4H), 7.47–7.37 (m, 2H), 7.35–7.27 (m, 1H), 7.03–6.94 (m, 2H), 3.86 (s, 3H).

^{13}C NMR (75 MHz, CDCl_3): δ_{C} (ppm) = 159.3, 141.0, 133.9, 128.9, 128.3, 126.9, 126.8, 114.3, 55.5.



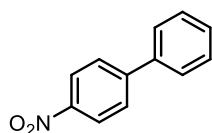
4-Methyl-1,1'-biphenyl (**24**)

4-Methyl-1,1'-biphenyl **24** was synthesized according to general procedure **GP-7** using 1-iodo-4-methylbenzene **23a** (218 mg, 1.00 mmol, 1.0 equiv.) or 1-bromo-4-methylbenzene **23b** (123 μL , 171 mg, 1.00 mmol, 1.0 equiv.), respectively, phenylboronic acid **9** (134 mg, 1.10 mmol, 1.1 equiv.), potassium carbonate (276 mg, 2.00 mmol, 2.0 equiv.), and 4 mL solvent (EtOH/ $\text{H}_2\text{O}_{\text{millipore}}$ 1/1) with the three times recycled palladium catalyst **22** (3 mg, 2 μmol , 0.2 mol%) at 50 °C. The crude product was purified by column chromatography (SiO_2 , hexanes) to afford a white solid (88.1 mg, 0.524 mmol, 52% or 103 mg, 0.612 mmol, 61%, respectively).

R_{f} = 0.38 (hexanes)

^1H NMR (300 MHz, CDCl_3): δ_{H} (ppm) = 7.63–7.56 (m, 2H), 7.55–7.48 (m, 2H), 7.48–7.40 (m, 2H), 7.38–7.30 (m, 1H), 7.30–7.24 (m, 2H), 2.41 (s, 3H).

^{13}C NMR (75 MHz, CDCl_3): δ_{C} (ppm) = 141.3, 138.5, 137.2, 129.6, 128.9, 127.1, 127.1, 21.3.



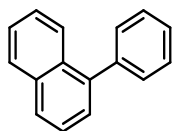
4-Nitro-1,1'-biphenyl (**26**)

4-Nitro-1,1'-biphenyl **26** was synthesized according to general procedure **GP-7** using 1-iodo-4-nitrobenzene **25a** (249 mg, 1.00 mmol, 1.0 equiv.) or 1-bromo-4-nitrobenzene **25b** (202 mg, 1.00 mmol, 1.0 equiv.), respectively, phenylboronic acid **9** (134 mg, 1.10 mmol, 1.1 equiv.), potassium carbonate (276 mg, 2.00 mmol, 2.0 equiv.), and 4 mL solvent (EtOH/ $\text{H}_2\text{O}_{\text{millipore}}$ 1/1) with the once recycled palladium catalyst **22** (3 mg, 2 μmol , 0.2 mol%) at 50 °C. The crude product was purified by column chromatography (SiO_2 , hexanes/ethyl acetate, 15:1) to afford a pale yellow solid (187 mg, 0.940 mmol, 94% or 184 mg, 0.926 mmol, 93%, respectively).

R_{f} = 0.35 (hexanes/ethyl acetate 15:1).

$^1\text{H NMR}$ (300 MHz, CDCl_3): δ_{H} (ppm) = 8.35–8.27 (m, 2H), 7.78–7.69 (m, 2H), 7.67–7.58 (m, 2H), 7.56–7.43 (m, 3H).

$^{13}\text{C NMR}$ (75 MHz, CDCl_3): δ_{C} (ppm) = 147.8, 147.2, 138.9, 129.3, 129.1, 128.0, 127.5, 124.3.



1-Phenylnaphthalene (28)

1-Phenylnaphthalene **28** was synthesized according to general procedure **GP-7** using 1-iodonaphthalene **27a** (149 μL , 254 mg, 1.00 mmol, 1.0 equiv.) or 1-bromonaphthalene **27b** (144 μL , 207 mg, 1.00 mmol, 1.0 equiv.), respectively, phenylboronic acid **9** (134 mg, 1.10 mmol, 1.1 equiv.), potassium carbonate (276 mg, 2.00 mmol, 2.0 equiv.), and 4 mL solvent ($\text{EtOH}/\text{H}_2\text{O}_{\text{millipore}}$ 1/1) with the twice recycled palladium catalyst **22** (3 mg, 2 μmol , 0.2 mol%) at 50 $^{\circ}\text{C}$. The crude product was purified by column chromatography (SiO_2 , hexanes) to afford a colorless oil (114 mg, 0.557 mmol, 56% or 33.9 mg, 0.166 mmol, 17%, respectively).

R_{f} = 0.33 (hexanes).

$^1\text{H NMR}$ (300 MHz, CDCl_3): δ_{H} (ppm) = 7.95–7.81 (m, 3H), 7.59–7.39 (m, 9H).

$^{13}\text{C NMR}$ (75 MHz, CDCl_3): δ_{C} (ppm) = 140.9, 140.4, 133.9, 130.2, 128.4, 127.8, 127.4, 127.1, 126.2, 125.9, 125.5.

3.3. Sample preparation and miscellaneous

Sample preparation for leaching experiments for ICP-OES

The organic phases were combined and dried over Na_2SO_4 . After filtering, the solvent was evaporated, internal standard (1,3,5-trimethoxybenzene, 25.0 mg, 150 μmol) was added, and dissolved in 5 mL CH_2Cl_2 . The resulting solution was filtered through a syringe filter (hydrophobic PTFE 0.2 μm), the solvent was evaporated, and the yield determined by quantitative NMR analysis in CDCl_3 . The combined dried product was treated with 2.4 mL $\text{HCl}_{\text{conc.}}$ and 0.8 mL $\text{HNO}_3_{\text{conc.}}$ and heated at 100 $^{\circ}\text{C}$ for 20 minutes. Upon cooling to room temperature, the mixture was washed with millipore water and the aqueous phase was transferred to a 10 mL volumetric flask with simultaneous filtering through a syringe filter (hydrophilic PTFE 0.2 μm) resulting in 32% *aqua regia* solution (v/v).

XPS spectra

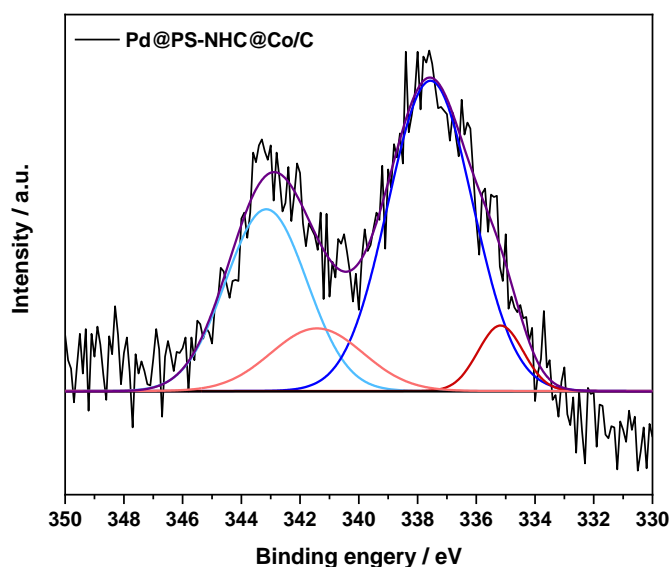
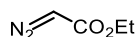


Figure 58. XPS spectra of **22**. Blue line shows Pd(II), red line shows Pd(0).

4. Cyclopropanation using chiral azaBOX-based copper catalysts

4.1. Synthesis of catalysts and starting materials



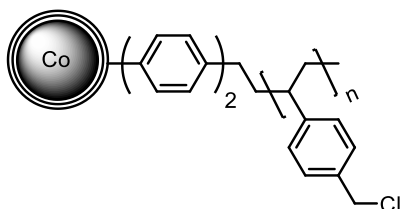
Ethyl diazoacetate (**34**)

34 was synthesized according to literature procedure,^[175] dissolving glycine ethyl hydrochloride (6.98 g, 50.0 mmol, 1.0 equiv.) in 12.5 mL H₂O_{dist} in a 100 mL three-necked flask. Subsequently, CH₂Cl₂ (30 mL) was added and the solution was cooled to -20 °C under vigorous stirring. A pre-cooled solution of sodium nitrite (4.14 g, 60.0 mmol, 1.2 equiv) in 12.5 mL H₂O_{dist} was added dropwise, followed by the dropwise addition of 5 wt% H₂SO₄ (4.75 g, 48.4 mmol, 0.97 equiv.) within 3 minutes. After 10 minutes, the mixture was transferred to a separating funnel and the organic phase was drained out into 50 mL ice-cold 5 wt% NaHCO₃ solution. The aqueous phase was extracted three times with CH₂Cl₂ (30 mL), all organic phases combined with the biphasic sodium bicarbonate mixture and shaken until neutral. The organic phase was dried over Na₂SO₄, the drying agent was filtered off, and the solution was concentrated under reduced pressure (13°C water bath, 170 mbar minimum pressure, cooling trap with liquid nitrogen) to yield **34** as a yellow solution in CH₂Cl₂ (123 g, 4.1 wt%, 88%). Yield and wt%

were determined by ^1H NMR relative to CH_2Cl_2 . The liquid was stored in the fridge over 3 Å molecular sieve under nitrogen atmosphere.

^1H NMR (300 MHz, CDCl_3): δ_{H} (ppm) = 4.73 (s, 1H), 4.21 (q, $J = 7.1$ Hz, 2H), 1.27 (t, $J = 7.1$ Hz, 3H).

4.1.1. Poly(benzyl halide)styrene- and Poly(benzyl azide)styrene-functionalized Co/C nanobeads

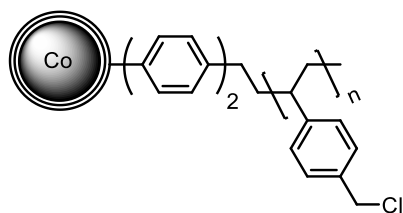


L (C) = 3.59 mmol/g

Poly(benzyl chloride)styrene-functionalized Co/C nanobeads PS-Cl@Co/C (20a)

PS-Cl@Co/C **20a** (L (C) = 3.59 mmol/g) was synthesized according to an adapted literature procedure,^[46] using freshly distilled 4-(chloromethyl)styrene **55** (942 μL , 916 mg, 6.00 mmol, 1.0 equiv.), vinylbiphenyl@Co/C **19** (450 mg, L (C) = 0.21 mmol/g, 94.5 μmol , 0.02 equiv.), and anhydrous DMF (1 mL) were introduced to a flame-dried Schlenk flask and degassed *via* three consecutive freeze-pump-thaw cycles. Subsequently, a solution of AIBN (29.6 mg, 180 μmol , 3 mol%) in degassed, anhydrous DMF (0.8 mL) was added dropwise and the slurry stirred at ambient temperature for 20 minutes. The resulting mixture was slowly heated to 100 °C and allowed to stir for 48 hours until a good polymerization was observed. Afterwards, the nanoparticles were collected, washed with acetone until the supernatant was clear (10 to 20x), and dried *in vacuo*. The particles were crushed with a pestle and washed again with acetone until the solution was clear (10x), CH_2Cl_2 (5x), and dried *in vacuo* at 50 °C to yield **20a** with 1.05 g.

Elemental microanalysis [%]: 51.1 C, 3.67 H, 0.26 N; **Loading (C):** 3.59 mmol/g.

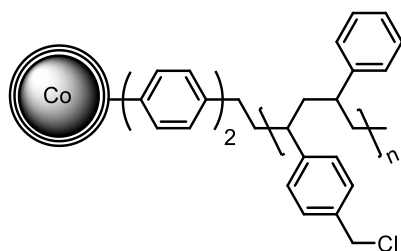


L (C) = 0.57 mmol/g

Poly(benzyl chloride)styrene-functionalized Co/C nanobeads PS-Cl@Co/C (20b)

PS-Cl@Co/C **20b** (0.57 mmol/g) was synthesized according to an adapted literature procedure,^[46] using freshly distilled 4-(chloromethyl)styrene **55** (2.09 mL, 2.03 g, 13.3 mmol, 1.0 equiv.), vinylbiphenyl@Co/C **19** (1.00 g, L(C) = 0.21 mmol/g, 213 μ mol, 0.02 equiv.), and anhydrous DMF (3 mL) were introduced to a flame-dried Schlenk flask and degassed *via* three consecutive freeze-pump-thaw cycles. Subsequently, a solution of AIBN (65.7 mg, 400 μ mol, 3 mol%) in degassed, anhydrous DMF (1 mL) was added dropwise and the slurry stirred at ambient temperature for 20 minutes. The resulting mixture was slowly heated to 100 °C and allowed to stir for 18 hours. Afterwards, the nanoparticles were collected, washed with acetone until the supernatant was clear (5 to 10x), and dried *in vacuo*. The particles were crushed with a pestle and washed again with acetone until the solution was clear (10x), CH₂Cl₂ (5x), and dried *in vacuo* at 50 °C to yield **20b** with 1.09 g.

Elemental microanalysis [%]: 14.1 C, 0.85 H, 0.10 N; **Loading (C):** 0.57 mmol/g.



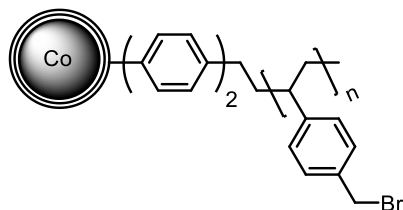
L (C) = 0.60 mmol/g

Co-polymer-functionalized Co/C nanobeads PS/PS-Cl@Co/C (56)

Freshly distilled 4-(chloromethyl)styrene **55** (283 μ L, 275 mg, 1.80 mmol, 1.0 equiv.), styrene **33** (137 μ L, 125 mg, 1.20 mmol, 0.7 equiv.), vinylbiphenyl@Co/C **19** (200 mg, L(C) = 0.21 mmol/g, 42.0 μ mol, 0.02 equiv.), and anhydrous DMF (1 mL) were introduced to a flame-dried Schlenk-flask and degassed *via* three consecutive freeze-pump-thaw cycles. Subsequently, a solution of AIBN (14.8 mg, 90.0 μ mol, 5 mol%) in degassed, anhydrous DMF (1 mL) was added dropwise and the slurry stirred at ambient temperature for 20 minutes. The resulting mixture was slowly heated to 85 °C and allowed to stir for 16 hours. Afterwards, the nanoparticles were collected, washed with acetone until the

supernatant was clear (5x), and dried *in vacuo*. The particles were crushed with a pestle and washed again with acetone (10x), CH₂Cl₂ (5x), and dried *in vacuo* at 50 °C to yield **56** with 214 mg.

Elemental microanalysis [%]: 14.5 C, 0.83 H, 0.08 N; **Loading (C):** 0.60 mmol/g.

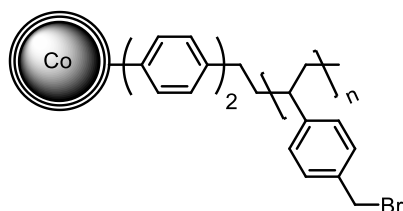


L (C) = 3.36 mmol/g

Poly(benzyl bromide)styrene-functionalized Co/C nanobeads PS-Br@Co/C (53a)

PS-Br@Co/C **53a** (3.59 mmol/g) was synthesized according to an adapted literature procedure,^[159] stirring PS-Cl@Co/C **20a** (200 mg, L (C) = 3.59 mmol/g, 718 μmol, 1.0 equiv.) with TBAB (1.51 g, 4.68 mmol, 6.5 equiv.), sodium bromide (5.82 g, 56.6 mmol, 79 equiv.) in a 1:1 mixture of benzene/H₂O_{dist} (43 mL) at 60 °C. After 5 days, the nanoparticles were collected, washed with CH₂Cl₂ (2x), H₂O_{millipore} (5x), acetone (5x), CH₂Cl₂ (3x). Drying *in vacuo* yielded **53a** with 128 mg.

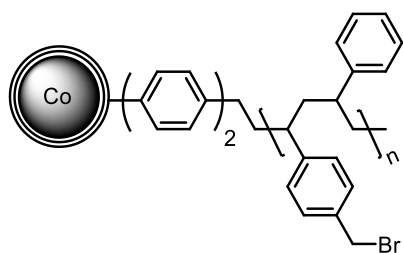
Elemental microanalysis [%]: 48.26 C, 4.06 H, 0.24 N; **Loading (C):** 3.36 mmol/g.



Poly(benzyl bromide)styrene-functionalized Co/C nanobeads PS-Br@Co/C (53b)

PS-Br@Co/C **53b** (0.57 mmol/g) was synthesized according to an adapted literature procedure,^[159] stirring PS-Cl@Co/C **20b** (200 mg, L (C) = 0.57 mmol/g, 114 μmol, 1.0 equiv.) with tetra-*n*-butylammonium bromide (TBAB) (503 mg, 1.56 mmol, 13.7 equiv.), sodium bromide (1.94 g, 18.9 mmol, 165 equiv.) in a 1:1 mixture of benzene/H₂O_{dist} (20 mL) at 60 °C. After 5 days, the nanoparticles were collected, washed with CH₂Cl₂ (2x), H₂O_{millipore} (5x), acetone (5x), CH₂Cl₂ (3x). Drying *in vacuo* yielded **20b** with 179 mg.

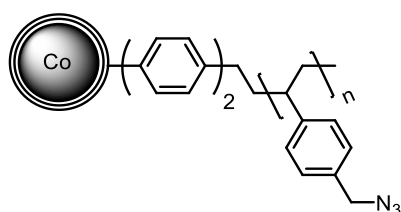
Elemental microanalysis [%]: not measured.



Co-polymer-functionalized Co/C nanobeads PS/PS-Br@Co/C (57)

PS/PS-Br@Co/C **57** was synthesized according to an adapted literature procedure,^[159] stirring PS/PS-Cl@Co/C **56** (200 mg, L (C) = 0.60 mmol/g, 120 μ mol, 1.0 equiv.) with TBAB (503 mg, 1.56 mmol, 13.0 equiv.), sodium bromide (1.94 g, 18.9 mmol, 157 equiv.) in a 1:1 mixture of benzene/H₂O_{dist} (20 mL) at 60 °C. After 5 days, the nanoparticles were collected, washed with CH₂Cl₂ (2x), H₂O_{millipore} (5x), acetone (5x), CH₂Cl₂ (3x). Drying *in vacuo* yielded **57** with 186 mg.

Elemental microanalysis [%]: not measured.



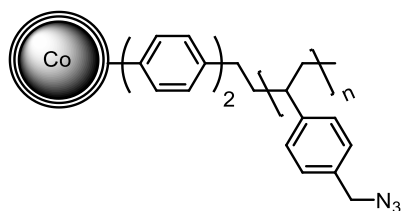
L (N) = 3.60 mmol/g

Poly(benzyl azide)styrene-functionalized Co/C nanobeads PS-N₃@Co/C (52a)

PS-N₃@Co/C **52a** (3.60 mmol/g) was synthesized according to an adapted literature procedure,^[156] dispersing PS-Cl@Co/C **20a** (250 mg, L (C) = 3.59 mmol/g, 898 μ mol, 1.0 equiv.) in 2.5 mL THF/H₂O_{millipore} (1:1) with the aid of an ultrasonic bath. Subsequently, sodium azide (406 mg, 6.25 mmol, 7.0 equiv.) was added and the mixture was stirred at 80 °C in a heavy-wall glass tube. After 3 days, the nanoparticles were collected, washed with a 1:1 mixture of THF/H₂O_{millipore} (5x), acetone (3x), and dried *in vacuo* at 50 °C to yield **52a** with 229 mg.

Elemental microanalysis [%]: 49.1 C, 3.74 H, 15.4 N; **Loading (N):** 3.60 mmol/g.

IR [cm⁻¹]: 3019, 2918, 2847, 2363, 2341, 2087, 1506, 1443, 1420, 1341, 1241, 1200, 1017, 805, 667.

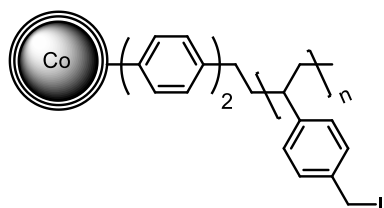


L (N) = 0.47 mmol/g

Poly(benzyl azide)styrene-functionalized Co/C nanobeads PS-N₃@Co/C (**52b**)

PS-N₃@Co/C **52b** (0.47 mmol/g) was synthesized according to an adapted literature procedure,^[156] dispersing PS-Cl@Co/C **20b** (250 mg, L (C) = 0.57 mmol/g, 143 μmol, 1.0 equiv.) in 2.5 mL THF/H₂O_{millipore} (1:1) with the aid of an ultrasonic bath. Subsequently, sodium azide (406 mg, 6.25 mmol, 44 equiv.) was added and the mixture was stirred at 80 °C in a heavy-wall glass tube. After 3 days, the nanoparticles were collected, washed with a 1:1 mixture of THF/H₂O_{millipore} (5x), acetone (3x), and dried *in vacuo* at 50 °C to yield **52b** with 253 mg.

Elemental microanalysis [%]: 14.4 C, 0.95 H, 2.08 N; **Loading (N):** 0.47 mmol/g.



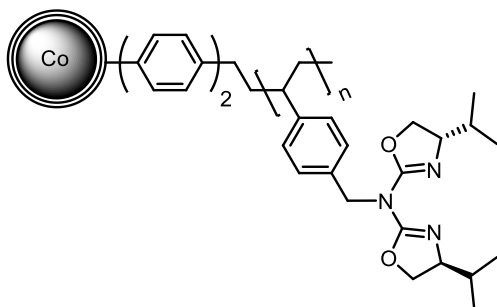
L (C) = 1.96 mmol/g

Poly(benzyl iodide)styrene-functionalized Co/C nanobeads PS-I@Co/C (**62**)

PS-I@Co/C **62** (1.96 mmol/g) was synthesized according to an adapted U.S. patent,^[176] stirring PS-Cl@Co/C **20a** (1.00 g, L (C) = 3.10 mmol/g, 3.10 mmol, 1.0 equiv.) in 6.5 mL anhydrous acetone. After dropwise adding a solution of sodium iodide (976 mg, 6.51 mmol, 2.1 equiv.) in 6.5 mL anhydrous acetone, the slurry was heated to 50 °C for 2 hours. The supernatant was decanted and the nanoparticles were washed thoroughly with diethyl ether until no white precipitate could be observed any longer (circa 20 to 25 times with each 10 mL). Drying *in vacuo* for 2 hours without heat yielded **62** with 1.47 g.

Elemental microanalysis [%]: 30.8 C, 2.60 H, 0.10 N; **Loading (C):** 1.96 mmol/g.

4.1.2. Immobilization of (*S,S*)-Bis(-4-isopropyl-4,5-dihydrooxazol-2-yl)amine ('Pr-40)



L (N) = 0.83 mmol/g

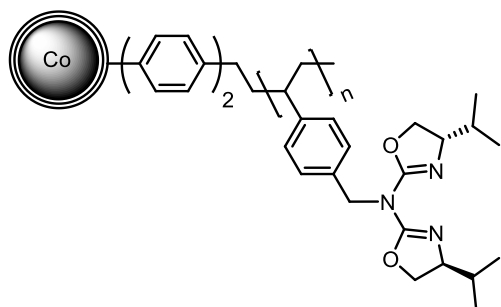
'Pr-azaBOX@PS-Br@Co/C (54a)

According to an adapted literature procedure,^{[152],[159]} (*S,S*)-Bis(-4-isopropyl-4,5-dihydrooxazol-2-yl)amine amine 'Pr-40* (172 mg, 720 μ mol, 1.0 equiv.) was dissolved in 10 mL anhydrous THF in a flame-dried Schlenk flask and degassed with three consecutive freeze-pump-thaw cycles under nitrogen atmosphere. The solution was cooled to -78 °C and *n*-butyllithium (473 μ L, 1.60 M in *n*-hexane, 756 μ mol, 1.1 equiv.) was added dropwise through a septum. The mixture was stirred for 15 minutes, before adding **53a** (100 mg, L (C) = 3.36 mmol/g, 336 μ mol, 0.5 equiv.) in portions. The solution was allowed to slowly reach room temperature and was further stirred for overall 48 hours. A saturated solution of Na₂CO₃ (5 mL) was added, stirred for 15 minutes and the nanoparticles were collected and washed with Na₂CO₃ solution (5x), H₂O_{millipore} (5x), acetone (5x), and CH₂Cl₂ (5x). Drying in vacuum at 50 °C yielded **54a** with 81.8 mg.

Elemental microanalysis [%]: 55.3 C, 5.37 H, 3.73 N; **Loading (N):** 0.83 mmol/g.

IR [cm⁻¹]: 3019, 2922, 2855 2340, 2322, 2117, 2091, 1632, 1509, 1409, 1077, 973, 812.

* This material was kindly provided by Dr. Peter Kreitmeier.^{[146],[152]}

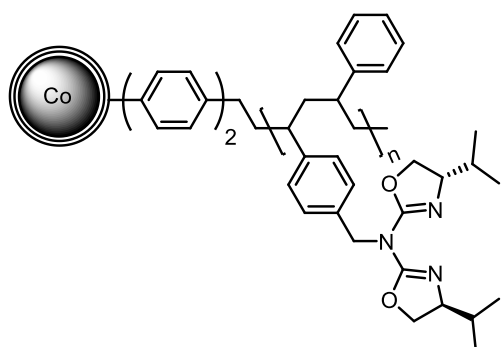


L (N) = 0.09 mmol/g

Pr-azaBOX@PS-Br@Co/C (54b)

According to an adapted literature procedure,^{[152],[159]} (*S,S*)-Bis(-4-isopropyl-4,5-dihydrooxazol-2-yl)amine **Pr-40** (172 mg, 720 μmol , 1.0 equiv.) was dissolved in 10 mL anhydrous THF in a flame-dried Schlenk flask and degassed with three consecutive freeze-pump-thaw cycles under nitrogen atmosphere. The solution was cooled to $-78\text{ }^{\circ}\text{C}$ and *n*-butyllithium (473 μL , 1.60 M in *n*-hexane, 756 μmol , 1.1 equiv.) was added dropwise through a septum. The mixture was stirred for 15 minutes, before adding 180 mg **53b** in portions. The solution was allowed to slowly reach room temperature and was further stirred for overall 48 hours. A saturated solution of Na_2CO_3 (5 mL) was added, stirred for 15 minutes and the nanoparticles were collected and washed with Na_2CO_3 solution (5x), $\text{H}_2\text{O}_{\text{millipore}}$ (5x), acetone (5x), and CH_2Cl_2 (5x). Drying in vacuum at $50\text{ }^{\circ}\text{C}$ yielded **54b** with 168 mg.

Elemental microanalysis [%]: 16.3 C, 1.35 H, 0.47 N; **Loading (N):** 0.09 mmol/g.



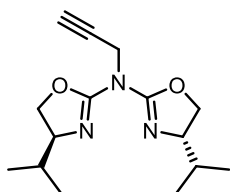
L (N) = 0.07 mmol/g

Pr-azaBOX@PS/PS-Br@Co/C (58)

According to an adapted literature procedure,^{[152],[159]} (*S,S*)-Bis(-4-isopropyl-4,5-dihydrooxazol-2-yl)amine **Pr-40** (172 mg, 720 μmol , 1.0 equiv.) was dissolved in 10 mL anhydrous THF in a flame-dried Schlenk flask and degassed with three consecutive freeze-pump-thaw cycles under nitrogen

atmosphere. The solution was cooled to $-78\text{ }^{\circ}\text{C}$ and *n*-butyllithium (473 μL , 1.60 M in *n*-hexane, 756 μmol , 1.1 equiv.) was added dropwise through a septum. The mixture was stirred for 15 minutes, before adding 175 mg of **57** in portions. The solution was allowed to slowly reach room temperature and was further stirred for overall 48 hours. A saturated solution of Na_2CO_3 (5 mL) was added, stirred for 15 minutes and the nanoparticles were collected and washed with Na_2CO_3 solution (5x), $\text{H}_2\text{O}_{\text{millipore}}$ (5x), acetone (5x), and CH_2Cl_2 (5x). Drying in vacuum at $50\text{ }^{\circ}\text{C}$ yielded **58** with 162 mg.

Elemental microanalysis [%]: 15.2 C, 1.09 H, 0.36 N; **Loading (N):** 0.07 mmol/g.

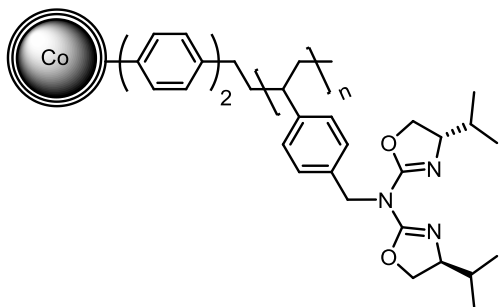


(S,S)-Bis-(4-isopropyl-4,5-dihydrooxazol-2-yl)-prop-2-ynyl-amine

According to literature procedure,^{[148],[151]} (*S,S*)-Bis-(4-isopropyl-4,5-dihydrooxazol-2-yl)amine *i*Pr-**40** (239 mg, 1.00 mmol, 1.0 equiv.) were dissolved in 8 mL anhydrous THF in a flame-dried Schlenk flask and degassed with three consecutive freeze-pump-thaw cycles under nitrogen atmosphere. The solution was cooled to $-78\text{ }^{\circ}\text{C}$ and *n*-butyllithium (656 μL , 1.60 M in *n*-hexane, 1.05 mmol, 1.1 equiv.) was added dropwise through a septum. The mixture was stirred for 15 minutes, before the dropwise addition of propargylbromide (456 μL , 80% (w/w) in toluene, 4.00 mmol, 4.0 equiv.). The solution was allowed to slowly reach room temperature and was further stirred for overall 22 hours. A saturated solution of Na_2CO_3 was added and the solution was concentrated, followed by extracting the aqueous phase three times with CH_2Cl_2 and drying over MgSO_4 . After removing the solvent *in vacuo*, the product was obtained as brown oil (272 mg, 981 μmol , 98%) and used without further purification.

$^1\text{H NMR}$ (300 MHz, CDCl_3): δ_{H} (ppm) = 4.64 (d, $J = 2.4\text{ Hz}$, 2H), 4.64 (d, $J = 2.4\text{ Hz}$, 2H), 4.40 (t, $J = 8.8\text{ Hz}$, 2H), 4.18 (dd, $J = 8.2, 6.8\text{ Hz}$, 2H), 3.99 – 3.86 (m, 2H), 2.24 (t, $J = 2.4\text{ Hz}$, 1H), 1.85 – 1.68 (m, 2H), 0.94 (d, $J = 6.8\text{ Hz}$, 6H), 0.87 (d, $J = 6.8\text{ Hz}$, 6H).

$^{13}\text{C NMR}$ (75 MHz, CDCl_3): δ_{C} (ppm) = 156.5, 79.2, 71.8, 71.7, 69.8, 39.8, 32.8, 18.7, 17.7.



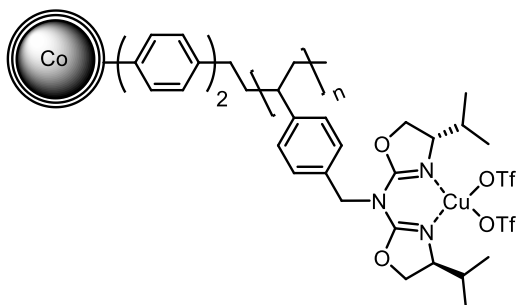
L (N) = 0.93 mmol/g

Pr-azaBOX@PS-I@Co/C (54c)

According to an adapted literature procedure, ^{[152],[159]} (*S,S*)-Bis(-4-isopropyl-4,5-dihydrooxazol-2-yl)amine **Pr-40** (742 mg, 3.10 mmol, 1.0 equiv.) was dissolved in 25 mL anhydrous THF in a flame-dried Schlenk flask and degassed with three consecutive freeze-pump-thaw cycles under nitrogen atmosphere. The solution was cooled to -78 °C and *n*-butyllithium (2.03 mL, 1.60 M in *n*-hexane, 3.26 mmol, 1.1 equiv.) was added dropwise through a septum. The mixture was stirred for 15 minutes, before adding **62** (500 mg, L (C) = 1.96 mmol/g, 980 μmol, 0.3 equiv.) in portions. The solution was allowed to slowly reach room temperature and was further stirred for overall 48 hours. A saturated solution of Na₂CO₃ (10 mL) was added, stirred for 15 minutes and the nanoparticles were collected and washed with Na₂CO₃ solution (5x), H₂O_{millipore} (5x), acetone (5x), and CH₂Cl₂ (5x). Drying in vacuum at 50 °C yielded **54c** with 393 mg.

Elemental microanalysis [%]: 40.5 C, 4.10 H, 4.01 N; **Loading (N):** 0.93 mmol/g.

4.1.3. Immobilization of copper(II) triflate onto functionalized nanobeads



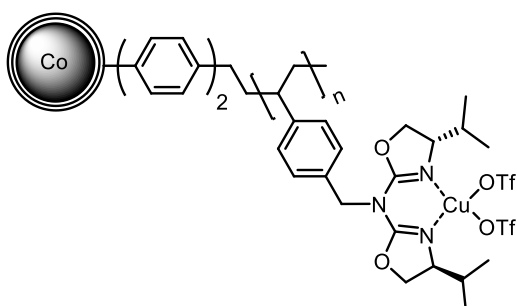
L (N) = 0.30 mmol/g

Cu(OTf)₂@ⁱPr-azaBOX@PS-Br@Co/C (30a)

A flame-dried Schlenk flask was charged with ⁱPr-azaBOX@PS-Br@Co/C **54a** (50.0 mg, L (N) = 0.83 mmol/g, 41.5 μmol, 1.0 equiv.) and set under vacuum for 1 hour. In a separate flame-dried Schlenk flask, copper(II) triflate (48.9 mg, 135 μmol, 3.3 equiv.) was dissolved in degassed, anhydrous CH₂Cl₂ (3 mL). The mixture was stirred at room temperature for 10 minutes, before adding **54a** in portions under nitrogen atmosphere. The flask was rinsed with degassed, anhydrous CH₂Cl₂ (1 mL) and stirred at room temperature for 3 days. After the given time, the nanoparticles were collected, washed with degassed, anhydrous CH₂Cl₂ (10x) and stored under nitrogen atmosphere to yield 78.0 mg of **30a**.

Elemental microanalysis [%]: 27.6 C, 3.93 H, 1.49 N; **Loading (N):** 0.30 mmol/g.

Loading (Cu): 1.32 mmol/g, 8.37 wt%.



L (N) = 0.06 mmol/g

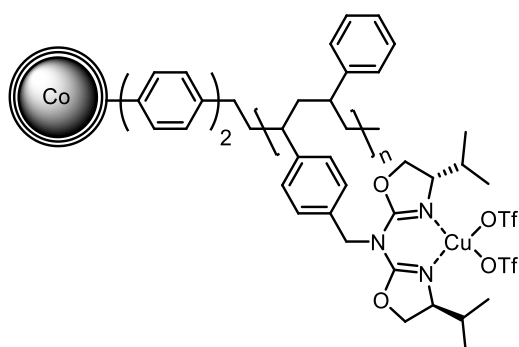
Cu(OTf)₂@ⁱPr-azaBOX@PS-Br@Co/C (30b)

A flame-dried Schlenk flask was charged with ⁱPr-azaBOX@PS-Br@Co/C **54b** (122 mg, L (N) = 0.09 mmol/g, 11.0 μmol, 1.0 equiv.) and set under vacuum for 1 hour. In a separate flame-dried Schlenk flask, copper(II) triflate (29.0 mg, 80.2 μmol, 7.3 equiv.) was dissolved in degassed, anhydrous

CH₂Cl₂ (3 mL). The mixture was stirred at room temperature for 10 minutes, before adding **54b** in portions under nitrogen atmosphere. The flask was rinsed with degassed, anhydrous CH₂Cl₂ (1 mL) and stirred at room temperature for 4 days. After the given time, the nanoparticles were collected, washed with degassed, anhydrous CH₂Cl₂ (10x) and stored under nitrogen atmosphere to yield 138 mg of **30b**.

Elemental microanalysis [%]: 13.5 C, 1.51 H, 0.35 N; **Loading (N):** 0.06 mmol/g.

Loading (Cu): 0.67 mmol/g, 4.25 wt%.



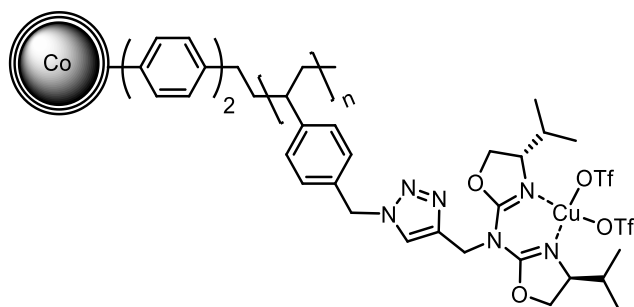
L (N) = 0.05 mmol/g

Cu(OTf)₂@ⁱPr-azaBOX@PS/PS-Br@Co/C (59)

A flame-dried Schlenk flask was charged with ⁱPr-azaBOX@PS-Br@Co/C **58** (100 mg, L (N) = 0.07 mmol/g, 7.00 μmol, 1.0 equiv.) and set under vacuum for 1 hour. In a separate flame-dried Schlenk flask, copper(II) triflate (25.3 mg, 70.0 μmol, 10 equiv.) was dissolved in degassed, anhydrous CH₂Cl₂ (3 mL). The mixture was stirred at room temperature for 10 minutes, before adding **58** in portions under nitrogen atmosphere. The flask was rinsed with degassed, anhydrous CH₂Cl₂ (1 mL) and stirred at room temperature for 3 days. After the given time, the nanoparticles were collected, washed with degassed, anhydrous CH₂Cl₂ (10x) and stored under nitrogen atmosphere to yield 125 mg of **59**.

Elemental microanalysis [%]: 13.2 C, 1.24 H, 0.27 N; **Loading (N):** 0.05 mmol/g.

Loading (Cu): 0.64 mmol/g, 4.08 wt%.



32a: L (N) = 1.20 mmol/g; **32b:** L (N) = 0.46 mmol/g

Cu(OTf)₂@ⁱPr-azaBOX@PS-N₃@Co/C (32a) and (32b)

A flame-dried Schlenk flask was charged with copper(II) triflate (231 mg, 638 μ mol, 1.0 equiv.) under nitrogen atmosphere. In a separate Schlenk flask, (*S,S*)-Bis-(4-isopropyl-4,5-dihydrooxazol-2-yl)-prop-2-ynyl-amine (197 mg, 708 μ mol, 1.1 equiv.) was dissolved in 3.5 mL anhydrous CH₂Cl₂, degassed with three consecutive freeze-pump-thaw cycles and added to the copper(II) triflate. After stirring for 22 hours at room temperature, the turquoise solution of **31** was separated in two portions:

32a was synthesized under nitrogen atmosphere using flame-dried Schlenk flasks. Therefore, degassed **52a** (100 mg, L (N) = 3.60 mmol/g, 360 μ mol, 1.0 equiv.), 3 mL of the freshly prepared copper-complexed solution **31** in CH₂Cl₂ (182 mM, 547 μ mol, 1.5 equiv. based on Cu(OTf)₂), copper(I) iodide (3.4 mg, 18 μ mol, 5 mol%), triethylamine (151 μ L, 109 mg, 1.08 mmol, 3.0 equiv.), and 1.5 mL anhydrous degassed CH₂Cl₂ were stirred at room temperature for 2 days to perform a copper(I)-catalyzed azide-alkyne cycloaddition. After the given time, the nanoparticles were collected, washed with degassed, anhydrous CH₂Cl₂ (10x) and stored under nitrogen atmosphere to yield 148 mg of **32a**.

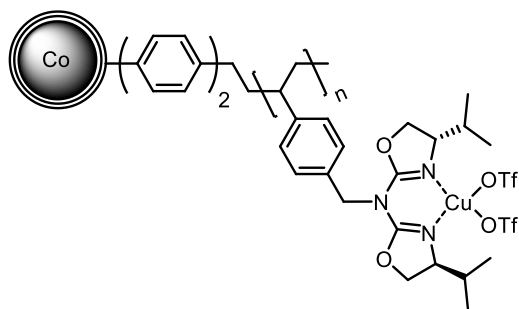
Elemental microanalysis [%]: 41.0 C, 4.70 H, 10.1 N; **Loading (N):** 1.20 mmol/g;

Loading (Cu): 1.28 mmol/g, 8.10 wt%.

32b was synthesized under nitrogen atmosphere using flame-dried Schlenk flasks. Therefore, degassed **52b** (100 mg, L (N) = 0.47 mmol/g, 47.0 μ mol, 1.0 equiv.), 0.5 mL of the freshly prepared copper-complexed solution **31** in CH₂Cl₂ (182 mM, 91.1 μ mol, 1.9 equiv. based on Cu(OTf)₂), copper(I) iodide (1.8 mg, 9.4 μ mol, 5 mol%), triethylamine (19.7 μ L, 14.3 mg, 141 μ mol, 3.0 equiv.), and 1.5 mL anhydrous degassed CH₂Cl₂ were stirred at room temperature for 2 days to perform a copper(I)-catalyzed azide-alkyne cycloaddition. After the given time, the nanoparticles were collected, washed with degassed, anhydrous CH₂Cl₂ (10x) and stored under nitrogen atmosphere to yield 155 mg of **32b**.

Elemental microanalysis [%]: 21.7 C, 2.13 H, 4.00 N; **Loading (N):** 0.46 mmol/g.

Loading (Cu): 0.96 mmol/g, 6.08 wt%.



L (N) = 0.63 mmol/g

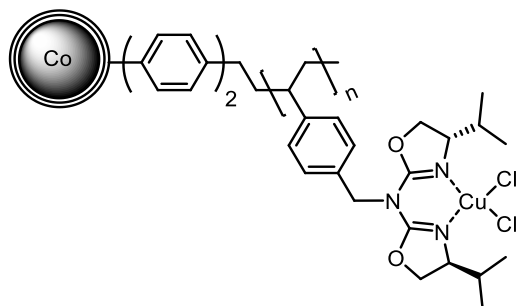
Cu(OTf)₂@ⁱPr-azaBOX@PS-I@Co/C (30c)

A flame-dried Schlenk flask was charged with ⁱPr-azaBOX@PS-I@Co/C **54c** (100 mg, L (N) = 0.93 mmol/g, 93.0 μmol, 1.0 equiv.) and set under vacuum for 1 hour. In a separate flame-dried Schlenk flask, copper(II) triflate (23.0 mg, 63.6 μmol, 0.7 equiv.) was dissolved in degassed, anhydrous CH₂Cl₂ (3 mL). The mixture was stirred at room temperature for 10 minutes, before adding **54c** in portions under nitrogen atmosphere. The flask was rinsed with degassed, anhydrous CH₂Cl₂ (1 mL) and stirred at room temperature for 3 days. After the given time, the nanoparticles were collected, washed with degassed, anhydrous CH₂Cl₂ (10x) and stored under nitrogen atmosphere to yield 78.0 mg of **30c**.

Elemental microanalysis [%]: 30.57 C, 3.28 H, 2.76 N; **Loading (N):** 0.63 mmol/g.

Loading (Cu): 0.66 mmol/g, 4.18 wt%.

4.1.4. Immobilization of copper(II) chloride and counterion exchange



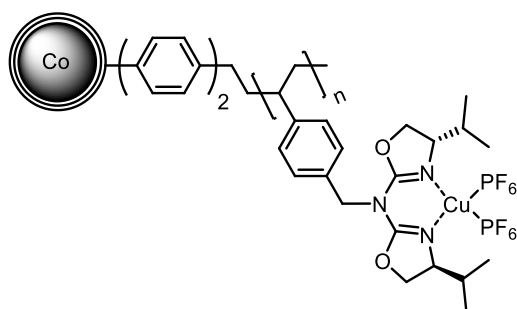
CuCl₂@ⁱPr-azaBOX@PS-Br@Co/C (60)

According to an adapted literature procedure,^[157] a flame-dried Schlenk flask was charged with ⁱPr-azaBOX@PS-Br@Co/C **54[†]** (150 mg, L (N) = 0.05 mmol/g, 7.50 μmol, 1.0 equiv.) and set under vacuum

[†] **54** was synthesized using **20a** (L (C) = 3.19 mmol/g). However, polymer loss occurred during the synthesis, resulting in a low polymer loading of (L (N) = 0.07 mmol/g). For this reason, the synthesis route *via* PS-I@Co/C is recommended.

for 1 hour. In a separate flame-dried Schlenk flask, copper(II) chloride (13.4 mg, 100 μmol , 13 equiv.) was dissolved in degassed, anhydrous CH_2Cl_2 (3 mL). The mixture was stirred at room temperature for 10 minutes, before adding **54** in portions under nitrogen atmosphere. The flask was rinsed with degassed, anhydrous CH_2Cl_2 (1 mL) and stirred at room temperature for 3 days. After the given time, the nanoparticles were collected, washed with degassed, anhydrous CH_2Cl_2 (6x) and stored under nitrogen atmosphere to yield 125 mg of **60**.

Loading (Cu): 0.68 mmol/g, 4.31 wt%.



$\text{Cu}(\text{PF}_6)_2@i\text{Pr-azaBOX@PS-Br@Co/C}$ (61**)**

According to an adapted literature procedure,^[157] a flame-dried heavy-wall Schlenk flask was charged with $\text{CuCl}_2@i\text{Pr-azaBOX@PS-Br@Co/C}$ **60** (46 mg, $L(\text{Cu}) = 0.68$ mmol/g, 31 μmol , 1.0 equiv.), potassium hexafluorophosphate (10 mg, 55 μmol , 1.8 equiv.), and 2 mL anhydrous CH_2Cl_2 . The slurry was stirred for 10 minutes, degassed with three consecutive freeze-pump-thaw cycles, and refluxed for 21 hours. Subsequently, the nanoparticles were collected, washed with degassed, anhydrous CH_2Cl_2 (6x) and stored under nitrogen atmosphere to yield 38 mg of **61**.

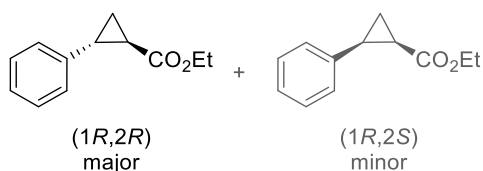
Loading (Cu): 0.47 mmol/g, 2.96 wt%.

4.2. Catalysis

General procedure for the cyclopropanation (GP-8)

A flame-dried 25 mL Schlenk flask was charged with copper catalyst **30c** (20 mg, $L(\text{Cu}) = 0.66$ mmol/g, 14 μmol , 1.4 mol%), 2 mL anhydrous CH_2Cl_2 and phenylhydrazine (5.0 μL , 5.5 mg, 51 μmol , 5 mol%) under nitrogen atmosphere and stirred at room temperature for 30 minutes. Subsequently, alkene (1.00 mmol, 1.0 equiv.) was added and rinsed with 2 mL anhydrous CH_2Cl_2 . After the flask was equipped with a septum and bubble counter, diazoacetate in CH_2Cl_2 (5 wt%, 1.50 mmol, 1.5 equiv.) was added dropwise over several hours by a syringe pump. The catalyst was collected by an external magnet, the

solution was decanted, and the nanoparticles washed three times with anhydrous CH_2Cl_2 (4 mL). The washing solutions were combined with the reaction solution, the solvent was evaporated, and the residue was purified by column chromatography (ethyl acetate/hexanes). The catalyst was directly reused without prior drying. Therefore, solely alkene (1.00 mmol, 1.0 equiv.) and 4 mL anhydrous CH_2Cl_2 were added to the recycled nanoparticles under nitrogen atmosphere, followed by dropwise addition of diazoacetate (1.50 mmol, 1.5 equiv.). The work-up and further recycling steps were performed as described above. In case of deactivation, new $\text{Cu}(\text{OTf})_2$ (1 mol%) and 4 mL anhydrous CH_2Cl_2 were added to the nanoparticles and stirred at r.t. under nitrogen atmosphere for 3 days. Afterwards, the solution was decanted, the nanoparticles washed three to five times with anhydrous CH_2Cl_2 (4 mL) and used in further cyclopropanation runs.



Ethyl (1R,2R)-2-phenylcyclopropane-1-carboxylate (*trans*-35)

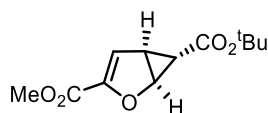
Ethyl (1R,2S)-2-phenylcyclopropane-1-carboxylate (*cis*-35)

According to general procedure **GP-8**, styrene **33** (115 μL , 104 mg, 1.00 mmol, 1.0 equiv.) was cyclopropanated with ethyl diazoacetate **34** (171 mg, 4.8 wt% in CH_2Cl_2 , 1.50 mmol, 1.5 equiv.) in 4 mL anhydrous CH_2Cl_2 and copper catalyst **30c** (16.9 mg, $L(\text{Cu}) = 0.80 \text{ mmol/g}$, 13.5 μmol , 1.3 mol%) at 22 °C. The ethyl diazoacetate **34** was added *via* a syringe pump (0.24 mL/h, corresponding to overall 13 hours). Afterwards, the resulting solution was stirred for another 9 hours and the reaction solution was separated from the catalyst and washed with anhydrous CH_2Cl_2 . The crude mixture was analyzed by gas chromatography.

GC-MS: 2 min at 50 °C, 20 °C/min to 250 °C (hold 3 min); retention time: styrene (4.54 min), dodecane (5.60 min), diethyl maleate (7.07 min), diethyl fumarate (7.21 min), *cis*-35 (9.10 min), *trans*-35 (9.44 min). Molecules verified by NIST Mass Spectral Library hits.

GC-FID: 3 min at 70 °C, 15 °C/min to 200 °C (hold 5 min); retention time: styrene (3.63 min), dodecane (5.50 min), *cis*-35 (10.34 min), *trans*-35 (10.83 min).

Chiral GC: 135 °C isotherm, 30 min: (1S,2R)-35 (13.51 min), (1R,2S)-35 (14.11 min), (1R,2R)-35 (15.23 min), (1S,2S)-35 (16.08 min).



(1S,5S,6S)-(-)-2-Oxabicyclo[3.1.0]hex-3-ene-3,6-dicarboxylic 6-*tert*-butyl ester 3-methyl ester (66)

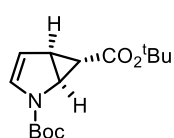
According to general procedure **GP-8**, methyl furan-2-carboxylate **63**[‡] (126 mg, 1.00 mmol, 1.0 equiv.) was cyclopropanated with *tert*-butyl diazoacetate **65**[‡] (213 mg, 5.2 wt% in CH₂Cl₂, 1.50 mmol, 1.5 equiv.) in 4 mL anhydrous CH₂Cl₂ and copper catalyst **30c** (20 mg, L (Cu) = 0.66 mmol/g, 14 μmol, 1.4 mol%) at 22 °C. The *tert*-butyl diazoacetate **65** was added *via* a syringe pump (1 mL/h, corresponding to overall 4 hours). Afterwards, the resulting solution was stirred for another hour and the reaction solution was separated from the catalyst and washed with anhydrous CH₂Cl₂. The solvent was evaporated and the crude product was purified by column chromatography (SiO₂, hexanes/ethyl acetate, 15:1) to afford a white solid (run 1 to run 4: 76.7 to 24.0 mg, 31.9 μmol to 10.0 μmol, 32 to 10% yield, 74 to 40% *ee*). **66** can be recrystallized with hexanes (87% *ee*).

R_f = 0.31 (hexanes/ethyl acetate 5:1, Vanillin).

¹H NMR (300 MHz, CDCl₃): δ_H (ppm) = 6.37 (d, *J* = 2.9 Hz, 1H), 4.90 (dd, *J* = 5.3, 1.1 Hz, 1H), 3.80 (s, 3H), 2.79 (dt, *J* = 5.4, 2.8 Hz, 1H), 1.44 (s, 9 H), 1.07 (dd, *J* = 2.7, 1.1 Hz, 1H).

¹³C NMR (75 MHz, CDCl₃): δ_C (ppm) = 171.2, 159.8, 149.2, 116.5, 81.6, 67.6, 52.4, 31.8, 28.2, 22.6.

HPLC analysis (Phenomenex Lux Cellulose-2, *n*-heptane/2-PrOH 99:1, 1.0 mL/min, 254 nm): *t_r* = **13.92 min**, 22.65 min, 87% *ee*).



Di-*tert*-butyl (1S,5S,6S)-2-azabicyclo[3.1.0]hex-3-ene-2,6-dicarboxylate (67)

According to general procedure **GP-8**, *N*-Boc-pyrrole **64**[‡] (167 mg, 1.00 mmol, 1.0 equiv.) was cyclopropanated with *tert*-butyl diazoacetate **65**[‡] (213 mg, 5.2 wt% in CH₂Cl₂, 1.50 mmol, 1.5 equiv.) in 4 mL anhydrous CH₂Cl₂ and four times recycled copper catalyst **30c** (20 mg, L (Cu) = 0.66 mmol/g, 14 μmol, 1.4 mol%) at 22 °C. The *tert*-butyl diazoacetate **65** was added *via* a syringe pump (1 mL/h, corresponding to overall 4 hours). Afterwards, the resulting solution was stirred for another 13 hours and the reaction solution was separated from the catalyst and washed with anhydrous CH₂Cl₂. The

[‡] These materials were kindly provided by Robert Eckl and Carina Sonnleitner.^[177]

solvent was evaporated and the crude product was purified by column chromatography (SiO₂, hexanes/ethyl acetate, 50:1) to afford a white solid (run 5: 90.3 mg, 32.1 μmol, 32% yield, 27% *ee*).

R_f = 0.53 (hexanes/ethyl acetate 5:1, Vanillin).

¹H NMR (300 MHz, CDCl₃): δ_H (ppm) = 6.73 – 6.25 (m, 1H), 5.49 – 5.25 (m, 1H), 4.50 – 4.10 (m, 1H), 2.86 – 2.51 (m, 1H), 1.51 (s, 9H), 1.44 (s, 9H), 1.04 – 0.71 (m, 1H).

¹³C NMR (75 MHz, CDCl₃): δ_C (ppm) = 172.5, 172.2, 151.4, 151.2, 129.8, 129.6, 110.2, 81.7, 80.9, 44.2, 43.9, 31.8, 30.8, 28.4, 28.3, 24.1 (signal doubling due to rotamers).

HPLC analysis (Phenomenex Lux Cellulose-2, *n*-heptane/*i*PrOH 98:2, 0.5 mL/min, 254 nm): t_r = 10.29 min, **15.63 min**, 27% *ee*)

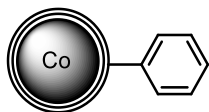
4.3. Sample preparation and miscellaneous

Sample preparation for leaching experiments for ICP-OES

The product solution was transferred into new glass ware, all volatile reagents were evaporated, and the residue was treated with 2.4 mL HCl_{conc.} and 0.8 mL HNO_{3 conc.}. After heating at 100 °C for 20 minutes, the mixture was transferred to a 10 mL volumetric flask. The flask was washed with H₂O_{millipore} and filled to the calibration mark. Filtering through a syringe filter (hydrophilic PTFE 0.2 μm) resulted in a 32% *aqua regia* solution (v/v).

5. Heavy metal extraction from water using microporous organic polymers

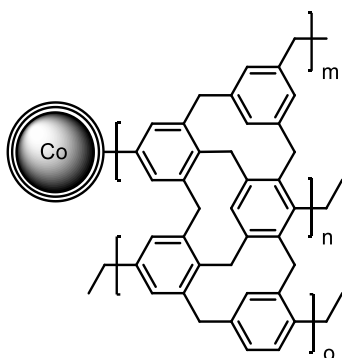
5.1. Synthesis of magnetic materials



Benzene-functionalized Co/C nanobeads (**70**)

According to literature procedure,^[37] unfunctionalized Co/C NPs **1** (1.00 g, 4.50% C, traces H), freshly distilled aniline (137 μ L, 140 mg, 1.50 mmol, 1.0 equiv.) and concentrated HCl (0.6 mL) were suspended in H₂O_{millipore} (25 mL) with the aid of an ultrasonic bath. A pre-cooled solution of sodium nitrite (158 mg, 2.29 mmol, 1.5 equiv.) in H₂O_{millipore} (12 mL) was added dropwise at 0 °C to *in-situ* generate the diazonium species. The slurry was stirred for another 30 minutes in the ice bath and subsequently sonicated at ambient temperature for 30 minutes. The nanobeads were retracted by magnetic decantation and washed with NaOH (1 M, 3x), water (3x), acetone (6x), diethylether (2x), and dried under vacuum to afford 955 mg of **70**.

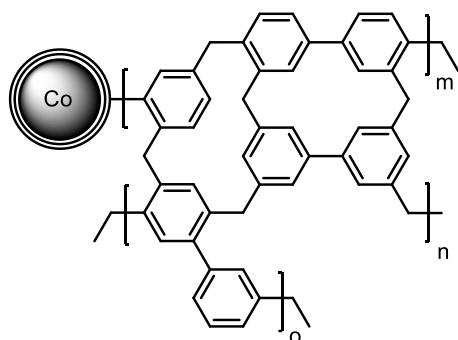
Elemental microanalysis [%]: 5.14 C, 0.06 H, 0 N; **Loading (C):** 0.09 mmol/g.



Benzene@Co/C (**71a**)

71a was synthesized according to **GP-2**, using 100 mg of **70**, anhydrous benzene (44.6 μ L, 39.1 mg, 500 μ mol, 1.0 equiv.), formaldehyde dimethyl acetal (111 μ L, 95.1 mg, 1.25 mmol, 2.5 equiv.), anhydrous iron (III) chloride (203 mg, 1.25 mmol, 2.5 equiv.), and 1,2-dichloroethane (9 mL) to afford 90.0 mg of **71a**.

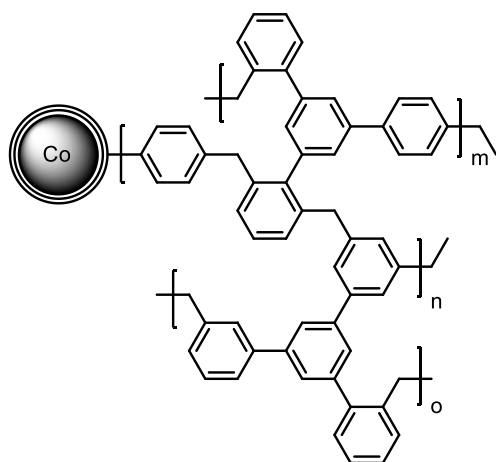
Elemental microanalysis [%]: 10.7 C, 0.49 H, 0 N.



1,1'-Biphenyl@Co/C (71b)

71b was synthesized by Andreas Hartl according to **GP-2**, using 100 mg of **70**, 1,1'-biphenyl (77.1 mg, 500 μmol , 1.00 equiv.), formaldehyde dimethyl acetal (55.3 μL , 47.6 mg, 625 μmol , 1.25 equiv.), anhydrous iron (III) chloride (101 mg, 625 μmol , 1.25 equiv.), and 1,2-dichloroethane (9 mL) to afford 153 mg of **71b**.

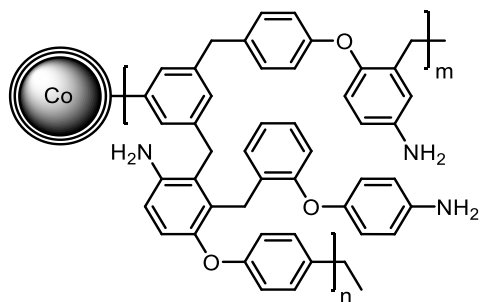
Elemental microanalysis [%]: 39.1 C, 2.30 H, 0 N.



1,3,5-Triphenylbenzene@Co/C (71c)

71c was synthesized by Andreas Hartl according to **GP-2**, using 100 mg of **70**, 1,3,5-triphenylbenzene (153 mg, 500 μmol , 1.0 equiv.), formaldehyde dimethyl acetal (265 μL , 228 mg, 3.00 mmol, 6.0 equiv.), anhydrous iron (III) chloride (487 mg, 3.00 mmol, 6.0 equiv.), and 1,2-dichloroethane (9 mL) to afford 147 mg of **71c**.

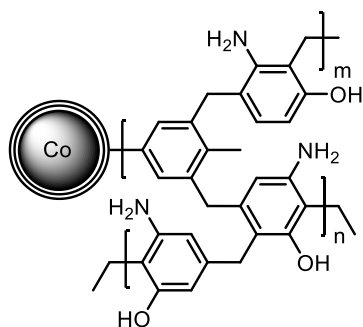
Elemental microanalysis [%]: 52.1 C, 3.16 H, 0 N.



4-Phenoxyaniline@Co/C (71d)

71d was synthesized according to **GP-2**, using 100 mg of **70**, 4-phenoxyaniline (92.6 mg, 500 μmol , 1.0 equiv.), formaldehyde dimethyl acetal (111 μL , 95.1 mg, 1.25 mmol, 2.5 equiv.), anhydrous iron (III) chloride (203 mg, 1.25 mmol, 2.5 equiv.), and 1,2-dichloroethane (9 mL) to afford 140 mg of **71d**.

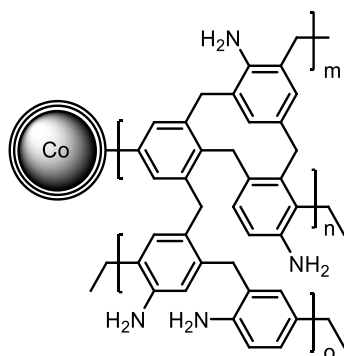
Elemental microanalysis [%]: 29.2 C, 2.03 H, 2.20 N; **Loading (N):** 1.57 mmol/g.



3-Aminophenol@Co/C (71e)

71e was synthesized according to **GP-2**, using 50.0 mg of **70**, 3-aminophenol (54.6 mg, 500 μmol , 1.0 equiv.), formaldehyde dimethyl acetal (88.8 μL , 76.1 mg, 1.00 mmol, 2.0 equiv.), anhydrous iron (III) chloride (162 mg, 1.00 mmol, 2.0 equiv.), and 1,2-dichloroethane (3 mL) to afford 97.0 mg of **71e**.

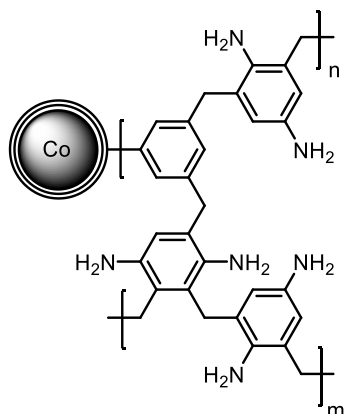
Elemental microanalysis [%]: 27.2 C, 2.34 H, 3.54 N; **Loading (N):** 2.53 mmol/g.



Aniline@Co/C (71f)

71f was synthesized according to **GP-2**, using 150 mg of **70**, anhydrous aniline (67.8 μ L, 70.0 mg, 750 μ mol, 1.0 equiv.), formaldehyde dimethyl acetal (133 μ L, 114 mg, 1.50 mmol, 2.0 equiv.), anhydrous iron (III) chloride (243 mg, 1.50 mmol, 2.0 equiv.), and 1,2-dichloroethane (4 mL) to afford 275 mg of **71f**.

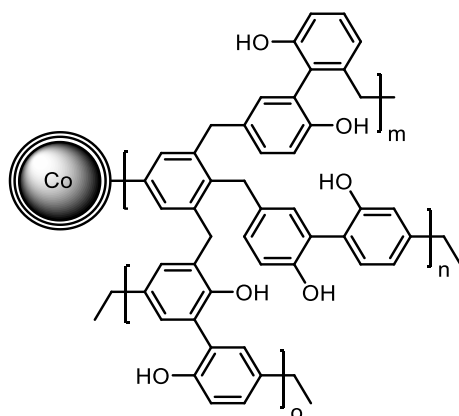
Elemental microanalysis [%]: 25.2 C, 1.97 H, 3.17 N; **Loading (N):** 0.64 mmol/g.



1,4-Phenylendiamine@Co/C (71g)

71g was synthesized according to **GP-2**, using 100 mg of **70**, 1,4-phenylendiamine (54.1 mg, 500 μ mol, 1.0 equiv.), formaldehyde dimethyl acetal (111 μ L, 95.1 mg, 1.25 mmol, 2.5 equiv.), anhydrous iron (III) chloride (203 mg, 1.25 mmol, 2.5 equiv.), and 1,2-dichloroethane (9 mL) to afford 130 mg of **71g**.

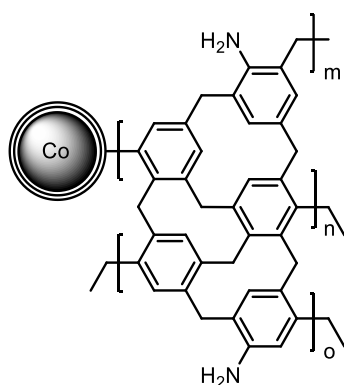
Elemental microanalysis [%]: 17.6 C, 1.35 H, 3.97 N; **Loading (N):** 1.42 mmol/g.



2,2'-Biphenol@Co/C (71h)

71h was synthesized according to **GP-2**, using 100 mg of **70**, 2,2'-biphenol (93.1 mg, 500 μ mol, 1.0 equiv.), formaldehyde dimethyl acetal (111 μ L, 95.1 mg, 1.25 mmol, 2.5 equiv.), anhydrous iron (III) chloride (203 mg, 1.25 mmol, 2.5 equiv.), and 1,2-dichloroethane (9 mL) to afford 107 mg of **71h**.

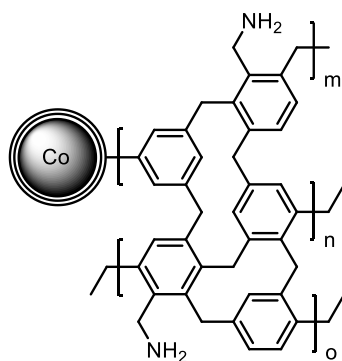
Elemental microanalysis [%]: 14.3 C, 0.79 H, 0 N.



Aniline/benzene@Co/C (71i)

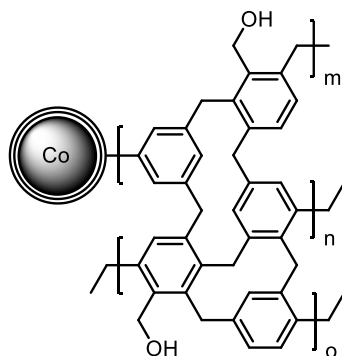
71i was synthesized according to **GP-2**, using 100 mg of **70**, anhydrous aniline (22.8 μ L, 23.3 mg, 250 μ mol, 1.0 equiv.), anhydrous benzene (22.3 μ L, 19.5 mg, 250 μ mol, 1.0 equiv.), formaldehyde dimethyl acetal (111 μ L, 95.1 mg, 1.25 mmol, 5.0 equiv.), anhydrous iron (III) chloride (203 mg, 1.25 mmol, 5.0 equiv.), and 1,2-dichloroethane (9 mL) to afford 97.5 mg of **71i**.

Elemental microanalysis [%]: 23.9 C, 1.66 H, 1.73 N; **Loading (N):** 1.24 mmol/g.

**Benzyl amine/benzene@Co/C (71j)**

71j was synthesized by Andreas Hartl according to **GP-2**, using 100 mg of **71j**, benzyl amine (27.3 μL , 26.8 mg, 250 μmol , 1.0 equiv.), anhydrous benzene (22.3 μL , 19.5 mg, 250 μmol , 1.0 equiv.), formaldehyde dimethyl acetal (88.5 μL , 76.1 mg, 1.00 mmol, 4.0 equiv.), anhydrous iron (III) chloride (162 mg, 1.00 mmol, 4.0 equiv.), and 1,2-dichloroethane (9 mL) to afford 120 mg of **71j**.

Elemental microanalysis [%]: 19.2 C, 1.14 H, 0.25 N; **Loading (N):** 0.18 mmol/g.

**Benzyl alcohol/benzene@Co/C (71k)**

71k was synthesized by Andreas Hartl according to **GP-2**, using 100 mg of **70**, benzyl alcohol (26.0 μL , 27.0 mg, 250 μmol , 1.0 equiv.), anhydrous benzene (22.3 μL , 19.5 mg, 250 μmol , 1.0 equiv.), formaldehyde dimethyl acetal (88.5 μL , 76.1 mg, 1.00 mmol, 4.0 equiv.), anhydrous iron (III) chloride (162 mg, 1.00 mmol, 4.0 equiv.), and 1,2-dichloroethane (9 mL) to afford 120 mg of **71k**.

Elemental microanalysis [%]: 28.1 C, 2.20 H, 0 N.

5.2. Heavy metal adsorption

5.2.1. Preparation of heavy metal stock solutions

The 1 mM stock solution was prepared by dissolving the desired metals in a 250 mL volumetric flask in $\text{H}_2\text{O}_{\text{millipore}}$. Therefore, $\text{BaCl}_2 \cdot 2\text{H}_2\text{O}$ (61.1 mg, 250 μmol), $\text{CdBr}_2 \cdot 4\text{H}_2\text{O}$ (86.1 mg, 250 μmol), $\text{CrCl}_3 \cdot 6\text{H}_2\text{O}$ (66.6 mg, 250 μmol), $\text{Cu}(\text{OAc})_2 \cdot \text{H}_2\text{O}$ (49.9 mg, 250 μmol), HgCl_2 (67.9 mg, 250 μmol), $\text{NiCl}_2 \cdot 6\text{H}_2\text{O}$ (59.4 mg, 250 μmol), $\text{Pb}(\text{OAc})_2 \cdot 3\text{H}_2\text{O}$ (94.8 mg, 250 μmol), $\text{FeCl}_2 \cdot 4\text{H}_2\text{O}$ (20.0 mg, 100 μmol) and $\text{CoCl}_2 \cdot 6\text{H}_2\text{O}$ (23.8 mg, 100 μmol) were dissolved in a 100 mL volumetric flask in $\text{H}_2\text{O}_{\text{millipore}}$. Diluting 10 mL of the 1 mM stock solution to 100 mL with $\text{H}_2\text{O}_{\text{millipore}}$, resulted in a 100 μM solution. Further diluting of 10 mL of the 100 μM solution to 100 mL with $\text{H}_2\text{O}_{\text{millipore}}$ resulted in a 10 μM solution.

In case of zinc as heavy metal, solely ZnBr_2 (22.5 mg, 100 μmol) was dissolved in a 100 mL volumetric flask with $\text{H}_2\text{O}_{\text{millipore}}$ to result in a 1 mM zinc solution. Subsequently, 5 mL of this solution were diluted to 50 mL with $\text{H}_2\text{O}_{\text{millipore}}$ to achieve a 100 μM zinc solution.

5.2.2. Procedures for the heavy metal extraction from water

Testing the adsorption of Ba^{2+} , Cr^{3+} , Cu^{2+} , Ni^{2+} , Pb^{2+} of various polymers

A 20 mL vial was charged with 10.0 mg of the magnetic Co/C polymer (**Co/C 1**, **70**, **4a- γ** , or **71a-k**) and 10 mL of a 100 μM heavy metal solution corresponding to 1.00 μmol of each metal: 137 μg Ba^{2+} , 52.0 μg Cr^{3+} , 63.6 μg Cu^{2+} , 58.7 μg Ni^{2+} , 207 μg Pb^{2+} in $\text{H}_2\text{O}_{\text{millipore}}$. The slurry was vigorously stirred (1000 rpm) at ambient temperature (25 $^\circ\text{C}$) for 20 hours. After the given time, the nanoparticles were collected by an external magnet and the solution was analyzed by ICP-OES. Adsorbed metals after 20 hours: **Co/C 1** (70% Cr^{3+} , 68% Cu^{2+} , 42% Ni^{2+} , 55% Pb^{2+}), **70** (88% Cr^{3+} , 88% Cu^{2+} , 17% Ni^{2+} , 81% Pb^{2+}), **71a** (98% Cr^{3+} , 93% Cu^{2+} , 40% Ni^{2+} , 93% Pb^{2+}), **71e** (23% Cu^{2+}), **71h** (100% Cr^{3+} , 99% Cu^{2+} , 58% Ni^{2+} , 99% Pb^{2+}).

Maximal combined metal uptake of Ba^{2+} , Cr^{3+} , Cu^{2+} , Ni^{2+} , Pb^{2+}

Maximal metal uptake for 71a: A 20 mL vial was charged with **71a** (2.1 mg) and 10 mL of a 100 μM heavy metal solution corresponding to 1.00 μmol of each metal: 137 μg Ba^{2+} , 52.0 μg Cr^{3+} , 63.6 μg Cu^{2+} , 58.7 μg Ni^{2+} , 207 μg Pb^{2+} in $\text{H}_2\text{O}_{\text{millipore}}$. The slurry was vigorously stirred (1000 rpm) at ambient temperature (25 $^\circ\text{C}$) for 20 hours. After the given time, the nanoparticles were collected by an external magnet and the solution was analyzed by ICP-OES. Adsorbed metals after 20 hours: 59% Cr^{3+} , 58% Cu^{2+} , 42% Pb^{2+} ; adsorption capacities for metal ions per gram of nanoparticles: 15 $\text{mg} \cdot \text{g}^{-1}$ Cr^{3+} , 18 $\text{mg} \cdot \text{g}^{-1}$ Cu^{2+} , 41 $\text{mg} \cdot \text{g}^{-1}$ Pb^{2+} .

Maximal combined metal uptake for 71h: A 20 mL vial was charged with **71h** (2.2 mg) and 10 mL of a 100 μM heavy metal solution corresponding to 1.00 μmol of each metal: 137 μg Ba^{2+} , 52.0 μg Cr^{3+} , 63.6 μg Cu^{2+} , 58.7 μg Ni^{2+} , 207 μg Pb^{2+} in $\text{H}_2\text{O}_{\text{millipore}}$. The slurry was vigorously stirred (1000 rpm) at ambient temperature (25 $^\circ\text{C}$) for 20 hours. After the given time, the nanoparticles were collected by an external magnet and the solution was analyzed by ICP-OES. Adsorbed metals after 20 hours: 65% Cr^{3+} , 66% Cu^{2+} , 60% Pb^{2+} ; adsorption capacities for metal ions per gram of nanoparticles: 15 $\text{mg}\cdot\text{g}^{-1}$ Cr^{3+} , 19 $\text{mg}\cdot\text{g}^{-1}$ Cu^{2+} , 57 $\text{mg}\cdot\text{g}^{-1}$ Pb^{2+} .

Maximal combined metal uptake for 71h within 5 days: A 20 mL vial was charged with **71h** (2.3 mg) and 10 mL of a 200 μM heavy metal solution corresponding to 2.00 μmol of each metal: 275 μg Ba^{2+} , 104 μg Cr^{3+} , 127 μg Cu^{2+} , 117 μg Ni^{2+} , 414 μg Pb^{2+} , in $\text{H}_2\text{O}_{\text{millipore}}$. The slurry was vigorously stirred (1000 rpm) at ambient temperature (30 $^\circ\text{C}$) for 20 hours. After the given time, the nanoparticles were collected by an external magnet and the solution was analyzed by ICP-OES. Adsorbed metals after 5 days: 97% Cr^{3+} , 71% Cu^{2+} , 2% Ni^{2+} , 55% Pb^{2+} ; adsorption capacities for metal ions per gram of nanoparticles: 44 $\text{mg}\cdot\text{g}^{-1}$ Cr^{3+} , 39 $\text{mg}\cdot\text{g}^{-1}$ Cu^{2+} , 98 $\text{mg}\cdot\text{g}^{-1}$ Pb^{2+} , 1 $\text{mg}\cdot\text{g}^{-1}$ Ni^{2+} .

Recycling of 71h with 100 μM solution (Cr^{3+} , Cu^{2+} , Pb^{2+})

A 20 mL vial was charged with **71h** (4.0 mg) and 10 mL of a 100 μM heavy metal solution corresponding to 1.00 μmol of each metal: 52.0 μg Cr^{3+} , 63.6 μg Cu^{2+} , 207 μg Pb^{2+} in $\text{H}_2\text{O}_{\text{millipore}}$. The slurry was vigorously stirred (1000 rpm) at ambient temperature (30 $^\circ\text{C}$) for 20 hours. After the given time, the nanoparticles were collected by an external magnet and the solution was analyzed by ICP-OES to determine the adsorbed metal content. The vessel was washed carefully with $\text{H}_2\text{O}_{\text{millipore}}$ (2x 3 mL) to remove non-adsorbed metals, before stirring the nanoparticles in 5 mL HCl (0.1 M in $\text{H}_2\text{O}_{\text{millipore}}$) at ambient temperature for 30 minutes. The nanoparticles were collected again with a magnet, the resulting acidic solution was removed and analyzed by ICP-OES to determine the desorbed metal content. Afterwards, the nanoparticles were regenerated with 5 mL Na_2CO_3 solution (0.5 M in $\text{H}_2\text{O}_{\text{millipore}}$) and washed five times with $\text{H}_2\text{O}_{\text{millipore}}$ (3 mL) until the washing solution was neutral (pH 6, pH indicator paper). For the next run, 10 mL of the metal solution (100 μM Cr^{3+} , Cu^{2+} , Pb^{2+}) were added and the procedure repeated.

Recycling of 71h with 10 μM solution (Cr^{3+} , Cu^{2+} , Pb^{2+})

A 20 mL vial was charged with **71h** (2.2 mg) and 10 mL of a 10 μM heavy metal solution corresponding to 0.10 μmol of each metal: 5.2 μg Cr^{3+} , 6.4 μg Cu^{2+} , 21 μg Pb^{2+} in $\text{H}_2\text{O}_{\text{millipore}}$. The slurry was vigorously

stirred (1000 rpm) at ambient temperature (30 °C) for 4 hours. After the given time, the nanoparticles were collected by an external magnet and the solution was analyzed by ICP-OES to determine the adsorbed metal content. For the next run, 10 mL of the metal solution (10 μM Cr^{3+} , Cu^{2+} , Pb^{2+}) were added and the procedure repeated. After three runs, the vessel was washed carefully with $\text{H}_2\text{O}_{\text{millipore}}$ (2x 3 mL) to remove non-adsorbed metals, before stirring the nanoparticles in 5 mL HCl (0.1 M in $\text{H}_2\text{O}_{\text{millipore}}$) at ambient temperature for 30 minutes. The nanoparticles were collected with a magnet and the resulting acidic solution was analyzed by ICP-OES to determine the desorbed metal content of the combined three runs. Afterwards, the nanoparticles were regenerated with 5 mL Na_2CO_3 solution (0.5 M in $\text{H}_2\text{O}_{\text{millipore}}$) and washed five times with $\text{H}_2\text{O}_{\text{millipore}}$ (3 mL) until the washing solution was neutral (pH 6, pH indicator paper). For the next run, 10 mL of the metal solution (10 μM Cr^{3+} , Cu^{2+} , Pb^{2+}) were added and the procedure repeated.

Recycling of 71h with 10 μM solution (Hg^{2+})

A 20 mL vial was charged with **71h** (2.4 mg) and 10 mL of a 10 μM mercury solution corresponding to 0.10 μmol (20 μg) Hg^{2+} in $\text{H}_2\text{O}_{\text{millipore}}$. The slurry was vigorously stirred (1000 rpm) at ambient temperature (30 °C) for 10 minutes. After the given time, the nanoparticles were collected by an external magnet and the solution was analyzed by ICP-OES to determine the adsorbed metal content. For the next run, 10 mL of the 10 μM Hg^{2+} solution were added and the procedure repeated. After three runs, the vessel was washed carefully with $\text{H}_2\text{O}_{\text{millipore}}$ (2x 3 mL) to remove non-adsorbed metals, before stirring the nanoparticles in 5 mL HCl (2 M in $\text{H}_2\text{O}_{\text{millipore}}$) at ambient temperature for 30 minutes. The nanoparticles were collected with a magnet and the resulting acidic solution was analyzed by ICP-OES to determine the desorbed metal content of the combined three runs. Afterwards, the nanoparticles were regenerated with 5 mL Na_2CO_3 solution (0.5 M in $\text{H}_2\text{O}_{\text{millipore}}$) and washed five times with $\text{H}_2\text{O}_{\text{millipore}}$ (3 mL) until the washing solution was neutral (pH 6, pH indicator paper). For the next run, 10 mL of the 10 μM Hg^{2+} solution were added and the procedure repeated.

Single metal capacity during recycling

A 20 mL vial was charged with **71h** (2.1 mg) and 10 mL ($c = 100 \mu\text{M}$, 1.00 μmol , 207 μg) Pb^{2+} in $\text{H}_2\text{O}_{\text{millipore}}$. The slurry was vigorously stirred (1000 rpm) at ambient temperature (30 °C) for 20 hours. After the given time, the nanoparticles were collected by an external magnet and the solution was analyzed by ICP-OES to determine the adsorbed metal content. For the next run, 10 mL ($c = 100 \mu\text{M}$, 1.00 μmol , 207 μg) Pb^{2+} in $\text{H}_2\text{O}_{\text{millipore}}$ were added and the procedure repeated. After three runs, the vessel was washed carefully with $\text{H}_2\text{O}_{\text{millipore}}$ (2x 3 mL) to remove non-adsorbed metals, before stirring the

nanoparticles in 5 mL HCl (0.1 M in H₂O_{millipore}) at ambient temperature for 30 minutes. The nanoparticles were collected with a magnet and the resulting acidic solution was analyzed by ICP-OES to determine the desorbed metal content of the combined three runs. The extraction was repeated with 5 mL HCl (0.1 M in H₂O_{millipore}) and analyzed equally. Afterwards, the nanoparticles were regenerated with 5 mL Na₂CO₃ solution (0.5 M in H₂O_{millipore}) and washed five times with H₂O_{millipore} (3 mL) until the washing solution was neutral (pH 6, pH indicator paper). For the next three runs, 10 mL (c = 100 μM, 1.00 μmol, 52.0 μg) Cr³⁺ in H₂O_{millipore} were used and the procedure repeated. In run 7 to 9, 10 mL (c = 100 μM, 1.00 μmol, 63.6 μg) Cu²⁺ in H₂O_{millipore} were used, followed by each 10 mL (c = 100 μM, 1.00 μmol, 201 μg) Hg²⁺ in H₂O_{millipore} for runs 10 to 12. However, the desorption of mercury was performed with 5 mL HCl (2 M in H₂O_{millipore}) both times. Adsorbed metals within the three runs of one heavy metal: 93% Pb²⁺, 52% Cr³⁺, 71% Cu²⁺, 33% Hg²⁺; adsorption capacities for metal ions per gram of nanoparticles: 273 mg·g⁻¹ Pb²⁺ (run 1 - 3), 39.9 mg·g⁻¹ Cr³⁺ (run 4 - 6), 54.9 mg·g⁻¹ Cu²⁺ (run 7 - 9), 94.3 mg·g⁻¹ Hg²⁺ (run 10 - 12).

Maximal mercury uptake, selectivity

Selectivity test for Co/C 1: A 20 mL vial was charged with Co/C 1 (2.6 mg, 4.92% C, 0.06% H) and 15 mL of a 1 mM heavy metal solution corresponding to 15.0 μmol of each metal: 2.06 mg Ba²⁺, 880 μg Cr³⁺, 953 μg Cu²⁺, 3.01 mg Hg²⁺, 880 μg Ni²⁺, 3.11 mg Pb²⁺ in H₂O_{millipore}. The slurry was vigorously stirred (1000 rpm) at ambient temperature (25 °C) for 89 hours. After the given time, the nanoparticles were collected by an external magnet and the solution was analyzed by ICP-OES to determine the adsorbed metal content. 52% (1.57 mg, 7.83 μmol) Hg²⁺ were adsorbed within 89 hours; Hg²⁺adsorption capacity: 604 mg·g⁻¹ NP.

Selectivity test for 71h: A 20 mL vial was charged with 71h (2.0 mg) and 15 mL of a 1 mM heavy metal solution corresponding to 15.0 μmol of each metal: 2.06 mg Ba²⁺, 880 μg Cr³⁺, 953 μg Cu²⁺, 3.01 mg Hg²⁺, 880 μg Ni²⁺, 3.11 mg Pb²⁺ in H₂O_{millipore}. The slurry was vigorously stirred (1000 rpm) at ambient temperature (25 °C) for 20 hours or 89 hours. After the given time, the nanoparticles were collected by an external magnet and the solution was analyzed by ICP-OES to determine the adsorbed metal content. 36% (1.09 mg, 5.43 μmol) Hg²⁺ were adsorbed within 20 hours; Hg²⁺adsorption capacity for 20 hours: 545mg·g⁻¹ NP. 54% (1.62 mg, 8.07 μmol) Hg²⁺ were adsorbed within 89 hours; Hg²⁺adsorption capacity for 89 hours: 810 mg·g⁻¹ NP.

Affinity to other heavy metals

Cd²⁺, Co²⁺, Fe²⁺: A 20 mL vial was charged with **71h** (2.5 mg) and 10 mL of a 100 μM heavy metal solution corresponding to 1.00 μmol of each metal: 112 μg Cd²⁺, 58.9 μg Co²⁺, 55.9 μg Fe²⁺ in H₂O_{millipore}. The slurry was vigorously stirred (1000 rpm) at ambient temperature (30 °C) for 20 hours. After the given time, the nanoparticles were collected by an external magnet and the solution was analyzed by ICP-OES to determine the adsorbed metal content. Furthermore, the brownish residue in the vial and the desorption were analyzed by ICP-OES. Adsorbed metals after 20 hours: 20% (0.197 μmol, 22.2 μg, 8.9 mg·g⁻¹ NP) Cd²⁺, no Co²⁺ (143 μg found in solution), 80% Fe²⁺ (24% as residue in vial, 33% (0.330 μmol, 18.4 μg, 9.2 mg·g⁻¹ NP) desorbed by NPs).

Zn²⁺: A 20 mL vial was charged with **71h** (2.0 mg) and 10 mL (c = 100 μM, 1.00 μmol, 65.4 μg) Zn²⁺ in H₂O_{millipore}. The slurry was vigorously stirred (1000 rpm) at ambient temperature (30 °C) for 20 hours. After the given time, the nanoparticles were collected by an external magnet and the solution was analyzed by ICP-OES to determine the adsorbed metal content. Adsorbed Zn²⁺ after 20 hours: 42% (0.422 μmol, 27.6 μg, 13 mg·g⁻¹ NP).

Hg²⁺: A 20 mL vial was charged with **71h** (2.3 mg) and 10 mL (c = 100 μM, 1.00 μmol, 201 μg) Hg²⁺ in H₂O_{millipore}. The slurry was vigorously stirred (1000 rpm) at ambient temperature (30 °C) for 10 minutes. After the given time, the nanoparticles were collected by an external magnet and the solution was analyzed by ICP-OES to determine the adsorbed metal content. Adsorbed Hg²⁺ after 10 minutes: 43% (0.435 μmol, 87.3 μg, 38.0 mg·g⁻¹ NP).

Real experiment

A 20 mL vial was charged with **71h** (2.3 mg) and 10 mL of a 10 μM heavy metal solution corresponding to 0.10 μmol of each metal: 5.2 μg Cr³⁺, 6.4 μg Cu²⁺, 20 μg Hg²⁺, 21 μg Pb²⁺ in mineral water.[§] The slurry was vigorously stirred (1000 rpm) at ambient temperature (30 °C) for 20 hours. After the given time, the nanoparticles were collected by an external magnet and the solution was analyzed by ICP-OES to determine the adsorbed metal content. The vessel was washed carefully with H₂O_{millipore} (2x 3 mL) to remove non-adsorbed metals, before stirring the nanoparticles in 5 mL HCl (2 M in H₂O_{millipore}) at ambient temperature for 30 minutes. The nanoparticles were collected again with a magnet, the

[§] Natural mineral water, non-carbonated, bottled in Quintus spring in Bruchsal (Germany) from EDEKA.

Mineral water analysis from Institute Romeis Bad Kissingen GmbH: sodium 20.0 mg·L⁻¹, potassium 2.0 mg·L⁻¹, magnesium 18.2 mg·L⁻¹, calcium 97.0 mg·L⁻¹, chloride 4.6 mg·L⁻¹, fluoride 0.35 mg·L⁻¹, sulfate 14.1 mg·L⁻¹, hydrogencarbonate 415.0 mg·L⁻¹. pH ≈ 8.

resulting acidic solution was removed and analyzed by ICP-OES to determine the desorbed metal content. Afterwards, the nanoparticles were regenerated with 5 mL Na₂CO₃ solution (0.5 M in H₂O_{millipore}) and washed five times with H₂O_{millipore} (3 mL) until the washing solution was neutral (pH 6, pH indicator paper). For the next run, 10 mL of the metal solution (10 μM Cr³⁺, Cu²⁺, Hg²⁺, Pb²⁺) were added and the procedure repeated. Adsorbed metals after 20 hours: 84% Cr³⁺, 89% Cu²⁺, 86% Hg²⁺, 93% Pb²⁺ in run 1. 84% Cr³⁺, 92% Cu²⁺, 87% Hg²⁺, 94% Pb²⁺ in run 2.

Metal adsorption for EDS measurement

A 20 mL vial was charged with **71h** (6.5 mg) and 10 mL of a 100 μM heavy metal solution corresponding to 1.00 μmol of each metal: 52.0 μg Cr³⁺, 63.6 μg Cu²⁺, 201 μg Hg²⁺, 207 μg Pb²⁺ in H₂O_{millipore}. The slurry was vigorously stirred (1000 rpm) at ambient temperature (30 °C) for 20 hours. After the given time, the nanoparticles were collected by an external magnet and the solution was analyzed by ICP-OES to determine the adsorbed metal content. The nanoparticles were washed with H₂O_{millipore} (3 mL), acetone (4x 4 mL), and dried in vacuum. Adsorbed metals after 20 hours: 99% Cr³⁺, 99% Cu²⁺, 99% Hg²⁺, 99% Pb²⁺.

5.2.3. ICP-OES

For ICP-OES measurements, a multi-metal calibration was performed, dissolving the following metal salts in 32% *aqua regia* (v/v): BaCl₂·2H₂O, CdBr₂·4H₂O, CoCl₂·6H₂O, CrCl₃·6H₂O, Cu(OAc)₂·H₂O, FeCl₂·4H₂O, HgCl₂, NiCl₂·6H₂O, Pb(OAc)₂·3H₂O. The zinc calibration was performed with ZnBr₂ in 10% HCl (v/v).

The metals were determined at the following wavelengths (additional wavelengths as control in brackets): Ba λ = 455.404 nm (λ = 233.527 nm), Cd λ = 214.438 nm (λ = 226.502 nm), Co λ = 228.616 nm (λ = 237.862 nm), Cr λ = 267.716 nm (λ = 283.563 nm), Cu λ = 324.754 nm (λ = 219.226 nm), Fe λ = 259.941 nm (λ = 275.573 nm), Hg λ = 184.950 nm (λ = 194.227 nm), Ni λ = 231.604 nm (λ = 221.648 nm), Pb λ = 220.353 nm (λ = 168.215 nm), Zn λ = 213.856 nm (λ = 206.200 nm, 334.502 nm).

ICP-OES sample preparation for adsorption:

To determine the adsorption of the various heavy metals, typically 10 mL of a metal solution with defined concentration was added to 2.0 mg of the functionalized Co/C nanobeads and stirred for a given time at room temperature (30 °C). The nanoparticles were collected by an external magnet and 5 mL (or 6 mL in case of recycling) of the supernatant was transferred to a 10 mL volumetric flask. After

adding 2.4 HCl_{conc.} and 1.2 mL HNO_{3 conc.}, the flask was filled with H₂O (millipore grade) to 10 mL. Subsequently, the solution was filtered through a syringe filter (hydrophilic PTFE 0.2 μm) resulting in a 32% *aqua regia* solution (v/v).

ICP-OES sample preparation for desorption:

To determine the desorption of the heavy metals into the acidic solution, the complete supernatant of the adsorption process was removed and the glass washed carefully with H₂O (millipore grade) to remove leftover metal solution with not-adsorbed metals. 5 mL of HCl (0.1 M, corresponding to 0.04 mL HCl_{conc.} or 2 M HCl in case of Hg²⁺ corresponding to 0.8 mL HCl_{conc.}) was added to the nanoparticles and stirred for 30 minutes at room temperature (30 °C). After magnetic decantation, the nanoparticles were washed two times with H₂O (millipore grade) and all combined solutions were collected in a 10 mL volumetric flask. 2.36 mL (or 1.6 mL in case of Hg²⁺) HCl_{conc.} and 0.8 mL HNO_{3 conc.} were added and the flask was filled with H₂O (millipore grade) and was filtered through a syringe filter (hydrophilic PTFE 0.2 μm) to result in a 32% *aqua regia* solution (v/v).

5.3. Additional figures and miscellaneous

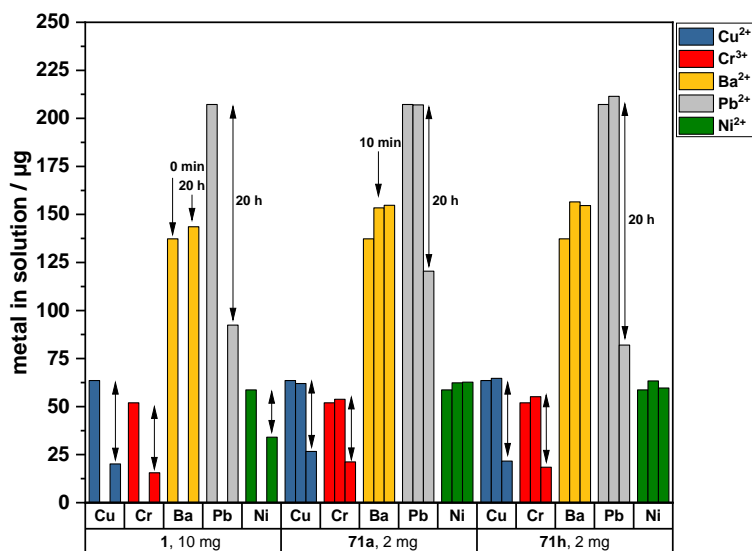


Figure 59. Metal extraction of **1** (10 mg) compared to **71a** and **71h** (2 mg) at t = 0 min, 10 minutes and 20 hours.

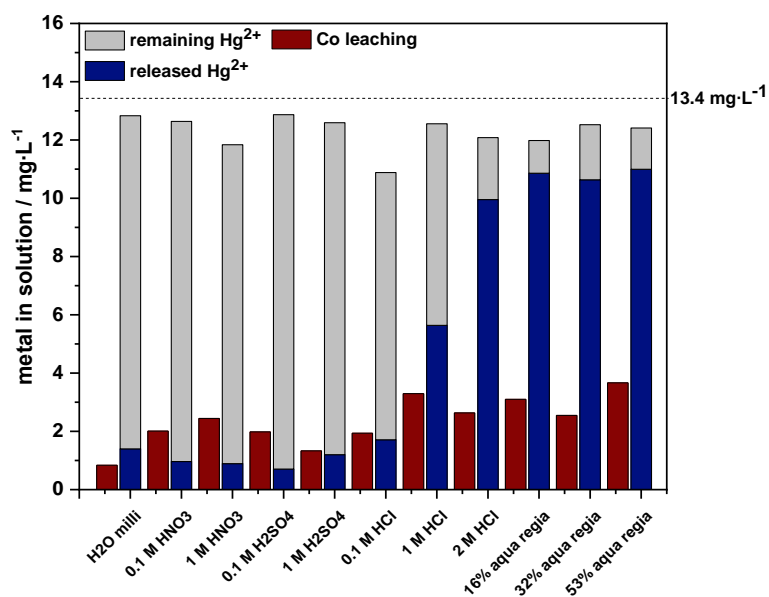


Figure 60. Initial mercury(II) release studies with water and different molarities of nitric acid, sulfuric acid, hydrochloric acid, and *aqua regia* with different (v/v). **71a** was investigated with previously adsorbed Hg²⁺ with a potential maximum of 1 μmol Hg²⁺ corresponding to 13.4 mg·L⁻¹ (dashed line) in 15 mL acid. The actual adsorbed value of each entry is illustrated *via* the gray bar (remaining Hg²⁺).

F. References

- [1] G. A. Ozin, L. Cademartiri, *Small* **2009**, *5*, 1240–1244.
- [2] G. A. Ozin, A. C. Arsenault, L. Cademartiri, *Nanochemistry. A chemical approach to nanomaterials*, 2nd ed. ed., Royal Society of Chemistry, Cambridge, **2008**.
- [3] M. N. Alam, N. Roy, D. Mandal, N. A. Begum, *RSC Adv.* **2013**, *3*, 11935–11956.
- [4] M. T. Amin, A. A. Alazba, U. Manzoor, *Adv. Mater. Sci. Eng.* **2014**, *2014*, 1–24.
- [5] L. A. Kolahalam, I. V. Kasi Viswanath, B. S. Diwakar, B. Govindh, V. Reddy, Y.L.N. Murthy, *Mater. Today: Proc.* **2019**, *18*, 2182–2190.
- [6] D. Vollath, *Nanomaterials. An introduction to synthesis, properties and application*, Wiley-VCH, Weinheim, **2008**.
- [7] D. Schaming, H. Remita, *Found. Chem.* **2015**, *17*, 187–205.
- [8] I. Freestone, N. Meeks, M. Sax, C. Higgitt, *Gold Bull.* **2007**, *40*, 270–277.
- [9] N. Serpone, S. Horikoshi, *Microwaves in nanoparticle synthesis. Fundamentals and applications*, Wiley-VCH, Berlin, **2013**.
- [10] a) C. A. Mirkin, *Small* **2005**, *1*, 14–16; b) R. Jin, Y. Cao, C. A. Mirkin, K. L. Kelly, G. C. Schatz, J. G. Zheng, *Science* **2001**, *294*, 1901–1903;
- [11] N. L. Rosi, C. A. Mirkin, *Chem. Rev.* **2005**, *105*, 1547–1562.
- [12] a) K. Li, B. Liu, *Chem. Soc. Rev.* **2014**, *43*, 6570–6597; b) K. Margulis-Goshen, S. Magdassi, *Curr. Opin. Colloid Interface Sci.* **2012**, *17*, 290–296; c) A. J. Clancy, M. K. Bayazit, S. A. Hodge, N. T. Skipper, C. A. Howard, M. S. P. Shaffer, *Chem. Rev.* **2018**, *118*, 7363–7408;
- [13] G. Koplovitz et al., *Small* **2019**, *15*, 1804557.
- [14] A. Akbarzadeh, M. Samiei, S. Davaran, *Nanoscale Res. Lett.* **2012**, *7*, 144.
- [15] a) S. Thakore, P. S. Rathore, R. N. Jadeja, M. Thounaojam, R. V. Devkar, *Mater. Sci. Eng., C* **2014**, *44*, 209–215; b) S. Dutz, R. Hergt, J. Mürbe, R. Müller, M. Zeisberger, W. Andrä, J. Töpfer, M. E. Bellemann, *J. Magn. Magn. Mater.* **2007**, *308*, 305–312;
- [16] A.-H. Lu, E. L. Salabas, F. Schüth, *Angew. Chem. Int. Ed.* **2007**, *46*, 1222–1244.
- [17] S. Mohan, S. O. Oluwafemi, N. Kalarikkal, S. Thomas, *Synthesis of Inorganic Nanomaterials. Advances and Key Technologies*, Elsevier Science & Technology, San Diego, **2018**.
- [18] D. Xiao, T. Lu, R. Zeng, Y. Bi, *Microchim. Acta* **2016**, *183*, 2655–2675.
- [19] Q. Zhang, X. Yang, J. Guan, *ACS Appl. Nano Mater.* **2019**, *2*, 4681–4697.
- [20] T. Hyeon, S. S. Lee, J. Park, Y. Chung, H. B. Na, *J. Am. Chem. Soc.* **2001**, *123*, 12798–12801.
- [21] J. Mosayebi, M. Kiyasatfar, S. Laurent, *Adv. Healthcare Mater.* **2017**, *6*, 1700306.
- [22] D. Langevin, *Annu. Rev. Phys. Chem.* **1992**, *43*, 341–369.

- [23] J. A. López Pérez, M. A. López Quintela, J. Mira, J. Rivas, S. W. Charles, *J. Phys. Chem. B* **1997**, *101*, 8045–8047.
- [24] H. Hayashi, Y. Hakuta, *Materials* **2010**, *3*, 3794–3817.
- [25] S. F. Hasany, I. Ahmed, R. J. A. Rehman, *Nanosci. Nanotechnol.* **2013**, *2*, 148–158.
- [26] J. J. M. Lenders, C. L. Altan, P. H. H. Bomans, A. Arakaki, S. Bucak, G. de With, N. A. J. M. Sommerdijk, *Cryst. Growth Des.* **2014**, *14*, 5561–5568.
- [27] a) H. T. Phan, A. J. Haes, *J. Phys. Chem. C* **2019**, *123*, 16495–16507; b) R. A. Andrievski, *J. Mater. Sci.* **2003**, *38*, 1367–1375;
- [28] L. Xu, H.-W. Liang, Y. Yang, S.-H. Yu, *Chem. Rev.* **2018**, *118*, 3209–3250.
- [29] S. Shylesh, V. Schünemann, W. R. Thiel, *Angew. Chem. Int. Ed.* **2010**, *49*, 3428–3459.
- [30] C.-J. Jia, F. Schüth, *Phys. Chem. Chem. Phys.* **2011**, *13*, 2457–2487.
- [31] V. V. Mody, A. Cox, S. Shah, A. Singh, W. Bevins, H. Parihar, *Appl. Nanosci.* **2014**, *4*, 385–392.
- [32] I. K. Herrmann, R. N. Grass, D. Mazunin, W. J. Stark, *Chem. Mater.* **2009**, *21*, 3275–3281.
- [33] M. Chen, S. Yamamuro, D. Farrell, S. A. Majetich, *J. Appl. Phys.* **2003**, *93*, 7551–7553.
- [34] a) X. Gao, K. M. K. Yu, K. Y. Tam, S. C. Tsang, *Chem. Commun.* **2003**, 2998–2999; b) T. Sen, A. Sebastianelli, I. J. Bruce, *J. Am. Chem. Soc.* **2006**, *128*, 7130–7131;
- [35] a) C. Xu, K. Xu, H. Gu, R. Zheng, H. Liu, X. Zhang, Z. Guo, B. Xu, *J. Am. Chem. Soc.* **2004**, *126*, 9938–9939; b) I. S. Lee, N. Lee, J. Park, B. H. Kim, Y.-W. Yi, T. Kim, T. K. Kim, I. H. Lee, S. R. Paik, T. Hyeon, *J. Am. Chem. Soc.* **2006**, *128*, 10658–10659;
- [36] J. Nishijo, C. Okabe, O. Oishi, N. Nishi, *Carbon* **2006**, *44*, 2943–2949.
- [37] R. N. Grass, E. K. Athanassiou, W. J. Stark, *Angew. Chem. Int. Ed.* **2007**, *46*, 4909–4912.
- [38] Q. M. Kainz, O. Reiser, *Acc. Chem. Res.* **2014**, *47*, 667–677.
- [39] J. H. J. Scott, Majetich, Sara, A., *Phys. Rev. B: Condens. Matter* **1995**, *52*, 12564–12571.
- [40] P. Mattila et al., *J. Nanopart. Res.* **2014**, *16*, e22.
- [41] X.-W. Wei, G.-X. Zhu, C.-J. Xia, Y. Ye, *Nanotechnology* **2006**, *17*, 4307–4311.
- [42] a) H. K. Kammler, L. Mädler, S. E. Pratsinis, *Chem. Eng. Technol.* **2001**, *24*, 583–596; b) W. Y. Teoh, R. Amal, L. Mädler, *Nanoscale* **2010**, *2*, 1324–1347;
- [43] N. T. Thanh, *Clinical Applications of Magnetic Nanoparticles. From Fabrication to Clinical Applications*, 1st ed. ed., CRC Press, Milton, **2018**.
- [44] C. M. Eichenseer, O. Reiser, *Nachr. Chem.* **2015**, *63*, 763–767.
- [45] a) C. A. Dyke, M. P. Stewart, F. Maya, J. M. Tour, *Synlett* **2004**, 155–160; b) F. M. Koehler, W. J. Stark, *Acc. Chem. Res.* **2013**, *46*, 2297–2306;
- [46] A. Schätz, M. Zeltner, T. D. Michl, M. Rossier, R. Fuhrer, W. J. Stark, *Chem. Eur. J.* **2011**, *17*, 10566–10573.

- [47] S. Wittmann, J.-P. Majoral, R. N. Grass, W. J. Stark, O. Reiser, *Green Process. Synth.* **2012**, *1*, 275–279.
- [48] M. Keller, A. Perrier, R. Linhardt, L. Travers, S. Wittmann, A.-M. Caminade, J.-P. Majoral, O. Reiser, A. Ouali, *Adv. Synth. Catal.* **2013**, *355*, 1748–1754.
- [49] Q. M. Kainz, M. Zeltner, M. Rossier, W. J. Stark, O. Reiser, *Chem. Eur. J.* **2013**, *19*, 10038–10045.
- [50] Q. M. Kainz, A. Späth, S. Weiss, T. D. Michl, A. Schätz, W. J. Stark, B. König, O. Reiser, *ChemistryOpen* **2012**, *1*, 125–129.
- [51] C. M. Eichenseer, B. Kastl, M. A. Pericàs, P. R. Hanson, O. Reiser, *ACS Sustainable Chem. Eng.* **2016**, *4*, 2698–2705.
- [52] Q. M. Kainz, S. Fernandes, C. M. Eichenseer, F. Besostri, H. Körner, R. Müller, O. Reiser, *Faraday discussions* **2014**, *175*, 27–40.
- [53] A. Schätz, T. R. Long, R. N. Grass, W. J. Stark, P. R. Hanson, O. Reiser, *Adv. Funct. Mater.* **2010**, *20*, 4323–4328.
- [54] Q. M. Kainz, R. Linhardt, P. K. Maity, P. R. Hanson, O. Reiser, *ChemSusChem* **2013**, *6*, 721–729.
- [55] S. Fernandes, C. M. Eichenseer, P. Kreitmeier, J. Rewitzer, V. Zlateski, R. N. Grass, W. J. Stark, O. Reiser, *RSC Adv.* **2015**, *5*, 46430–46436.
- [56] S. Wittmann, A. Schätz, R. N. Grass, W. J. Stark, O. Reiser, *Angew. Chem. Int. Ed.* **2010**, *49*, 1867–1870.
- [57] M. Keller, V. Collière, O. Reiser, A.-M. Caminade, J.-P. Majoral, A. Ouali, *Angew. Chem. Int. Ed.* **2013**, *52*, 3626–3629.
- [58] F. M. Koehler, M. Rossier, M. Waelle, E. K. Athanassiou, L. K. Limbach, R. N. Grass, D. Günther, W. J. Stark, *Chemical communications (Cambridge, England)* **2009**, 4862–4864.
- [59] R. Fuhrer, I. K. Herrmann, E. K. Athanassiou, R. N. Grass, W. J. Stark, *Langmuir* **2011**, *27*, 1924–1929.
- [60] Q. M. Kainz, R. Linhardt, R. N. Grass, G. Vilé, J. Pérez-Ramírez, W. J. Stark, O. Reiser, *Adv. Funct. Mater.* **2014**, *24*, 2020–2027.
- [61] a) N. Mizuno, M. Misono, *Chem. Rev.* **1998**, *98*, 199–218; b) J. D. A. Pelletier, J.-M. Basset, *Accounts of chemical research* **2016**, *49*, 664–677; c) D. C. Bailey, S. H. Langer, *Chem. Rev.* **1981**, *81*, 109–148;
- [62] a) M. Benaglia, A. Puglisi, F. Cozzi, *Chem. Rev.* **2003**, *103*, 3401–3429; b) D. E. Bergbreiter, Y.-S. Liu, *Tetrahedron Lett.* **1997**, *38*, 7843–7846; c) N. E. Leadbeater, M. Marco, *Chem. Rev.* **2002**, *102*, 3217–3274; d) Y. Uozumi, H. Danjo, T. Hayashi, *Tetrahedron Lett.* **1998**, *39*, 8303–8306; e) W. Zhang, Y. Sun, L. Zhang, *Ind. Eng. Chem. Res.* **2016**, *55*, 12398–12406; f) Y. Uozumi, *Bull. Chem. Soc. Jpn.* **2008**, *81*, 1183–1195;

- [63] a) R. Andrés, E. de Jesús, J. C. Flores, *New J. Chem.* **2007**, *31*, 1161; b) R. Touzani, H. Alper, *Journal of Molecular Catalysis A: Chemical* **2005**, *227*, 197–207;
- [64] a) S. S. Acharyya, S. Ghosh, R. Bal, *ACS Sustainable Chem. Eng.* **2014**, *2*, 584–589; b) A. C. Atesin, N. A. Ray, P. C. Stair, T. J. Marks, *J. Am. Chem. Soc.* **2012**, *134*, 14682–14685; c) B. Dong, D. L. Miller, C. Y. Li, *J. Phys. Chem. Lett.* **2012**, *3*, 1346–1350; d) K. B. Vu, K. V. Bukhryakov, D. H. Anjum, V. O. Rodionov, *ACS Catal.* **2015**, *5*, 2529–2533; e) H. Zhong, Y. Su, C. Cui, F. Zhou, X. Li, R. Wang, *ACS Sustainable Chem. Eng.* **2017**, *5*, 8061–8069;
- [65] S. B. Kalidindi, B. R. Jagirdar, *ChemSusChem* **2012**, *5*, 65–75.
- [66] M. Rai, S. S. da Silva (Eds.) *Green Chemistry and Sustainable Technology*, Springer International Publishing, Cham, **2017**.
- [67] A. Schätz, R. N. Grass, W. J. Stark, O. Reiser, *Chem. Eur. J.* **2008**, *14*, 8262–8266.
- [68] J. Zhi, S. Mitchell, J. Pérez-Ramírez, O. Reiser, *ChemCatChem* **2015**, *7*, 2585–2589.
- [69] R. Linhardt, Q. M. Kainz, R. N. Grass, W. J. Stark, O. Reiser, *RSC Adv.* **2014**, *4*, 8541.
- [70] a) L. Stadler, M. Homafar, A. Hartl, S. Najafishirtari, M. Colombo, R. Zboril, P. Martin, M. B. Gawande, J. Zhi, O. Reiser, *ACS Sustainable Chem. Eng.* **2019**, *7*, 2388–2399; b) G. Purohit, D. S. Rawat, O. Reiser, *ChemCatChem* **2020**, *12*, 569–575;
- [71] M. Zeltner, A. Schätz, M. L. Hefti, W. J. Stark, *J. Mater. Chem.* **2011**, *21*, 2991–2996.
- [72] A. Schätz, R. N. Grass, Q. Kainz, W. J. Stark, O. Reiser, *Chem. Mater.* **2010**, *22*, 305–310.
- [73] P. Xu et al., *Sci. Total Environ.* **2012**, *424*, 1–10.
- [74] A. Pratt in *Frontiers of Nanoscience, Vol. 6* (Ed.: C. Binns), Elsevier Science, Oxford, **2014**.
- [75] S. C. N. Tang, I. M. C. Lo, *Water Res.* **2013**, *47*, 2613–2632.
- [76] P. Biswas, C.-Y. Wu, *J. Air Waste Manage. Assoc.* **2005**, *55*, 708–746.
- [77] a) M. N. Moore, *Environ. Int.* **2006**, *32*, 967–976; b) N. Wilson, *BioScience* **2018**, *68*, 241–246;
- [78] M. Rossier, A. Schaetz, E. K. Athanassiou, R. N. Grass, W. J. Stark, *Chem. Eng. J.* **2011**, *175*, 244–250.
- [79] P. K. Maity et al., *Org. Lett.* **2011**, *13*, 8–10.
- [80] P. K. Maity, Q. M. Kainz, S. Faisal, A. Rolfe, T. B. Samarakoon, F. Z. Basha, O. Reiser, P. R. Hanson, *Chem. Commun.* **2011**, *47*, 12524–12526.
- [81] Q. M. Kainz, S. Fernandes, C. M. Eichenseer, F. Besostri, H. Körner, R. Müller, O. Reiser, *Faraday Discuss.* **2014**, *175*, 27–40.
- [82] Q. M. Kainz, A. Schätz, A. Zöpfl, W. J. Stark, O. Reiser, *Chem. Mater.* **2011**, *23*, 3606–3613.
- [83] a) I. K. Herrmann et al., *Nanoscale* **2013**, *5*, 8718–8723; b) C. M. Schumacher, I. K. Herrmann, S. B. Bubenhofer, S. Gschwind, A.-M. Hirt, B. Beck-Schimmer, D. Günther, W. J. Stark, *Adv. Funct. Mater.* **2013**, *23*, 4888–4896; c) I. K. Herrmann, M. Urner, F. M. Koehler, M. Hasler, B.

- Roth-Z'graggen, R. N. Grass, U. Ziegler, B. Beck-Schimmer, W. J. Stark, *Small* **2010**, *6*, 1388–1392;
- [84] a) A. Levin, A. Hartl, O. Reiser, C. Czeslik, *Coll. Surf. B: Biointerfaces* **2019**, *182*, 110344; b) V. Zlateski, R. Fuhrer, F. M. Koehler, S. Wharry, M. Zeltner, W. J. Stark, T. S. Moody, R. N. Grass, *Bioconjugate Chem.* **2014**, *25*, 677–684;
- [85] a) G. Song, M. Kenney, Y.-S. Chen, X. Zheng, Y. Deng, Z. Chen, S. X. Wang, S. S. Gambhir, H. Dai, J. Rao, *Nat. Biomed. Eng.* **2020**, *4*, 325–334; b) J. Yu, F. Chen, W. Gao, Y. Ju, X. Chu, S. Che, F. Sheng, Y. Hou, *Nanoscale Horiz.* **2017**, *2*, 81–88; c) W. S. Seo et al., *Nature Mater.* **2006**, *5*, 971–976;
- [86] W. Bonrath, J. Medlock, J. Schütz, B. Wüstenberg, T. Netscher, *Hydrogenation. Chapter 3: Hydrogenation in the Vitamins and Fine Chemicals Industry – An Overview.* (Ed.: I. Karam), InTech, Rijeka, Croatia, **2012**.
- [87] a) P. T. Anastas, J. C. Warner, *Green chemistry: theory and practice*, Oxford University Press, Oxford, **1998**; b) P. T. Anastas, M. M. Kirchhoff, *Acc. Chem. Res.* **2002**, *35*, 686–694; c) R. A. Sheldon, *Chem. Commun.* **2008**, 3352–3365;
- [88] a) A.-H. Lu, E. L. Salabas, F. Schüth, *Angew. Chem. Int. Ed.* **2007**, *46*, 1222–1244; b) S. Shylesh, V. Schünemann, W. R. Thiel, *Angew. Chem. Int. Ed.* **2010**, *49*, 3428–3459; c) M. B. Gawande, P. S. Branco, R. S. Varma, *Chem. Soc. Rev.* **2013**, *42*, 3371–3393; d) M. B. Gawande, R. Luque, R. Zboril, *ChemCatChem* **2014**, *6*, 3312–3313; e) A. Schätz, O. Reiser, W. J. Stark, *Chem. Eur. J.* **2010**, *16*, 8950–8967; f) V. Polshettiwar, R. Luque, A. Fihri, H. Zhu, M. Bouhrara, J.-M. Basset, *Chem. Rev.* **2011**, *111*, 3036–3075; g) V. Polshettiwar, B. Baruwati, R. S. Varma, *Green Chem.* **2009**, *11*, 127–131;
- [89] N. B. McKeown, P. M. Budd, *Chem. Soc. Rev.* **2006**, *35*, 675–683.
- [90] B. Li, F. Su, H.-K. Luo, L. Liang, B. Tan, *Microporous Mesoporous Mater.* **2011**, *138*, 207–214.
- [91] a) D. Dang, P. Wu, C. He, Z. Xie, C. Duan, *J. Am. Chem. Soc.* **2010**, *132*, 14321–14323; b) X. Du, Y. Sun, B. Tan, Q. Teng, X. Yao, C. Su, W. Wang, *Chem. Commun.* **2010**, *46*, 970–972;
- [92] a) H. Furukawa, O. M. Yaghi, *J. Am. Chem. Soc.* **2009**, *131*, 8875–8883; b) N. B. McKeown, B. Gahnem, K. J. Msayib, P. M. Budd, C. E. Tattershall, K. Mahmood, S. Tan, D. Book, H. W. Langmi, A. Walton, *Angew. Chem. Int. Ed.* **2006**, *118*, 1836–1839; c) C. D. Wood et al., *Chem. Mater.* **2007**, *19*, 2034–2048;
- [93] R. Dawson, T. Ratvijitvech, M. Corker, A. Laybourn, Y. Z. Khimyak, A. I. Cooper, D. J. Adams, *Polym. Chem.* **2012**, *3*, 2034–2038.
- [94] G. Ferey, C. Mellot-Draznieks, C. Serre, F. Millange, J. Dutour, S. Surble, I. Margiolaki, *Science* **2005**, *309*, 2040–2042.

- [95] A. P. Cote, A. I. Benin, N. W. Ockwig, M. O'Keeffe, Matzger, A. J., O. M. Yaghi, *Science* **2005**, *310*, 1166–1170.
- [96] T. Tozawa et al., *Nat. Mater.* **2009**, *8*, 973–978.
- [97] K. Song, P. Liu, J. Wang, L. Pang, J. Chen, I. Hussain, B. Tan, T. Li, *Dalton Trans.* **2015**, *44*, 13906–13913.
- [98] B. Li, R. Gong, W. Wang, X. Huang, W. Zhang, H. Li, C. Hu, B. Tan, *Macromolecules* **2011**, *44*, 2410–2414.
- [99] V. A. Davankov, S. V. Rogozhin, M. P. Tsyurupa, US Patent 3, 729, 457, 1971.
- [100] a) J. H. Ahn, J. E. Jang, C. G. Oh, S. K. Ihm, J. Cortez, D. C. Sherrington, *Macromolecules* **2006**, *39*, 627–632; b) F. S. Macintyre, D. C. Sherrington, L. Tetley, *Macromolecules* **2006**, *39*, 5381–5384;
- [101] M. P. Tsyurupa, V. A. Davankov, *React. Funct. Polym.* **2006**, *66*, 768–779.
- [102] B. Li, Z. Guan, W. Wang, X. Yang, J. Hu, B. Tan, T. Li, *Adv. Mater.* **2012**, *24*, 3390–3395.
- [103] a) Q. Liang, J. Liu, Y. Wei, Z. Zhao, M. J. MacLachlan, *Chem. Commun.* **2013**, *49*, 8928–8930; b) S. Ogasawara, S. Kato, *J. Am. Chem. Soc.* **2010**, *132*, 4608–4613;
- [104] R. Andrés, E. de Jesús, J. C. Flores, *New J. Chem.* **2007**, *31*, 1161–1191.
- [105] R. Pauthenet, *J. Appl. Phys.* **1982**, *53*, 8187–8192.
- [106] a) K. S. W. Sing, *Pure Appl. Chem.* **1985**, *57*, 603–619; b) L. Li, H. Zhao, J. Wang, R. Wang, *ACS Nano* **2014**, *8*, 5352–5364;
- [107] J. Weber, J. Schmidt, A. Thomas, W. Böhlmann, *Langmuir* **2010**, *26*, 15650–15656.
- [108] B. Basu, S. Paul, *Appl. Organomet. Chem.* **2013**, *27*, 588–594.
- [109] a) H. Yang, X. Han, Z. Ma, R. Wang, J. Liu, X. Ji, *Green Chem.* **2010**, *12*, 441–451; b) H. Yang, Y. Wang, Y. Qin, Y. Chong, Q. Yang, G. Li, L. Zhang, W. Li, *Green Chem.* **2011**, *13*, 1352–1361; c) X. Feng, M. Yan, T. Zhang, Y. Liu, M. Bao, *Green Chem.* **2010**, *12*, 1758–1766;
- [110] B. Yuan, Y. Pan, Y. Li, B. Yin, H. Jiang, *Angew. Chem.* **2010**, *122*, 4148–4152.
- [111] M. Cano, A. Benito, W. K. Maser, E. P. Urriolabeitia, *Carbon* **2011**, *49*, 652–658.
- [112] Q. M. Kainz, R. Linhardt, R. N. Grass, G. Vilé, J. Pérez-Ramírez, W. J. Stark, O. Reiser, *Adv. Funct. Mater.* **2014**, *24*, 2020–2027.
- [113] C. D. Wagner, W. M. Riggs, L. E. Davis, J. Moulder, *Handbook of X-ray Photoelectron Spectroscopy: A Reference Book of Standard Data for Use in X-ray Photoelectron Spectroscopy*, Perkin-Elmer Corporation, Physical Electronics Division, Minnesota, **1979**.
- [114] M. Liao, Q. Hu, J. Zheng, Y. Li, H. Zhou, C.-J. Zhong, B. H. Chen, *Electrochim. Acta* **2013**, *111*, 504–509.

- [115] S. Ranjbar, *Dissertation*, Universitat Rovira I Virgili (ICIQ), Tarragona; Universität Regensburg, Regensburg, **2016**.
- [116] L. Stadler, M. Homafar, A. Hartl, S. Najafishirtari, M. Colombo, R. Zboril, P. Martin, M. B. Gawande, J. Zhi, O. Reiser, *ACS Sustainable Chem. Eng.* **2019**, *7*, 2388–2399.
- [117] a) C. E. Garrett, K. Prasad, *Adv. Synth. Catal.* **2004**, *346*, 889–900; b) V. L. Budarin, P. S. Shuttleworth, J. H. Clark, R. Luque, *Curr. Org. Synth.* **2010**, *7*, 614–627;
- [118] a) X. Duan, J. Liu, J. Hao, L. Wu, B. He, Y. Qiu, J. Zhang, Z. He, J. Xi, S. Wang, *Carbon* **2018**, *130*, 806–813; b) N. Jiao, Z. Li, C. Xia, J. Liu, *ChemistrySelect* **2017**, *2*, 4545–4556; c) S.-T. Yang, P. Shen, B.-S. Liao, Y.-H. Liu, S.-M. Peng, S.-T. Liu, *Organometallics* **2017**, *36*, 3110–3116; d) M. Shokouhimehr, K. Hong, T. H. Lee, C. W. Moon, S. P. Hong, K. Zhang, J. M. Suh, K. S. Choi, R. S. Varma, H. W. Jang, *Green Chem.* **2018**, *20*, 3809–3817;
- [119] a) C. V. Rode, M. J. Vaidya, R. V. Chaudhari, *Org. Process Res. Dev.* **1999**, *3*, 465–470; b) C. V. Rode, M. J. Vaidya, R. Jaganathan, R. V. Chaudhari, *Chem. Eng. Sci.* **2001**, *56*, 1299–1304;
- [120] A. Biffis, P. Centomo, A. Del Zotto, M. Zecca, *Chem. Rev.* **2018**, *118*, 2249–2295.
- [121] A. Fihri, M. Bouhrara, B. Nekoueishahraki, J.-M. Basset, V. Polshettiwar, *Chem. Soc. Rev.* **2011**, *40*, 5181–5203.
- [122] G. C. Fortman, S. P. Nolan, *Chem. Soc. Rev.* **2011**, *40*, 5151–5169.
- [123] C. C. C. Johansson Seechurn, M. O. Kitching, T. J. Colacot, V. Snieckus, *Angew. Chem. Int. Ed.* **2012**, *51*, 5062–5085.
- [124] a) N. Miyaura, A. Suzuki, *Chem. Rev.* **1995**, *95*, 2457–2483; b) F.-S. Han, *Chem. Soc. Rev.* **2013**, *42*, 5270–5298;
- [125] N. T. S. Phan, M. Van Der Sluys, C. W. Jones, *Adv. Synth. Catal.* **2006**, *348*, 609–679.
- [126] D. B. Eremin, V. P. Ananikov, *Coord. Chem. Rev.* **2017**, *346*, 2–19.
- [127] A. Y. Kostyukovich, A. M. Tsedilin, E. D. Sushchenko, D. B. Eremin, A. S. Kashin, M. A. Topchiy, A. F. Asachenko, M. S. Nechaev, V. P. Ananikov, *Inorg. Chem. Front.* **2019**, *6*, 482–492.
- [128] a) R. K. Arvela, N. E. Leadbeater, M. S. Sangi, V. A. Williams, P. Granados, R. D. Singer, *J. Org. Chem.* **2005**, *70*, 161–168; b) N. E. Leadbeater, M. Marco, *Angew. Chem. Int. Ed.* **2003**, *42*, 1407–1409;
- [129] a) M. García-Melchor, A. A. C. Braga, A. Lledós, G. Ujaque, F. Maseras, *Acc. Chem. Res.* **2013**, *46*, 2626–2634; b) M. Pérez-Lorenzo, *J. Phys. Chem. Lett.* **2012**, *3*, 167–174; c) I. Hussain, J. Capricho, M. A. Yawer, *Adv. Synth. Catal.* **2016**, *358*, 3320–3349; d) A. S. Kashin, V. P. Ananikov, *J. Org. Chem.* **2013**, *78*, 11117–11125; e) M. V. Polynski, V. P. Ananikov, *ACS Catal.* **2019**, *9*, 3991–4005; f) P. Veerakumar, P. Thanasekaran, K.-L. Lu, K.-C. Lin, S. Rajagopal, *ACS Sustainable Chem. Eng.* **2017**, *5*, 8475–8490; g) A. Zecchina, S. Bordiga, E. Groppo, *Selective nanocatalysts*

- and nanoscience. Concepts for heterogeneous and homogeneous catalysis*, Wiley-VCH-Verl., Weinheim, **2011**;
- [130] M. Górna, M. S. Szulmanowicz, A. Gniewek, W. Tylus, A. M. Trzeciak, *J. Organomet. Chem.* **2015**, *785*, 92–99.
- [131] A. V. Astakhov, O. V. Khazipov, A. Y. Chernenko, D. V. Pasyukov, A. S. Kashin, E. G. Gordeev, V. N. Khrustalev, V. M. Chernyshev, V. P. Ananikov, *Organometallics* **2017**, *36*, 1981–1992.
- [132] B. Kastl, *Dissertation*, Universität Regensburg, Regensburg, **2018**.
- [133] P. D. Stevens, J. Fan, H. M. R. Gardimalla, M. Yen, Y. Gao, *Org. Lett.* **2005**, *7*, 2085–2088.
- [134] C. G. Tan, R. N. Grass, *Chem. Commun.* **2008**, 4297–4299.
- [135] J.-W. Byun, Y.-S. Lee, *Tetrahedron Lett.* **2004**, *45*, 1837–1840.
- [136] Y. Ding, M. A. Clark, *ACS Comb. Sci.* **2015**, *17*, 1–4.
- [137] M. L. Malone, B. M. Paegel, *ACS Comb. Sci.* **2016**, *18*, 182–187.
- [138] A. L. Satz, J. Cai, Y. Chen, R. Goodnow, F. Gruber, A. Kowalczyk, A. Petersen, G. Naderi-Oboodi, L. Orzechowski, Q. Strebels, *Bioconjugate Chem.* **2015**, *26*, 1623–1632.
- [139] H. Nozaki, S. Moriuti, H. Takaya, R. Noyori, *Tetrahedron Lett.* **1966**, *7*, 5239–5244.
- [140] H. Fritschi, U. Leutenegger, A. Pfaltz, *Helv. Chim. Acta* **1988**, *71*, 1553–1565.
- [141] U. Leutenegger, G. Umbricht, C. Fahrni, P. von Matt, A. Pfaltz, *Tetrahedron* **1992**, *48*, 2143–2156.
- [142] R. E. Lowenthal, A. Abiko, S. Masamune, *Tetrahedron Lett.* **1990**, *31*, 6005–6008.
- [143] D. A. Evans, K. A. Woerpel, M. M. Hinman, M. M. Faul, *J. Am. Chem. Soc.* **1991**, *113*, 726–728.
- [144] a) H. Brunner, U. Obermann, P. Wimmer, *Organometallics* **1989**, *8*, 821–826; b) H. Brunner, U. Obermann, *Chem. Ber.* **1989**, *122*, 499–507;
- [145] M. Glos, O. Reiser, *Org. Lett.* **2000**, *2*, 2045–2048.
- [146] H. Werner, R. Vicha, A. Gissibl, O. Reiser, *J. Org. Chem.* **2003**, *68*, 10166–10168.
- [147] a) C. Geiger, P. Kreitmeier, O. Reiser, *Adv. Synth. Catal.* **2005**, *347*, 249–254; b) R. Rasappan, M. Hager, A. Gissibl, O. Reiser, *Org. Lett.* **2006**, *8*, 6099–6102;
- [148] A. Gissibl, M. G. Finn, O. Reiser, *Org. Lett.* **2005**, *7*, 2325–2328.
- [149] L. K. A. Pils, T. Ertl, O. Reiser, *Org. Lett.* **2017**, *19*, 2754–2757.
- [150] R. B. Chhor, B. Nosse, S. Sörgel, C. Böhm, M. Seitz, O. Reiser, *Chem. Eur. J.* **2003**, *9*, 260–270.
- [151] A. Schätz, M. Hager, O. Reiser, *Adv. Funct. Mater.* **2009**, *19*, 2109–2115.
- [152] H. Werner, C. I. Herrerías, M. Glos, A. Gissibl, J. M. Fraile, I. Pérez, J. A. Mayoral, O. Reiser, *Adv. Synth. Catal.* **2006**, *348*, 125–132.
- [153] a) R. Rasappan, T. Olbrich, O. Reiser, *Adv. Synth. Catal.* **2009**, *351*, 1961–1967; b) J. M. Fraile, J. I. García, C. I. Herrerías, J. A. Mayoral, O. Reiser, A. Socuélamos, H. Werner, *Chem. Eur. J.*

- 2004**, *10*, 2997–3005; c) A. Gissibl, C. Padié, M. Hager, F. Jaroschik, R. Rasappan, E. Cuevas-Yañez, C.-O. Turrin, A.-M. Caminade, J.-P. Majoral, O. Reiser, *Org. Lett.* **2007**, *9*, 2895–2898; d) J. M. Fraile, I. Pérez, J. A. Mayoral, O. Reiser, *Adv. Synth. Catal.* **2006**, *348*, 1680–1688; e) J. I. García, C. I. Herrerías, B. López-Sánchez, J. A. Mayoral, O. Reiser, *Adv. Synth. Catal.* **2011**, *353*, 2691–2700;
- [154] a) J. M. Fraile, J. I. García, V. Martínez-Merino, J. A. Mayoral, L. Salvatella, *J. Am. Chem. Soc.* **2001**, *123*, 7616–7625; b) M. I. Burguete, J. M. Fraile, E. García-Verdugo, S. V. Luis, V. Martínez-Merino, J. A. Mayoral, *Ind. Eng. Chem. Res.* **2005**, *44*, 8580–8587; c) A.I. Fernández, J.M. Fraile, J.I. García, C.I. Herrerías, J.A. Mayoral, L. Salvatella, *Catal. Commun.* **2001**, *2*, 165–170; d) J.M. Fraile, J.I. García, M.A. Harmer, C.I. Herrerías, J.A. Mayoral, *J. Mol. Catal. A: Chem.* **2001**, *165*, 211–218; e) J. M. Fraile, J. I. García, C. I. Herrerías, J. A. Mayoral, O. Reiser, M. Vaultier, *Tetrahedron Lett.* **2004**, *45*, 6765–6768; f) A. Schätz, A. Scarel, E. Zangrando, L. Mosca, C. Carfagna, A. Gissibl, B. Milani, O. Reiser, *Organometallics* **2006**, *25*, 4065–4068;
- [155] a) O. Reiser, *Isr. J. Chem.* **2016**, *56*, 531–539; b) H. M. L. Davies, S. J. Hedley, *Chem. Soc. Rev.* **2007**, *36*, 1109–1119;
- [156] Q. M. Kainz, A. Späth, S. Weiss, T. D. Michl, A. Schätz, W. J. Stark, B. König, O. Reiser, *ChemistryOpen* **2012**, *1*, 125–129.
- [157] C. N. Slattery, L.-A. Clarke, A. Ford, A. R. Maguire, *Tetrahedron* **2013**, *69*, 1297–1301.
- [158] J. M. Fraile, J. I. García, J. A. Mayoral, T. Tarnai, *J. Mol. Catal. A: Chem.* **1999**, *144*, 85–89.
- [159] H. Werner, *Dissertation*, Universität Regensburg, Regensburg, **2003**.
- [160] B. Liu, S.-F. Zhu, W. Zhang, C. Chen, Q.-L. Zhou, *J. Am. Chem. Soc.* **2007**, *129*, 5834–5835.
- [161] H. B. Bradl, *Heavy Metals in the Environment: Origin, Interaction and Remediation*, 1st ed., Elsevier Academic Press, London, **2005**.
- [162] P. A. Kobielska, A. J. Howarth, O. K. Farha, S. Nayak, *Coord. Chem. Rev.* **2018**, *358*, 92–107.
- [163] R. Goyer, *U.S. Environmental Protection Agency Risk Assessment Forum* **2004**.
- [164] a) Ihsanullah, A. Abbas, A. M. Al-Amer, T. Laoui, M. J. Al-Marri, M. S. Nasser, M. Khraisheh, M. A. Atieh, *Sep. Purif. Technol.* **2016**, *157*, 141–161; b) F. Fu, Q. Wang, *J. Environ. Manage.* **2011**, *92*, 407–418;
- [165] Z. Yang, X. Huang, X. Yao, H. Ji, *J. Appl. Polym. Sci.* **2018**, *135*, 45568.
- [166] a) P. Xu et al., *Sci. Total Environ.* **2012**, *424*, 1–10; b) M. Hua, S. Zhang, B. Pan, W. Zhang, L. Lv, Q. Zhang, *J. Hazard. Mater.* **2012**, *211-212*, 317–331; c) F. Lu, D. Astruc, *Coord. Chem. Rev.* **2018**, *356*, 147–164;
- [167] F. M. Koehler, M. Rossier, M. Waelle, E. K. Athanassiou, L. K. Limbach, R. N. Grass, D. Günther, W. J. Stark, *Chem. Commun.* **2009**, 4862–4864.

- [168] M. Rossier, F. M. Koehler, E. K. Athanassiou, R. N. Grass, B. Aeschlimann, D. Günther, W. J. Stark, *J. Mater. Chem.* **2009**, *19*, 8239–8243.
- [169] M. Rossier, F. M. Koehler, E. K. Athanassiou, R. N. Grass, M. Waelle, K. Birbaum, D. Günther, W. J. Stark, *Ind. Eng. Chem. Res.* **2010**, *49*, 9355–9362.
- [170] M. Rossier, M. Schreier, U. Krebs, B. Aeschlimann, R. Fuhrer, M. Zeltner, R. N. Grass, D. Günther, W. J. Stark, *Sep. Purif. Technol.* **2012**, *96*, 68–74.
- [171] L. Stadler, M. Homafar, A. Hartl, S. Najafshirtari, M. Colombo, R. Zboril, P. Martin, M. B. Gawande, J. Zhi, O. Reiser, *ACS Sustainable Chem. Eng.* **2019**, *7*, 2388–2399.
- [172] World Health Organization WHO, "International Programme on Chemical Safety. Ten chemicals of major public health concern", to be found under https://www.who.int/ipcs/assessment/public_health/chemicals_phc/en/.
- [173] S. Hünig, G. Märkl, J. Sauer, P. Kreitmeier, A. Ledermann, *Arbeitsmethoden in der organischen Chemie*, 2nd ed., Verlag Lehmanns Media, Berlin, **2008**.
- [174] R. Linhardt, *Dissertation*, Universität Regensburg, Regensburg, **2014**.
- [175] N. E. Searle, *Org. Synth.* **1956**, *36*, 25.
- [176] S. V. McKinley, U.S. Patent 3,923,911, U.S. Patent 3,923,911, Dec 2, 1975, **1975**.
- [177] a) D. A. Nicewicz, G. Brétéché, J. S. Johnson, *Org. Synth.* **2008**, *85*, 278–286; b) L. Grehn, U. Ragnarsson, *Angew. Chem. Int. Ed.* **1984**, *23*, 296–301; c) H. N. C. Wong, *Synthesis* **1985**, 1111–1115;

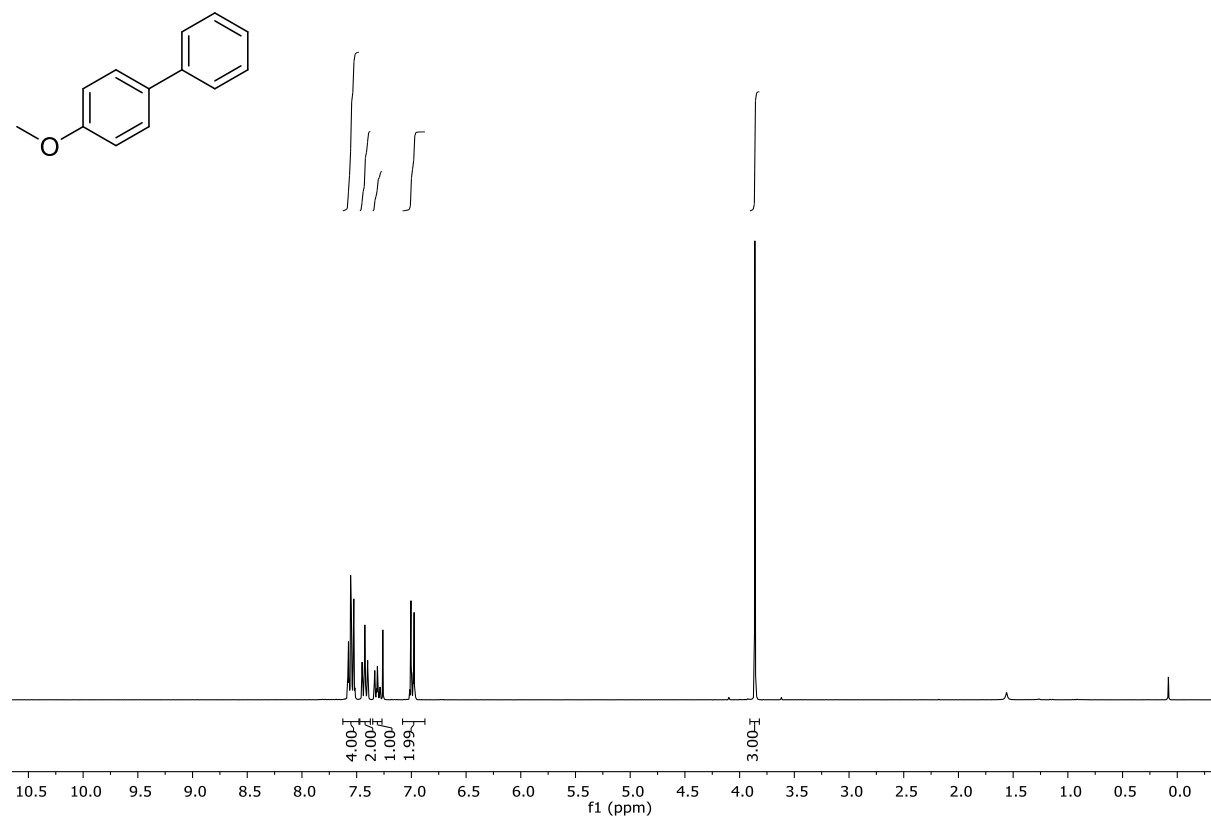
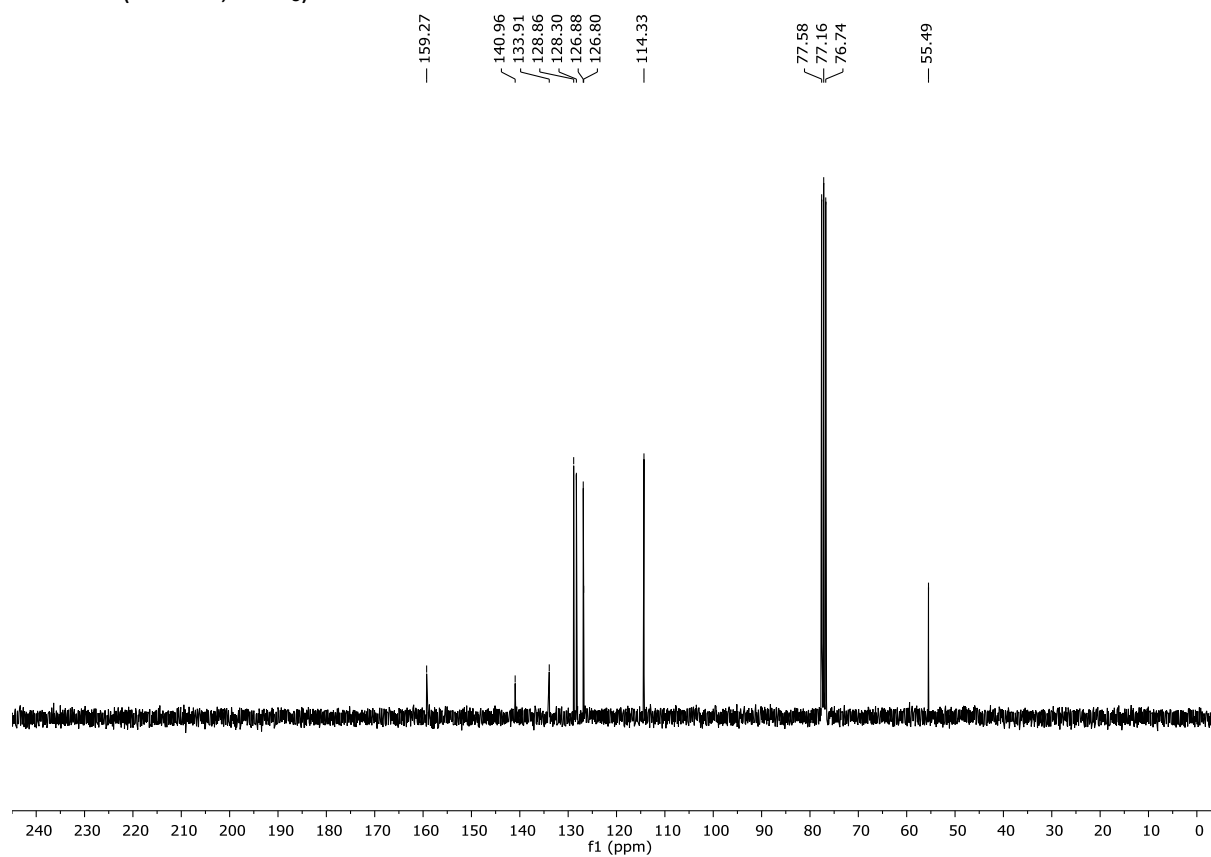
G. Appendix

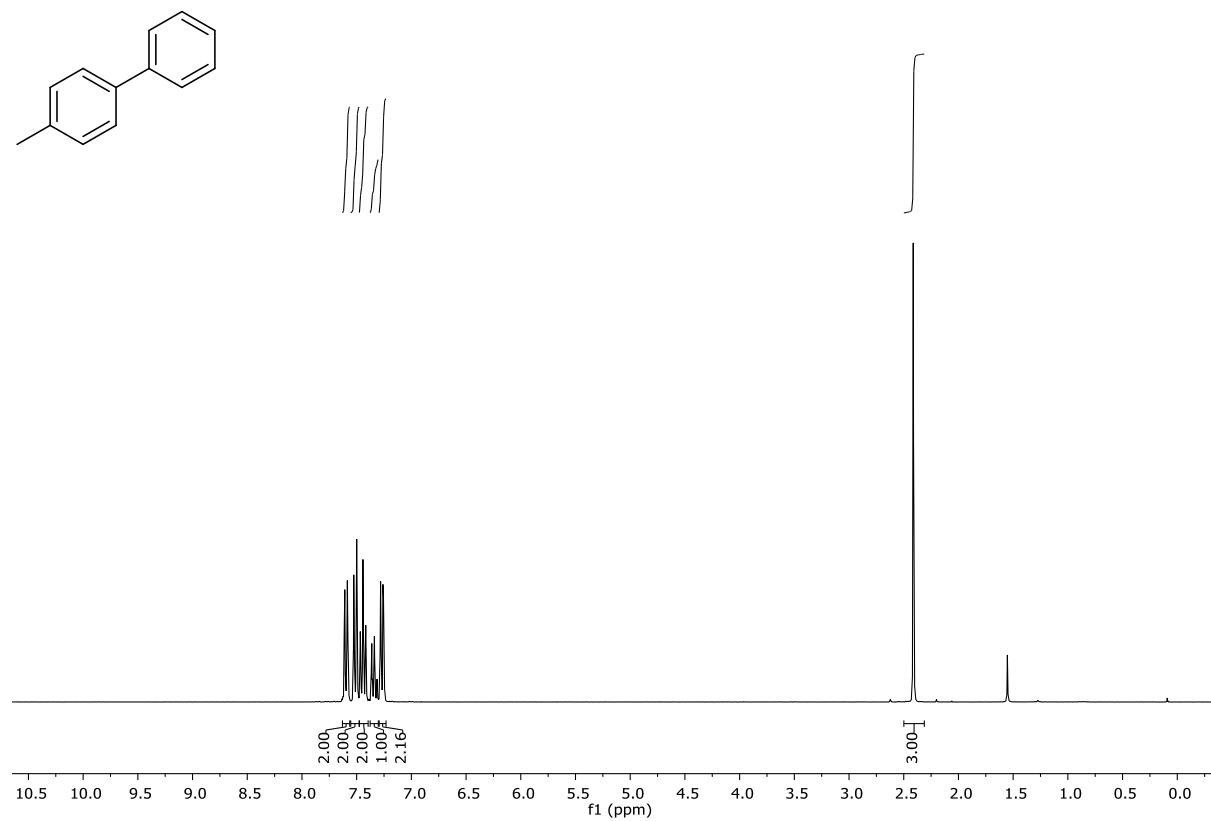
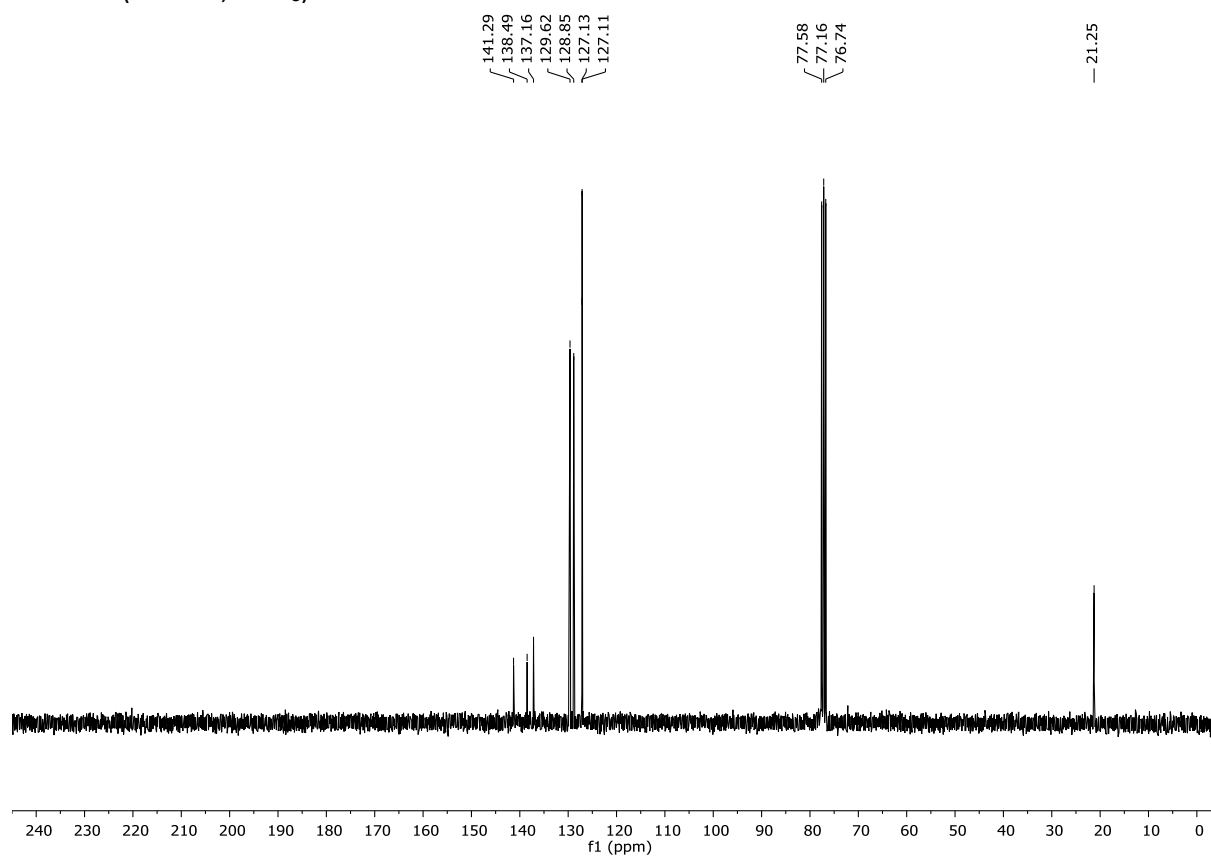
1. NMR spectra

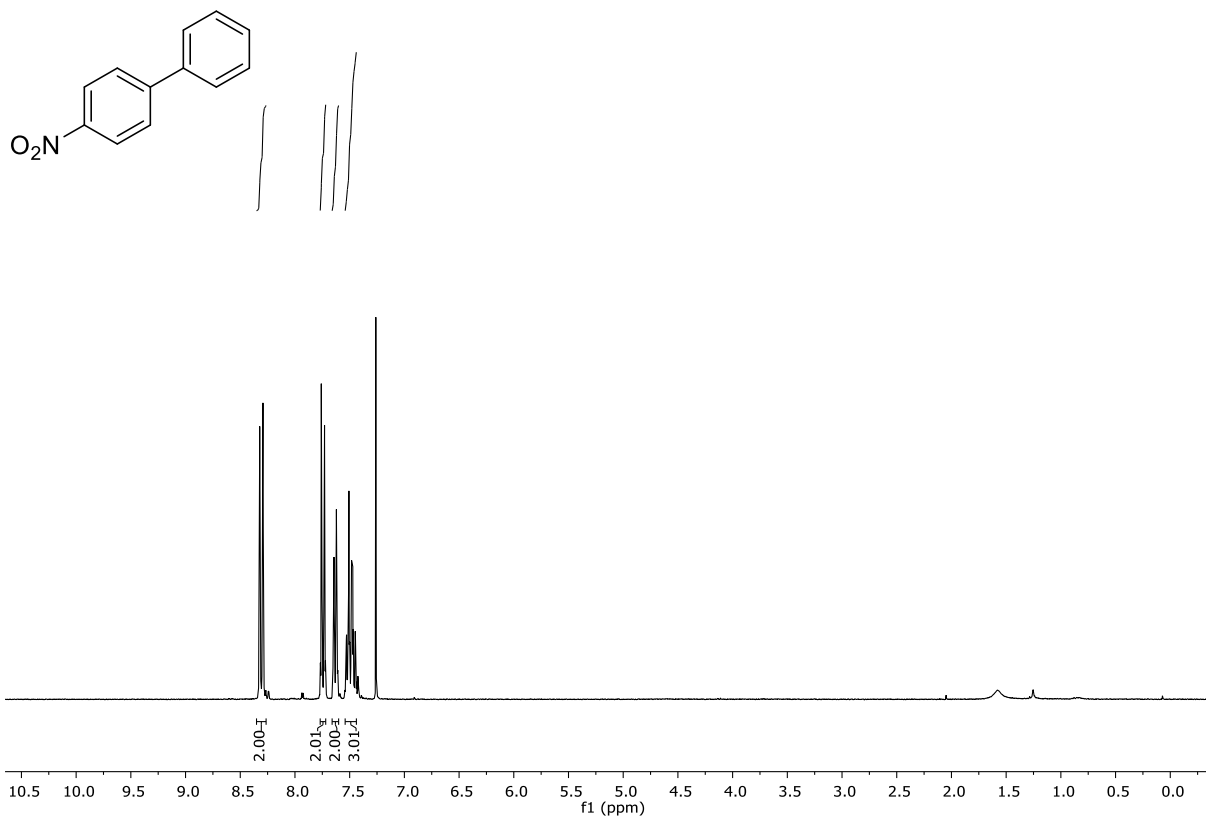
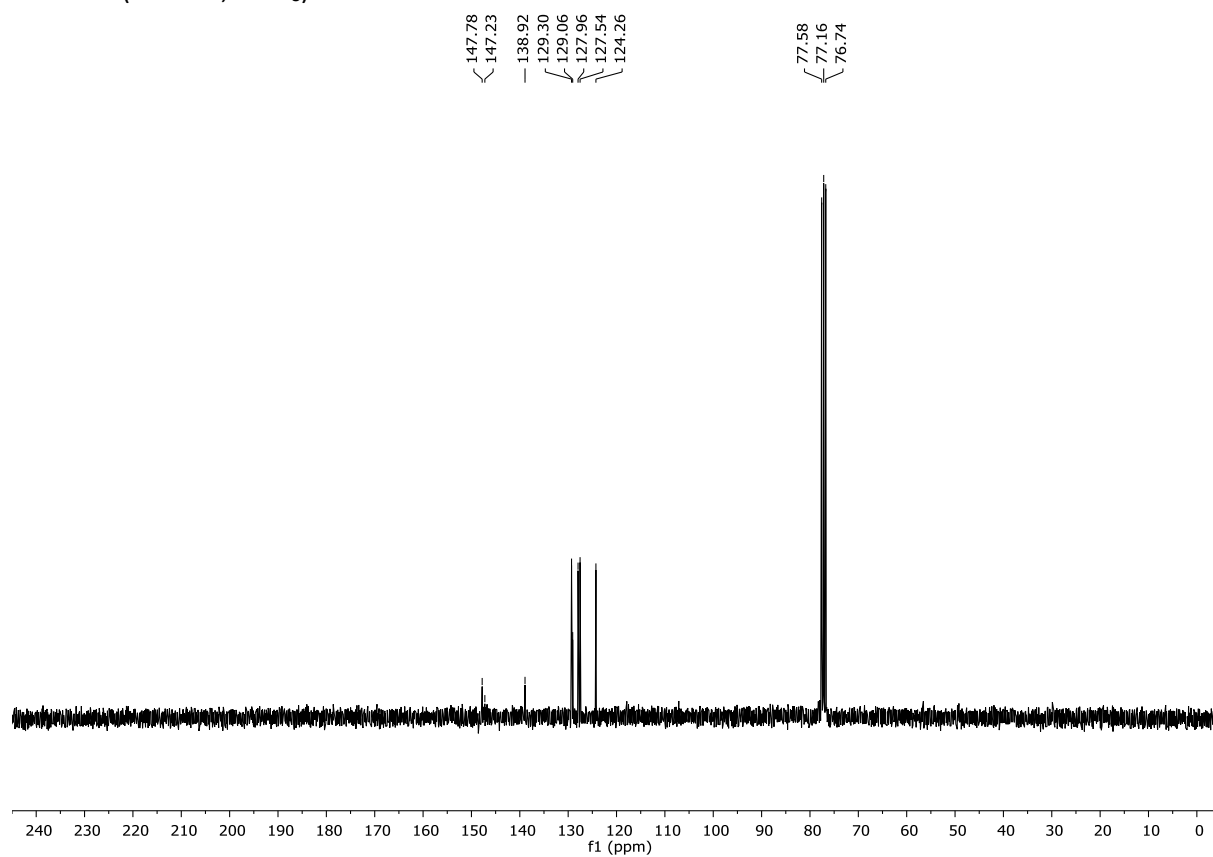
^1H NMR spectra: upper image

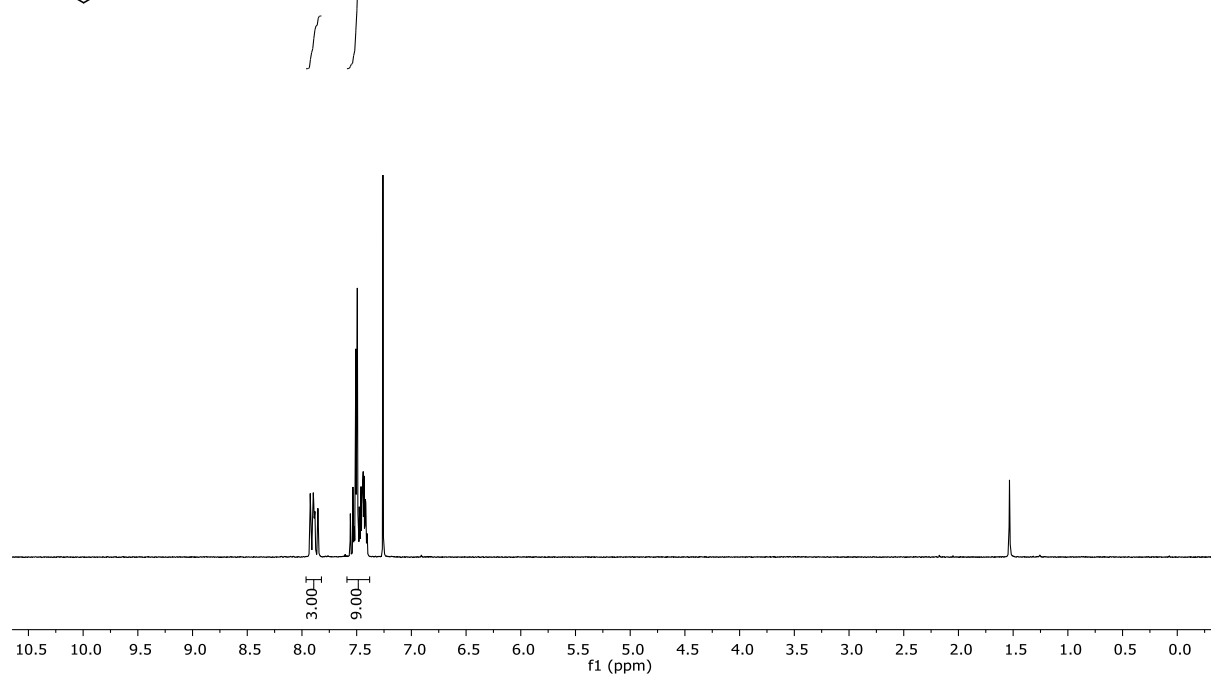
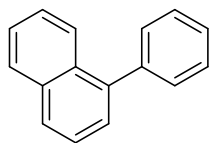
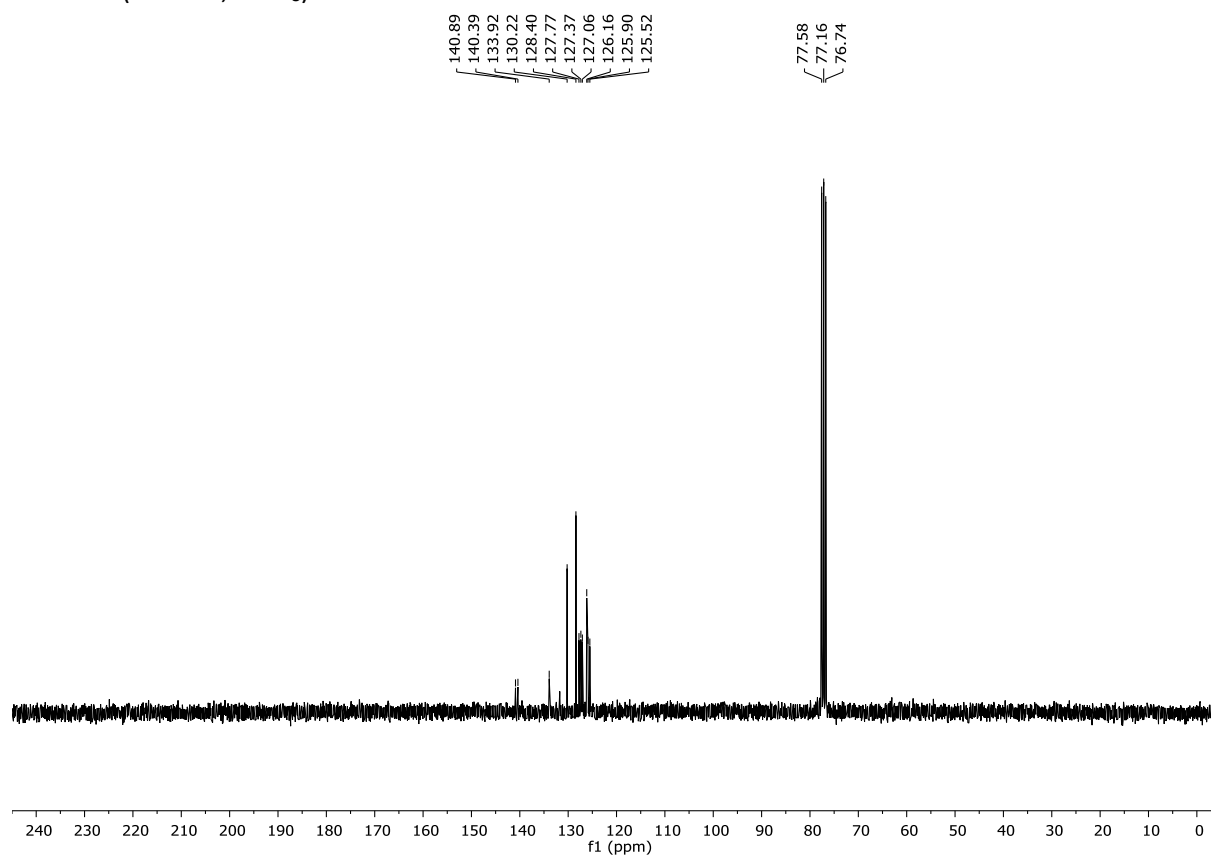
^{13}C NMR spectra: lower image

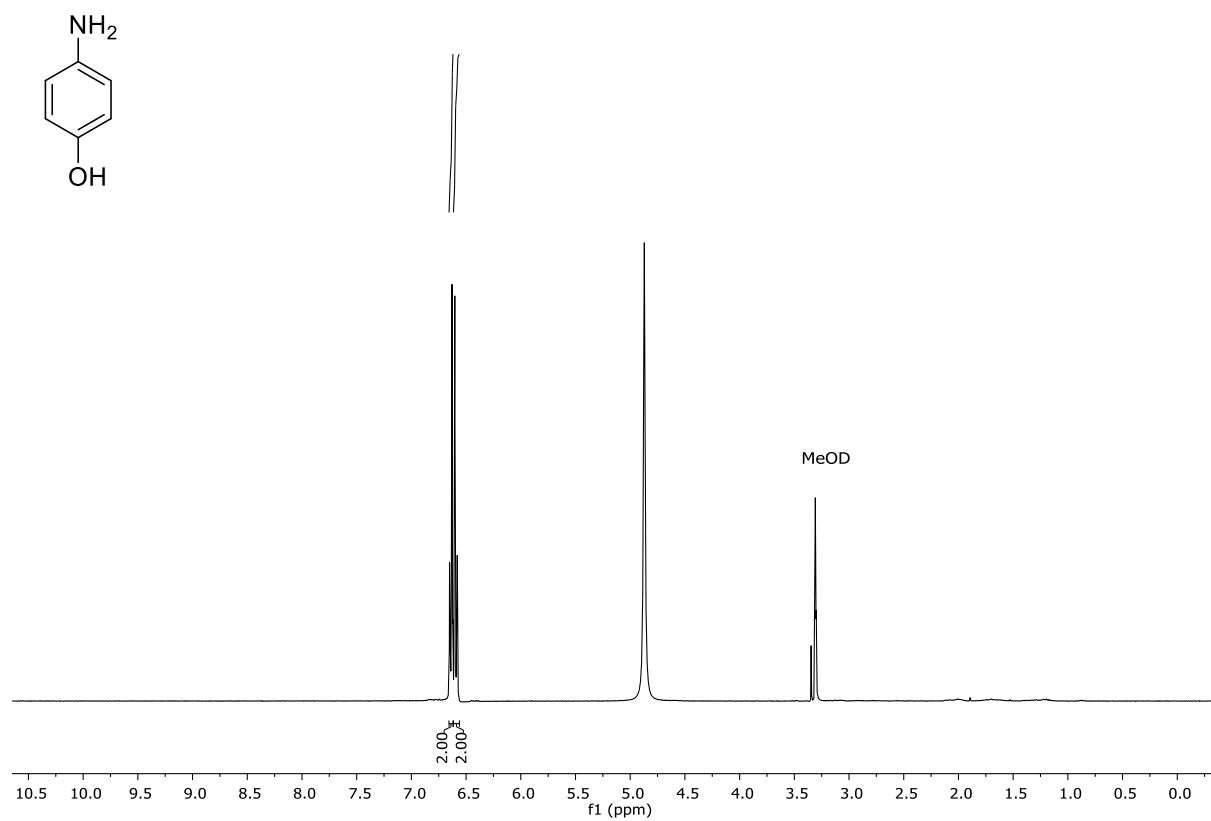
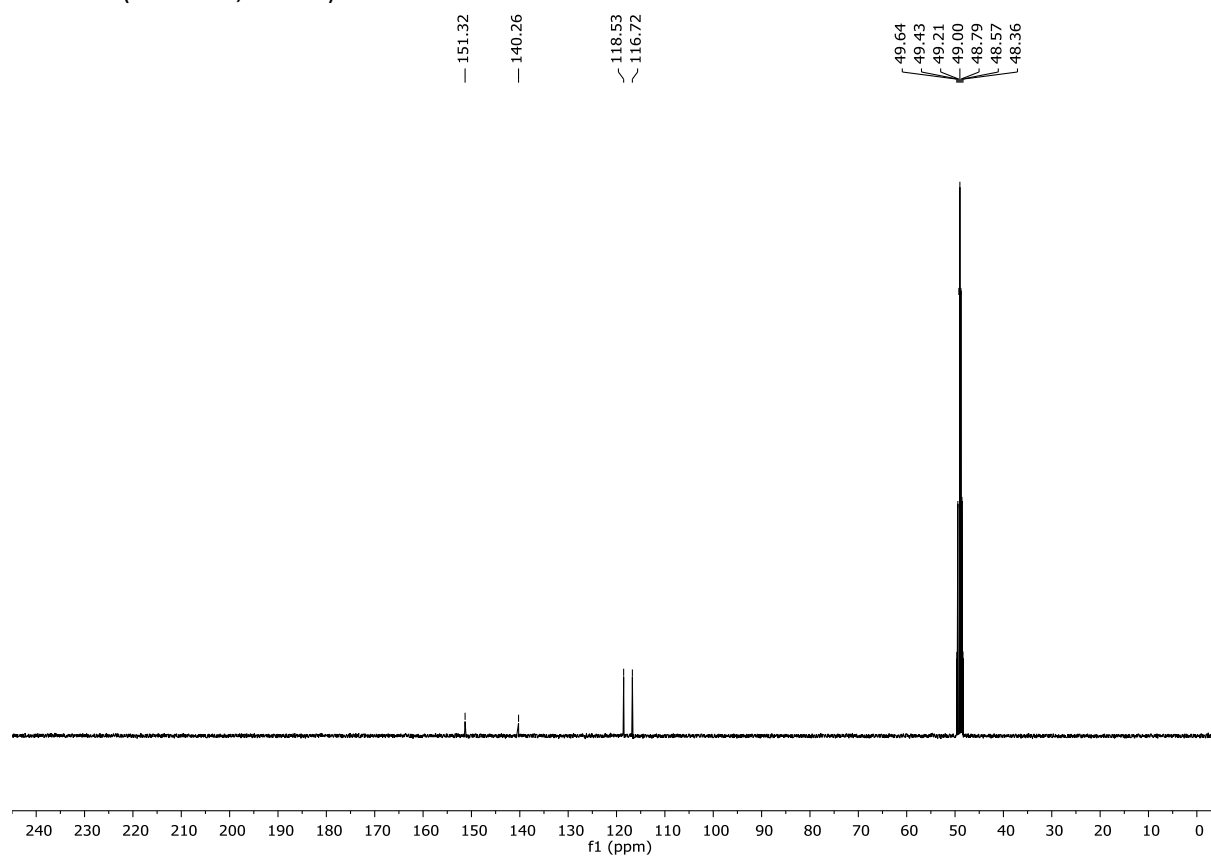
Frequency and solvent are noted at the top of the spectra.

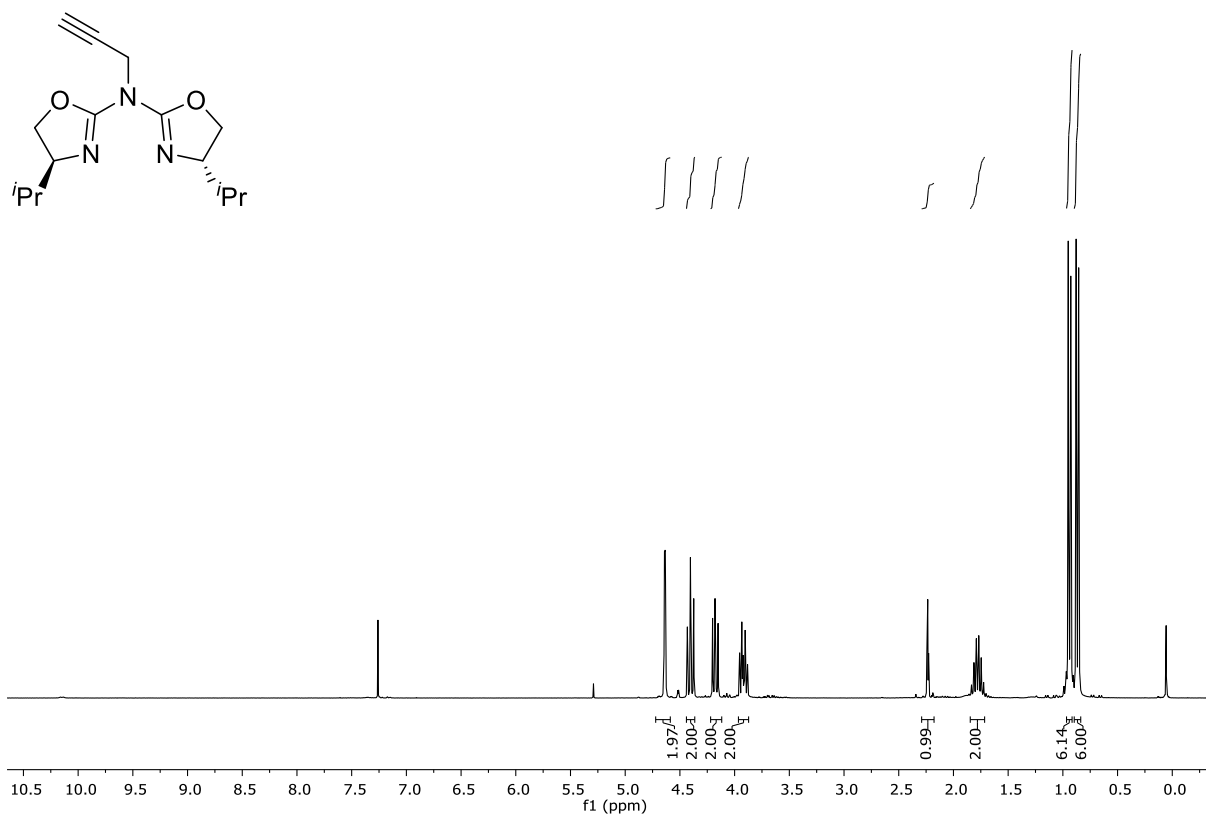
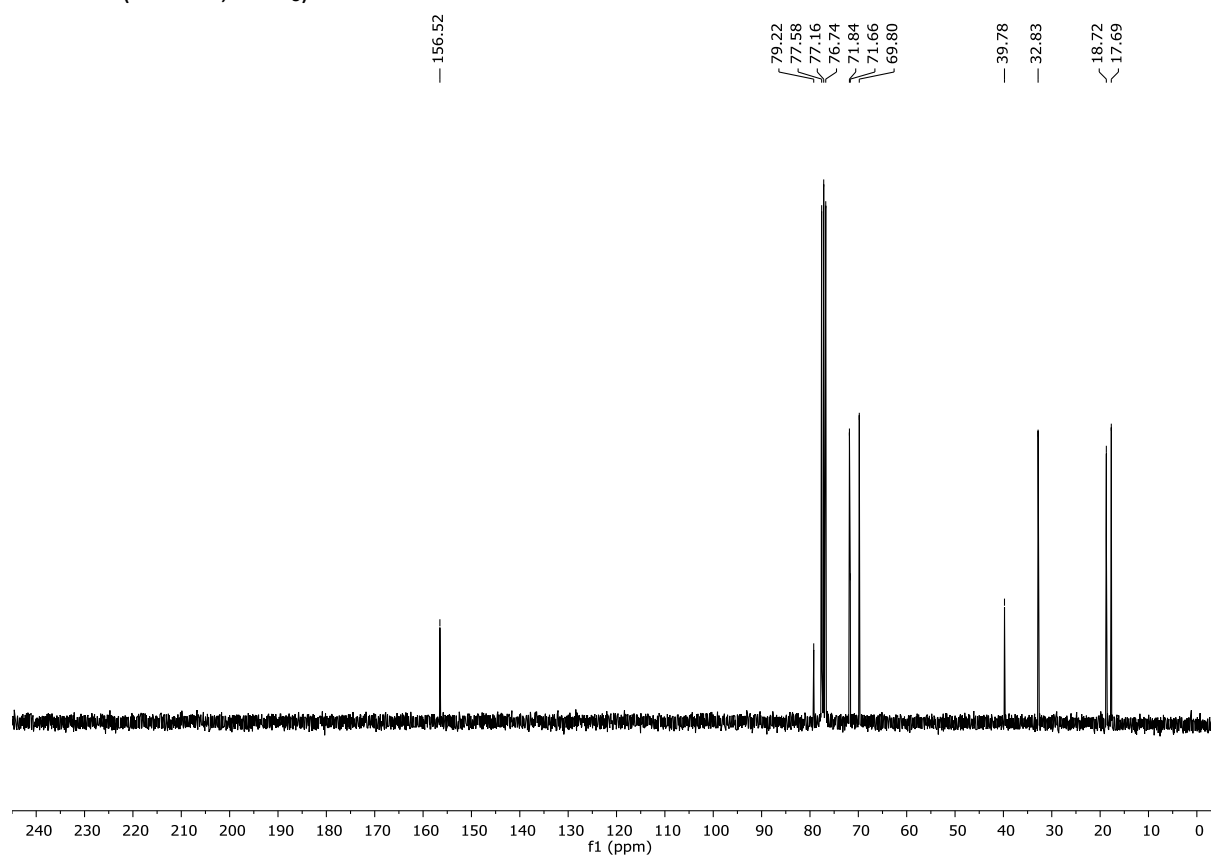
4-Methoxy-1,1'-biphenyl (16) **^1H NMR (300 MHz, CDCl_3)** **^{13}C NMR (75 MHz, CDCl_3)**

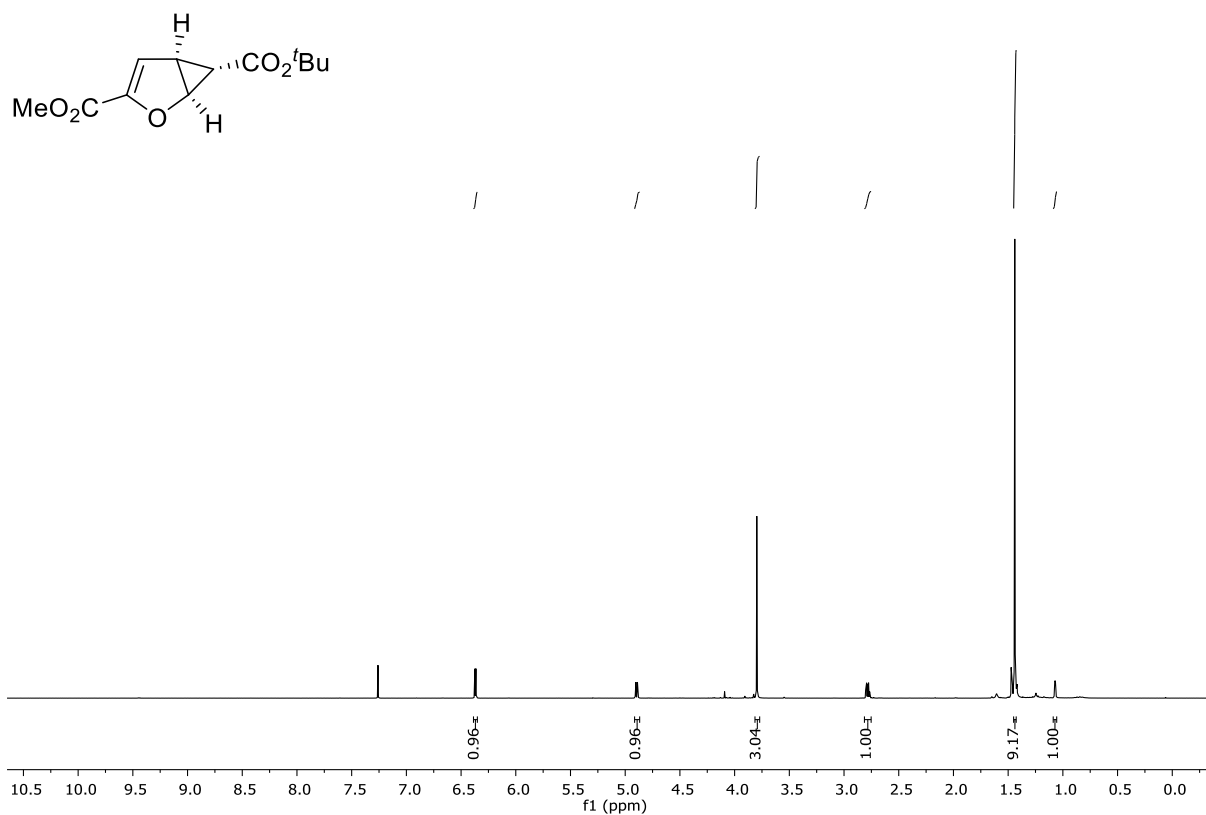
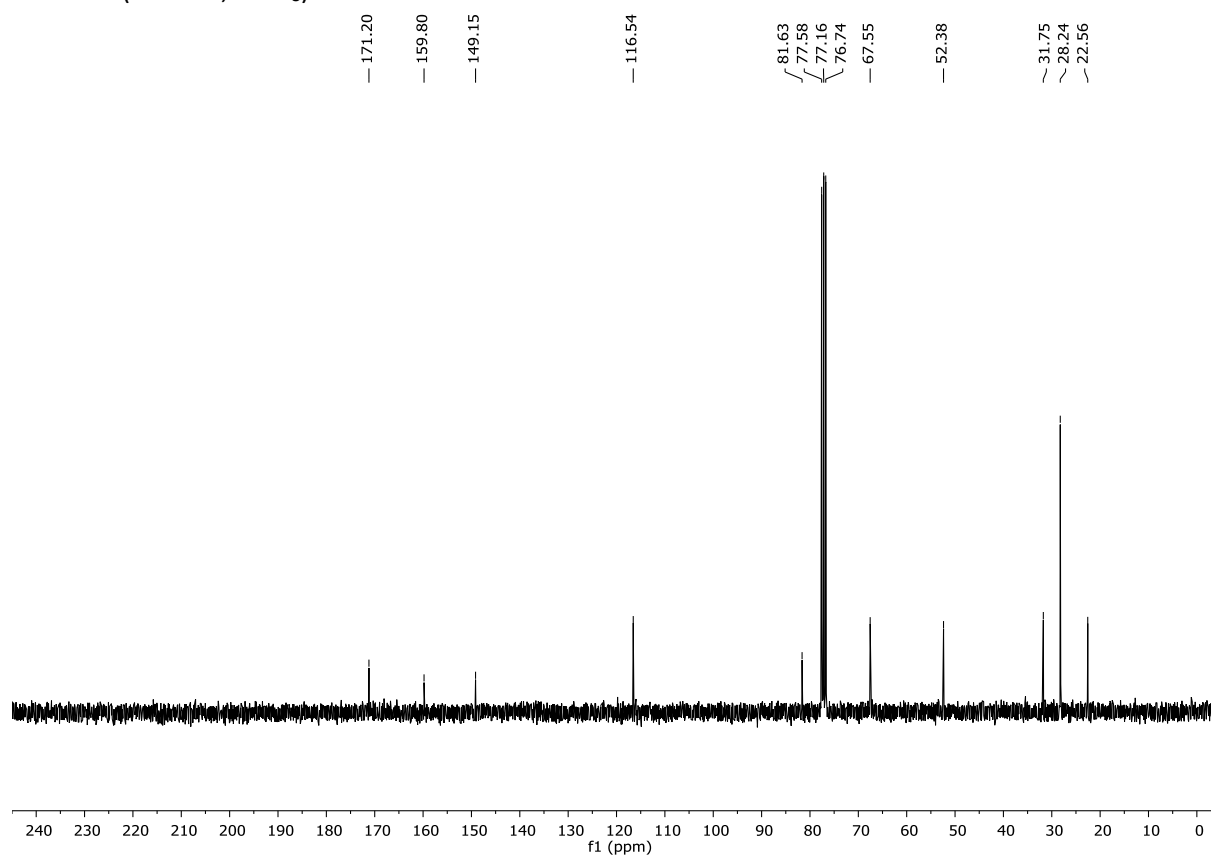
4-Methyl-1,1'-biphenyl (24) $^1\text{H NMR}$ (300 MHz, CDCl_3) $^{13}\text{C NMR}$ (75 MHz, CDCl_3)

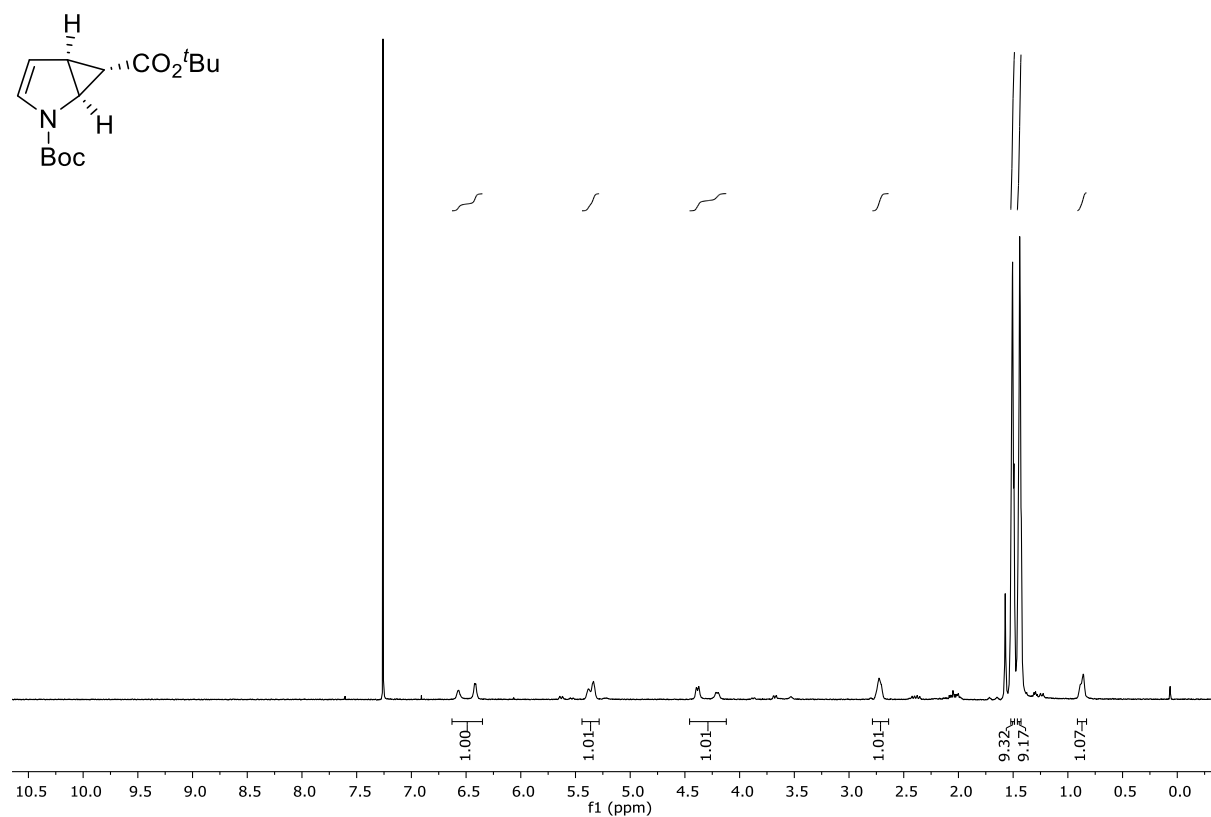
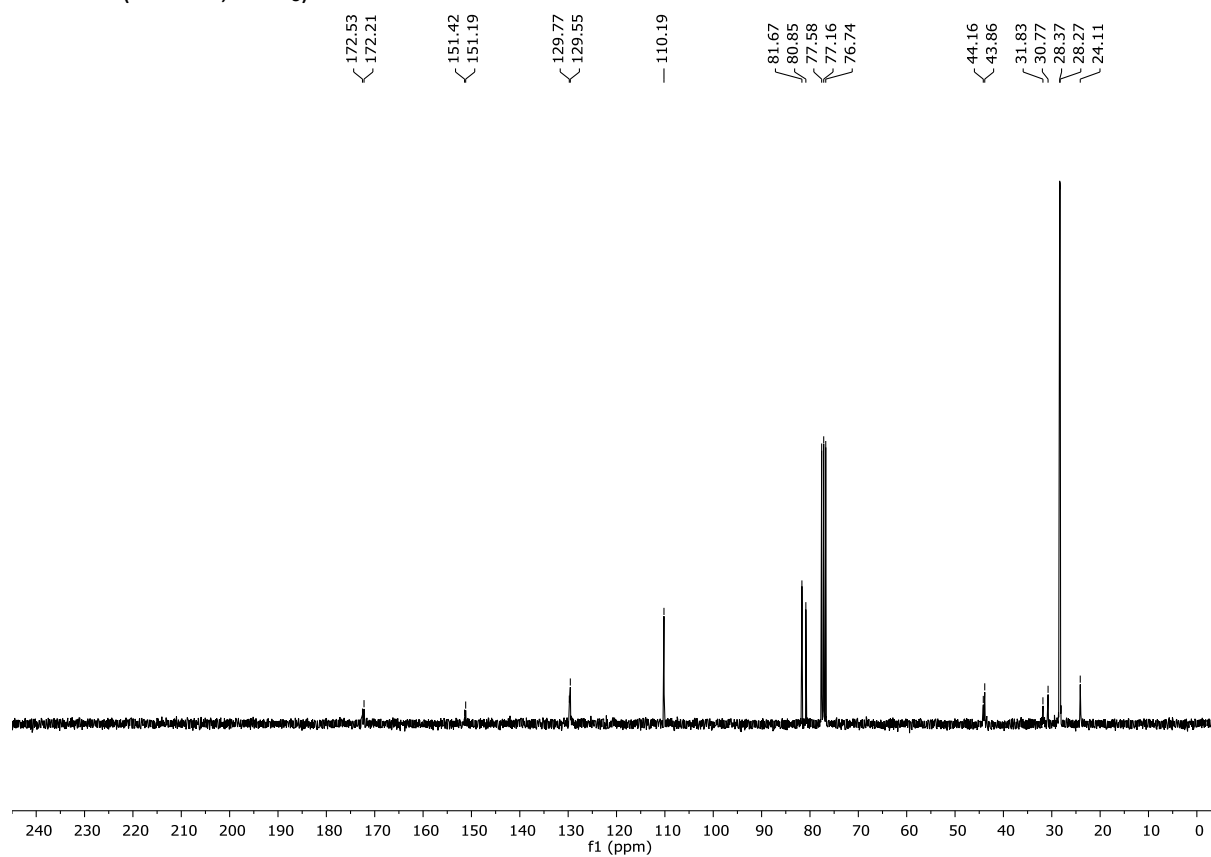
4-Nitro-1,1'-biphenyl (26)**¹H NMR (300 MHz, CDCl₃)****¹³C NMR (75 MHz, CDCl₃)**

1-Phenylnaphthalene (28)**¹H NMR (300 MHz, CDCl₃)****¹³C NMR (75 MHz, CDCl₃)**

4-Aminophenol**¹H NMR (400 MHz, MeOD)****¹³C NMR (101 MHz, MeOD)**

(S,S)-Bis(4-isopropyl-4,5-dihydrooxazol-2-yl)prop-2-ynylamine¹H NMR (300 MHz, CDCl₃)¹³C NMR (75 MHz, CDCl₃)

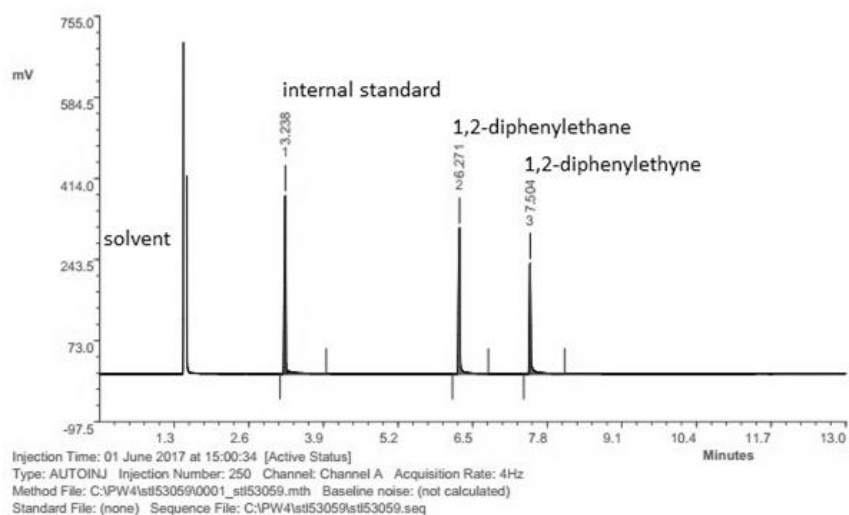
(1*S*,5*S*,6*S*)-(-)-2-Oxabicyclo[3.1.0]hex-3-ene-3,6-dicarboxylic 6-*tert*-butyl ester 3-methyl ester (66)¹H NMR (300 MHz, CDCl₃)¹³C NMR (75 MHz, CDCl₃)

(1*S*,5*S*,6*S*)-Di-*tert*-butyl-2-azabicyclo[3.1.0]hex-3-ene-2,6-dicarboxylate (67)¹H NMR (300 MHz, CDCl₃)¹³C NMR (75 MHz, CDCl₃)

2. GC chromatograms

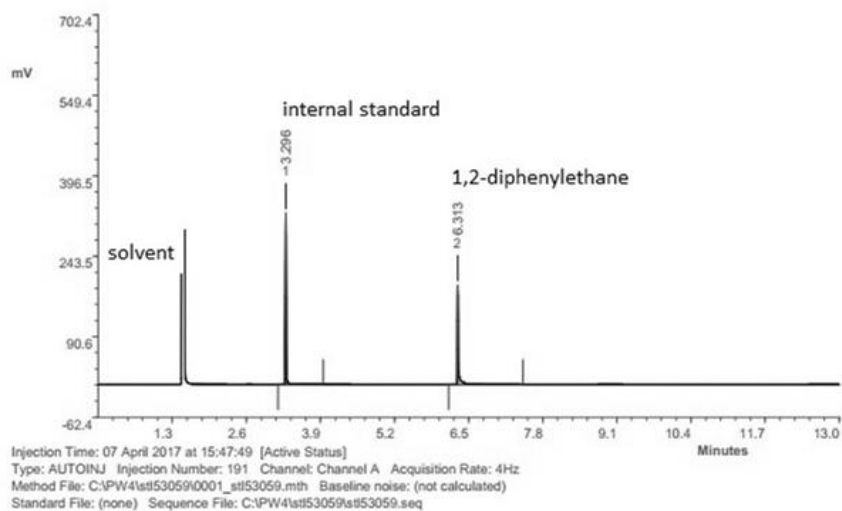
1,2-Diphenylethane (7)

Calibration with dodecane as internal standard, starting material, and product.



| Peak | RT | Area | %Ar | Conc. (Ar) | Height | M | Units | Name |
|------|-------|---------|-------|----------------|---------|---|-------|------|
| 1 | 3.238 | 614.018 | 39.41 | Not Calculated | 374.631 | 1 | | |
| 2 | 6.271 | 544.397 | 34.94 | Not Calculated | 306.147 | 1 | | |
| 3 | 7.504 | 399.744 | 25.65 | Not Calculated | 231.672 | 1 | | |

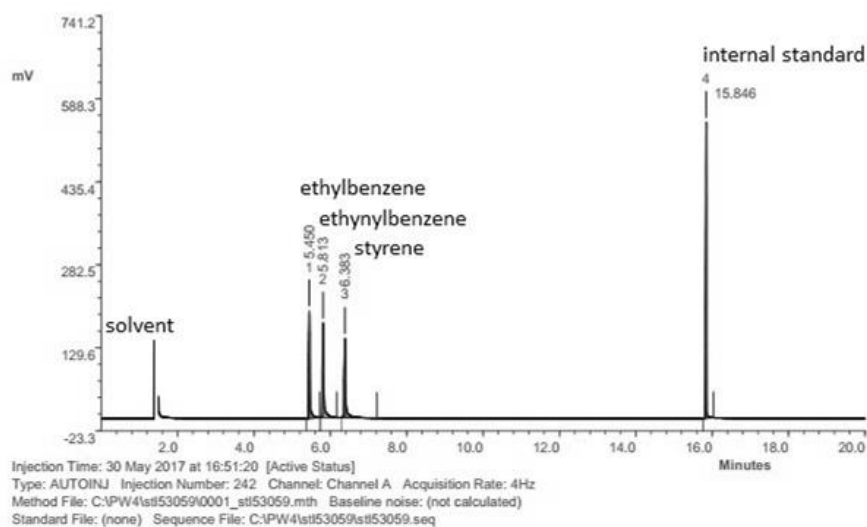
Measurement of reaction sample with dodecane as internal standard.



| Peak | RT | Area | %Ar | Conc. (Ar) | Height | M | Units | Name |
|------|-------|---------|-------|----------------|---------|---|-------|------|
| 1 | 3.296 | 466.428 | 59.42 | Not Calculated | 324.874 | 1 | | |
| 2 | 6.313 | 318.540 | 40.58 | Not Calculated | 188.196 | 1 | | |

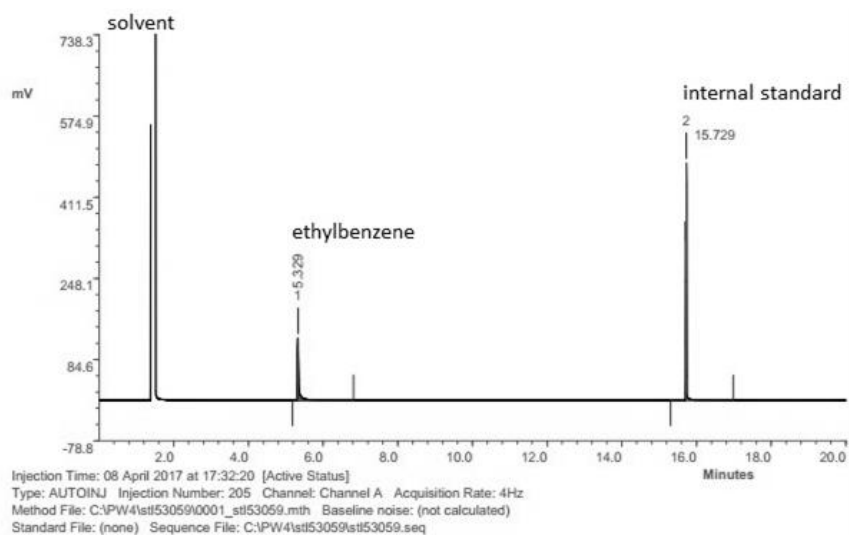
Ethylbenzene (with ethynylbenzene as starting material)

Calibration with dodecane as internal standard, starting material, and product.



| Peak | RT | Area | %Ar | Conc. (Ar) | Height | M | Units Name |
|------|--------|---------|-------|----------------|---------|---|------------|
| 1 | 5.450 | 502.018 | 21.87 | Not Calculated | 198.090 | 1 | |
| 2 | 5.813 | 451.838 | 19.68 | Not Calculated | 174.061 | 1 | |
| 3 | 6.383 | 434.199 | 18.92 | Not Calculated | 146.180 | 1 | |
| 4 | 15.846 | 907.377 | 39.53 | Not Calculated | 545.216 | 1 | |

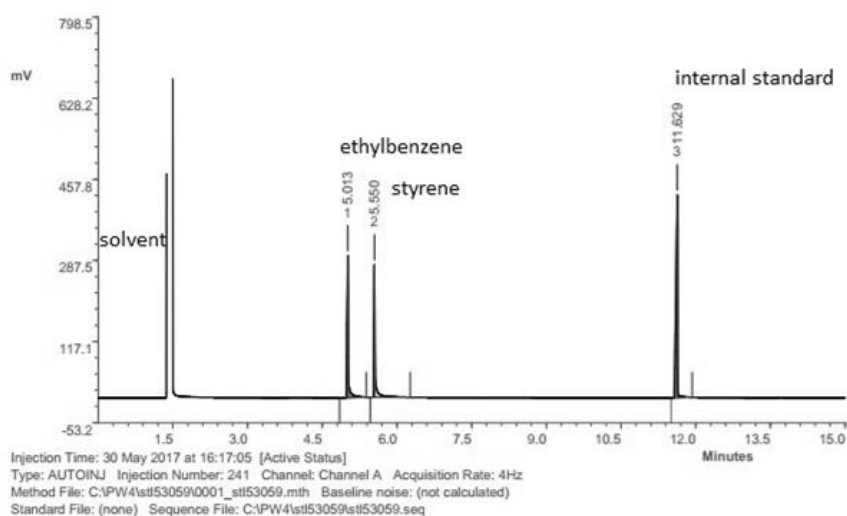
Measurement of reaction sample with dodecane as internal standard.



| Peak | RT | Area | %Ar | Conc. (Ar) | Height | M | Units Name |
|------|--------|---------|-------|----------------|---------|---|------------|
| 1 | 5.329 | 357.819 | 33.01 | Not Calculated | 124.955 | 1 | |
| 2 | 15.729 | 726.224 | 66.99 | Not Calculated | 476.988 | 1 | |

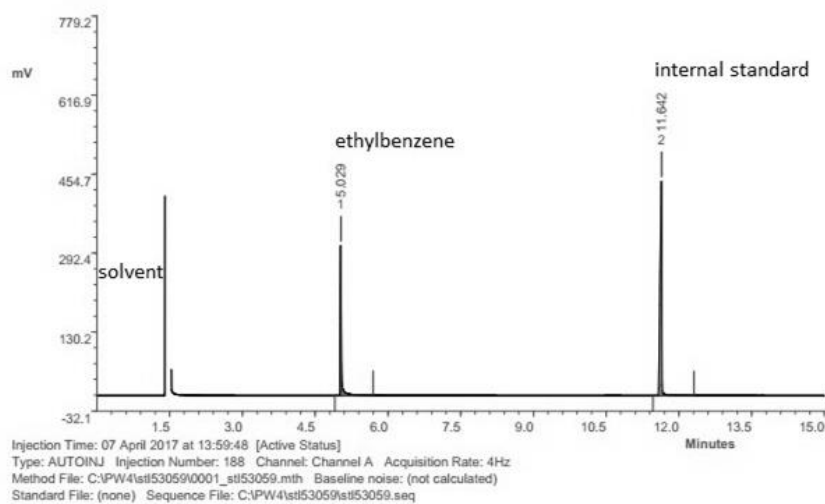
Ethylbenzene (with styrene as starting material)

Calibration with dodecane as internal standard, starting material, and product.



| Peak | RT | Area | %Ar | Conc. (Ar) | Height | M | Units | Name |
|------|--------|----------|-------|----------------|---------|---|-------|------|
| 1 | 5.013 | 536.709 | 26.07 | Not Calculated | 297.414 | 1 | | |
| 2 | 5.550 | 510.808 | 24.81 | Not Calculated | 278.130 | 1 | | |
| 3 | 11.629 | 1011.439 | 49.12 | Not Calculated | 425.388 | 1 | | |

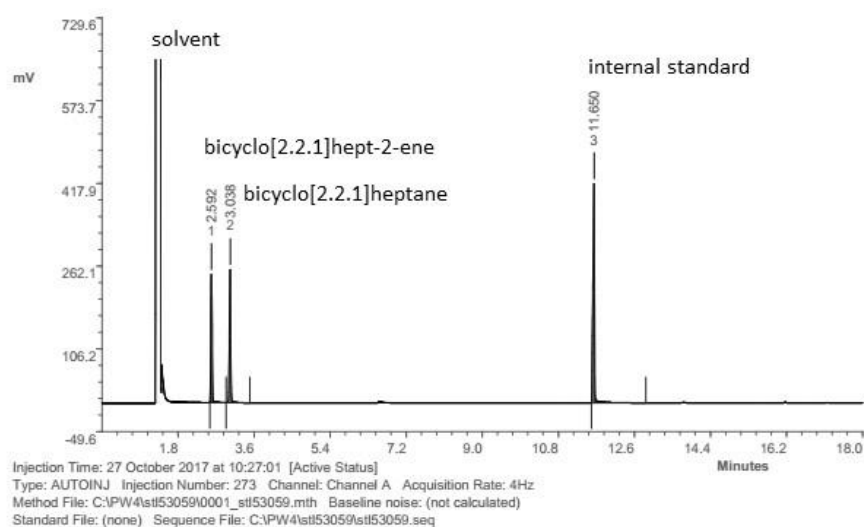
Measurement of reaction sample with dodecane as internal standard.



| Peak | RT | Area | %Ar | Conc. (Ar) | Height | M | Units | Name |
|------|--------|----------|-------|----------------|---------|---|-------|------|
| 1 | 5.029 | 558.646 | 34.04 | Not Calculated | 307.320 | 1 | | |
| 2 | 11.642 | 1082.368 | 65.96 | Not Calculated | 439.706 | 1 | | |

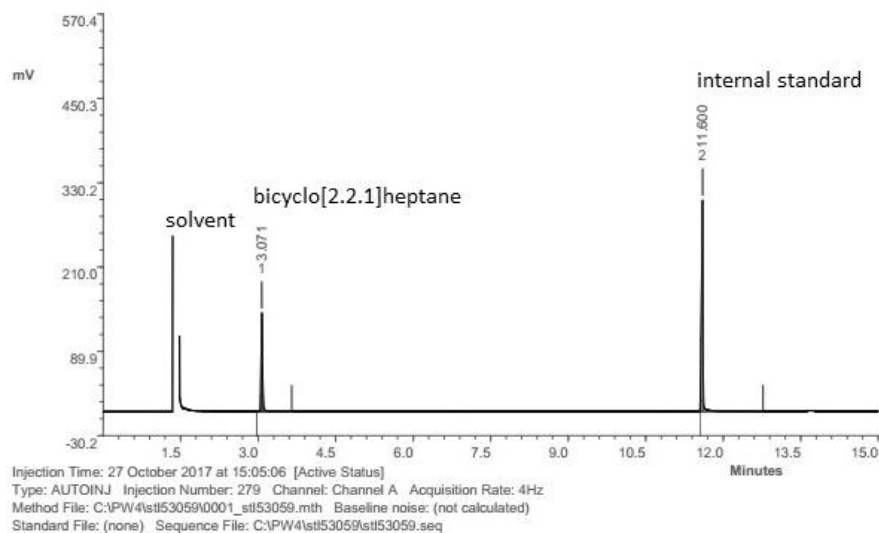
Bicyclo[2.2.1]heptane

Calibration with dodecane as internal standard, starting material, and product.



| Peak | RT | Area | %Ar | Conc. (Ar) | Height | M | Units | Name |
|------|--------|----------|-------|----------------|---------|---|-------|------|
| 1 | 2.592 | 472.816 | 23.44 | Not Calculated | 241.242 | 0 | | |
| 2 | 3.038 | 524.395 | 25.99 | Not Calculated | 250.771 | 0 | | |
| 3 | 11.650 | 1020.333 | 50.57 | Not Calculated | 412.645 | 0 | | |

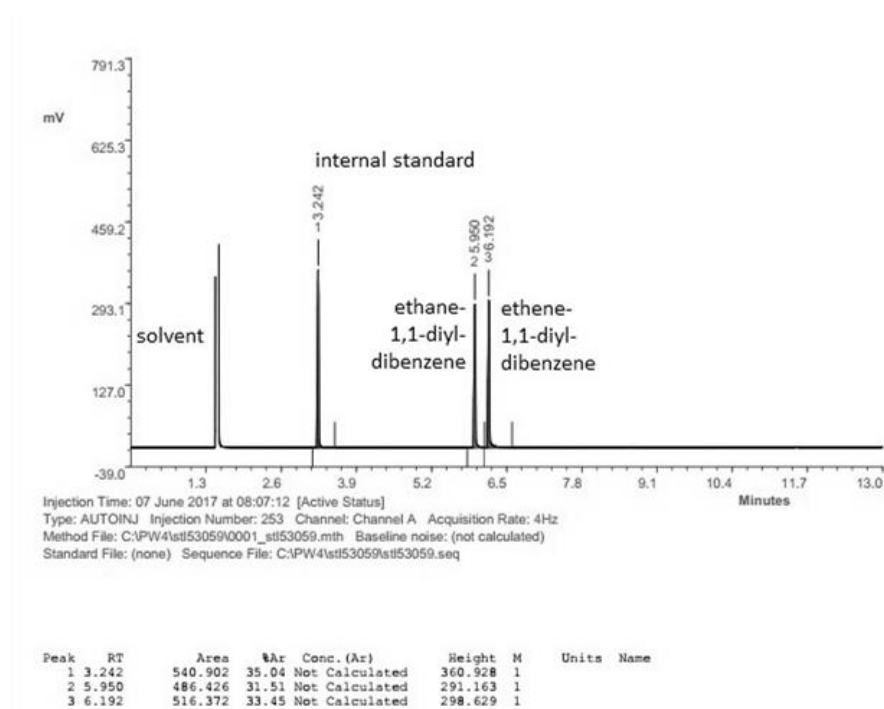
Measurement of reaction sample with dodecane as internal standard.



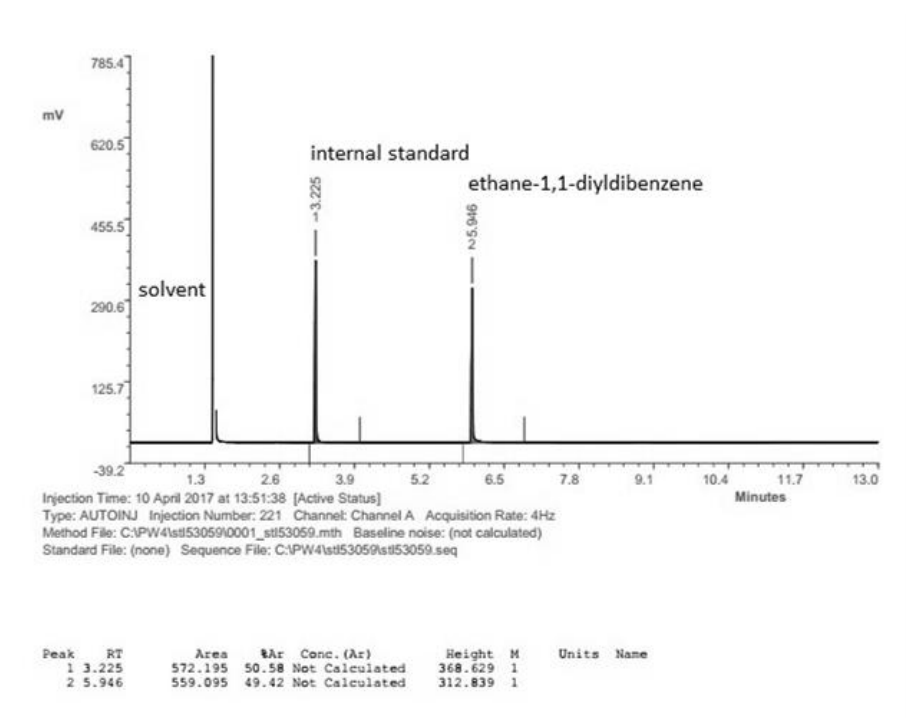
| Peak | RT | Area | %Ar | Conc. (Ar) | Height | M | Units | Name |
|------|--------|---------|-------|----------------|---------|---|-------|------|
| 1 | 3.071 | 265.237 | 30.04 | Not Calculated | 140.138 | 0 | | |
| 2 | 11.600 | 617.808 | 69.96 | Not Calculated | 300.747 | 0 | | |

Ethane-1,1-diyl-dibenzene

Calibration with dodecane as internal standard, starting material, and product.

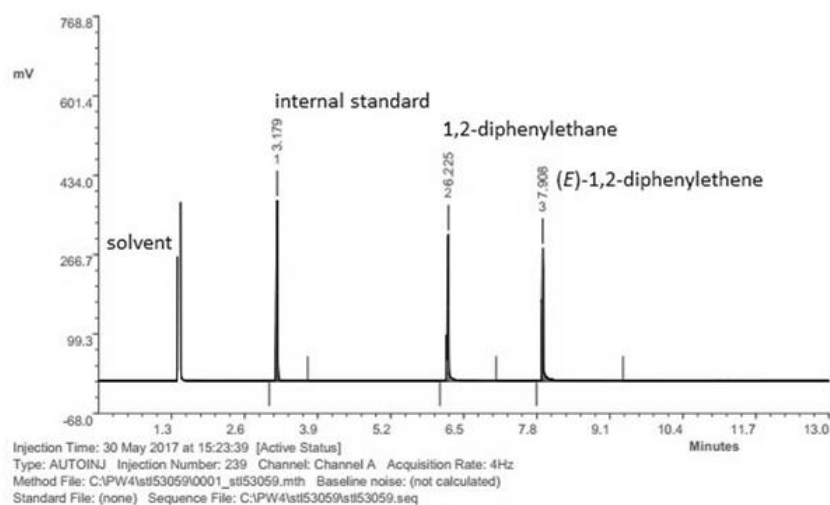


Measurement of reaction sample with dodecane as internal standard.



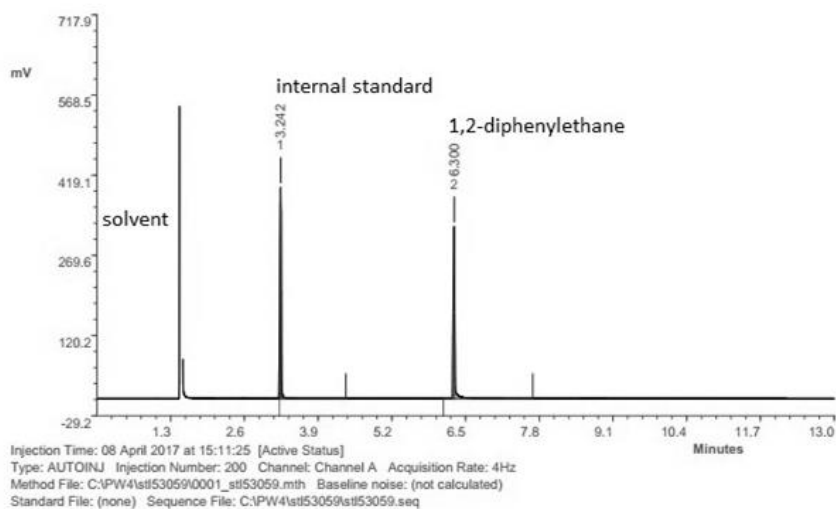
1,2-Diphenylethane (7)

Calibration with dodecane as internal standard, starting material, and product.



| Peak | RT | Area | SAr | Conc. (Ar) | Height | M | Units | Name |
|------|-------|---------|-------|----------------|---------|---|-------|------|
| 1 | 3.179 | 587.243 | 35.17 | Not Calculated | 380.476 | 1 | | |
| 2 | 6.225 | 553.193 | 33.13 | Not Calculated | 308.164 | 1 | | |
| 3 | 7.908 | 529.288 | 31.70 | Not Calculated | 279.721 | 1 | | |

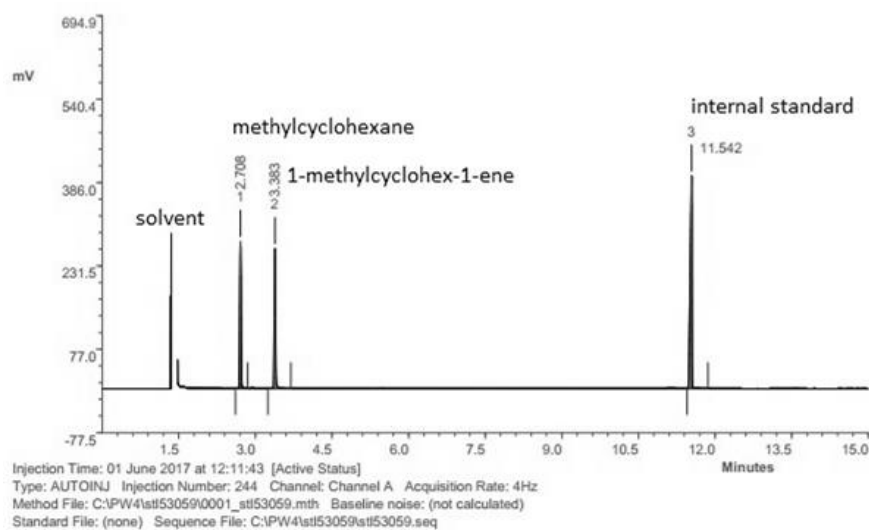
Measurement of reaction sample with dodecane as internal standard.



| Peak | RT | Area | SAr | Conc. (Ar) | Height | M | Units | Name |
|------|-------|---------|-------|----------------|---------|---|-------|------|
| 1 | 3.242 | 598.870 | 49.90 | Not Calculated | 393.246 | 0 | | |
| 2 | 6.300 | 601.357 | 50.10 | Not Calculated | 320.017 | 1 | | |

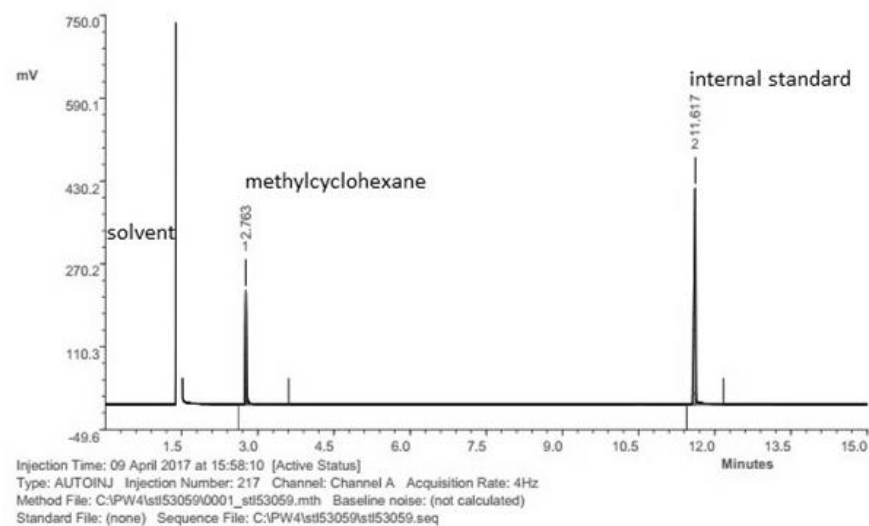
Methylcyclohexane

Calibration with dodecane as internal standard, starting material, and product.



| Peak | RT | Area | %Ar | Conc. (Ar) | Height | M | Units | Name |
|------|--------|---------|-------|----------------|---------|---|-------|------|
| 1 | 2.708 | 448.347 | 24.65 | Not Calculated | 272.506 | 1 | | |
| 2 | 3.383 | 446.984 | 24.58 | Not Calculated | 259.028 | 1 | | |
| 3 | 11.542 | 923.184 | 50.77 | Not Calculated | 393.809 | 1 | | |

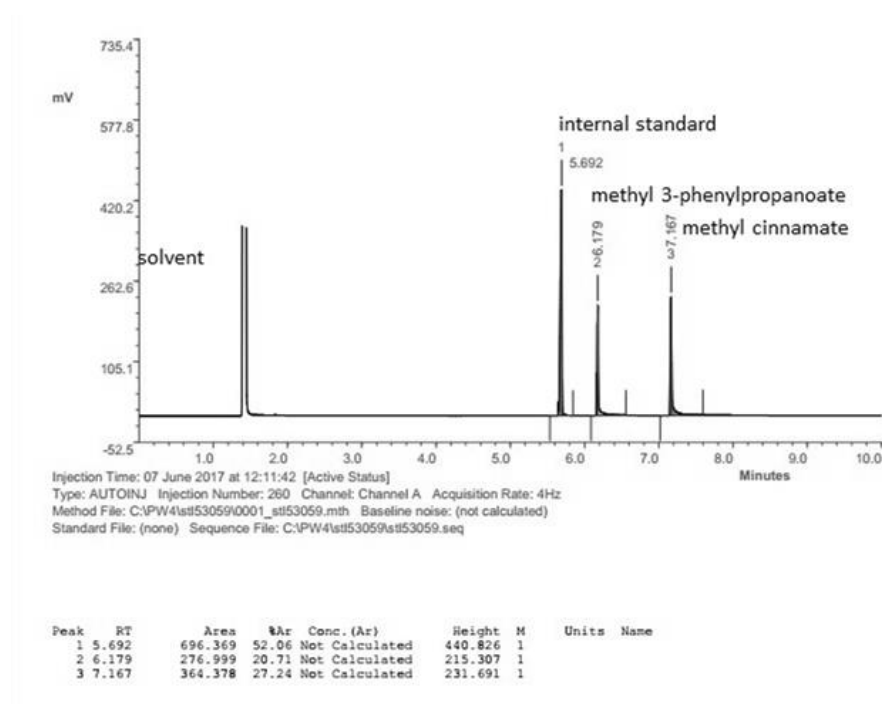
Measurement of reaction sample with dodecane as internal standard.



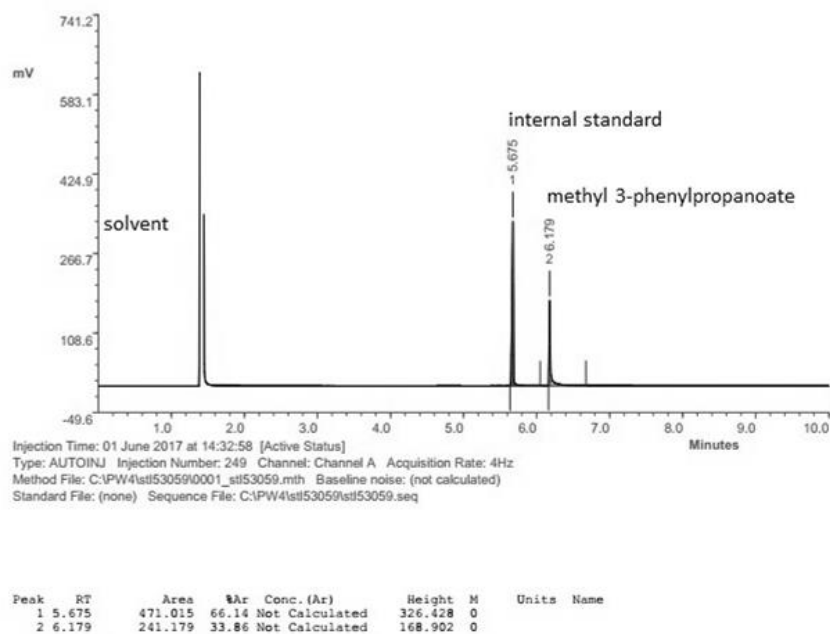
| Peak | RT | Area | %Ar | Conc. (Ar) | Height | M | Units | Name |
|------|--------|---------|-------|----------------|---------|---|-------|------|
| 1 | 2.763 | 377.109 | 27.73 | Not Calculated | 219.384 | 1 | | |
| 2 | 11.617 | 982.823 | 72.27 | Not Calculated | 416.475 | 1 | | |

Methyl 3-phenylpropanoate

Calibration with dodecane as internal standard, starting material, and product.

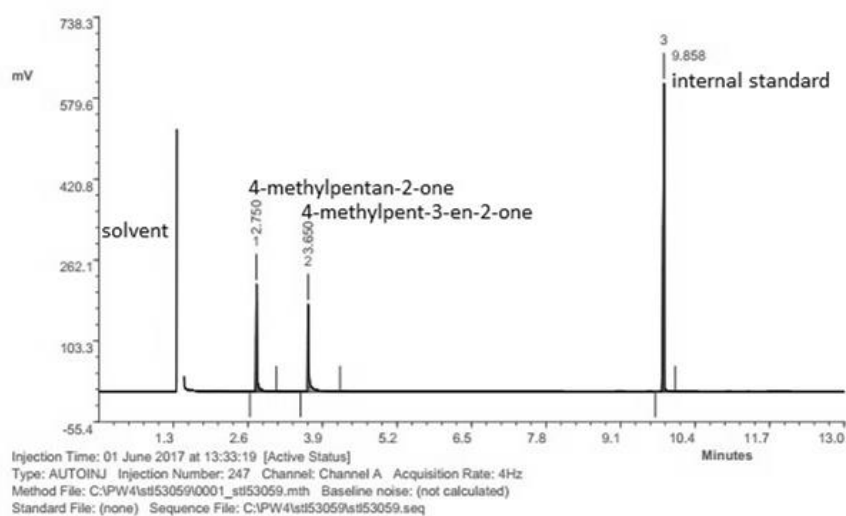


Measurement of reaction sample with dodecane as internal standard.



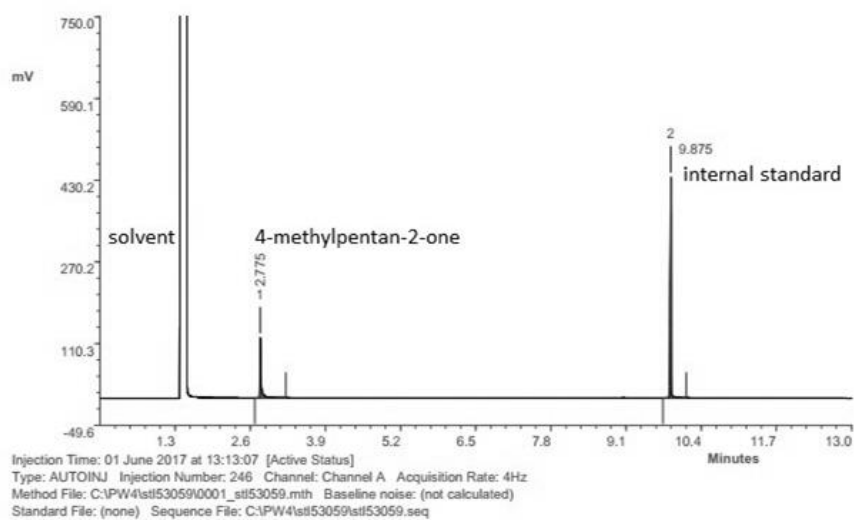
4-Methylpentan-2-one

Calibration with dodecane as internal standard, starting material, and product.



| Peak | RT | Area | %Ar | Conc. (Ar) | Height | M | Units | Name |
|------|-------|---------|-------|----------------|---------|---|-------|------|
| 1 | 2.750 | 307.871 | 20.17 | Not Calculated | 210.411 | 1 | | |
| 2 | 3.650 | 284.350 | 18.63 | Not Calculated | 170.986 | 1 | | |
| 3 | 9.858 | 934.303 | 61.20 | Not Calculated | 604.722 | 1 | | |

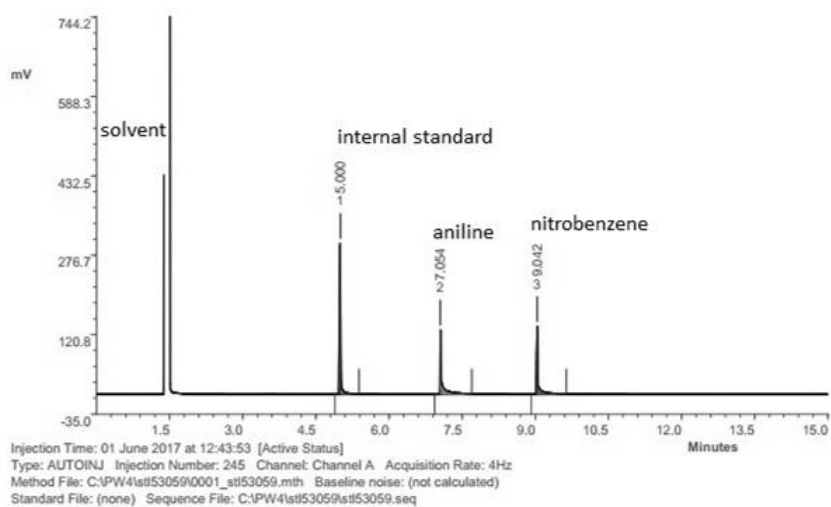
Measurement of reaction sample with dodecane as internal standard.



| Peak | RT | Area | %Ar | Conc. (Ar) | Height | M | Units | Name |
|------|-------|---------|-------|----------------|---------|---|-------|------|
| 1 | 2.775 | 182.584 | 24.88 | Not Calculated | 117.833 | 1 | | |
| 2 | 9.875 | 551.364 | 75.12 | Not Calculated | 432.648 | 1 | | |

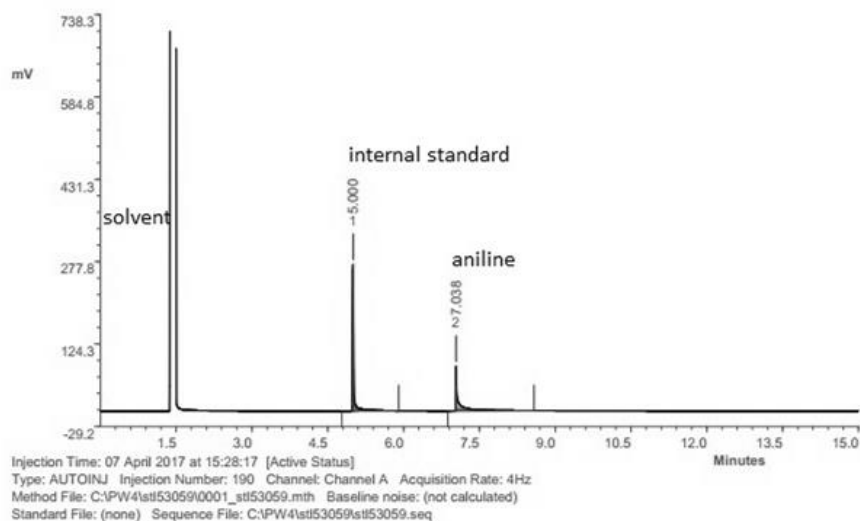
Aniline

Calibration with ethylbenzene as internal standard, starting material, and product.



| Peak | RT | Area | %Ar | Conc. (Ar) | Height | M | Units | Name |
|------|-------|---------|-------|----------------|---------|---|-------|------|
| 1 | 5.000 | 530.401 | 45.31 | Not Calculated | 296.475 | 1 | | |
| 2 | 7.054 | 316.316 | 27.02 | Not Calculated | 126.138 | 1 | | |
| 3 | 9.042 | 323.868 | 27.67 | Not Calculated | 132.938 | 1 | | |

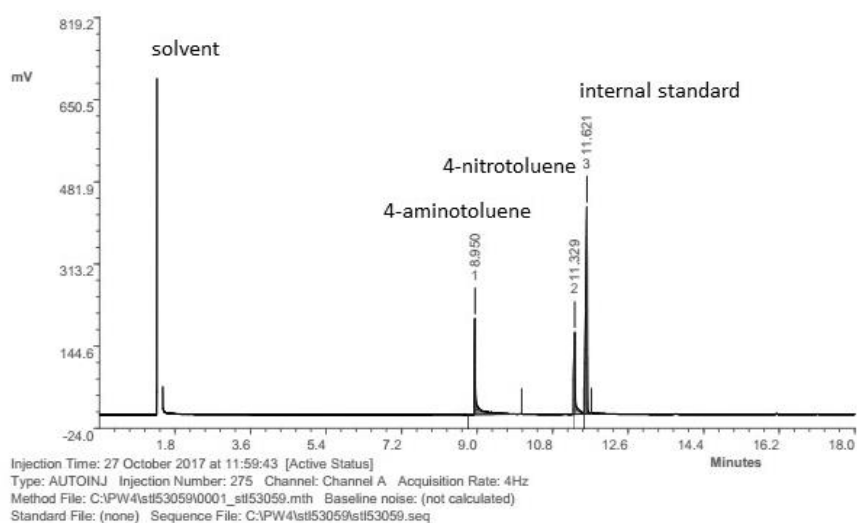
Measurement of reaction sample with ethylbenzene as internal standard.



| Peak | RT | Area | %Ar | Conc. (Ar) | Height | M | Units | Name |
|------|-------|---------|-------|----------------|---------|---|-------|------|
| 1 | 5.000 | 492.750 | 63.57 | Not Calculated | 272.683 | 1 | | |
| 2 | 7.038 | 282.335 | 36.43 | Not Calculated | 82.843 | 1 | | |

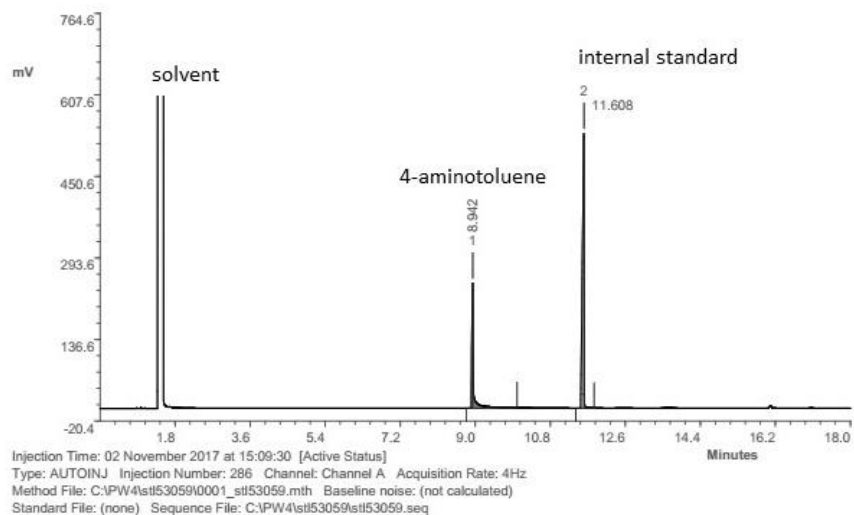
4-Aminotoluene

Calibration with dodecane as internal standard, starting material, and product.



| Peak | RT | Area | %Ar | Conc. (Ar) | Height | M | Units | Name |
|------|--------|----------|-------|----------------|---------|---|-------|------|
| 1 | 8.950 | 521.553 | 25.74 | Not Calculated | 196.303 | 1 | | |
| 2 | 11.329 | 438.264 | 21.63 | Not Calculated | 167.991 | 0 | | |
| 3 | 11.621 | 1066.469 | 52.63 | Not Calculated | 424.781 | 0 | | |

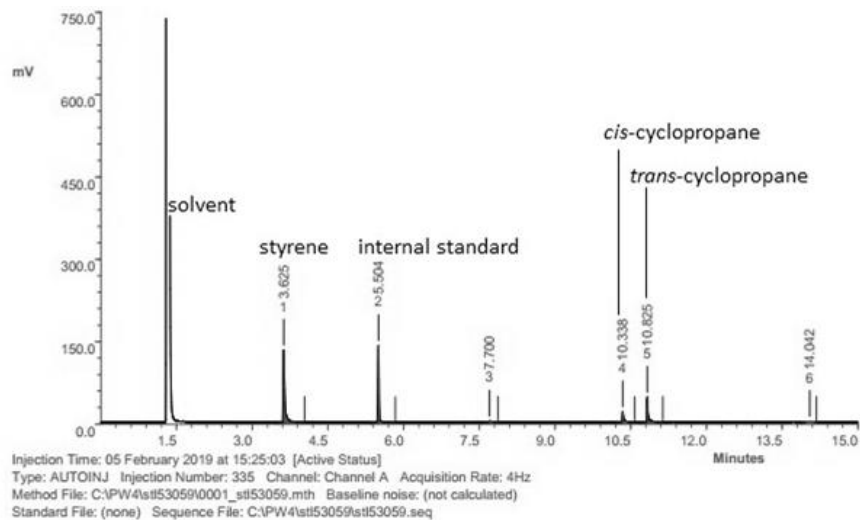
Measurement of reaction sample with dodecane as internal standard.



| Peak | RT | Area | %Ar | Conc. (Ar) | Height | M | Units | Name |
|------|--------|----------|-------|----------------|---------|---|-------|------|
| 1 | 8.942 | 633.491 | 30.26 | Not Calculated | 240.839 | 1 | | |
| 2 | 11.608 | 1459.756 | 69.74 | Not Calculated | 528.909 | 1 | | |

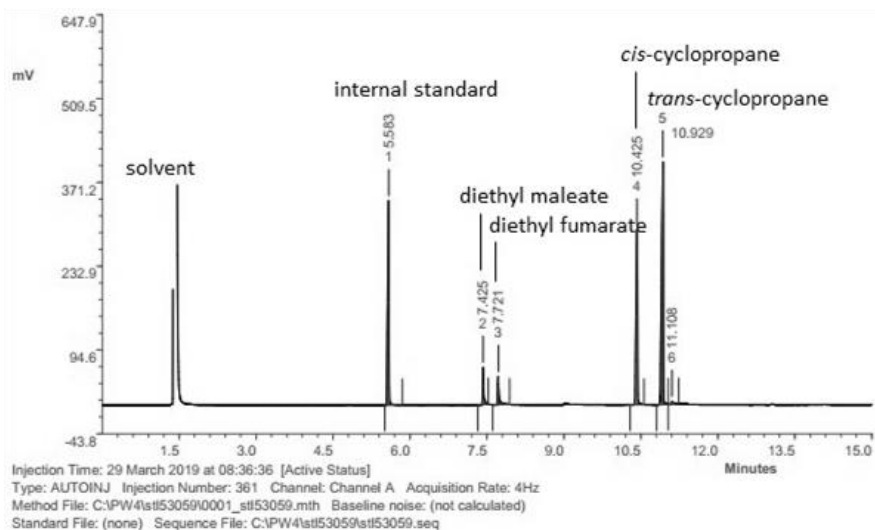
Ethyl (1*R*,2*R*)-2-phenylcyclopropane-1-carboxylate (*trans*-cyclopropane 35)Ethyl (1*R*,2*S*)-2-phenylcyclopropane-1-carboxylate (*cis*-cyclopropane 35)

Calibration with dodecane as internal standard, starting material, and product.

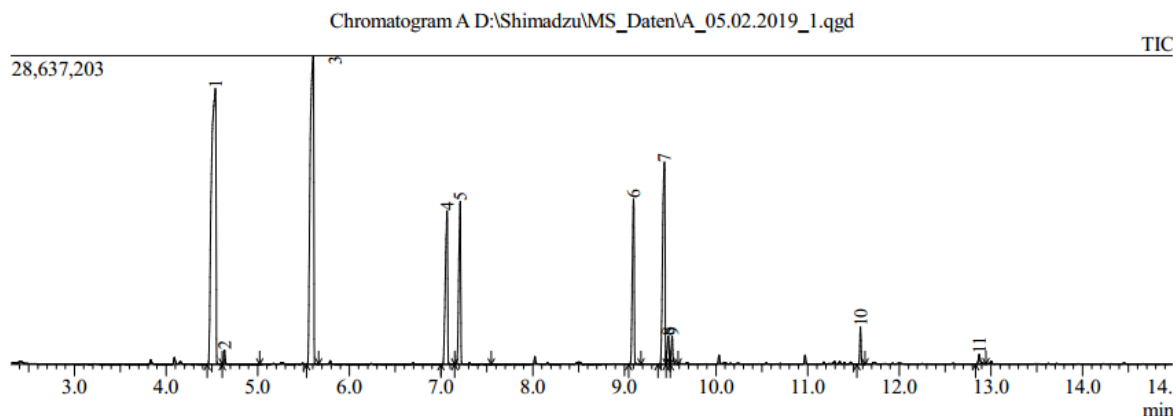


| Peak | RT | Area | %Ar | Conc. (Ar) | Height | M | Units | Name |
|------|--------|---------|-------|----------------|---------|---|-------|------|
| 1 | 3.625 | 309.465 | 46.40 | Not Calculated | 131.819 | 1 | | |
| 2 | 5.504 | 212.503 | 31.86 | Not Calculated | 139.888 | 1 | | |
| 3 | 7.700 | 7.108 | 1.07 | Not Calculated | 1.942 | 1 | | |
| 4 | 10.338 | 40.289 | 6.04 | Not Calculated | 19.013 | 1 | | |
| 5 | 10.825 | 85.079 | 12.76 | Not Calculated | 45.604 | 1 | | |
| 6 | 14.042 | 12.563 | 1.88 | Not Calculated | 1.323 | 1 | | |

Measurement of reaction sample with dodecane as internal standard.



| Peak | RT | Area | %Ar | Conc. (Ar) | Height | M | Units | Name |
|------|--------|---------|-------|----------------|---------|---|-------|------|
| 1 | 5.583 | 576.969 | 26.65 | Not Calculated | 336.914 | 1 | | |
| 2 | 7.425 | 87.199 | 4.03 | Not Calculated | 61.209 | 1 | | |
| 3 | 7.721 | 77.416 | 3.58 | Not Calculated | 45.904 | 1 | | |
| 4 | 10.425 | 542.236 | 25.04 | Not Calculated | 288.349 | 1 | | |
| 5 | 10.929 | 869.778 | 40.17 | Not Calculated | 400.121 | 1 | | |
| 6 | 11.108 | 11.594 | 0.54 | Not Calculated | 4.282 | 1 | | |

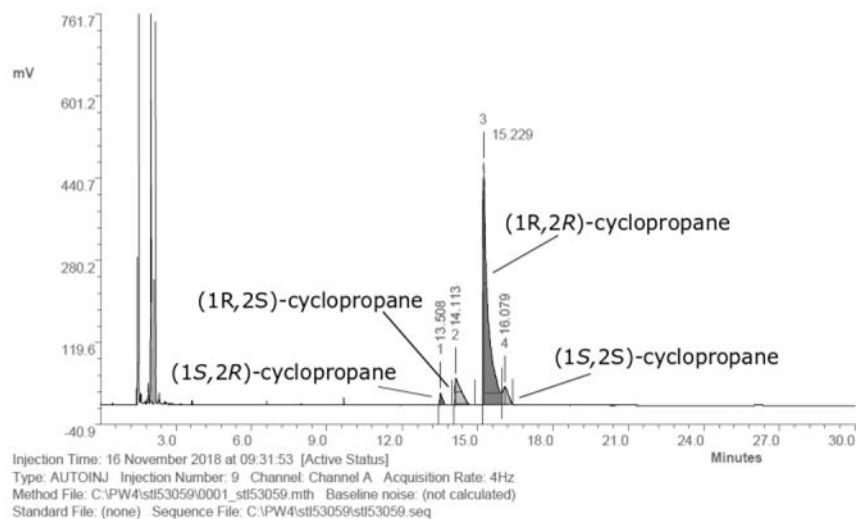
GC-MS chromatogram of *trans*- and *cis*-cyclopropane **35**

Peak Report TIC

| Peak# | R.Time | Area | Area% | Height | Height% | A/H | Mark | Name |
|-------|--------|-----------|--------|-----------|---------|------|------|----------------------------------------------|
| 1 | 4.537 | 87837176 | 31.56 | 25489176 | 19.93 | 3.45 | | Styrene |
| 2 | 4.636 | 1317057 | 0.47 | 1267809 | 0.99 | 1.04 | SV | |
| 3 | 5.604 | 76916659 | 27.63 | 28577127 | 22.35 | 2.69 | V | Decane |
| 4 | 7.065 | 23992879 | 8.62 | 14177121 | 11.09 | 1.69 | SV | 2-Butenedioic acid (Z)-, diethyl ester |
| 5 | 7.208 | 21717350 | 7.80 | 14975430 | 11.71 | 1.45 | SV | Diethyl fumarate |
| 6 | 9.101 | 21340179 | 7.67 | 15229423 | 11.91 | 1.40 | V | <i>trans</i> -1-Carboxy-2-phenylcyclopropane |
| 7 | 9.437 | 33568090 | 12.06 | 18741930 | 14.66 | 1.79 | V | <i>trans</i> -1-Carboxy-2-phenylcyclopropane |
| 8 | 9.480 | 3787631 | 1.36 | 2559381 | 2.00 | 1.48 | V | |
| 9 | 9.522 | 3117236 | 1.12 | 2595314 | 2.03 | 1.20 | V | |
| 10 | 11.577 | 3328627 | 1.20 | 3362146 | 2.63 | 0.99 | V | |
| 11 | 12.872 | 1425147 | 0.51 | 887688 | 0.69 | 1.61 | V | |
| | | 278348031 | 100.00 | 127862545 | 100.00 | | | |

Chiral GC chromatogram (Cyclodex- β column) of *trans*- and *cis*-cyclopropane **35**

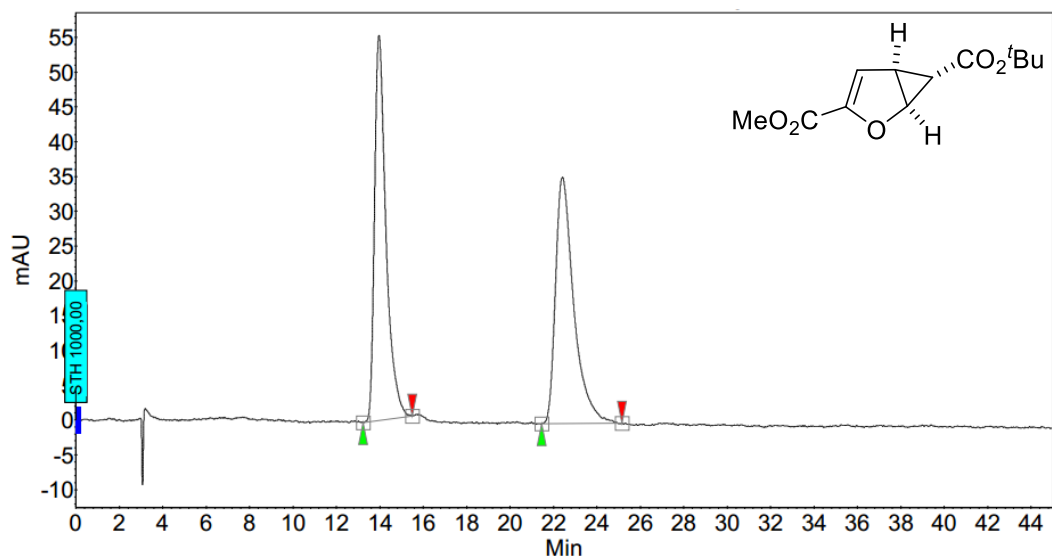
Measurement of reaction sample (oven temperature: 135 °C isotherm).



| Peak | RT | Area | %Ar | Conc.(Ar) | Height | M | Units | Name |
|------|--------|----------|-------|----------------|---------|---|-------|------|
| 1 | 13.508 | 178.207 | 2.27 | Not Calculated | 24.009 | 0 | | |
| 2 | 14.113 | 881.691 | 11.23 | Not Calculated | 53.002 | 0 | | |
| 3 | 15.229 | 6231.628 | 79.40 | Not Calculated | 472.630 | 0 | | |
| 4 | 16.079 | 556.411 | 7.09 | Not Calculated | 35.201 | 0 | | |

3. HPLC chromatograms

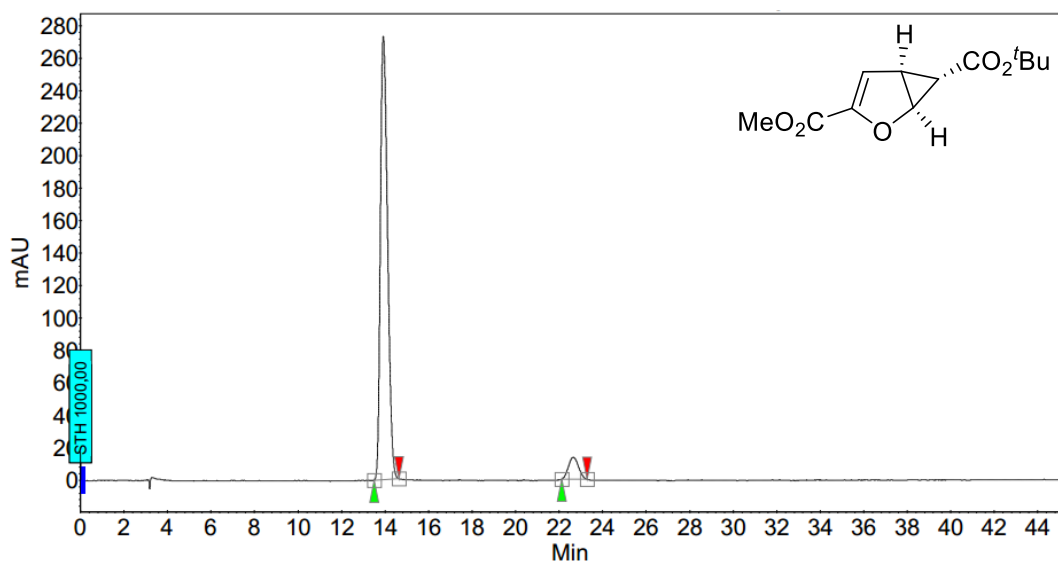
2-Oxabicyclo[3.1.0]hex-3-ene-3,6-dicarboxylic 6-*tert*-butyl ester 3-methyl ester (66)



Peak Results :

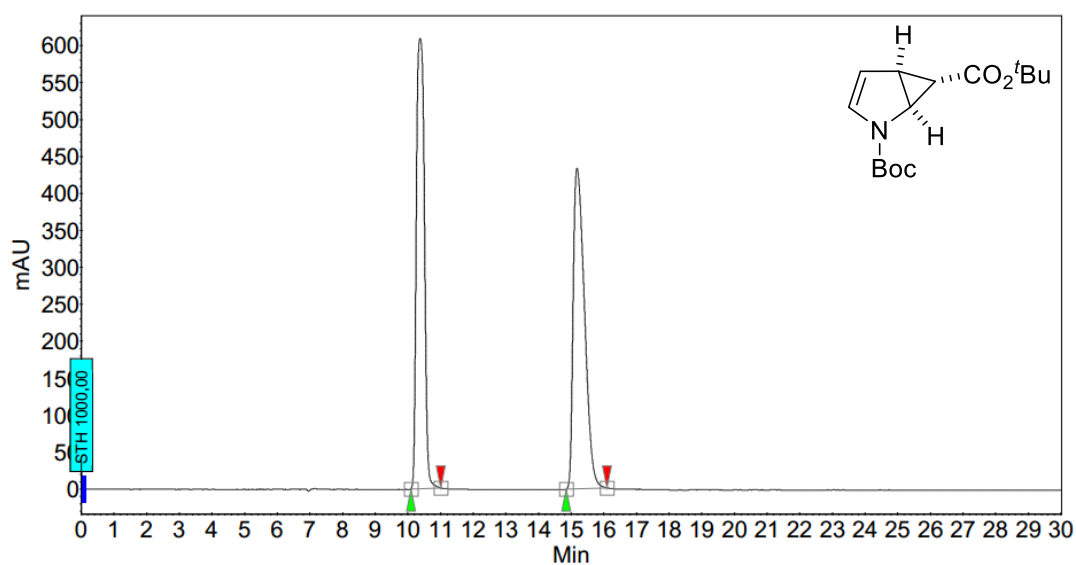
| Index | Name | Time [Min] | Quantity [% Area] | Height [mAU] | Area [mAU.Min] | Area % [%] |
|-------|---------|------------|-------------------|--------------|----------------|------------|
| 1 | UNKNOWN | 13.96 | 49.52 | 55.4 | 33.9 | 49.522 |
| 2 | UNKNOWN | 22.42 | 50.48 | 35.4 | 34.5 | 50.478 |
| Total | | | 100.00 | 90.8 | 68.4 | 100.000 |

(1*S*,5*S*,6*S*)-(-)-2-Oxabicyclo[3.1.0]hex-3-ene-3,6-dicarboxylic 6-*tert*-butyl ester 3-methyl ester (66)



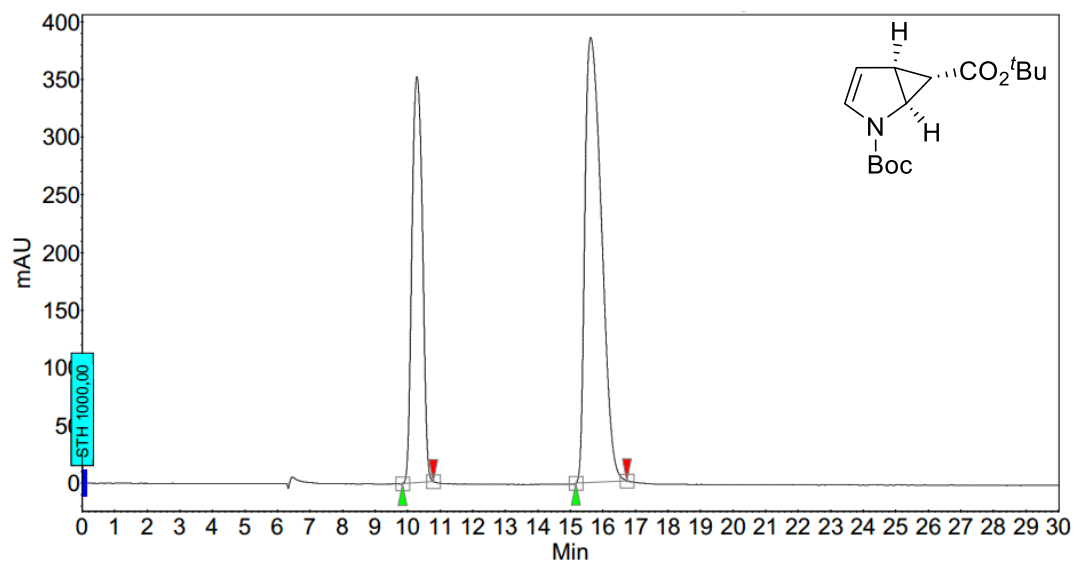
Peak Results :

| Index | Name | Time [Min] | Quantity [% Area] | Height [mAU] | Area [mAU.Min] | Area % [%] |
|-------|---------|------------|-------------------|--------------|----------------|------------|
| 1 | UNKNOWN | 13.92 | 93.49 | 273.0 | 104.4 | 93.489 |
| 2 | UNKNOWN | 22.65 | 6.51 | 13.6 | 7.3 | 6.511 |
| Total | | | 100.00 | 286.6 | 111.7 | 100.000 |

Di-*tert*-butyl-2-azabicyclo[3.1.0]hex-3-ene-2,6-dicarboxylate (67)

Peak Results :

| Index | Name | Time [Min] | Quantity [% Area] | Height [mAU] | Area [mAU.Min] | Area % [%] |
|-------|---------|------------|-------------------|--------------|----------------|------------|
| 1 | UNKNOWN | 10.37 | 49.79 | 609.2 | 172.8 | 49.791 |
| 2 | UNKNOWN | 15.18 | 50.21 | 433.9 | 174.2 | 50.209 |
| Total | | | 100.00 | 1043.1 | 347.0 | 100.000 |

Di-*tert*-butyl (1*S*,5*S*,6*S*)-2-azabicyclo[3.1.0]hex-3-ene-2,6-dicarboxylate (67)

Peak Results :

| Index | Name | Time [Min] | Quantity [% Area] | Height [mAU] | Area [mAU.Min] | Area % [%] |
|-------|---------|------------|-------------------|--------------|----------------|------------|
| 1 | UNKNOWN | 10.29 | 36.68 | 352.0 | 132.1 | 36.677 |
| 2 | UNKNOWN | 15.63 | 63.32 | 385.9 | 228.1 | 63.323 |
| Total | | | 100.00 | 738.0 | 360.3 | 100.000 |

4. Curriculum Vitae

Personal data

| | |
|---------------|------------------------------|
| Name | Lisa Stadler |
| Date of birth | August 30, 1993 in Starnberg |
| Nationality | German |
| Email | stadler_lisa@t-online.de |

Education

| | |
|-------------------|----------------------------------------------------------------------------------------------------------|
| 11/2016 – current | PhD thesis in the research group of <i>Prof. Dr. O. Reiser</i> (University of Regensburg, Germany) |
| 09/2016 | Master of Science in chemistry |
| 04/2016 – 09/2016 | Master thesis in the research group of <i>Prof. Dr. O. Reiser</i> (University of Regensburg, Germany) |
| 10/2014 – 09/2016 | Advanced studies in chemistry (University of Regensburg, Germany) |
| 09/2014 | Bachelor of Science in chemistry |
| 02/2014 – 05/2014 | Bachelor thesis in the research group of <i>Prof. Dr. J. Wegener</i> (University of Regensburg, Germany) |
| 10/2011 – 09/2014 | Studies in chemistry (University of Regensburg, Germany) |
| 09/2003 – 07/2011 | Abitur (<i>A-levels</i>), Anton-Bruckner-Gymnasium (<i>secondary school</i>) Straubing, Germany. |

Publications

L. Stadler, M. Homafar, A. Hartl, S. Najafishirtari, M. Colombo, R. Zboril, P. Martin, M. B. Gawande, J. Zhi, O. Reiser, *ACS Sustainable Chem. Eng.* **2019**, *7*, 2388-2399.

“Recyclable magnetic microporous organic polymer (MOP) encapsulated with palladium nanoparticles and Co/C nanobeads for hydrogenation reactions.”

L. Stadler, O. Reiser, *Manuscript in preparation.*

“Magnetic microporous polymers as high capacity adsorbents for the effective reversible extraction of toxic heavy metals from water.”

Conferences

7th EuCheMS Chemistry Congress – Liverpool (United Kingdom), August 26-30, 2018.

“Functionalized carbon-coated magnetic nanoparticles as a recyclable catalyst for Suzuki-Miyaura couplings under mild reaction conditions” (poster presentation).

GDCh-Wissenschaftsforum – Berlin (Germany), September 10-14, 2017.

“Magnetically recyclable palladium nanocatalysts based on microporous organic polymers for hydrogenation reactions” (poster presentation).

26th ISHC Congress – Regensburg (Germany), August 03-08, 2017.

“Microporous organic polymers embedded with magnetic Co/C nanobeads and transition metal nanoparticles as recyclable multifunctional catalysts” (poster presentation).

1st German-Russian Interdisciplinary Student Workshop – Moscow (Russia), April 25-27, 2016

“Palladium nanoparticles embedded in magnetic microporous organic polymers: Highly active and recyclable catalysts for hydrogenation reactions” (oral communication, 15 min).

4th International Scientific Conference “Advances in Synthesis and Complexing” – Moscow (Russia), April 25-27, 2016

6th EuCheMS Chemistry Congress – Seville (Spain), September 11-15, 2016.

“Microporous organic polymers encapsulated with metal nanoparticles and Co/C nanobeads and its use as magnetic recyclable catalyst” (poster presentation).

Professional References

Prof. Dr. Oliver Reiser

Institut für Organische Chemie

Universität Regensburg, Universitätsstr. 31

93053 Regensburg, Germany

Phone: 0049 941 943 4631

Email: Oliver.Reiser@chemie.uni-regensburg.de

H. Acknowledgment - Danksagung

Bedanken möchte ich mich zunächst herzlich bei Prof. Dr. Oliver Reiser für die Überlassung des interessanten Themas und seine beständige Unterstützung während der gesamten Arbeit.

Für die Messung von diversen TEM, BET, TGA und XPS-Messungen, den fachlichen Diskussionen und der bereitwilligen Hilfestellung bei Problemen, danke ich Dr. Sharif Najafishirtari, Prof. Dr. Josef Zweck, Dr. Manoj Gawande, Dr. Massimo Colombo, Dr. Rainer Müller und Thomas-Norbert-Gerhard Meier.

Allen Mitarbeitern der Zentralen Analytik der Universität Regensburg danke ich für sämtliche Messungen, insbesondere Barbara Baumann und Helmut Schüller. Mein Dank gebührt ebenso Vanessa Tomanek und Joachim Rewitzer für die unproblematischen und schnellen Termine, eure Geduld bei den unzähligen ICP-Messungen, als auch der guten Unterhaltung währenddessen.

Ein herzliches Dankeschön an die Mitarbeiterinnen des Sekretariats der Arbeitsgruppe, Antje Weigert und Michaela Schüle, für die Bearbeitung aller bürokratischen und organisatorischen Angelegenheiten und ihr offenes Ohr für Probleme jeglicher Art.

Besonderer Dank gilt Dr. Peter Kreitmeier für die zahllosen fachlichen Ratschläge, Hilfestellungen, Tüfteleien und sonstige unterhaltsame Gespräche. Für die technische sowie synthetische Unterstützung danke ich desweiteren unseren aktuellen und ehemaligen Mitarbeitern Klaus Döring, Simone Dürmeier, Brigitte Eichenseher, Johannes Floß, Roxane Harteis und Helena Konkel.

Für die Integration in die Arbeitsgruppe und die herzliche und freundschaftliche Atmosphäre möchte ich mich bei allen aktuellen und ehemaligen Mitarbeitern des Arbeitskreises bedanken. Besonderer Dank gilt hierbei meinen damaligen und heutigen guten Freunden und Kollegen Tobias Babl, Simon Budde, Robert Eckl, Peter Ehrnsberger, Christian Eichinger, Sebastian Engl, Dr. Thomas Ertl, Sebastian Fischer, Dr. Thomas Föll, Dr. Matthias Gnahn, Andreas Hartl, Dr. Martin Hofmann, Dr. Benjamin Kastl, Dr. Sabine Kerres, Tomislav Krolo, Dr. Verena Lehner, Michael Leitner, Natalija Moor, Dr. Saerom Park, Eva Plut, Anna Rustler, Carina Sonnleitner, Lukas Traub und Lisa Uhlstein. Vor allem möchte ich mich für alle gemeinsamen Unternehmungen inner- und außerhalb der Universität bedanken. Seien es fachliche Diskussionen, aufmunternde Worte, der Kaffee am Morgen, ein Ausflug zum See oder auch eine gemütliche Runde in der Küche. Ich bin unendlich dankbar, dass wir so eine schöne Zeit miteinander hatten. Mit euch war und wird es nie langweilig!

Meinem guten Freund und ehemaligem Laborkollegen, Dr. Benjamin Kastl, möchte ich besonders danken. Nicht nur für die gemeinsame schöne und entspannte Zeit im Labor und die vielen lustigen Momente, die wir sowohl in der Universität als auch außerhalb hatten, sondern vor allem für deine

mittlerweile langjährige Freundschaft. Du hast mich mit deiner freundlichen Art von Anfang an herzlich aufgenommen und hast jeden Tag in der Arbeit ein Stück weit erheitert. Ich danke dir für alles!

Meinen Nanopartikel-Kollegen Andreas Hartl und Christian Eichinger danke ich für die unzähligen fachlichen Diskussionen, als auch nicht-fachlichen Gespräche. Hierzu gehören natürlich auch Simon Budde und Dr. Thomas Föll. Ihr hattet immer ein offenes Ohr und stets einen Rat oder Scherz auf Lager.

Herzlichen Dank an meine Bürokollegen und Leidensgenossen Michael Leitner, Lukas Traub und Peter Ehrnsberger für die Hilfestellung, die Motivationssuche und die unterhaltsamen Nachmittage und Abende. Peter, dir möchte ich zusätzlich für die zwar kurze, aber sehr schöne und entspannte Zeit im Labor danken und auch für so einige Online-Treffen, während des „Home-Office“.

Dr. Corina Neumeister danke ich für die schöne Zeit während meines Forschungspraktikums. Ich konnte bei dir viel lernen und ohne deine aufgeschlossene, herzliche und lustige Art wäre ich womöglich nicht da, wo ich jetzt bin.

Für das schnelle und gewissenhafte Korrekturlesen dieser Arbeit danke ich Dr. Martin Hofmann, Dr. Benjamin Kastl, Natalija Moor, Robert Eckl, Sebastian Fischer und Anna Stadler.

Zudem danke ich meinen ehemaligen Bachelorstudenten und Forschungspraktikant(inn)en Martin Gawron, Sebastian Graf, Matthias Pertl, Christina Pfab, Daniel Schmidhuber und Ulrike Wirth.

Meinen lieben Freunden von zuhause und außerhalb der Universität möchte ich ebenso herzlich danken: Julia Bauer, Jacqueline Baumann, Karin Bogner, Jessica Hennek, Katrin Holzleitner, Alexandra Kersch, Theresa Kränzle, Sabrina Weiß. Auch wenn es bei manchen Freundschaft auf den zweiten Blick war oder wir den ein oder anderen Streit hatten, bin ich froh, jede einzelne von euch als Freundin zu haben. Wir haben viel gemeinsam erlebt und ich freue mich immer, euch nach langer Zeit wieder zu sehen. Es ist jedesmal, als wären wir nie getrennt gewesen!

Lieber Jimmy, ich bin dir aus tiefstem Herzen für alles dankbar, was wir gemeinsam erlebt und durchgemacht haben. Es war nicht immer einfach, aber ich danke dir für deine unermüdliche Unterstützung, deine Geduld, deine häufig gefragte Hilfe, sowie den Rückhalt, den ich von dir in allen Lebenslagen seit Jahren täglich erhalte. Danke, dass du immer an mich glaubst und für mich da bist.

Abschließend bedanke ich mich von ganzem Herzen bei meiner Familie. Von euch habe ich seit jeher bedingungslose Unterstützung und Rückhalt erfahren. Danke, dass ihr das möglich gemacht habt und mich immer unterstützt und ermutigt habt!

I. Declaration

Herewith I declare that this present thesis is a presentation of my original work prepared single-handed. Wherever contributions from others are involved, all of them are marked clearly, with reference to the literature, license, and acknowledgment of collaborative research.

Regensburg, June 30, 2020

Lisa Stadler